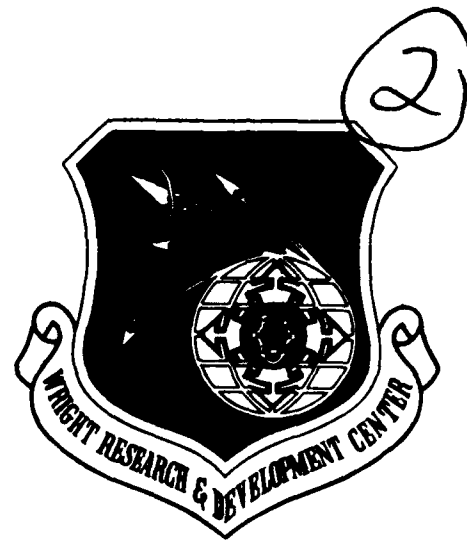


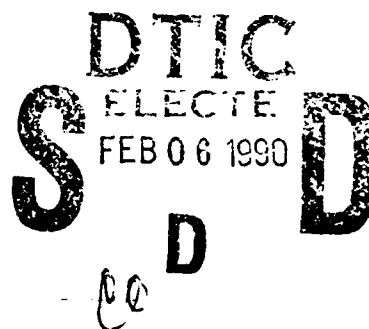
DTIC FILE COPY

WRDC-TR-89-4107



## OPTIMIZATION OF LAMINATED COMPOSITE PLATES

Antonio Miravete  
Mechanics & Surface Interactions Branch  
Nonmetallic Materials Division



September 1989

Final Report for Period September 1988--August 1989

Approved for public release; distribution is unlimited.

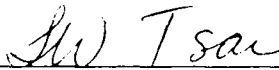
MATERIALS LABORATORY  
AIR FORCE WRIGHT RESEARCH AND DEVELOPMENT CENTER  
AIR FORCE SYSTEMS COMMAND  
WRIGHT-PATTERSON AIR FORCE BASE, OHIO 45433-6533

## NOTICE

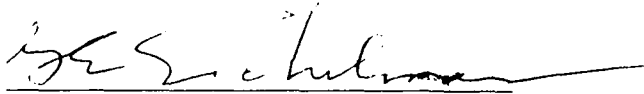
WHEN GOVERNMENT DRAWINGS, SPECIFICATIONS, OR OTHER DATA ARE USED FOR ANY PURPOSE OTHER THAN IN CONNECTION WITH A DEFINITELY GOVERNMENT-RELATED PROCUREMENT, THE UNITED STATES GOVERNMENT INCURS NO RESPONSIBILITY OR ANY OBLIGATION WHATSOEVER. THE FACT THAT THE GOVERNMENT MAY HAVE FORMULATED OR IN ANY WAY SUPPLIED THE SAID DRAWINGS, SPECIFICATIONS OR OTHER DATA, IS NOT TO BE REGARDED BY IMPLICATION, OR OTHERWISE IN ANY MANNER CONSTRUED, AS LICENSING THE HOLDER, OR ANY OTHER PERSON OR CORPORATION; OR AS CONVEYING ANY RIGHTS OR PERMISSION TO MANUFACTURE, USE, OR SELL ANY PATENTED INVENTION THAT MAY IN ANY WAY BE RELATED THERETO.

THIS REPORT HAS BEEN REVIEWED BY THE OFFICE OF PUBLIC AFFAIRS (ASD/PA) AND IS RELEASABLE TO THE NATIONAL TECHNICAL INFORMATION SERVICE (NTIS). AT NTIS IT WILL BE AVAILABLE TO THE GENERAL PUBLIC INCLUDING FOREIGN NATIONS.

THIS TECHNICAL REPORT HAS BEEN REVIEWED AND IS APPROVED FOR PUBLICATION.

  
STEPHEN W. TSAI, Chief  
Mechanics & Surface Interactions Branch  
Nonmetallic Materials Division

FOR THE COMMANDER

  
GAIL E. EICHELMAN  
Assistant Director  
Nonmetallic Materials Division

IF YOUR ADDRESS HAS CHANGED, IF YOU WISH TO BE REMOVED FROM OUR MAILING LIST, OR IF THE ADDRESSEE IS NO LONGER EMPLOYED BY YOUR ORGANIZATION PLEASE NOTIFY WRDC/MLBM, WRIGHT-PATTERSON AFB, OH 45433-6533 TO HELP MAINTAIN A CURRENT MAILING LIST.

COPIES OF THIS REPORT SHOULD NOT BE RETURNED UNLESS RETURN IS REQUIRED BY SECURITY CONSIDERATIONS, CONTRACTUAL OBLIGATIONS, OR NOTICE ON A SPECIFIC DOCUMENT.

UNCLASSIFIED

SECURITY CLASSIFICATION OF THIS PAGE

REPORT DOCUMENTATION PAGE				Form Approved OMB No. 0704-0188		
1a. REPORT SECURITY CLASSIFICATION Unclassified			1b. RESTRICTIVE MARKINGS			
2a. SECURITY CLASSIFICATION AUTHORITY			3. DISTRIBUTION/AVAILABILITY OF REPORT Approved for public release; distribution is unlimited			
2b. DECLASSIFICATION/DOWNGRADING SCHEDULE						
4. PERFORMING ORGANIZATION REPORT NUMBER(S) WRDC-TR-89-4107			5. MONITORING ORGANIZATION REPORT NUMBER(S)			
6a. NAME OF PERFORMING ORGANIZATION Systran Corp		6b. OFFICE SYMBOL (If applicable)	7a. NAME OF MONITORING ORGANIZATION Materials Laboratory (WRDC/MLRM) Wright Research and Development Center			
6c. ADDRESS (City, State, and ZIP Code) 4126 Linden Ave Dayton OH 45432			7b. ADDRESS (City, State, and ZIP Code) Wright-Patterson AFB OH 45433-6533			
8a. NAME OF FUNDING/SPONSORING ORGANIZATION		8b. OFFICE SYMBOL (If applicable)	9. PROCUREMENT INSTRUMENT IDENTIFICATION NUMBER F33615-88-C-5402			
8c. ADDRESS (City, State, and ZIP Code)			10. SOURCE OF FUNDING NUMBERS			
			PROGRAM ELEMENT NO. 62102F	PROJECT NO. 2418	TASK NO. 04	WORK UNIT ACCESSION NO. 51
11. TITLE (Include Security Classification) Optimization of Laminated Composite Plates						
12. PERSONAL AUTHOR(S) Antonio Miravete						
13a. TYPE OF REPORT Final		13b. TIME COVERED FROM 9/1988 TO 8/1989		14. DATE OF REPORT (Year, Month, Day) Sep 1989		
15. PAGE COUNT 190						
16. SUPPLEMENTARY NOTATION						
17. COSATI CODES			18. SUBJECT TERMS (Continue on reverse if necessary and identify by block number)			
FIELD	GROUP	SUB-GROUP				
11	04		composite materials; optimization; finite elements			
19. ABSTRACT (Continue on reverse if necessary and identify by block number)						
<p>Optima laminate configurations for laminated rectangular plates under transverse and buckling loads are investigated. Laminate thickness and fiber orientation are treated as design variables, the thickness laminate being variable along the plate. A fully stressed iterative procedure and a quadratic failure criterion have been applied in order to get the minimum weight plate using strength as a design criterion. A finite element method accounting for in-plane and interlaminar stresses has been used. Results for thin and thick plates, different boundary conditions and some types of loading are shown.</p> <p><i>... showing the effect of material properties</i></p>						
20. DISTRIBUTION/AVAILABILITY OF ABSTRACT <input checked="" type="checkbox"/> UNCLASSIFIED/UNLIMITED <input type="checkbox"/> SAME AS RPT <input type="checkbox"/> DTIC USERS			21. ABSTRACT SECURITY CLASSIFICATION Unclassified			
22a. NAME OF RESPONSIBLE INDIVIDUAL Dr Stephen W. Tsai			22b. TELEPHONE (Include Area Code) (513-255-3068)		22c. OFFICE SYMBOL WRDC/MLRM	

DD Form 1473, JUN 86

Previous editions are obsolete.

SECURITY CLASSIFICATION OF THIS PAGE

UNCLASSIFIED

## FOREWORD

This report was prepared in the Mechanics and Surface Interactions Branch (WRDC/MLBM), Nonmetallic Material Division, Materials Laboratory, Wright Research and Development Center, Wright-Patterson Air Force Base, Ohio.

The work report herein was performed from September 1988 to August 1989. Dr Antonio Miravete is a Professor at the Department of Mechanical Engineering, Escuela Tecnica Superior de Ingenieros Industriales, University of Zaragoza, 50015 Zaragoza, Spain under contract F33615-88-C-5402.

The author is grateful to Dr Stephen W. Tsai for his encouragement and guidance in the course of this work.

Accession For	
NTIS CR&I	<input checked="" type="checkbox"/>
DTIC TAB	<input type="checkbox"/>
Unannounced	<input type="checkbox"/>
Justification	
By	
Date	
Availability Codes	
Dist	
A-1	



## TABLE OF CONTENTS

	Page
1. <u>INTRODUCTION</u> .....	1
1.1 LITERATURE REVIEW.....	2
1.2 PROJECT SUMMARY.....	7
2. <u>SYMBOLS AND NOTATION</u> .....	9
3. <u>LAMINATED COMPOSITE PLATES SUBJECTED TO TRANSVERSE LOADS</u> .....	16
3.1 ANALYTICAL FORMULATION.....	17
3.1.1 Equations of Analysis.....	17
3.1.2 Failure Criterion.....	20
3.1.3 Recurrence Relations.....	22
3.2 ANALYSIS OF THE VARIABLE THICKNESS PROBLEM.....	25
3.2.1 Model assumptions and Method of Analysis.....	26
3.2.2 Through-Thickness Stress Distributions.....	27
3.2.3 Failure Mechanisms.....	30
3.2.4 Experimental Study and Verification of the Theoretical Model.....	34
3.3 DESCRIPTION OF RESULTS.....	43
3.3.1 Model Assumptions and Method of Analysis.....	44
3.3.2 Determination of elastic constants and strengths.....	46
3.3.3 One-dimensional Laminated Composite Plates.....	48
3.3.4 Two-dimensional Laminated Composite Plates.....	51
4. <u>LAMINATED COMPOSITE PLATES SUBJECTED TO BUCKLING LOADS</u> .....	62
4.1 ANALYTICAL FORMULATION.....	62
4.2 DESCRIPTION OF RESULTS.....	64
4.2.1 Model Assumptions and Method of Analysis.....	64
4.2.2 One-dimensional Laminated Composite Plates.....	66
4.2.3 Two-dimensional Laminated Composite Plates.....	68

5.	<u>CONCLUDING REMARKS</u> .....	75
	<u>REFERENCES</u> .....	77

## LIST OF FIGURES

<u>No.</u>	<u>Page</u>
1. Schematic representation of a variable-thickness composite plate.....	86
2. Representation of the optimization procedure.....	86
3. Distribution of $\sigma_1$ for a two-sides tapered plate and $\partial M/\partial x > 0...$	87
4. Distribution of $\sigma_3$ for a two-sides tapered plate and $\partial M/\partial x > 0...$	87
5. Distribution of $\sigma_5$ for a two-sides tapered plate and $\partial M/\partial x > 0...$	88
6. Distribution of $\sigma_1$ for a one-side tapered plate and $\partial M/\partial x > 0....$	88
7. Distribution of $\sigma_3$ for a one-side tapered plate and $\partial M/\partial x > 0....$	89
8. Distribution of $\sigma_5$ for a one-side tapered plate and $\partial M/\partial x > 0....$	89
9. Distribution of $\sigma_1$ for a two-sides tapered plate and $\partial M/\partial x < 0...$	90
10. Distribution of $\sigma_3$ for a two-sides tapered plate and $\partial M/\partial x < 0...$	90
11. Distribution of $\sigma_5$ for a two-sides tapered plate and $\partial M/\partial x < 0...$	91
12. Distribution of $\sigma_1$ for a one-side tapered plate and $\partial M/\partial x < 0....$	91
13. Distribution of $\sigma_3$ for a one-side tapered plate and $\partial M/\partial x < 0....$	92
14. Distribution of $\sigma_5$ for a one-side tapered plate and $\partial M/\partial x < 0....$	92
15. Distribution of $\sigma_1$ for a one-side tapered plate, $t_1/t=0.3$ , M/Pt=5 and $\partial M/\partial x > 0.....$	93
16. Distribution of $\sigma_3$ for a one-side tapered plate, $t_1/t=0.3$ , M/Pt=5 and $\partial M/\partial x > 0.....$	93
17. Distribution of $\sigma_5$ for a one-side tapered plate, $t_1/t=0.2$ , M/Pt=5 and $\partial M/\partial x > 0.....$	94

## TABLE OF CONTENTS

		Page
1.	<u>INTRODUCTION</u> .....	1
	1.1 LITERATURE REVIEW.....	2
	1.2 PROJECT SUMMARY.....	7
2.	<u>SYMBOLS AND NOTATION</u> .....	9
3.	<u>LAMINATED COMPOSITE PLATES SUBJECTED TO TRANSVERSE LOADS</u> .....	16
	3.1 ANALYTICAL FORMULATION.....	17
	3.1.1 Equations of Analysis.....	17
	3.1.2 Failure Criterion.....	20
	3.1.3 Recurrence Relations.....	22
	3.2 ANALYSIS OF THE VARIABLE THICKNESS PROBLEM.....	25
	3.2.1 Model assumptions and Method of Analysis.....	26
	3.2.2 Through-Thickness Stress Distributions.....	27
	3.2.3 Failure Mechanisms.....	30
	3.2.4 Experimental Study and Verification of the Theoretical Model.....	34
	3.3 DESCRIPTION OF RESULTS.....	43
	3.3.1 Model Assumptions and Method of Analysis.....	44
	3.3.2 Determination of elastic constants and strengths.....	46
	3.3.3 One-dimensional Laminated Composite Plates.....	48
	3.3.4 Two-dimensional Laminated Composite Plates.....	51
4.	<u>LAMINATED COMPOSITE PLATES SUBJECTED TO BUCKLING LOADS</u> .....	62
	4.1 ANALYTICAL FORMULATION.....	62
	4.2 DESCRIPTION OF RESULTS.....	64
	4.2.1 Model Assumptions and Method of Analysis.....	64
	4.2.2 One-dimensional Laminated Composite Plates.....	66
	4.2.3 Two-dimensional Laminated Composite Plates.....	68



5.	<u>CONCLUDING REMARKS</u> .....	75
	<u>REFERENCES</u> .....	77

## LIST OF FIGURES

<u>No.</u>	<u>Page</u>
1. Schematic representation of a variable-thickness composite plate.....	86
2. Representation of the optimization procedure.....	86
3. Distribution of $\sigma_1$ for a two-sides tapered plate and $\partial M/\partial x > 0...$	87
4. Distribution of $\sigma_3$ for a two-sides tapered plate and $\partial M/\partial x > 0...$	87
5. Distribution of $\sigma_5$ for a two-sides tapered plate and $\partial M/\partial x > 0...$	88
6. Distribution of $\sigma_1$ for a one-side tapered plate and $\partial M/\partial x > 0....$	88
7. Distribution of $\sigma_3$ for a one-side tapered plate and $\partial M/\partial x > 0....$	89
8. Distribution of $\sigma_5$ for a one-side tapered plate and $\partial M/\partial x > 0....$	89
9. Distribution of $\sigma_1$ for a two-sides tapered plate and $\partial M/\partial x < 0...$	90
10. Distribution of $\sigma_3$ for a two-sides tapered plate and $\partial M/\partial x < 0...$	90
11. Distribution of $\sigma_5$ for a two-sides tapered plate and $\partial M/\partial x < 0...$	91
12. Distribution of $\sigma_1$ for a one-side tapered plate and $\partial M/\partial x < 0....$	91
13. Distribution of $\sigma_3$ for a one-side tapered plate and $\partial M/\partial x < 0....$	92
14. Distribution of $\sigma_5$ for a one-side tapered plate and $\partial M/\partial x < 0....$	92
15. Distribution of $\sigma_1$ for a one-side tapered plate, $t_1/t=0.3$ , $M/Pt=5$ and $\partial M/\partial x > 0.....$	93
16. Distribution of $\sigma_3$ for a one-side tapered plate, $t_1/t=0.3$ , $M/Pt=5$ and $\partial M/\partial x > 0.....$	93
17. Distribution of $\sigma_5$ for a one-side tapered plate, $t_1/t=0.2$ , $M/Pt=5$ and $\partial M/\partial x > 0.....$	94

18.	Distribution of $\sigma_3$ for a one-side tapered plate, $t_1/t=0.2$ , $M/Pt=5$ and $\partial M/\partial x > 0$ .....	94
19.	Distribution of $\sigma_5$ for a one-side tapered plate, $t_1/t=0.2$ , $M/Pt=5$ and $\partial M/\partial x > 0$ .....	95
20.	Distribution of $\sigma_1$ for a one-side tapered plate, $t_1/t=0.1$ , $M/Pt=5$ and $\partial M/\partial x > 0$ .....	95
21.	Distribution of $\sigma_1$ for a one-side tapered plate, $t_1/t=0.1$ , $M/Pt=5$ and $\partial M/\partial x > 0$ .....	96
22.	Distribution of $\sigma_3$ for a one-side tapered plate, $t_1/t=0.1$ , $M/Pt=5$ and $\partial M/\partial x > 0$ .....	96
23.	Distribution of $\sigma_5$ for a one-side tapered plate, $t_1/t=0.1$ , $M/Pt=5$ and $\partial M/\partial x > 0$ .....	97
24.	Three-point bending test.....	97
25.	Delamination failure in the midplane.....	98
26.	Delamination failure in the tapered surface.....	98
27.	SEM photograph of delamination fracture surface.....	99
28.	SEM photograph of detail of delamination fracture surface.....	99
29.	Photograph showing a mixed compression-interlaminar normal failure mode.....	100
30.	SEM photograph of mixed mode fracture surface.....	101
31.	SEM image of top of mixed failure mode surface. Crushing due to a compressive interlaminar stress is detected.....	101
32.	SEM photograph of the upper part of the mixed failure mode surface.....	101

33.	SEM photograph of the center part of the mixed failure mode surface.....	102
34.	SEM image of the inner part of the mixed failure mode surface..	102
35.	SEM image of the bottom of the mixed failure mode surface.....	103
36.	Photograph showing specimen OLCP_7001.....	103
37.	Measurements of specimen OLCP_7001.....	104
38.	Photograph showing detail of tapering of specimen OLCP_7001.	104
39.	Image of failure in specimen OLCP_7001.....	105
40.	Representation of specimen OLCP_7001 and position of gauges..	105
41.	Photograph showing specimen OLCP_7002.....	106
42.	Measurements of specimen OLCP_7002 in inches (meters).....	106
43.	Image of failure in specimen OLCP_7002.....	107
44.	Representation of specimen OLCP_7002 and position of gauges..	107
45.	Photograph showing specimen OLCP_7003.....	108
46.	Measurements of specimen OLCP_7003 in inches (meters).....	108
47.	Image of failure in specimen OLCP_7003.....	109
48.	Representation of specimen OLCP_7003 and position of gauges..	109
49.	Representation of sections AA and BB.....	110
50.	Distribution of $\epsilon_5$ through the thickness in section AA.....	110
51.	Distribution of $\epsilon_5$ through the thickness in section BB.....	110
52.	Description of structure used to compare both 2-D plane strain model and shear deformation plate model.....	111

53.	Distribution of $\sigma_1$ through the thickness from a 2-D plane strain model and a shear deformation plate model.....	111
54.	Distribution of $\sigma_5$ through the thickness from a 2-D plane strain model and a shear deformation plate model.....	112
55.	Variation of interlaminar normal modulus in function of $m$ and $n$ in a laminate T300/N5208 $[90m/0n]_s$ .....	112
56.	Variation of interlaminar shear modulus in function of $\phi$ in a laminate T300/N5208 $[+\phi/-\phi]_s$ .....	113
57.	Definition of coordinates axis and key to colors for one-dimensional plates.....	113
58.	Representation of optimal thin one-dimensional plates subjected to a uniform distributed transverse load.....	114
59.	Representation of optimal thick one-dimensional plates subjected to a uniform distributed transverse load.....	114
60.	Representation of optimal one-dimensional sandwich panels subjected to a uniform distributed transverse load.....	115
61.	Representation of optimal thin one-dimensional plates subjected to a point transverse load.....	115
62.	Representation of optimal thick one-dimensional plates subjected to a point transverse load.....	116
63.	Representation of optimal one-dimensional sandwich panels subjected to a point transverse load.....	116
64.	Definition of a coordinate axis and key to colors for two-dimensional plates subjected to a transverse load.....	117
65.	Weight saving and normalized deflection for a thin, simply supported plate subjected to a uniform distributed transverse load.....	117

66.	Representation of an optimal thin, simply supported plate subjected to a uniform distributed transverse load for aspect ratios between 1 and 1.75.....	118
67.	Representation of an optimal thin, simply supported plate subjected to a uniform distributed transverse load for aspect ratios between 1.75 and 2.25.....	118
68.	Representation of an optimal thin, simply supported plate subjected to a uniform distributed transverse load for aspect ratios between 2.25 and 3.5.....	119
69.	Representation of an optimal thin, simply supported plate subjected to a uniform distributed transverse load for aspect ratios higher than 3.5.....	119
70.	Weight saving and normalized deflection for a thin, clamped plate subjected to a uniform distributed transverse load.....	120
71.	Representation of an optimal thin, clamped plate subjected to a uniform distributed transverse load for aspect ratios between 1 and 1.5.....	120
72.	Representation of an optimal thin, clamped plate subjected to a uniform distributed transverse load for aspect ratios between 1.5 and 4.4.....	121
73.	Representation of an optimal thin, clamped plate subjected to a uniform distributed transverse load for aspect ratios between 1.5 and 4.4.....	121
74.	Weight saving and normalized deflection for a thick, simply supported plate subjected to a uniform distributed transverse load.....	122
75.	Representation of an optimal thick, simply supported plate subjected to a uniform distributed transverse load plates for aspect ratios between 1 and 3.5.....	122
76.	Representation of an optimal thick, simply supported plate subjected to a uniform distributed transverse load for aspect ratios higher than 3.5.....	123

77.	Weight saving and normalized deflection for a thick, clamped plate subjected to a uniform distributed transverse load.....	123
78.	Representation of an optimal thick, clamped plate subjected to a uniform distributed transverse load for aspect ratios between 1 and 3.5.....	124
79.	Representation of an optimal thick, clamped plate subjected to a uniform distributed transverse load for aspect ratios higher than 3.5.....	124
80.	Weight saving and normalized deflection for a simply supported sandwich panel subjected to a uniform distributed transverse load.....	125
81.	Representation of an optimal simply supported sandwich panel subjected to a uniform distributed transverse load for aspect ratios between 1 and 1.5.....	125
82.	Representation of an optimal simply supported sandwich panel subjected to a uniform distributed transverse load for aspect ratios higher than 1.5.....	126
83.	Weight saving and normalized deflection for a clamped sandwich panel subjected to a uniform distributed transverse load.....	126
84.	Representation of an optimal clamped sandwich panel subjected to a uniform distributed transverse load for aspect ratios between 1 and 1.5.....	127
85.	Representation of an optimal clamped sandwich panel subjected to a uniform distributed transverse load for aspect ratios between 1.5 and 2.5.....	127
86.	Representation of an optimal clamped sandwich panel subjected to a uniform distributed transverse load for aspect ratios higher than 2.5.....	128
87.	Weight saving for a thin, simply supported plate subjected to a point transverse load.....	128

88.	Representation of an optimal thin, simply supported plate subjected to a point transverse load for aspect ratios between 1 and 2.....	129
89.	Representation of an optimal thin, simply supported plate subjected to a point transverse load for aspect ratios between 2 and 5.....	129
90.	Representation of an optimal thin, simply supported plate subjected to a point transverse load for aspect ratios higher than 5.....	130
91.	Weight saving for a thin, clamped plate subjected to a point transverse load.....	130
92.	Representation of an optimal thin, clamped plate subjected to a point transverse load for aspect ratios between 1 and 1.5.....	131
93.	Representation of an optimal thin, clamped plate subjected to a point transverse load for aspect ratios between 1.5 and 5.....	131
94.	Representation of an optimal thin, clamped plate subjected to a point transverse load for aspect ratios higher than 5.....	132
95.	Weight saving for a thick, simply supported plate subjected to a point transverse load.....	132
96.	Representation of an optimal thick, simply supported plate subjected to a point transverse load for aspect ratios between 1 and 2.25.....	133
97.	Representation of an optimal thick, simply supported plate subjected to a point transverse load for aspect ratios higher than 2.25.....	133
98.	Weight saving for a thick, clamped plate subjected to a point transverse load.....	134
99.	Representation of an optimal thick, clamped plate subjected to a point transverse load for aspect ratios between 1 and 2.5.....	134
100.	Representation of an optimal thick, clamped plate subjected to a point transverse load for aspect ratios between 2.5 and 5.....	135



101.	Representation of an optimal thick, clamped plate subject to a point transverse load for aspect ratios higher than 5.....	135
102.	Weight saving for a simply supported sandwich panel subjected to a point transverse load.....	136
103.	Representation of an optimal simply supported sandwich panel subjected to a point transverse load for aspect ratios between 1 and 2.....	136
104.	Representation of an optimal simply supported sandwich panel subjected to a point transverse load for aspect ratios between 2 and 5.....	137
105.	Representation of an optimal simply supported sandwich panel subjected to a point transverse load for aspect ratios higher than 5.....	137
106.	Weight saving for a clamped sandwich panel subjected to a point transverse load.....	138
107.	Representation of an optimal clamped sandwich panel subjected to a point transverse load for aspect ratios between 1 and 1.5.....	138
108.	Representation of an optimal clamped sandwich panel subjected to a point transverse load for aspect ratios between 1.5 and 5.....	139
109.	Representation of an optimal clamped sandwich panel subjected to a point transverse load for aspect ratios higher than 5.....	139
110.	Definition of coordinate axis for one-dimensional plates subjected to a uniform uniaxial compression load.....	140
111.	Critical load and optimum angle for an one-dimensional simply supported plate.....	140
112.	Comparison between critical loads of optimum configuration and quasi-isotropic laminate (one-dimensional simply supported plates).....	141

113.	Weight saving for different cross sections whose height is twice the laminate thickness (one-dimensional simply supported plates).....	141
114.	Weight saving for different cross sections whose height is ten times the laminate thickness (one-dimensional simply supported plates).....	142
115.	Critical load and optimum angle for an one-dimensional clamped plate.....	142
116.	Comparison between critical loads of optimum configuration and quasi-isotropic laminate (one-dimensional clamped plates).....	143
117.	Weight saving for different cross sections whose height is twice the laminate thickness (one-dimensional clamped plates).....	143
118.	Weight saving for different cross sections whose height is ten times the laminate thickness (one-dimensional simply supported plates).....	144
119.	Critical load and optimum angle for an one-dimensional cantilever plate.....	144
120.	Comparison between critical loads of optimum configuration and quasi-isotropic laminate (cantilever simply supported plates).....	145
121.	Weight saving for different cross sections whose height is twice the laminate thickness (one-dimensional cantilever plates).....	145
122.	Weight saving for different cross sections whose height is ten times the laminate thickness (one-dimensional simply supported plates).....	146
123.	Definition of coordinate axis for two-dimensional plates subjected to uniform uniaxial compression, biaxial compression, shear or combined load.....	146
124.	Critical load and optimum angle for a simply supported plate subjected to a uniform uniaxial compression load.....	147

125.	Comparison between critical loads of optimum configuration and quasi-isotropic laminate (simply supported plates subjected to a uniform uniaxial compression load).....	147
126.	Comparison of critical loads for cross-ply and quasi-isotropic laminate for a square plate (simply supported plates subjected to as uniform uniaxial compression load).....	148
127.	Comparison between weights of aluminium and the optimum configuration of T300/N5208 (simply supported plates subjected to a uniform uniaxial compression load).....	148
128.	Critical load and optimum angle for a simply supported plate subjected to a uniform biaxial compression load ( $N_y=N_x/2$ ).....	149
129.	Comparison between critical loads of optimum configuration and quasi-isotropic laminate (simply supported plates subjected to a uniform biaxial compression load ( $N_y=N_x/2$ )).....	149
130.	Comparison of critical loads for cross-ply and quasi-isotropic laminate for a square plate (simply supported plates subjected to a uniform biaxial compression load ( $N_y=N_x/2$ )).....	150
131.	Comparison between weights of aluminium and the optimum configuration of T300/N5208 (simply supported plates subjected to a uniform biaxial compression load ( $N_y=N_x/2$ )).....	150
132.	Critical load and optimum angle for a simply supported plate subjected to a uniform biaxial compression load ( $N_y=N_x$ ).....	151
133.	Comparison between critical loads of optimum configuration and quasi-isotropic laminate (simply supported plates subjected to a uniform biaxial compression load ( $N_y=N_x$ )).....	151
134.	Comparison of critical loads for cross-ply and quasi-isotropic laminate for a square plate (simply supported plates subjected to a uniform biaxial compression load ( $N_y=N_x$ )).....	152
135.	Comparison between weights of aluminium and the optimum configuration of T300/N5208 (simply supported plates subjected to a uniform biaxial compression load ( $N_y=N_x$ )).....	152

136.	Critical load and optimum angle for a simply supported plate subjected to a uniform biaxial compression load ( $N_y=2*N_x$ ).....	153
137.	Comparison between critical loads of optimum configuration and quasi-isotropic laminate (simply supported plates subjected to a uniform biaxial compression load ( $N_y=2*N_x$ )).....	153
138.	Comparison of critical loads for cross-ply and quasi-isotropic laminate for a square plate (simply supported plates subjected to a uniform biaxial compression load ( $N_y=2*N_x$ )).....	154
139.	Comparison between weights of aluminium and the optimum configuration of T300/N5208 (simply supported plates subjected to a uniform biaxial compression load ( $N_y=2*N_x$ )).....	154
140.	Critical load and optimum angle for a clamped plate subjected to a uniform uniaxial compression load.....	155
141.	Comparison between critical loads of optimum configuration and quasi-isotropic laminate (clamped plates subjected to a uniform uniaxial compression load).....	155
142.	Comparison of critical loads for cross-ply and quasi-isotropic laminate for a square plate (clamped plates subjected to a uniform uniaxial compression load).....	156
143.	Comparison between weights of aluminium and the optimum configuration of T300/N5208 (clamped plates subjected to a uniform uniaxial compression load).....	156
144.	Critical load and optimum angle for a clamped plate subjected to a uniform biaxial compression load ( $N_y=N_x/2$ ).....	157
145.	Comparison between critical loads of optimum configuration and quasi-isotropic laminate (clamped plates subjected to a uniform biaxial compression load ( $N_y=N_x/2$ )).....	157
146.	Comparison of critical loads for cross-ply and quasi-isotropic laminate for a square plate (clamped plates subjected to a uniform biaxial compression load ( $N_y=N_x/2$ )).....	158

147.	Comparison between weights of aluminium and the optimum configuration of T300/N5208 (clamped plates subjected to a uniform biaxial compression load ( $N_y=N_x/2$ )).....	158
148.	Critical load and optimum angle for a clamped plate subjected to a uniform biaxial compression load ( $N_y=N_x$ ).....	159
149.	Comparison between critical loads of optimum configuration and quasi-isotropic laminate (clamped plates subjected to a uniform biaxial compression load ( $N_y=N_x$ )).....	159
150.	Comparison of critical loads for cross-ply and quasi-isotropic laminate for a square plate (clamped plates subjected to a uniform biaxial compression load ( $N_y=N_x$ )).....	160
151.	Comparison between weights of aluminium and the optimum configuration of T300/N5208 (clamped plates subjected to a uniform biaxial compression load ( $N_y=N_x$ )).....	160
152.	Critical load and optimum angle for a clamped plate subjected to a uniform biaxial compression load ( $N_y=2*N_x$ ).....	161
153.	Comparison between critical loads of optimum configuration and quasi-isotropic laminate (clamped plates subjected to a uniform biaxial compression load ( $N_y=2*N_x$ )).....	161
154.	Comparison of critical loads for cross-ply and quasi-isotropic laminate for a square plate (clamped plates subjected to a uniform biaxial compression load ( $N_y=2*N_x$ )).....	162
155.	Comparison between weights of aluminium and the optimum configuration of T300/N5208 (clamped plates subjected to a uniform biaxial compression load ( $N_y=2*N_x$ )).....	162
156.	Critical load and optimum angle for a simply supported plate subjected to a uniform shear load.....	163
157.	Comparison between critical loads of optimum configuration and quasi-isotropic laminate (simply supported plates subjected to a uniform shear load).....	163

158.	Comparison of critical loads for cross-ply and quasi-isotropic laminate for a square plate (simply supported plates subjected to a uniform shear load).....	164
159.	Comparison between weights of aluminium and the optimum configuration of T300/N5208 (simply supported plates subjected to a uniform shear load).....	164
160.	Critical load and optimum angle for a clamped plate subjected to a uniform shear load.....	165
161.	Comparison between critical loads of optimum configuration and quasi-isotropic laminate (clamped plates subjected to a uniform shear load).....	165
162.	Comparison of critical loads for cross-ply and quasi-isotropic laminate for a square plate (clamped plates subjected to a uniform shear load).....	166
163.	Comparison between weights of aluminium and the optimum configuration of T300/N5208 (clamped plates subjected to a uniform shear load).....	166
164.	Buckling parameters for simply supported plates subjected to a combined uniform uniaxial compression and shear.....	167
165.	Buckling parameters for clamped plates subjected to a combined uniform uniaxial compression and shear.....	167

## LIST OF TABLES

<u>No.</u>		<u>Page</u>
1.	Coordinates x and z of strain guages.....	35
2.	Longitudinal strains in specimen OLCP_7001.....	36
3.	Interlaminar shear strains in specimen OLCP_7001.....	36
4.	Maximum vertical displacement in specimen OLCP_7001.....	37
5.	Longitudinal strains in specimen OLCP_7002.....	38
6.	Interlaminar shear strains in specimen OLCP_7002.....	38
7.	Maximum vertical displacement in specimen OLCP_7002.....	39
8.	Longitudinal strains in specimen OLCP_7003.....	39
9.	Interlaminar shear strains in specimen OLCP_7003.....	40
10.	Maximum vertical displacement in specimen OLCP_7003.....	40
11.	Longitudinal strains in specimens OLCP_7001, OLCP_7002 and OLCP_7003.....	41
12.	Interlaminar shear strains in specimens OLCP_7001, OLCP_7002 and OLCP_7003.....	41
13.	Maximum vertical displacement in specimens OLCP_7001, OLCP_7002 and OLCP_7003.....	42

## 1. INTRODUCTION

Composite materials have been increasingly used during the last decades, in order to lighten structures in fields like aeronautics and space. Two steps are essential in the process of taking advantage of this kind of materials: design and optimization.

Optimization of composite structures is a recent issue, because both optimization techniques and composite structures have been developed during the last few decades and therefore, the conjunction of both of them is even more recent. Composite materials being an expensive but efficient technology to get minimum weight structures, it is logical to make an attempt to find out how to design properly optimum laminated composite plates with no reduction in their strength. A general scheme is depicted in Figure 1.

Since many kinds of ground and air vehicles have rectangular plates as a common structural element, an increasing demand for improved structural efficiency in such applications has resulted. Composite materials offer a number of advantages other than their high stiffness to density values: for example, their capability of being tailored by orientation of the filaments in the various layers in order to optimize the desired structural behavior.

Actually, although there is a lot of literature related to plate analysis, the most modern references lack adequate information which could allow a designer to tailor or synthesize an optimal design. The reason for that can be found in two aspects: first, the difficulty of accurately assessing the level of strains and stresses in any point of a laminated composite plate and, secondly, the need of implementing an optimization procedure able to find the minimum weight structure.

Fortunately, the current development of numerical techniques and the existence of powerful computers make possible a solution to the two problems mentioned above.



The interest of the optimization of laminated composite plates is focussed on three different fields: in-plane loads, transverse loads, and buckling. It is noticeable by reviewing the literature, that the problem dealing with in-plane loads has already been studied, and a number of technical publications and software packages can be found.

In the present report, an optimization of rectangular laminated composite plates subjected to transverse loads and buckling is carried out. Plates (both thin and thick) and sandwich panels, subjected to uniformly distributed and point loads, are analyzed in the chapter about transverse loads, considering clamped and simply supported as boundary conditions. Uniform uni-, bi-axial compression, shear, and combined loads are also studied in the section devoted to buckling.

## 1.1 LITERATURE REVIEW

### *Optimization procedures applied to laminated composite plates*

The earliest attempt in composite optimization seems to be due to Foye [1], who studied the minimum weight optimum design of laminated for strength and membrane stiffness. Multiple in-plane loading conditions were considered, and a random search method was used to find ply orientation angles, such that the strength and stiffness requirement would be satisfied with the smallest number of plies. Another procedure for the optimum design of laminates was reported by Waddoups [2]. Minimum weight designs are obtained by considering strength constraints under multiple distinct loading conditions. Either the Tsai-Hill or the maximum strain criterion may be used, and all laminae are assumed to behave linearly to failure.

Waddoups and co-workers [3] reported a structural synthesis capability for a class of anisotropic plate structures. The basic concepts of structural synthesis were developed by Schmit and his associates [4,5]. This technique

was successfully applied to the optimum design of integrally stiffened cylindrical shells by Kicher [6] and Morrow-Kicher [7]. The most general problem dealing with this method was formulated by Waddoups and his workers [3] and involves 21 design variables, 45 distinct failure modes, and 3 independent loading conditions. Kicher and Chao [8] reported the development of a structural optimization capability for stiffened fiber-composite cylinders. Multiple load conditions were considered and strength, as well as buckling failure modes, were guarded against. The design variables include stiffener dimensions and spacing, fiber volume content, and ply orientation angles. In these last two references, [3] and [8], the optimization problem is cast in mathematical programming form and then a SUMT-type method, based on the Fiacco-McCormick interior penalty function and the Davidson-Fletcher-Powell algorithm for unconstrained minimization, is employed to obtain numerical results. Verette [9] extended the laminate optimization procedure reported by Waddoups [2].

Morz [10] tried to obtain the optimal reinforcement using strength as a design criterion. Bryzgalin [11] and Love and Melchers [12] used a stiffness criterion to get an optimal design of constant thickness composites. Lai and Abenbach [13] used a direct search procedure to obtain an optional design for minimum tensile stress at the interface in a layered structure subjected to time harmonic and transient loads.

Khot [14] suggested an efficient optimization technique based on strain energy distribution and a numerical search for the minimum weight design of structures. The procedure takes into account multiple loading conditions and displacement constraints on the structure. Schmit and Farshi [15,16] presented a method for minimum weight design of symmetric composite laminates subjected to multiple in-plane loading conditions. Hayashi [17] optimized the fiber volume fractions for columns and orientation angle for plates and cylinders for corresponding buckling strength.

Chao and others [18] determined the optimum fiber orientation for a symmetric orthotropic composite laminate with in-plane loading. The fiber orientation of each ply is treated as a design variable. Hayashi [19] and Bert

[20] performed a similar analysis. Housner and Stein [21] calculated the optimum fiber direction of graphite-epoxy sandwich panels under axial compression, assuming that the angle of all the plies was the same. Hirano [22] optimized the buckling load of laminated plates under uniaxial and biaxial compression.

Bert [23] presented a technique for obtaining the optimal laminate design for a thin plate which consisted of multiple layers of equal thickness composite laminae, the design criterion being maximization of fundamental frequency. By means of this technique, Bert [24] analyzed clamped composite-materials plates, Adali [25] reported the design of shear-deformable antisymmetric angle-ply laminates, and Pedersen [26,27] studied the sensitivity analysis and optimal design for laminates.

Joshi and Iyengar [28] studied the minimum weight design of composite plates subjected to in-plane and transverse loads treating fiber orientation and thickness of plies as design variables. Soni and Iyengar [29] reported their studies on optimum design of clamped laminated plates. In a design paper Joshi and Iyengar [30] presented their studies on optimum design under in-plane loads with multiple design variables.

Khot [31] presented a computer program (OPTCOMP) for analyzing composite structures subjected to in-plane and transverse loads. The recurrence relations used are remarkable, but this technique does not account for interlaminar stresses. McKeown [32], Starnes and Haftka [33], and Schmit and Mehrinfar [34] reported studies on structural synthesis systems dealing with optimization of composite structures, but the design flexibility is limited. Sobieszczanski-Sobiesky [35] described a design system, but he did not fully consider the interaction of all the design variables.

Park [36] analyzed the optimal design of simple symmetric laminates under the first ply failure criterion. Donaldson [37] reported simplified weight-saving techniques for composite panels. Wurzel [38] studied optimal design of bidirectional composites.

Massard [39] reported a computer sizing study dealing with optimization of composite laminates subjected to in-plane loads. Maksimovic [40] developed a procedure for obtaining near-minimum weight design of large composite structures subjected to statically applied loads by means of the method of inscribed hyperspheres. Tsai [41] described a computer program (LAMRANK) to optimize and rank composite laminates subjected to in-plane loads. Watkins and Morris [42] presented a multicriteria objective function optimization scheme, with application to laminated plates subjected to in-plane and transverse loads.

Iyengar [43] obtained an optimum weight design of hybrids laminates of fiber-reinforced composites made of boron/epoxy and aramid/epoxy. Pedersen [44] studied how an orthotropic material must be oriented in order to obtain extreme energy density.

A thorough study of buckling problems for laminated composite plates was presented by Leissa [45]. Muc [46] obtained three types of optimal angle in closed analytical form for laminated rectangular plates under uniaxial and biaxial compression. These directions are functions of the material properties, the geometrical properties and the type of buckling mode.

After reviewing the literature related to optimization of composite plates, it is noticeable that laminated composite plates under in-plane loads can be optimized by following the papers described above. There is no difficulty in any case, and commercial software, from personal computers to macro-systems, is available.

In the chapter about laminated composite plates subjected to transverse loads, none of the papers mentioned above considered interlaminar stresses, and there are no solutions available in the literature for different aspect ratios, boundary conditions, and types of loading. Owing to the complexity of the problem, laminated composite plates subjected to transverse loads were analyzed by means of the Reissner-Stavsky theory [47] and therefore, interlaminar stresses were neglected.

Though thousands of papers dealing with buckling of plates have been written up to now, there is no publication related to the optima solutions to different problems dealing with one-dimensional and two-dimensional laminated composite plates.

### *The finite element method applied to laminated composite plates*

In the process of optimizing a composite structure, not only an optimization procedure is needed, but a finite element formulation is also required. The following paragraphs describe a brief review about the finite element formulation applied to laminated composite plates.

The classical lamination theory based on the Kirchhoff [48] hypothesis was the first attempt in the development of laminated plate theory. This theory is not computationally efficient from the simple finite element formulation point of view [49] neither is it suitable for composite structures analysis, owing to its simplifying assumptions, the most important of which are the neglect of the transverse shear deformations, and the transverse normal stresses.

Reissner [50] and Mindlin [51] were the first to provide first-order shear deformable theories based on the thin plate assumptions for variation of stresses and displacements through the thickness of the plate, respectively. Studies of low order elements i.e., 3-noded triangles, 4-noded and 8-noded quadrilaterals showed violent stress oscillations. Some techniques, such as reduced and selective integrations [52-55], modified shear strain methods [56], and hybrid and mixed methods [57], succeeded in generating efficient elements. But, even so, these numerical analysis have certain limitations: the transverse shearing strains are assumed constant through the plate thickness, and a fictitious shear correction coefficient is introduced.

Lo, Christensen and Wu [58-59], and Reissner [60] presented a theory for plates based on an assumed higher order displacement field. Kant, Owen, and Zienkiewicz [61] presented, for the first time, a  $C^0$  plate bending finite

element formulation of a higher order theory. This element is a 9-noded Lagrange quadrilateral and has six degrees of freedom per node. Reddy [62] presented a higher order shear theory in which in-plane displacements are expanded as cubic functions of the thickness coordinate, while the transverse deflection is kept only a function of  $x$  and  $y$ .

Recently, Pandya and Kant [63] presented a refined higher order  $C^0$  plate bending element in which the transverse deflection is expressed as a quadratic function of the thickness. This element is a 9-noded Lagrange quadrilateral. Lakshminarayana and Ramani [64] studied some shear flexible triangular laminated composite plate finite elements. Prathap and Somashekar [65] studied a 8-noded laminated anisotropic finite element. Tessler [66] analyzed a higher order theory in which the transverse deflection is expressed as a quadratic function of the thickness. Miravete [67] presented a finite element formulation applied to three-dimensional laminated composite plates, based on [62] and the penalty function method [68].

A more detailed description of the finite element formulations mentioned above can be found in [69].

In this report some finite elements have been used, the formulation varying in function on the type of problem to solve.

## 1.2 PROJECT SUMMARY

In this work, an attempt is made to optimize rectangular laminated composite plates. Laminate thickness and fiber orientation are treated as design variables. Since optimization of composite plates subjected to in-plane loads has already been reported, the present study is focussed on transverse loads and buckling.

In Section 2 the symbols and the notation used in this report are described. Basically, this reports follows the notation introduced by Tsai and Hahn [71]

in those sections related to design of composites, the symbology and notation used by Khot [31] in those chapters dealing with optimization, and finally, the notation introduced by Zienkiewicz [68], in the paragraphs devoted to the finite element method.

Optimization of laminated composite plates subjected to transverse loads is treated in Section 3. First, the equations of the analysis are formulated. Since strength has been the design criterion, a failure criterion must be chosen. Next, recurrence relations dealing with the optimization procedure are described.

Once the analytical formulation has been reported, the variable thickness problem is analyzed by means of a 2-D model. Through-thickness stress distributions are determined for different cases, and the influence of geometric parameters and the applied load on the strength of the plate is also analyzed. The failure mechanisms reported on experimental testings are described next. Finally, verification of the theoretical model by means of a number of experimental testings is carried out.

The final part of the chapter, related to optimization of laminated composite plates subjected to transverse loads, is devoted to describe the numerical results. The 6-component stress tensor is accounted for. Normal and shear interlaminar effects are present in the analysis and, therefore, elastic constants and strengths must be determined. Optima configurations of variable-thicknesses and angles of orientation of fibers are presented for one- and two-dimensional plates. Weight savings are also reported.

Section 4 deals with the optimization of laminated composite plates subjected to buckling. First, the analytical formulation is described. Numerical results are presented for uniform uniaxial compressive loads (one-dimensional plates) and uniform uniaxial, biaxial compressive, shear, and combined loads (two-dimensional plates). The optimization criterion used has been the critical compressive force.

Concluding remarks are outlined in Section 5.

## 2. SYMBOLS AND NOTATION

$a$	Length of the plate; or nodal displacement vector.
$a'$	Relative nodal displacement.
$a^e$	Nodal displacement vector of the finite element $e$ .
$B$	Geometric matrix used in the finite element method; $B = L N$ .
$b$	Width of the plate.
$C_{ij}$	Stiffness matrix in the generalized Hooke's law; in concentrated notation, $i, j=1,2,3,4,5,6$ .
$c$	Strain-displacement matrix, or core thickness in a sandwich panel.
$D$	Matrix of elastic constants.
$e_{ij}$	Strain energy of the $j$ th layer of the element $i$ .
$\tilde{e}_{ij}$	Strain energy density of the $j$ th layer of the element $i$ .
$\tilde{e}'_{ij}$	Strain energy density of the $j$ th layer of the element $i$ .
$e'_{ij}$	Relative strain energy of the $j$ th layer of the element $i$ .
$F_{ij}, F_i$	Strength parameters in stress formulation of the quadratic failure criterion.
$f^e$	Nodal forces in the finite element $e$ .
$K$	Stiffness matrix of the whole plate.



$K'$	Relative stiffness matrix of the whole plate.
$K_B$	Stiffness matrix of the whole plate due to bending stresses.
$K_s$	Geometric matrix of the whole plate.
$k^e$	Elemental stiffness matrix .
$l$	Diagonal of a plate.
$l_i$	Surface area of the element $i$ .
$M$	Applied bending moment.
$N$	Shape function matrix.
$N_x$	Applied compressive force in x-direction per unit width.
$N_x \text{ cr}$	Critical compressive force in x-direction per unit width.
$N_y$	Applied compressive force in y-direction per unit width.
$N_y \text{ cr}$	Critical compressive force in y-direction per unit width.
$N_{xy}$	Applied compressive force in xy- or 12-plane per unit width.
$N_{xy \text{ cr}}$	Critical compressive force in xy- or 12-plane per unit width.
$P$	Applied transverse load.
$Q$	Reduced stiffness matrix for plane stress.
$q^e$	Distributed forces in the finite element $e$ .
$Q_{yy}$	Term of the reduced matrix for plane stress. $Q_{yy} = E_y / (1 - \nu_{12}\nu_{21})$ .
$r$	Strength/stress ratio or strength ratio.
$S$	Positive pure shear strength in the xy- or 12-plane of a ply.

$S'$	Negative pure shear strength in the xy- or 12-plane of a ply.
$t$	Total laminate thickness.
$t_1$	Difference between the total laminate thickness( $t$ ) and the minor thickness of a tapered plate.
$t_{ij}$	Thickness of the $j$ th layer of the $i$ th element.
$u$	Deflection in the x-direction.
$V$	Strain energy of a single plate element subjected to in-plane stresses.
$V_B$	Strain energy of a single plate element due to plate bending.
$V_e$	Volume of the finite element $e$ .
$V_{ij}$	Volume of the $j$ th layer of the $i$ th element.
$V_s$	Strain energy of a single plate element due to in-plane stresses.
$v$	Deflection in the y-direction.
$w$	Deflection in the z-direction.
$X$	Uniaxial tensile strength of a ply along the x-axis.
$X'$	Uniaxial compressive strength of a ply along the x-axis.
$Y$	Uniaxial tensile strength of a ply along the y-axis.
$Y'$	Uniaxial compressive strength of a ply along the y-axis.
$Z$	Uniaxial tensile strength of a ply along the z-axis.
$Z'$	Uniaxial compressive strength of a ply along the z-axis.
$\alpha_{ij}$	Thickness of the $j$ th layer of the $i$ th element normalized to maximum thickness.

$\delta \epsilon$	Strain generated by a virtual displacement.
$\delta u$	Displacement generated by a virtual displacement.
$\delta e$	Vector of nodal deflections.
$\delta a^e$	Virtual displacements in the finite element $e$ .
$\epsilon_i$	Strain component.
$\epsilon'_i$	Relative strain component.
$\epsilon_o$	Initial strains.
$\theta$	Angle between x-axis and fiber or principal axis of layer.
$\Lambda$	Scaling parameter.
$\lambda$	Lagrangian parameter; or coefficient used to formulate a eigenvalue problem.
$v$	Number of cycle of iteration.
$\phi$	Angle of variation of thickness.
$\rho_{ij}$	Mass density of the $j$ th layer of the $i$ th element.
$\sigma_i$	Stress component.
$\sigma'_i$	Relative stress component.
$\sigma_o$	Initial stresses.



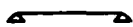
One-dimensional thin plate.



One-dimensional thick plate.



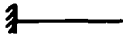
One-dimensional sandwich plate.



One-dimensional simply supported plate.



One-dimensional clamped plate.



One-dimensional cantilever plate.



Two-dimensional thin plate.



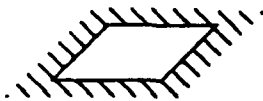
Two-dimensional thick plate.



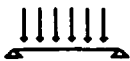
Two-dimensional sandwich plate.



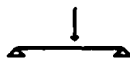
Two-dimensional simply supported plate.



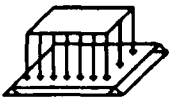
Two-dimensional clamped plate.



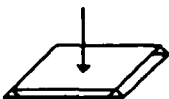
One-dimensional plate subjected to a uniform transverse load.



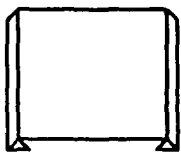
One-dimensional plate subjected to a point transverse load.



Two-dimensional plate subjected to a uniform transverse load.



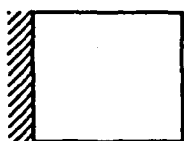
Two-dimensional plate subjected to a point transverse load.



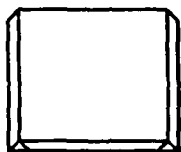
One-dimensional simply supported plate.



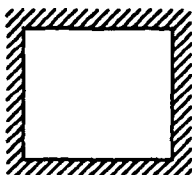
One-dimensional clamped plate.



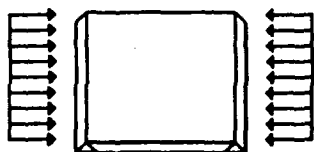
One-dimensional cantilever plate.



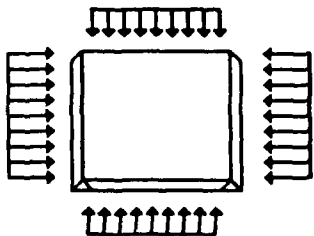
Two-dimensional simply supported plate.



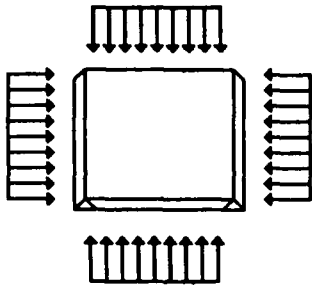
Two-dimensional simply supported plate.



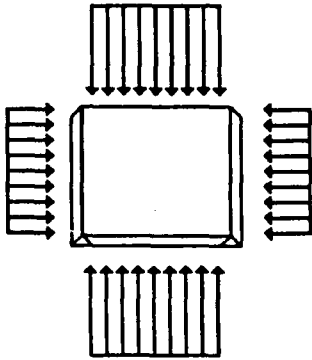
Two-dimensional plate subjected to a uniaxial uniform compression load.



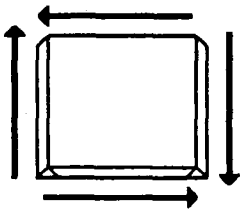
Two-dimensional plate subjected to a biaxial uniform compression load ( $N_y = N_x/2$ ).



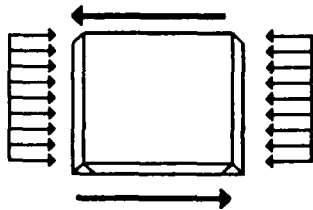
Two-dimensional plate subjected to a biaxial uniform compression load ( $N_y = N_x$ ).



Two-dimensional plate subjected to a biaxial uniform compression load ( $N_y = N_x * 2$ ).



Two-dimensional plate subjected to a uniform in-plane shear load .



Two-dimensional plate subjected to a uniaxial uniform compression and in-plane shear load .

### **3. OPTIMIZATION OF LAMINATED COMPOSITE PLATES SUBJECTED TO TRANSVERSE LOADS**

This section deals with transverse loads. The study of the optimization of laminated composite plates subjected to this type of load is extremely complex.

On the one hand, the whole stress tensor must be considered: the three in-plane stress components are present owing to the bending effects, and so are the two interlaminar shear stress components, owing to the shear effects. Finally, the interlaminar normal stress component must also be considered because of the variable thickness, as equilibrium equations predict.

On the other hand, the minimum weight plate must be found. Therefore, accuracy and efficiency should be combined in order to analyze the structure properly and then, to solve the optimization problem by means of an iterative procedure.

Thus, first of all, the analytical formulation is exposed. General procedures for analyzing the structure, predicting the laminate failure, and optimizing the laminate composite plate are described.

Secondly, the variable thickness problem is analyzed. The behavior of a bidimensional plate with variable thickness is extremely difficult to understand, because it is a 3-D problem, and because bending, shear, and variable thickness effects appear simultaneously. Therefore, a one-dimensional plate with variable thickness is studied here by means of a 2-D plane strain finite element model.

Finally, once the failure mechanisms are identified, and the 2-D plane strain model has been verified by means of an experimental study, a number of results are presented.

One-dimensional laminated composite plates are studied by applying the 2-D plane strain model mentioned above. Optima configurations and weight savings are reported for different kinds of plates, types of loading, and boundary conditions.

Two-dimensional laminated composite plates are also analyzed. Since the 2-D plane strain model can only be used for the one-dimensional case, a more general model based on a higher order shear theory is used. This method is efficient and accurate, not only because the analysis is carried out very fast, but also because the required number of nodes of the mesh is not large, and the results from the shear deformation theory used here and the 2-D plane strain model are very close.

### 3.1 ANALYTICAL FORMULATION

The formulation used here deals with the following three aspects :

- Analysis of the plate. The aim is to get strains and stresses in any point of the plate.
- Failure criterion. Once the stress tensor is known, a failure criterion is needed in order to know the relationship between the stress tensor and the strength/stress ratio.
- Optimization procedure. The objective is to find the minimum weight plate, using strength as a design criterion.

#### *3.1.1 Equations of analysis*



The analysis of the structure has been carried out by means of the finite element method. By means of this technique, strains and stresses can be obtained in any point of the plate.

With the finite element method, the interior of the plate is idealized as an assembly of discrete elements over which the unknown displacements are represented approximately by linear, quadratic, etc., variations. Thus, the governing equation of internal equilibrium is satisfied approximately.

Let  $\delta a^e$  be a virtual displacement of the nodes. This displacement generates the following displacements inside the finite element:

$$\delta u = N \delta a^e \quad (3.1)$$

and the following strains inside the finite element:

$$\delta \epsilon = B \delta a^e \quad (3.2)$$

The work done by the node forces is equal to the addition of the products of each component of force by the corresponding displacement:

$$\delta a^{eT} q^e \quad (3.3)$$

Analogously, the internal work-normalized to volume-done by distributed stresses and forces is

$$\delta \epsilon^T \sigma - \delta u^T \quad (3.4)$$

or

$$\delta a^T (B^T \sigma - N^T b) \quad (3.5)$$

The external work must be equal to the internal work integrated on the elemental volume. Therefore,

$$\delta a^e T q^e = \delta a^e T \left( \int_v B^T \sigma dv - \int_v N^T b dv \right) \quad (3.6)$$

This expression is valid for any virtual displacement. Thus,

$$q^e = \int_v B^T \sigma dv - \int_v N^T b dv \quad (3.7)$$

For a linear relationship between stresses and strains, the following expression can be obtained:

$$q^e = k^e a^e + f^e \quad (3.8)$$

where  $k^e$  is the elemental stiffness matrix

$$k^e = \int_v B^T D B dv \quad (3.9)$$

and

$$f^e = - \int_v N^T b dv - \int_v B^T D \epsilon_0 dv + \int_v B^T \sigma_0 dv \quad (3.10)$$

The force-displacement relation for the whole plate is given by:

$$[K] \{a\} = q \quad (3.11)$$

where  $[K]$  is the stiffness matrix of the structure,  $\{a\}$  is the displacement vector, and  $\{q\}$  is the force vector.

The strain energy  $e_{ij}$  of the  $j$ th layer of the  $i$ th element is given by:

$$e_{ij} = \{a\}_i^T [k]_{ij} \{a\}_i \quad (3.12)$$

The element strains  $\{\epsilon\}_i$  in the  $i$ th element are expressed by:

$$\{\epsilon\}_i = [c] \{a\}_i \quad (3.13)$$

where  $[c]$  is the strain-displacement matrix. The stresses  $\{\sigma\}_{ij}$  in the  $j$ th layer of the  $i$ th element are given by:

$$\{\sigma\}_{ij} = [Q]_{ij} \{\epsilon\}_i \quad (3.14)$$

where  $[Q]_{ij}$  is the matrix of elastic constants of the  $j$ th layer of the  $i$ th element.

### 3.1.2 Failure criterion

Once we know how to calculate strains and stresses in any point of the plate, we need to apply a failure criterion in order to assess the stress level in each layer.

For optimization processes, the concept of strength/stress ratio is extremely useful. Thus, the chosen failure criterion must have a unique strength/stress ratio for each combined state of stress and the corresponding state of strain. For this reason, a quadratic criterion has been applied.

According to Tsai and Wu [72], there exists a failure surface in the stress-space in the following scalar form:

$$F_{ij} \sigma_{ij} + F_i \sigma_i = 1 \quad i, j = 1, 2, 3, 4, 5, 6 \quad (3.15)$$

where the contracted notation is used;  $F_i$  and  $F_{ij}$  are strength tensors of the second and fourth rank, respectively.

One method of applying the strength criterion is to transform the stress components into the material-symmetry axes. The final expression will be composed by the following terms:

$$\begin{aligned}
 &F_1 \sigma_1' + F_2 (\sigma_2' + \sigma_3') + F_{11} \sigma_1'^2 \\
 &+ F_{22} (\sigma_2'^2 + \sigma_3'^2 + 2 \sigma_4'^2) + F_{66} (\sigma_5'^2 + \sigma_6'^2) \\
 &+ 2 F_{12} (\sigma_1' \sigma_2' + \sigma_1' \sigma_3') + 2 F_{23} (\sigma_2' \sigma_3' + \sigma_4'^2) = 1
 \end{aligned} \tag{3.16}$$

where

$$F_1 = 1/X - 1/X' \tag{3.17}$$

$$F_{11} = 1/(X X') \tag{3.18}$$

$$F_2 = 1/Y - 1/Y' \tag{3.19}$$

$$F_{22} = 1/(Y Y') \tag{3.20}$$

$$F_{33} = 1/(Z Z') \tag{3.21}$$

$$F_{66} = 1/(S S') \tag{3.22}$$

The coupling or interaction terms can be calculated by means of the following formula:

$$F_{ij} = F_{ij}^* [F_{ii} F_{jj}]^{1/2} \quad i \neq j \tag{3.23}$$

$$\text{and } F_{ij}^* = -0.5 \tag{3.24}$$

The strength/stress ratio  $r$  is the ratio between the maximum, ultimate or allowable strength, and the applied stress:

$$\{\sigma\}_{\max} = r \{\sigma\}_{\text{applied}} \tag{3.25}$$

Since each combination of stress components in Equation 3.26

$$F_{ij} \sigma_i \sigma_j + F_i \sigma_i = 1 \quad (3.26)$$

reaches its maximum when the left-hand side reaches unity, we can substitute Equation 3.25 into Equation 3.26 :

$$[F_{ij} \sigma_i \sigma_j] r^2 + [F_i \sigma_i] r - 1 = 0 \quad (3.27)$$

If we define

$$a = F_{ij} \sigma_i \sigma_j \quad (3.28)$$

$$b = F_i \sigma_i \quad (3.29)$$

Then, the strength/stress ratio  $r$  is the positive square root in the quadratic formula :

$$r = - ( b / 2a ) + [ ( b / 2a )^2 + 1/a ]^{1/2} \quad (3.30)$$

### *3.1.3 Recurrence relations*

The recurrence relations proposed here for resizing the elements are based on the optimality criteria, which are not rigorous in the mathematical sense, but which are found to give near optimum weight designs for large structures in a very efficient way.

The optimality criterion for the generalized stiffness requirement can be stated as, "the optimum structure is the one in which the ratio of the average

strain energy density to the mass density is the same in all the elements" [73]. This criterion can be written as:

$$l = \lambda \tilde{e}_{ij} / \rho_{ij} \quad \begin{matrix} i=1, \dots, m \\ j=1, \dots, m \end{matrix} \quad (3.31)$$

where  $\lambda$  is the Lagrangian parameter,  $\tilde{e}_{ij}$  is the strain energy density of the  $j$ th layer of the  $i$ th element, and  $\rho_{ij}$  is the mass density. The strain energy density is given by:

$$\tilde{e}_{ij} = e_{ij} / V_{ij} \quad (3.32)$$

where  $V_{ij}$  is the volume of the element defined by:

$$V_{ij} = t_{ij} l_i \quad (3.33)$$

where  $t_{ij}$  is the thickness of the  $j$ th layer of the  $i$ th element and  $l_i$  is the surface area of the  $i$ th element. The design variable  $t_{ij}$  can be written as:

$$t_{ij} = \Lambda \alpha_{ij} \quad (3.34)$$

where  $\alpha_{ij}$  is the relative thickness (normalized to the maximum thickness) of the  $j$ th layer of the  $i$ th element, and  $\Lambda$  is the scaling parameter. Introducing the scaling parameter in Equation 3.11 gives:

$$\Lambda [K'] \{a\} = \{q\} \quad (3.35)$$

or

$$[K'] \{a'\} = \{q\} \quad (3.36)$$

where

$$\{a\} = \{a'\} / \Lambda \quad (3.37)$$

and  $[K']$  is the stiffness matrix for the whole structure obtained by using the relative design vector  $\alpha_{ij}$ . Introducing the scaling parameter into Equations 3.12 to 3.14, the relations between the actual quantities and the relative quantities at element level can be expressed as:

$$[K]_{ij} = \Lambda [K']_{ij} \quad (3.38)$$

$$\{a\}_i = \{a'\}_i / \Lambda \quad (3.39)$$

$$\{\epsilon\}_i = \{\epsilon'\}_i / \Lambda \quad (3.40)$$

$$\{\sigma\}_{ij} = \{\sigma'\}_{ij} / \Lambda \quad (3.41)$$

where the prime quantities are the relative values.

Introducing Equations 3.32, 3.38 and 3.39 in Equation 3.31 gives:

$$1 = \lambda \tilde{e}'_{ij} / (\Lambda^2 \rho_{ij}) \quad (3.42)$$

where

$$\tilde{e}'_{ij} = \{r'\}_i^t [K']_{ij} \{r'\}_i / (\alpha_{ij} l_i) \quad (3.43)$$

Multiplying both sides of Equation 3.42 by  $\alpha_{ij}^2$  and taking the square root gives:

$$\alpha_{ij} = B \alpha_{ij} (\tilde{e}'_{ij} / \rho_{ij})^{1/2} \quad (3.44)$$

where B is a constant. Equation 3.44 can be rewritten in an iterative form as:

$$(\alpha_{ij})_{v+1} = B (\alpha_{ij})_v (\tilde{e}'_{ij} / \rho_{ij})^{1/2} \quad (3.45)$$

where  $v$  and  $v+1$  refer to the cycles of iteration.

In this procedure the resizing of an element is done by dividing the design variable by the minimum actual strength/stress ratio for that element:

$$(\alpha_{ij})_{v+1} = (\alpha_{ij})_v / (r)_{\min v} \quad (3.46)$$

Therefore, the election of the appropriate failure criterion is critical. If the strength/stress ratio defined by the failure criterion is unique for each combined state of stress and the corresponding state of strain, the application of Equation 3.46 is efficient and simple. Otherwise, the application of the procedure becomes more complicated.

### 3.2 ANALYSIS OF THE VARIABLE THICKNESS PROBLEM

The aim of this study is to find out what happens inside the laminate when the laminate thickness varies and one transverse load is applied. The behavior of a two-dimensional plate with variable thickness is extremely difficult to understand because it is a 3-D problem, and because bending, shear and variable thickness effects appear simultaneously. In other words, the whole stress tensor must be considered: the three in-plane stress components are present owing to the bending effects, and so are the two interlaminar shear stress components because of the shear effects. Finally, the interlaminar normal stress component must also be considered because of the variable thickness effect.

In order to simplify the problem and to understand the variable thickness phenomenon, a one-dimensional plate with variable thickness is studied here by means of a 2-D plane strain finite element model.

The next section refers to the attempts for obtaining through-thickness stress distributions in a cross section where the laminate thickness varies.



Once the stress level is known, the laminate failure will be predicted by means of a quadratic failure criterion. The aim of this study is to analyze theoretically the influence of the different parameters on the mechanical behavior of variable-thickness laminated composite plates.

A study of the damage in variable thickness laminated composites caused by a transverse load provided an understanding of composite failure mechanisms (caused by transverse loads) and identified the essential parameters causing the damage in composite plates.

Finally, an experimental study will assess the accuracy of the theory, as well as analyze the influence of the different parameters on the mechanical behavior of variable-thickness laminated composite plates.

### *3.2.1. Model assumptions and method of analysis*

The model used here assumes:

- This study is limited to one-dimensional laminated composite plates, in order to avoid three-dimensional effects and to analyze properly the consequences of the variable thickness effect.
- The fiber orientation is longitudinal (x-direction). This is the optimal direction for one-dimensional laminated composite plates.
- The material used is graphite/epoxy AS4/3501-6.

The method of analysis is explained by the following points:

- A 2-D plane strain finite element model.
- The mesh is composed by 1891 nodes.

- Different types of loading and boundary conditions have been studied to analyze the variable thickness problem from a theoretical point of view as well as to obtain through-thickness stress distributions.
- A three-point bending model has been used for analyzing theoretically the influence of the different parameters on the mechanical behavior of variable-thickness laminated composite plates.
- A three-point bending testing in fatigue and static conditions have been carried out for identifying the failure mechanisms .
- A three-point bending testing in static conditions has been used to verify the theoretical model, and to analyze experimentally the influence of the different parameters on the mechanical behavior of variable-thickness laminated composite plates.

### *3.2.2.Through-thickness stresses distributions*

This section explains the attempts to obtain through-thickness stresses distributions in a cross section, where the laminate thickness varies from  $t$  to  $t-t_1$ .

The solution of the problem is a function of a number of parameters :

- $\theta$  : angle of variation of thickness
- $t/t_1$  : thickness ratio
- Stacking sequence
- Bending moment distribution
- Shear force distribution
- Characteristic length / laminate thickness ratio

## • Material.

The model described in Section 3.2.1 has been applied to different cases in order to find out what happens inside the laminate when the laminate thickness varies and to study the sensitivity of the the parameters mentioned above. Thus, once the relationship between each parameter and the mechanical behavior of the plate is known, some design changes can be made in order to improve the mechanical characteristics of the plate.

Figures 3, 4, and 5 show the distributions of  $\sigma_1$ ,  $\sigma_3$  and  $\sigma_5$  through the thickness for one-dimensional two-sides tapered plates and linear bending moment distributions with  $\partial M/\partial x > 0$ . These stress components present remarkable differences with respect to the constant-thickness plate distributions. Especially, those related to  $\sigma_3$  and  $\sigma_5$ , because  $\sigma_5$  has two maxima near the top and bottom surfaces and  $\sigma_3$  reaches much higher values than in the case of constant thickness.

In Figures 6, 7, and 8, the distributions of  $\sigma_1$ ,  $\sigma_3$ , and  $\sigma_5$  through the thickness for one-dimensional one-side tapered plates and linear bending moment distributions with  $\partial M/\partial x > 0$ . Obviously, to tape the plate in just one side leads to non-symmetrical distributions with peaks of interlaminar stresses near the surface tapered.

Figures 9, 10, and 11 show the distributions of  $\sigma_1$ ,  $\sigma_3$ , and  $\sigma_5$  through the thickness for one-dimensional two-sides tapered plates and linear bending moment distributions with  $\partial M/\partial x < 0$ . The sign of  $\partial M/\partial x$  has a strong influence on the distributions of longitudinal and interlaminar stresses.

Finally, Figures 12, 13, and 14 represent the distributions of  $\sigma_1$ ,  $\sigma_3$ , and  $\sigma_5$  through the thickness for one-dimensional one side tapered plates and linear bending moment distributions with  $\partial M/\partial x < 0$ .

In Figures 15, 16, and 17,  $\sigma_1$ ,  $\sigma_3$ , and  $\sigma_5$  distributions are represented for  $t_1/t=0.3$ ,  $M/Pt=5$ , and  $\partial M/\partial x < 0$ , respectively. Two angles of variation of thickness have been considered: 15 and 90 degrees. To reduce the angle of

variation of thickness from  $90^\circ$  to  $15^\circ$  leads to decrease considerably the values of the peaks in the distributions of  $\sigma_1$ ,  $\sigma_3$  and  $\sigma_5$ , especially these last two.

Figures 18, 19, and 20, show the distributions of  $\sigma_1$ ,  $\sigma_3$ , and  $\sigma_5$  for  $t_1/t=0.2$ ,  $M/Pt=5$ , and  $\partial M/\partial x < 0$ , respectively. As expected, maxima values decrease considerably with respect to Figures 15, 16 and 17, because of the smaller value of  $t_1/t$ .

Distributions of  $\sigma_1$ ,  $\sigma_3$ , and  $\sigma_5$  for  $t_1/t=0.1$ ,  $M/Pt=5$ , and  $\partial M/\partial x < 0$  are presented in Figures 21, 22, and 23, respectively. Numerical values keep decreasing because of the value of  $t_1/t=0.1$ . Also, the effect of the angle of variation of thickness can be seen by comparing the distributions for  $\theta=90^\circ$  and  $\theta=15^\circ$ .

The following conclusions can be drawn after analyzing the results described above:

- The examination of Figures 3 through 14 leads to the conclusion that the variable-thickness effect presents a strong influence on the distributions of longitudinal and interlaminar stresses. High peaks of interlaminar stresses appear near the areas of change of thickness.
- Comparison of Figures 3, 4, and 5 and Figures 6, 7, and 8 shows that the distributions of the through-thickness stresses vary in function of the sign of  $\partial M/\partial x$ .
- Stress distributions are strongly dependent on  $t/t_1$  or thickness ratio, as the comparisons of Figures 15 through 23 reflect.
- $\theta$ , or angle of variation of thickness has a remarkable influence on interlaminar stress distributions through the laminate thickness. This fact is shown in Figures 15 through 23.

Focusing on optimization of laminated composite plates, the last four parameters in the list mentioned at the beginning of section 3.2.2 will be input data, and the optimization procedure will determine the rest of parameters of the list except for the angle of variation of thickness. Therefore, the sensitivity study of this parameter becomes more and more important since the angle of variation of thickness is critical for the mechanical behavior of variable thickness plates.

### *3.2.3 Failure mechanisms*

A variable-thickness unidirectional laminated composite exhibits a variety of failure mechanisms when subjected to transverse loads. The knowledge of these modes is very important for the understanding of what happens inside the laminate. Once we know which the critical failure mechanisms are, we will be able to identify the strain components associated with them.

A number of laminated composite plates were tested in fatigue and static conditions:

- AS4/3501-6 Graphite/Epoxy was used for this work.
- The types of testing performed were three-point static and dynamic bending.
- The load rate for the static testing was 0.06 in/min (0.001524 m/min).
- For the fatigue testing, the frequency was 5 cycles/second, and the load was 60 % of the static failure load. The vertical displacement was controlled.

Figure 24 shows the three-point-bending testing.

After studying the results, the following failure mechanisms have been reported:

1. **Delamination.** This is the most usual failure mode when the angle of variation of thickness is high. It is due to a sharp thickness variation that generates a peak of interlaminar shear stress near the areas of change of thickness. In Figure 25, a delamination failure in a tapered surface is shown. This mechanism can also be detected in thick plates, though the angle of variation of thickness is low. A representation of this failure mechanism can be seen in Figure 26. Figure 27 shows a SEM image of a delamination fracture surface. This damage was originated by a interlaminar shear stress near the midplane of the laminate. A detail of this fracture surface can be seen in Figure 28.
2. **Bending modes (compression).** This mechanism occurs when the plate is very thin, the variable thickness effect is negligible, and the compression strength is lower than the tension strength in the fiber direction. The following in-plane compression failure modes can be distinguished:
  - 2.1. **Induced transverse tensile failure.** Unidirectional composites can fracture along the fibers when loaded by compression by a transverse tensile failure mode, because of the weakness of the matrix and the fiber-matrix interface, compared with the strength of the fibers.
  - 2.2. **Compressive delamination failure.** If a fiber buckles, the fiber-matrix interface may fracture in shear and lead to ultimate failure.
  - 2.3. **Euler failure.** If the matrix is ductile and the interface is strong, the fiber can bend without matrix failure and will eventually fracture in bending.
  - 2.4. **Microbuckling.** A more likely failure mode of unidirectional composite laminates associated with fiber microbuckling and fiber kinking, is shear crippling. Macroscopically, shear crippling looks like a shear

failure on a plane at an angle to the direction of loading. Microscopic inspection, however, indicates that shear crippling is frequently the result of kink-band formation.

- 2.5. Strength failure. The final failure mode exhibited in unidirectional composites is associated with pure compression failure of the fibers. In this case, the fracture surface is likely to be at an angle to the loading direction, usually about  $45^\circ$ .
3. Bending modes (tension). This mechanism occurs when the plate is very thin, the variable thickness effect is negligible, and the compression strength is higher than tension strength in the fiber direction. The following in-plane tension failure modes can be distinguished:
  - 3.1. Unidirectional composite subjected to longitudinal tensile load. Brittle failure. In this mode, stress concentrations created at the broken fiber ends will lead to specimen separation at a given cross section.
  - 3.2. Unidirectional composite subjected to longitudinal tensile load. Brittle failure with fiber pullout. Variations in bond strength and local load transfer mechanisms from matrix to fiber can lead to the pull-out of the fibers from the matrix at fracture.
  - 3.3. Unidirectional composite subjected to longitudinal tensile load. Brittle failure with debonding and/or matrix failure. Finally, in other cases, cracks at different cross sections of the laminate may join together at fracture through fiber-matrix debonding or by shear failure of the matrix. *This interfiber matrix shear failure and fiber-matrix debonding can occur either independently or in combination; that is, portions of the failure path may exhibit debonding, while matrix shear failure is evident in other regions.*
4. Mixed modes. A mixed failure mechanism has been detected in the regions close to the application of the load. There exists a compressive delamination because of bending mode (compression), and crushing

because of compressive peeling or interlaminar normal stress. This mechanism was observed in the three-point-bending fatigue testing, after 50,000 cycles. Figure 29 shows a representation of this mixed mode. The SEM photograph of Figure 30, points clearly the fracture area. In Figures 31 through 35, some SEM images show the different mechanisms. At the top (Figure 31), a crushing failure because of compressive interlaminar normal stress is shown. In Figures 32 through 35, some surface views reflect a clear compressive delamination failure because of the bending mode (compression). No kinking was reported in the SEM images. This mixed mode does not appear in the four-point-bending testing and it can also be avoided by placing a hard rubber pad (60-80 durometer) between the load point and the specimen.

After analyzing the failure mechanisms described above, the following conclusions can be drawn:

- The critical failure modes are related to two strain components:  $\epsilon_1$  or longitudinal normal strain and  $\epsilon_5$  or interlaminar shear strain.
- The bending (compression or tension) modes are likely to occur when the plate is thin and the variable thickness effect is negligible.
- The delamination mechanisms are usual in cases where the variable thickness effect is critical (sharp change of thickness). The failure appears in the tapered surface. This mechanism also occurs when the plate is thick, even if the variable thickness is negligible. In this case, the failure appears near the middle plane of the laminate.
- The mode related to interlaminar normal strains (mixed mode) is due to stress concentrations in the areas near the application of the load. This mechanism can be easily avoided by means of the solutions mentioned above.



### *3.2.4 Experimental study and verification of the theoretical model*

An experimental study assessed the accuracy of the theoretical model, and the influence of the angle of variation of thickness on the strength of a composite plate:

- AS4/3501-6 Graphite/Epoxy was used for this work.
- The type of testing performed was three-point static bending.
- The load rate was 0.06 in/min (0.001524 m/min).
- Three types of specimens were tested. Maximum, minimum thickness, and span were the same for the three specimens. The only variable parameter was the angle of variation of thickness:
  - Specimen OLCP\_7001. Angle of variation of thickness:  $60^\circ$
  - Specimen OLCP\_7002. Angle of variation of thickness:  $45^\circ$
  - Specimen OLCP\_7003. Angle of variation of thickness:  $90^\circ$
- The span was 8 inches (0.2032 meters).
- The maximum thickness was at the center of the beam: 0.66 inches (0.0167 meters).
- The minimum thickness was at the end of the beam: 0.28 inches (0.007 meters).
- Longitudinal and interlaminar strains were measured by using strain gauges. The collocation of the gauges is reported in Table 3.1. The election of the points was carried out in function of the theoretical

analysis. Strain gauges were disposed in those points whose strain value was critical, according to the results from the finite element method applied to variable thickness laminated composite plates.

Table 3.1 Coordinates x and z of strain gauges. Values are expressed in inches (meters).

POINT	x		z	
1	0.0	(0.0000)	0.100	(0.00254)
2	0.0	(0.0000)	0.200	(0.00508)
3	1.0	(0.0254)	0.350	(0.00889)
4	2.0	(0.0508)	0.415	(0.01054)
5	3.0	(0.0762)	0.600	(0.01524)
6	4.0	(0.1016)	0.510	(0.01295)
7	4.0	(0.1016)	0.350	(0.00889)
8	4.0	(0.1016)	0.000	(0.00000)

The study on failure mechanisms shows that critical strain components are the longitudinal strain  $\epsilon_1$ , and the interlaminar shear strain is  $\epsilon_5$ . An analysis of both components for specimens described OLCP\_7001, OLCP\_7002, and OLCP\_7003 follows.

The scheme of the specimen OLCP\_7001 is depicted in Figure 36. Measurements are reported in Figure 37. This specimen was made by tapering the plate in its inner part (Figure 38) and the angle of variation of thickness is  $6^\circ$ . The failure load was 4950 lb (22000N). The failure mode is

shown in Figure 39. The upper surface does not present any failure, in spite of being tapered. Instead of that, a crack appears near the middle plane at the end of the plate where interlaminar shear strains are maxima. The reason for this is that the angle of variation of thickness is very low. A scheme of the situation of the gauges is depicted in Figure 40. The numerical results of the specimen OLCP\_7001 are presented in Tables 3.2, 3.3, and 3.4. Tables 3.2 and 3.3 show longitudinal and interlaminar shear strains in the critical points for the failure load, respectively. The maximum value is registered in point number 1 ( $\epsilon_5=0.0131$ ).

Table 3.2 Longitudinal strains in specimen OLCP\_7001. Load: 4950 lb (22000 N).

POINT	$\epsilon_1 * 1E-3$ TESTING	$\epsilon_1 * 1E-3$ THEORY
8	8.9	8.6

Table 3.3 Interlaminar shear strains in specimen OLCP\_7001. Load: 4950 lb (22000 N).

POINT	$\epsilon_5 * 1E-3$ TESTING	$\epsilon_5 * 1E-3$ THEORY
1	13.1 (FAILURE)	12.5
2	9.0	8.1
3	6.3	7.3
4	5.7	6.7
5	4.2	5.8
6	3.7	3.1
7	12.7	12.1

The maximum vertical displacement is reported in Table 3.4. In both fields, strains and displacements, an excellent agreement is found between the data and the prediction.

Table 3.4 Maximum vertical displacement in specimen OLCP\_7001. Load: 4950 lb (22000 N).

POINT	$d_z$ TESTING	$d_z$ THEORY
8	- 0.173 (0.00439)	- 0.161 (0.00409)

The scheme of the specimen OLCP\_7002 is depicted in Figure 41. Measurements are reported in Figure 42. The angle of change of thickness is  $45^\circ$ . Six steps were designed along the specimen. The failure load was 2960 lb (13150 N). The failure mode is shown in Figure 43. Owing to the high angle of variation of thickness, failure appears at the upper surface in the thinnest area of change of thickness. Failure mechanism is a kind of interlaminar shear mode. As theoretical results predict, there is a peak of interlaminar shear strains in the places where the thickness changes. A scheme of the situation of the gauges is depicted in Figure 44. The numerical results of the specimen OLCP\_7002 are presented in Tables 3.5, 3.6, and 3.7. Tables 3.5 and 3.6 show longitudinal and interlaminar shear strains in the critical points for the failure load, respectively. The maximum value is registered in point number 3 ( $\epsilon_5=0.0131$ ).

Table 3.5 Longitudinal strains in specimen OLCP\_7002. Load: 2960 lb (13150 N).

POINT	$\epsilon_1 * 1E-3$ TESTING	$\epsilon_1 * 1E-3$ THEORY
8	4.4	3.96

Table 3.6 Interlaminar shear strains in specimen OLCP\_7002. Load: 2960 lb (13150 N).

POINT	$\epsilon_5 * 1E-3$ TESTING	$\epsilon_5 * 1E-3$ THEORY
1	6.0	5.7
3	13.1 (FAILURE)	12.5
4	11.0	11.6
5	10.0	9.8
7	2.8	2.3

The maximum vertical displacement is reported in Table 3.7. In both fields, strains and displacements, an excellent agreement is found between the data and the prediction.

Table 3.7 Maximum vertical displacement in specimen OLCP\_7002. Load: 2960 lb (13150 N).

POINT	$d_z$ TESTING	$d_z$ THEORY
8	- 0.157 (0.004)	- 0.141 (0.0036)

The scheme of the specimen OLCP\_7003 is depicted in Figure 45. Measurements are reported in Figure 46. The angle of change of thickness is 90°. Six steps were designed along the specimen. The failure load was 2485 lb (11046 N). The failure mode is shown in Figure 47. Owing to the high angle of variation of thickness, failure appears at the upper surface in the thinnest area of change of thickness at a low failure load. As with specimen OLCP\_7002, failure mechanism is a kind of interlaminar shear mode. As theoretical results predict, there is a remarkable peak of interlaminar shear strains in the places where the thickness changes. A scheme of the situation of the gauges is depicted in Figure 48. The numerical results of the specimen OLCP\_7003 are presented in Tables 3.8, 3.9, and 3.10. Tables 3.8 and 3.9 show longitudinal and interlaminar shear strains in the critical points for the failure load, respectively. The maximum value is registered in point number 3 ( $\epsilon_5=0.0139$ ).

Table 3.8 Longitudinal strains in specimen OLCP\_7003. Load: 2485 lb (11046 N).

POINT	$\epsilon_1 * 1E-3$ TESTING	$\epsilon_1 * 1E-3$ THEORY
8	5.13	4.6

Table 3.9 Interlaminar shear strains in specimen OLCP\_7003. Load: 2485 lb (11046 N)

POINT	$\xi_5 * 1E-3$ TESTING	$\xi_5 * 1E-3$ THEORY
1	7.25	7.5
3	13.9 (FAILURE)	12.5
4	12.18	11.6
5	11.02	9.8
7	3.77	3.4

The maximum vertical displacement is reported in Table 3.7. In both fields, strains and displacements, an excellent agreement is found between the data and the prediction.

Table 3.10 Maximum vertical displacement in specimen OLCP\_7003. Load: 2485 lb (11046 N).

POINT	$d_z$ TESTING	$d_z$ THEORY
8	- 0.171 (0.00432)	- 0.157 (0.004)

Tables 3.11, 3.12, and 3.13 compare the three specimens tested. These tables show the values of longitudinal, interlaminar shear strains and maxima vertical displacements, respectively, for a load of 1000 lb (4445 N).

Table 3.11 Longitudinal strains in specimens OLCP\_7001, OLCP\_7002 and OLCP\_7003. Load: 1000 lb (4445 N).

POINT	$\epsilon_1 * 1E-3$ OLCP_7001	$\epsilon_1 * 1E-3$ OLCP_7002	$\epsilon_1 * 1E-3$ OLCP_7003
8	1.78	1.77	1.76

As expected, the longitudinal strains at the inner surface in the middle of the span are very similar for the three specimens tested. That is because the three specimens present the same thickness at the middle of the span and, therefore, the longitudinal strains and stresses should be very close in the three cases.

Table 3.12 Interlaminar shear strains in specimens OLCP\_7001, OLCP\_7002 and OLCP\_7003. Load: 1000 lb (4445 N).

POINT	$\epsilon_5 * 1E-3$ OLCP_7001	$\epsilon_5 * 1E-3$ OLCP_7002	$\epsilon_5 * 1E-3$ OLCP_7003
1	2.62	2.5	2.4
3	1.26	4.8	5.24
4	1.14	4.2	4.4
5	0.84	3.8	4.0
7	2.54	1.3	1.12

Table 3.12 shows very nice results. On the one hand, the maxima values are registered in specimens OLCP\_7002 and OLCP\_7003, whose angles of variation of thickness present high values (45 and 90 degrees, respectively). On the other hand, in these two cases, the values given by gauges number 3, 4, and 5 are critical, which means that the upper surface is the critical one



from the failure point of view. Instead of that, specimen OLCP\_7001 does not present its maximum value in any of these points and, therefore, the tapered surface is not critical at all.

Table 3.13 Maximum vertical displacement in specimens OLCP\_7001, OLCP\_7002 and OLCP\_7003. Load: 1000 lb (4445 N).

POINT	$d_z$ OLCP_7001	$d_z$ OLCP_7002	$d_z$ OLCP_7003
8	-0.0346 (0.00087)	-0.059 (0.00149)	-0.0628 (0.00159)

The results reported in Table 3.13 point out a higher stiffness of specimen OLCP\_7001 with respect to the other two. The lower the angle of variation of thickness, the better the fiber works. Hence, according to these results, there is no linearity, and the angle of variation of thickness must be very low in order to get a high quality design from the point of view of stiffness and strength.

Figures 50 and 51 compare the distributions of interlaminar strains through the laminate thickness. Both graphics refer to the three-point-bending testing and the specimen OLCP\_7001 described above. Figure 50 shows the theoretical and experimental distributions of interlaminar shear strain  $\epsilon_5$  in section AA. As shown in Figure 49, section AA corresponds to the end of the beam. This section is critical because the laminate thickness is minimum. Figure 51 represents the same distributions of  $\epsilon_5$  in section BB, at the middle of the span (Figure 50). In both cases, theoretical and experimental distributions are very close.

Comparison of these results shows:

- For low values of the angle of variation of thickness, the strength is outstanding and the variable thickness effect does not alter the

mechanical behavior of the plate. Failure occurs at the middle plane of the plate and corresponds to a delamination mechanism (owing to interlaminar shear stresses).

- For high values of the angle of variation of thickness, the strength is low and the variable thickness effect does alter the mechanical behavior of the plate. Failure occurs at the area where the thickness varies, and corresponds to a delamination mechanism (owing to high interlaminar shear stresses provoked by the variable thickness effect).
- The numerical results from theory and testing are very close both in the fields of deflections and longitudinal and interlaminar strains.
- Theoretical and experimental distributions of through-thickness strains are also very close.

### 3.3 DESCRIPTION OF RESULTS

This section describes a number of numerical results for one- and two-dimensional laminated composite plates. First, the method of analysis. The conclusions drawn in the last section are the key for the formulation of the present problem. The results obtained from the 2-D plane strain model are very close to the data given by the experimental study. This model can be directly applied for analyzing one-dimensional laminated composite plates. And that model can also be the base for a more general one, applicable to the analysis of two-dimensional laminated composite plates.

Once the method of analysis is known, the different input data required for the calculation must be obtained. In a structural optimization problem, there are two types of input data: geometric and those related to the material itself. There is no problem in getting to know the geometric data of the plate, but the elastic constants and strengths of the material require a special treatment. In-plane constants are given in the literature, though some doubts

exist about compression strength. However, through-thickness properties are hard to get, and even some constants like interlaminar normal and interlaminar shear moduli are a function of the stacking sequence. Therefore, the elastic constants and strengths will be obtained for the material used in this work.

Finally, one- and two-dimensional laminated composite plates will be studied, and a number of figures will show the optima configurations for different kinds of plates, types of loading, and boundary conditions.

### *3.3.1 Model assumptions and method of analysis*

In the last section, a 2-D plane strain model has been verified by means of an experimental study. Hence, there are two options to optimize two-dimensional plates:

- Generalizing to a 3-D model, by using a three-dimensional finite element theory and
- Using a 2-D model, by applying a shear deformation plate theory.

The first option is expensive, especially from the point of view of the optimization and, therefore, the subsequent application of an iterative procedure.

The second option is efficient, because the analysis is carried out very fast and the required number of nodes of the mesh is not large. But the following question remains to be answered: is a 2-D shear deformation plate theory accurate enough to study two-dimensional plates with variable thickness ?

This question has two possible answers:

- If the angle of variation of thickness is 90 degrees, there are discontinuities in the exterior surface(s) of the laminated composite plates, there are free edges effects, and a 3-D finite element theory should be used.
- If the angle of variation of thickness is low, and the plate exterior surfaces are continuous as shown in Figure 36, a two-dimensional plate with variable thickness can be studied very accurately by means of a 2-D shear deformation theory. This fact is based on a number of verifications made between 2-D plane strain models and 1-D models using a shear deformation plate theory. In all cases, deflections were very close and, according to the conclusions of failure mechanisms, the critical stress components  $\sigma_1$  and  $\sigma_5$  presented very small differences. One verification is presented in Figures 52, 53, and 54. The geometry is shown in Figure 52. In Figures 53 and 54, distributions of  $\sigma_1$  and  $\sigma_5$  from both models are depicted, respectively .

Both theoretical and experimental studies about variable thickness (Section 3.2) showed that the angle of variation of thickness has a strong influence on the failure load, and that, the lower the angle, the higher the failure load. Hence, it is logical to design tapered plates with low angles of variation of thickness and continuous exterior surfaces. In this case, a 2-D shear deformation plate theory is applicable.

The finite element used [67] here is based on the higher order shear theory [62] and on the penalty function theory. This scheme makes it possible to analyze thin and thick plates, because of its general formulation.

The results given by the finite element method are optimized by means of the iterative procedure described in Section 3.1.3. Laminate thickness and fiber orientation are the design variables. Laminate thickness is modified in each step by means of an iterative procedure based on optimality criteria to

design a minimum weight structure. In order to assess the stress level, a quadratic failure criterion is applied in each element. If the stresses in all the elements satisfy this criterion, the process is over. If they do not, another iteration starts. Usually, around ten iterations are needed to get convergence.

The optimization of fiber orientations is complex because of:

- Practical considerations. Only four angles have been used :  
0°, 45°, -45°, and 90° .
- Practical considerations. The optimum laminate should be defined in function of repetitive sublaminate.
- Stacking sequence. A strong influence on the strain and stress level is due to bending and interlaminar effects.

No acceptable result was obtained, by using the optimization procedures available. Hence, 2-D shear deformation model being so fast and playing with discrete variables, all the possible combinations were tried as possible optima sublaminate.

Finally, the following assumptions have been made in the development of the analysis :

- The analysis is static.
- The theory applied is valid for small deformations.
- The material used is supposed to be elastic.

### *3.3.2 Determination of elastic constants and strengths*

The analysis and optimization of a composite structure require the determination of elastic constants and strengths.

T300/N5208 is a unidirectional graphite/epoxy laminate. Thus, each layer can be considered as a transversely isotropic material. The stiffness matrix for such material is represented in Table 3.7. There are five independent constants and 12 nonzero components.

Table 3.7 Stiffness matrix for a transversely isotropic material.

	$\epsilon_1$	$\epsilon_2$	$\epsilon_3$	$\epsilon_4$	$\epsilon_5$	$\epsilon_6$
$\sigma_1$	$C_{11}$	$C_{12}$	$C_{12}$	0	0	0
$\sigma_2$	$C_{21}$	$C_{22}$	$C_{23}$	0	0	0
$\sigma_3$	$C_{21}$	$C_{32}$	$C_{22}$	0	0	0
$\sigma_4$	0	0	$0 \ (C_{22} - C_{23})/2$	0	0	0
$\sigma_5$	0	0	0	0	$C_{66}$	0
$\sigma_6$	0	0	0	0	0	$C_{66}$

The five independent constants present the following values :

$$\begin{aligned}
 C_{11} &= 181.8 \quad \text{GPa} \\
 C_{12} &= 2.90 \quad \text{GPa} \\
 C_{22} &= 10.35 \quad \text{GPa} \\
 C_{23} &= 7.05 \quad \text{GPa} \\
 C_{66} &= 7.17 \quad \text{GPa}
 \end{aligned}$$

For a laminate, the components that relate  $\sigma_3 / \epsilon_3$  and  $\sigma_5 / \epsilon_5$  are a function of the stacking sequence. According to Roy and Tsai [74], Figure 55

gives some values of the interlaminar normal modulus in function of  $m$  and  $n$  in a laminate T300/N5208  $[90_m/0_n]_s$ .

Figure 56 [74] shows the variation of the interlaminar shear modulus in function of  $\phi$  in a laminate T300/N5208  $[+\phi/-\phi]_s$ .

The strengths for this material are given by the following values:

$X$	$=$	1500	MPa
$X'$	$=$	1500	MPa
$Y$	$=$	40	MPa
$Y'$	$=$	246	MPa
$Z$	$=$	40	MPa
$Z'$	$=$	246	MPa
$S$	$=$	68	MPa
$S'$	$=$	68	MPa

### 3.3.3 One-dimensional laminated composite plates

The following points analyze the problem:

- The objective is to get the minimum weight structure by using strength as a design criterion.
- The laminate used is  $[0]_n$  because it is the optimum for one-dimensional laminated composite plates subjected to transverse loads.
- Two-sided tapered laminates have been considered.
- Three kinds of plates have been analyzed:
  - thin plates ( $l/t \gg 10$ ),
  - thick plates ( $l/t \ll 10$ ),
  - sandwich panels.

- Boundary conditions are restricted to :
  - simply supported plates,
  - clamped plates,
  - cantilever plates.
- Two types of loading have been applied:
  - uniform load, and
  - point load, at the center of the plate for simply supported and clamped plates, and at the free end of the plate for cantilever plates.
- The mesh was composed by 400 nodes.
- The material used is T300/N5208.

Figure 57 shows the definition of coordinates axis and the key to colors for one-dimensional plates.

*Thin plates subjected to a uniform load*

Optimal thin plates subjected to a uniform load are represented in Figure 58. Whatever the boundary condition, the optimum laminate thickness is :

$$t = 2 k a (P/X)^{1/2} \quad (3.47)$$

where  $a$  is the plate span,  $P$  is the load applied,  $X$  is the uniaxial tensile strength of a ply along the  $x$ -axis, and  $k$  is a coefficient that varies in function of  $x$ . The value of the non-dimensional coefficient  $k$  in function of  $x$  is given for the following boundary conditions: simply supported, clamped, and cantilever one-dimensional plate. Also, the weight savings (WS) are reported for these three cases. The 45.7 % WS for the cantilever plate is remarkable.



### *Thick plates subjected to a uniform load*

Figure 59 shows the optimal thick plates subjected to a uniform load. In this case, the optimum laminate thickness is :

$$t = 2 k a P/S \quad (3.48)$$

where  $S$  is the shear strength in the  $xy$ - or  $12$ -plane of a ply. The value of the non-dimensional coefficient  $k$  in function of  $x$  and the optimal configurations are given for the boundary conditions mentioned above. The weight saving is the same for the three boundary conditions: 45.7 %.

### *Sandwich panels subjected to a uniform load*

Optimal one-dimensional uniform loaded sandwich panels are represented in Figure 60. In this case, only failure mode dealing with the faces have been considered. The optimum laminate thickness can be calculated by means of the following expression:

$$t = 2 k (a^2 P/c X) \quad (3.49)$$

where  $c$  is the core thickness. Optimal sandwiches and the value of  $k$  as a function of  $x$  are presented for different boundary conditions. The weight saving is 31.2 % for simply supported plates, 58.5 % for clamped plates, and 56.9 % for cantilever plates.

### *Thin plates subjected to a point load*

Optimal thin plates subjected to a point load are represented in Figure 61. Whatever the boundary condition, the optimum laminate thickness is :

$$t = 2 k (P a/X)^{1/2} \quad (3.50)$$

The value of the non-dimensional coefficient  $k$  in function of  $x$  is given for the following boundary conditions: simply supported, clamped, and

cantilever one-dimensional plate. Also, the weight savings (WS) are reported for these three cases. The 44.0 % WS for clamped plates is remarkable.

#### *Thick plates subjected to a point load*

Figure 62 shows the optimal thick plates subjected to a point load. In this case, the optimum laminate thickness is :

$$t = 2 k \ P/S \quad (3.51)$$

The value of the non-dimensional coefficient  $k$  in function of  $x$  and the optimal configurations are given for the boundary conditions mentioned above. There is not weight saving in this case for any boundary condition.

#### *Sandwich panels subjected to a point load*

Optimal one-dimensional sandwiches subjected to a point load, are represented in Figure 63. In this case, only failure mode dealing with the faces have been considered. The optimum laminate thickness can be calculated by means of the following expression:

$$t = 2 k (a \ P/c \ X) \quad (3.52)$$

Optimal sandwiches and the value of  $k$  as a function of  $x$  are presented for different boundary conditions. The weight saving is 45.7 % for simply support plates, 41.4 % for clamped plates, and 45.7 % for cantilever plates.

#### *3.3.4 Two-dimensional laminated composite plates*

The following points analyze the problem:

- The objective is to get the minimum weight structure by using strength as a design criterion.

- Only symmetric and balanced laminates have been considered.
- Two-sided tapered laminates have been considered.
- Three kind of plates have been analyzed:
  - thin plates ( $l/t \gg 10$ ),
  - thick plates ( $l/t \ll 10$ ),
  - sandwich panels.
- Boundary conditions are restricted to :
  - simply supported plates along the four edges of the plate,
  - clamped plates along the four edges of the plate.
- Two types of loading have been applied:
  - uniform load, and
  - point load at the center of the plate.
- Owing to practical considerations, only four angles have been used :  $0^\circ, 45^\circ, -45^\circ$ , and  $90^\circ$ .
- Plate aspect ratios between 1 and 10 have been considered.
- The mesh was composed by 400 nodes.
- The material used is T300/N5208.

Figure 64 shows the definition of coordinates axis and key to colors for one-dimensional plates.

*Thin, simply supported plates subjected to a uniform load*

Weight saving and normalized deflection for thin, simply supported, uniform loaded plates are shown in Figure 65. The weight saving is a function of the aspect ratio, the maximum value being 27% for a square plate. The optimum sublamine also varies in the function of the aspect ratio:

- [45/-45] for b/a between 1 and 1.75,
- [0/45/-45] for b/a between 1.75 and 2.25,
- [0<sub>5</sub>/45/-45] for b/a between 2.25 and 3.5,
- [0] for b/a higher than 3.5.

The quasi-isotropic sublamine [0/45/-45/90] presents low-weight saving with respect to the rest of sublamines, maximum value being 18 % for a square plate.

The optimum laminate thickness can be calculated by means of the following expression:

$$t = 2 k a (P/X)^{1/2} \quad (3.53)$$

where a is the length of the plate, P is the load applied, X is the uniaxial tensile strength of a ply along the x-axis, and k is a non-dimensional coefficient that is a function of x and y. Figures 66 through 69 show the values of k along the x-axis and the diagonal.

*Thin, clamped plates subjected to a uniform load*

Weight saving and normalized deflection for thin, clamped, uniform loaded plates are shown in Figure 70. The weight saving is a function of the aspect ratio, the maximum value being 48 % for b/a=2. The optimum sublamine also varies in the function of the aspect ratio:

- [0/90] for b/a between 1 and 1.5,
- [0<sub>5</sub>/90<sub>2</sub>] for b/a between 1.5 and 4.4,

- [0] for b/a higher than 4.4.

The quasi-isotropic sublaminate [0/45/-45/90] presents low-weight saving with respect to the rest of sublaminates, maximum value being 40 % for a square plate.

The optimum laminate thickness can be calculated by means of the following expression:

$$t = 2 k a (P/X)^{1/2} \quad (3.54)$$

Figures 71, 72, and 73 show the values of the non-dimensional parameter k along the x-axis and the diagonal.

*Thick, simply supported plates subjected to a uniform load*

Weight saving and normalized deflection for thick, simply supported, uniform loaded plates are shown in Figure 74. The weight saving is a function of the aspect ratio, the maximum value being 46 % for b/a=10. The optimum sublaminate also varies in the function of the aspect ratio:

- [45/-45] for b/a between 1 and 3.5,
- [0] for b/a higher than 3.5.

The quasi-isotropic sublaminate [0/45/-45/90] presents low-weight saving with respect to the rest of sublaminates, the maximum value being 20 % for b/a=10.

The optimum laminate thickness can be calculated by means of the following expression:

$$t = 2 k a P/S \quad (3.55)$$

Figures 75 and 76 show the values of the non-dimensional parameter  $k$  along the x-axis and the diagonal.

*Thick, clamped plates subjected to a uniform load*

Weight saving and normalized deflection for thick, clamped, uniform loaded plates are shown in Figure 77. The weight saving is a function of the aspect ratio, the maximum value being 46 % for  $b/a=10$ . The optimum sublaminate also varies in the function of the aspect ratio:

- [45/-45] for  $b/a$  between 1 and 3.5,
- [0] for  $b/a$  higher than 3.5.

The quasi-isotropic sublaminate [0/45/-45/90] presents low-weight saving with respect to the rest of sublaminate, the maximum value being 20 % for  $b/a=10$ .

The optimum laminate thickness can be calculated by means of the following expression:

$$t = 2 k a P/S \quad (3.56)$$

Figures 78 and 79 show the values of the non-dimensional parameter  $k$  along the x-axis and the diagonal.

*Simply supported sandwich panels subjected to a uniform load*

Weight saving and normalized deflection for simply supported, uniform loaded sandwiches are shown in Figure 80. The weight saving is a function of the aspect ratio, the maximum value being 35 % for  $b/a=10$ . The optimum sublaminate also varies in the function of the aspect ratio:

- [45/-45] for  $b/a$  between 1 and 2,

- [0] for b/a higher than 2.

The quasi-isotropic sublamine [0/45/-45/90] presents low weight saving with respect to the rest of sublaminates, the maximum value being 20 % for b/a=10.

The optimum laminate thickness can be calculated by means of the following expression:

$$t = 2 k (a^2 P/c X) \quad (3.57)$$

Figures 81 and 82 show the values of the non-dimensional parameter k along the x-axis and the diagonal.

#### *Clamped sandwich panels subjected to a uniform load*

Weight saving and normalized deflection for clamped, uniform loaded sandwiches are shown in Figure 83. The weight saving is a function of the aspect ratio, the maximum value being 60 % for b/a=2. The optimum sublamine also varies in the function of the aspect ratio:

- [0/90] for b/a between 1 and 1.5,
- [0<sub>5</sub>/90<sub>2</sub>] for b/a between 1.5 and 2.5,
- [0] for b/a higher than 2.5.

The quasi-isotropic sublamine [0/45/-45/90] presents low-weight saving with respect to the rest of sublaminates, maximum value being 50 % for b/a=10.

The optimum laminate thickness can be calculated by means of the following expression:

$$t = 2 k (a^2 P/c X) \quad (3.58)$$

Figures 84, 85, and 86 show the values of the non-dimensional parameter  $k$  along the x-axis and the diagonal.

*Thin, simply supported plates subjected to a point load*

Weight saving for thin, simply supported plates subjected to a point load, is shown in Figure 87. The weight saving is a function of the aspect ratio, the maximum value being 76 % for  $b/a=2$ . The optimum sublaminate is [0] for all plate aspect ratios analyzed.

The quasi-isotropic sublaminate [0/45/-45/90] presents low-weight saving with respect to the optimum sublaminate, the maximum value being 63 % for  $b/a=2$ .

Since no general formula for expressing the optimum laminate thickness has been found, the following particular case has been calculated:

- $a=7.87$  in (0.2 m),
- $P=1.125$  E4 lb (5 E4 N).

Figures 88, 89, and 90 show the values of the thickness in meters along the x-axis and the diagonal.

*Thin, clamped plates subjected to a point load*

Weight saving for thin, clamped plates subjected to a point load, is shown in Figure 91. The weight saving is a function of the aspect ratio, the maximum value being 83 % for  $b/a=10$ . The optimum sublaminate also varies in the function of the aspect ratio:

- [45/-45] for  $b/a$  between 1 and 1.5,
- [0] for  $b/a$  higher than 1.5.



The quasi-isotropic sublamine [0/45/-45/90] presents low-weight saving with respect to the optimum sublamine, the maximum value being 80 % for  $b/a=10$ .

Since no general formula for expressing the optimum laminate thickness has been found, the following particular case has been calculated:

- $a=7.87$  in (0.2 m),
- $P=1.125 \text{ E4 lb}$  (5 E4 N).

Figures 92, 93, and 94 show the values of the thickness in meters along the x-axis and the diagonal.

*Thick, simply supported plates subjected to a point load*

Weight saving for thick, simply supported plates subjected to a point load, is shown in Figure 95. The weight saving is a function of the aspect ratio, the maximum value being 82 % for  $b/a=2$ . The optimum sublamine also varies in the function of the aspect ratio:

- [45/-45] for  $b/a$  between 1 and 2.25,
- [0] for  $b/a$  higher than 2.25.

The quasi-isotropic sublamine [0/45/-45/90] presents low-weight saving with respect to the optimum sublamine, the maximum value being 78 % for  $b/a=2$ .

Since no general formula for expressing the optimum laminate thickness has been found, the following particular case has been calculated:

- $a=7.87$  in (0.2 m),

- $P=1.125 \text{ E4 lb (5 E4 N)}$ .

Figures 96 and 97 show the values of the thickness in meters along the x-axis and the diagonal.

*Thick, clamped plates subjected to a point load*

Weight saving for thick, clamped plates subjected to a point load, is shown in Figure 98. The weight saving is a function of the aspect ratio, the maximum value being 82 % for  $b/a=10$ . The optimum sublaminate also varies in the function of the aspect ratio:

- [45/-45] for  $b/a$  between 1 and 2.5,
- [0] for  $b/a$  higher than 2.5.

The quasi-isotropic sublaminate [0/45/-45/90] presents low-weight saving with respect to the optimum sublaminate, the maximum value being 78 % for  $b/a=10$ .

Since no general formula for expressing the optimum laminate thickness has been found, the following particular case has been calculated:

- $a=7.87 \text{ in (0.2 m)}$ ,
- $P=1.125 \text{ E4 lb (5 E4 N)}$ .

Figures 99 through 101 show the values of the thickness in meters along the x-axis and the diagonal.

*Simply supported sandwich panels subjected to a point load*

Weight saving for simply supported sandwiches subjected to a point load, is shown in Figure 102. The weight saving is a function of the aspect ratio, the maximum value being 94 % for  $b/a=2$ . The optimum sublaminate is [0] for all the plate aspect ratios analyzed.

The quasi-isotropic sublaminate [0/45/-45/90] presents low-weight saving with respect to the optimum sublaminate, maximum value being 80 % for  $b/a=2$ .

Since no general formula for expressing the optimum laminate thickness has been found, the following particular case has been calculated:

- $a=7.87$  in (0.2 m),
- $P=1.125 \text{ E4 lb}$  (5 E4 N).

In Figures 103 through 105 show the values of the thickness in meters along the x-axis and the diagonal.

*Clamped sandwich panels subjected to a point load*

Weight saving for simply supported sandwiches subjected to a point load, is shown in Figure 106. The weight saving is a function of the aspect ratio, the maximum value being 96 % for  $b/a=10$ . The optimum sublaminate also varies in the function of the aspect ratio:

- [0/90] for  $b/a$  between 1 and 1.5,
- [0<sub>5</sub>/90<sub>2</sub>] for  $b/a$  between 1.5 and 5,
- [0] for  $b/a$  higher than 5.

The quasi-isotropic sublaminate [0/45/-45/90] presents low-weight saving with respect to the optimum sublaminate, the maximum value being 94 % for  $b/a=2$ .

Since no general formula for expressing the optimum laminate thickness has been found, the following particular case has been calculated:

- $a=7.87$  in (0.2 m),

•  $P=1.125 \text{ E4 lb (5 E4 N)}$ .

Figures 107 through 109 show the values of the thickness in meters along the x-axis and the diagonal.

#### 4. OPTIMIZATION OF LAMINATED COMPOSITE PLATES SUBJECTED TO BUCKLING

This section analyzes the case dealing with buckling loads. The use of laminated composite materials in aircrafts and space structures offers a unique opportunity for obtaining weight savings over conventional constructions. Also, composite materials adds versatility to the design process by allowing the structure to be tailored to meet the design criteria. One such design criterion is the prevention of compressive and shear buckling in laminated composite plates.

First, the analytical formulation of buckling of plates is reported. As usual, the theory of plates requires a numerical technique in order to simulate different boundary conditions and types of loading. The same finite element used in Section 3 (Optimization of laminated composite plates subjected to transverse loads) has been applied in this work.

Finally, results of one- and two-dimensional laminated composite plates have been described. Optima angles of orientation of the fiber and critical uniform compressive and shear loads are given for different boundary conditions and types of loading. Relative weights with respect to aluminium and the quasi-isotropic configuration are also reported.

##### 4.1 ANALYTICAL FORMULATION

The strain energy of a single plate element subject to in-plane stresses can be written as

$$V = V_B + V_s \quad (4.1)$$

where  $V_s$  is the strain energy owing to in-plane stresses acting on the second order strains, and  $V_B$  is the strain energy owing to plate bending.  $V_s$  can be expressed as

$$V_s = -\frac{1}{2} \iint \left[ \sigma_x \left( \frac{\partial w}{\partial x} \right)^2 + \sigma_y \left( \frac{\partial w}{\partial y} \right)^2 + 2\tau_{xy} \frac{\partial w}{\partial x} \frac{\partial w}{\partial y} \right] t \, dx \, dy \quad (4.2)$$

or written in matrix form as

$$V_s = -\frac{1}{2} \iint \left[ \frac{\partial w}{\partial x} \frac{\partial w}{\partial y} \right] \begin{bmatrix} \sigma_x & \tau_{xy} \\ \tau_{xy} & \sigma_y \end{bmatrix} \begin{bmatrix} \frac{\partial w}{\partial x} \\ \frac{\partial w}{\partial y} \end{bmatrix} t \, dx \, dy \quad (4.3)$$

Now, the lateral displacement  $w$  can be written as

$$w = [\bar{N}] \{\delta^e\} \quad (4.4)$$

where  $N$  is the shape function vector and  $\{\delta_e\}$  is a vector of nodal deflections. Writing

$$\begin{bmatrix} \frac{\partial w}{\partial x} \\ \frac{\partial w}{\partial y} \end{bmatrix} = \begin{bmatrix} \frac{\partial \bar{N}}{\partial x} \\ \frac{\partial \bar{N}}{\partial y} \end{bmatrix} \{\delta^e\} = [S] \{\delta^e\} \quad (4.5)$$

the following expression can be obtained

$$V_s = -\frac{1}{2} \iint \{\delta^e\}^T [S]^T [\sigma] [S] \{\delta^e\} t \, dx \, dy \quad (4.6)$$

On differentiating with respect to the nodal displacements this component of strain energy gives a "geometric stiffness"

$$\frac{\partial V^e}{\partial \delta_1}$$

$$[ \quad ] = - [k_s]^e \{ \delta^e \}$$

$$\frac{\partial V^e}{\partial \delta_N}$$

(4.7)

with

$$[k_s]^e = - \iint [S]^T [\sigma] [S] t \, dx \, dy$$

(4.8)

For the whole plate, the element matrices can be assembled:

$$([K_B] - [K_s]) \{ \delta \} = \{ Q \}$$

(4.9)

If all the in-plane stresses can be increased by a factor  $\lambda$ , this will increase the geometric stiffness proportionately. It is possible, therefore, to find a  $\lambda$  which, with no external loading  $Q$ , gives

$$([K_B] - \lambda [K_s]) \{ \delta \} = 0$$

(4.10)

that expresses an eigenvalue problem.

## 4.2 DESCRIPTION OF RESULTS

In this part of the report, some results of laminates composite plates subjected to compression, shear and combined loads are presented. Only thin plates have been analyzed.

In the case of one-dimensional plates, all the cases reported are for an angle of orientation of the fibers of  $0^\circ$ . Critical loads, weight savings for flat plates and different cross sections are presented.

In the chapter about two-dimensional plates, the study of variable thickness plates has not generated interesting results. The only author that has published in this area was Ashton [75], who obtained results for linearly tapered plates subjected to uniaxial loading, but no weight saving was reported. Instead of that, very interesting results have appeared when the angle of orientation of the fiber varies.

#### *4.2.1 Model assumptions and method of analysis*

The model used presents the following assumptions:

- The analysis is static.
- The theory applied is valid for small deformations.
- The material used is supposed to be elastic.
- The finite element used here is based on the higher order shear theory[62] and the penalty function method. A 2-D model has been applied for both one- and two-dimensional laminated composite plates.
- The design criterion used is the critical compressive force to prevent the plate from buckling.



#### 4.2.2 One-dimensional laminated composite plates

The following points analyze the problem:

- The objective is to get the minimum weight structure by using critical compressive force as a design criterion.
- The laminate used is  $[0]_n$ , because it is the optimum for one-dimensional laminated composite plates subjected to uniform uniaxial loads.
- Boundary conditions are restricted to :
  - simply supported plates,
  - clamped plates,
  - cantilever plates.
- Uniform uniaxial compression loading has been applied.
- Plate aspect ratios between 1 and 10 have been considered.
- The mesh was composed by 400 nodes.
- The material used was T300/N5208.

Figure 110 shows a definition of coordinates axis for one-dimensional plates subjected to uniform uniaxial compression loads.

*One-dimensional simply supported plates subjected to a uniaxial compression load*

Figures 111 and 112 show critical loads for one-dimensional simply supported plates subjected to uniform uniaxial compression loads. Figure 111

also shows the optimum angle. Since this case is one-dimensional, this angle is  $0^\circ$ . A comparison between the optimum angle and the quasi-isotropic laminate is shown in Figure 112. This laminate presents very low critical loads for low-aspect ratios.

Optima configurations for one-dimensional simply supported plates subjected to uniform uniaxial compression loads are depicted in Figures 113 and 114. For a maximum height of twice the thickness, the triangular configuration presents a higher weight saving than the other two (Figure 113). The T configuration is the lightest if the height is ten times the thickness (Figure 114).

#### *One-dimensional clamped plates subjected to a uniaxial compression load*

Figures 115 through 118 refer to one-dimensional clamped plates subjected to uniform uniaxial compression loads. A comparison between the optimum angle,  $0^\circ$  (Figure 115) and the quasi-isotropic laminate is shown in Figure 116. The critical load for this case is four times higher than it was in the case of simply supported plates. The reason for this is that a clamped plate is stiffer than a simply supported one and thus, the capability of supporting uniform uniaxial compression loads is also higher. In the chapter of optima configurations, similar results to the case of simply supported plates are reported (Figures 117 and 118).

#### *One-dimensional cantilever plates subjected to a uniaxial compression load*

Finally, one-dimensional cantilever plates subjected to uniform uniaxial compression loads are analyzed in Figures 119 through 122. The critical load for this case is 4 times lower than it was in the case of simply supported plates, and 16 times lower than in the case of clamped plates (Figure 119). A comparison between the optimum angle and the quasi-isotropic laminate is shown in Figure 120. In the chapter of optima configurations, similar results to the two boundary conditions treated above are reported (Figures 121 and 122).

#### *4.2.3 Two-dimensional laminated composite plates*

The following points analyze the problem:

- The objective is to get the minimum weight structure by using critical compressive force as a design criterion.
- Only symmetric and balanced laminates have been considered.
- Boundary conditions are restricted to :
  - simply supported plates along the four edges of the plate, and
  - clamped plates along the four edges of the plate.
- Six types of loading have been applied:
  - uniform uniaxial compression load,
  - uniform biaxial compression load ( $N_y = N_x/2$ ),
  - uniform biaxial compression load ( $N_y = N_x$ ),
  - uniform biaxial compression load ( $N_y = 2 * N_x$ ),
  - uniform shear load,
  - combined load: uniform uniaxial and uniform shear load.
- The mesh was composed by 400 nodes.
- The material used is T300/N5208.

Figure 123 shows a definition of coordinates axis for two-dimensional plates subjected to uniform uniaxial, biaxial, shear and combined compression loads.

*Two-dimensional simply supported plates subjected to a uniaxial compression*

In Figures 124 and 125, critical loads are reported for two-dimensional simply supported plates subjected to uniform uniaxial compression loads. Figure 124 also shows the optimum angle. Both critical load and optimum angle are a function of the plate aspect ratio, though they present constant values for aspect ratios higher than four. A comparison between the optimum configuration and the quasi-isotropic laminate is shown in Figure 125.

A comparison between critical loads for angle-ply and quasi-isotropic laminate in function of the angle of fiber orientation is carried out in Figure 126. For angles between 27 and 66 degrees, the critical load for angle-ply laminates is higher than for quasi-isotropic laminates.

Figure 127 shows normalized weights of aluminum and quasi-isotropic T300/N5208 to the optimum laminate of T300/N5208.

*Two-dimensional simply supported plates subjected to a biaxial compression ( $N_y=N_x/2$ )*

Figures 128 and 129 report critical loads for two-dimensional simply supported plates subjected to uniform biaxial compression loads ( $N_y=N_x/2$ ). Figure 128 also shows the optimum angle. Both critical load and optimum angle are a function of the plate aspect ratio, though they present constant values for aspect ratios higher than two. A comparison between the optimum configuration and the quasi-isotropic laminate is shown in Figure 129.

A comparison between critical loads for angle-ply and quasi-isotropic laminate in function of the angle of fiber orientation is carried out in Figure 130. For angles between 27 and 66 degrees, the critical load for angle-ply laminates is higher than for quasi-isotropic laminates.

Figure 131 shows normalized weights of aluminum and quasi-isotropic T300/N5208 to the optimum laminate of T300/N5208.

*Two-dimensional simply supported plates subjected to a biaxial compression ( $N_y=N_x$ )*

Figures 132 and 133 reports critical loads for two-dimensional simply supported plates subjected to uniform biaxial compression loads ( $N_y=N_x$ ). Figure 132 also shows the optimum angle. Both critical load and optimum angle are a function of the plate aspect ratio, though they present constant values for aspect ratios higher than three. A comparison between the optimum configuration and the quasi-isotropic laminate is shown in Figure 133.

A comparison between critical loads for angle-ply and quasi-isotropic laminate in function of the angle of fiber orientation is carried out in Figure 134. For angles between 27 and 66 degrees, the critical load for angle-ply laminates is higher than for quasi-isotropic laminates.

Figure 135 reports normalized weights of aluminum and quasi-isotropic T300/N5208 to the optimum laminate of T300/N5208.

*Two-dimensional simply supported plates subjected to a biaxial compression ( $N_y=2*N_x$ )*

Figures 136 and 137 show the critical loads for two-dimensional simply supported plates subjected to uniform biaxial compression loads ( $N_y=2*N_x$ ). Figure 136 also shows the optimum angle. Both critical load and optimum angle are a function of the plate aspect ratio, though they present constant values for aspect ratios higher than two. A comparison between the optimum configuration and the quasi-isotropic laminate is shown in Figure 137.

A comparison between critical loads for angle-ply and quasi-isotropic laminate in function of the angle of fiber orientation is carried out in Figure 138. For angles between 27 and 66 degrees, the critical load for angle-ply laminates is higher than for quasi-isotropic laminates.

Figure 139 shows normalized weights of aluminum and quasi-isotropic T300/N5208 to the optimum laminate of T300/N5208.

*Two-dimensional clamped plates subjected to a uniaxial compression*

Figures 140 and 141 report critical loads for two-dimensional clamped plates subjected to uniform uniaxial compression loads. Figure 140 also shows the optimum angle. Both critical load and optimum angle are a function of the plate aspect ratio. A comparison between the optimum configuration and the quasi-isotropic laminate is shown in Figure 141.

A comparison between critical loads for angle-ply and quasi-isotropic laminate in function of the angle of fiber orientation is carried out in Figure 142. For angles lower than 42 degrees, the critical load for angle-ply laminates is higher than for quasi-isotropic laminates.

Figure 143 reports normalized weights of aluminum and quasi-isotropic T300/N5208 to the optimum laminate of T300/N5208.

*Two-dimensional clamped plates subjected to a biaxial compression ( $N_y=N_x/2$ )*

Figures 144 and 145 reports critical loads for two-dimensional clamped plates subjected to uniform biaxial compression loads ( $N_y=N_x/2$ ). Figure 144 also shows the optimum angle. Both critical load and optimum angle are a function of the plate aspect ratio. A comparison between the optimum configuration and the quasi-isotropic laminate is shown in Figure 145.

Comparison between critical loads for angle-ply and quasi-isotropic laminate in function of the angle of fiber orientation is carried out in Figure 146. For angles between 21 and 40 degrees, the critical load for angle-ply laminates is higher than for quasi-isotropic laminates.

Figure 147 reports normalized weights of aluminum and quasi-isotropic T300/N5208 to the optimum laminate of T300/N5208.

*Two-dimensional clamped plates subjected to a biaxial compression ( $N_y=N_x$ )*

Figures 148 and 149 report critical loads for two-dimensional clamped plates subjected to uniform biaxial compression loads ( $N_y=N_x$ ). Figure 148 also shows the optimum angle. Both critical load and optimum angle are a function of the plate aspect ratio. A comparison between the optimum configuration and the quasi-isotropic laminate is shown in Figure 149.

Comparison between critical loads for angle-ply and quasi-isotropic laminate in function of the angle of fiber orientation is carried out in Figure 150. For angles between 43 and 47 degrees, the critical load for angle-ply laminates is higher than for quasi-isotropic laminates.

Figure 151 shows normalized weights of aluminum and quasi-isotropic T300/N5208 to the optimum laminate of T300/N5208.

*Two-dimensional clamped plates subjected to a biaxial compression ( $N_y=2*N_x$ )*

Figures 152 and 153 report critical loads for two-dimensional clamped plates subjected to uniform biaxial compression loads ( $N_y=2*N_x$ ). Figure 152 also shows the optimum angle. Both critical load and optimum angle are a function of the plate aspect ratio. A comparison between the optimum configuration and the quasi-isotropic laminate is shown in Figure 153.

A comparison between critical loads for angle-ply and quasi-isotropic laminate in function of the angle of fiber orientation is carried out in Figure 154. For angles between 52 and 66 degrees, the critical load for angle-ply laminates is higher than for quasi-isotropic laminates.

Figure 155 shows normalized weights of aluminum and quasi-isotropic T300/N5208 to the optimum laminate of T300/N5208.

*Two-dimensional simply supported plates subjected to a shear load.*

Figures 156 and 157 reports critical loads for two-dimensional simply supported plates subjected to uniform shear loads. Figure 156 also shows the optimum angle. Both critical load and optimum angle are a function of the plate aspect ratio. A comparison between the optimum configuration and the quasi-isotropic laminate is shown in Figure 157.

A comparison between critical loads for angle-ply and quasi-isotropic laminate in function of the angle of fiber orientation is carried out in Figure 158. For angles between 24 and 66 degrees, the critical load for angle-ply laminates is higher than for quasi-isotropic laminates.

Figure 159 reports normalized weights of aluminum and quasi-isotropic T300/N5208 to the optimum laminate of T300/N5208.

*Two-dimensional clamped plates subjected to a shear load.*

Figures 160 and 161 report critical loads for two-dimensional clamped plates subjected to uniform shear loads. Figure 160 also shows the optimum angle. Both critical load and optimum angle are a function of the plate aspect ratio. A comparison between the optimum configuration and the quasi-isotropic laminate is shown in Figure 161.

A comparison between critical loads for angle-ply and quasi-isotropic laminate in function of the angle of fiber orientation is carried out in Figure 162. For angles between 26 and 64 degrees, the critical load for angle-ply laminates is higher than for quasi-isotropic laminates.

Figure 163 shows normalized weights of aluminum and quasi-isotropic T300/N5208 to the optimum laminate of T300/N5208.

*Two-dimensional simply supported and clamped plates subjected to a combined load (uniaxial compression and shear)*



Finally, Figures 164 and 165 represent the buckling parameters for simply supported and clamped plates subjected to combined uniform uniaxial compression and shear, respectively.

## 5. CONCLUDING REMARKS

A study on optimization of laminated composite plates has been presented. Plates subjected to transverse loads and buckling have been treated. Optima configurations for different boundary conditions and types of loading have been reported.

In the chapter of transverse loads, the following conclusions can be drawn:

- The variable thickness effect has a remarkable influence on the behavior of a tapered laminated composite plate. The distributions of through-thickness stresses are very sensitive to the thickness ratio ( $t/t_1$ ) and the angle of variation of thickness. Especially, the interlaminar shear stress reaches very high values in the areas of change of thickness. The peak value can be controlled by modifying some parameters: thickness ratio, angle of variation of thickness, type of loading.... The distributions of interlaminar stresses vary in function of the sign of the bending moment.
- The failure mechanisms reported in variable-thickness composite plates can be grouped in three general modes:
  - 1) Interlaminar shear mode: It is due to interlaminar shear stresses, and appears in the tapered surfaces when the change of thickness is sharp (high angles of variation of thickness) . It can also appear in the midplane, in thick plates.
  - 2) Bending modes: They are due to bending stresses. These modes are usual in thin plates, very low angles of variation of thickness and low thickness ratios. They are the typical failure modes in thin untapered plates.

3) Mixed modes: A compression-interlaminar normal mode has been found in the area of application of the load in the fatigue testing. This mode does not appear in the 4-point bending test.

- For uniformly distributed loads, optimal configurations have been shown. Some general formulas have been presented for designing variable-thickness laminated composite plates (3.47 ) to (3.52). High weight savings have also been reported.
- For point loads, we have found a general formula only for one-dimensional plates. Hence, a particular case has been analyzed for two-dimensional plates. For both cases, one- and two-dimensional plates, the optimal configurations have been reported. Very high weight saving have also been presented.

From the chapter of buckling loads, the following conclusions can be drawn:

- Optimal configurations are presented for one-dimensional plates. Critical compressive forces are also represented. Different variable-thickness solutions are depicted, and their weight savings given (from 15 to 66%).
- Finally, optimal two-dimensional plates subjected to uniform uni-,biaxial compression, shear, and combined loads are shown. Optima angles of orientation of fibers, critical compressive and shear forces have been presented for all cases, and relative weights with respect to aluminium given. The highest weight saving have been reported for low aspect ratios.

## REFERENCES

1. R. Foye, "Advanced design concepts for advanced composite frames ", Volume I-II Air Force Materials Laboratory, Wright Patterson Air Force Base, Ohio, AFML-TR-68-91, 1968.
2. M. E. Waddoups, "Structural airframe application of advanced composite materials- analytical methods", Volume IV Air Force Materials Laboratory, Wright Patterson Air Force Base, Ohio, AFML-TR-69-101, 1969.
3. M. E. Waddoups, L. A. McCullers, F.O. Olsen and J. E. Ashton, "Structural synthesis of anisotropic plates ", Presented at AIAA/ASME 11th Structures, Structural Dynamics and Material Conference, Denver, Colorado, 1970.
4. Schmit, L. A., " Structural Design by Systematic Synthesis", Proceedings of 2nd National Conference on Electrical Computation, Structure Division, ASCE , pp. 105, 1960.
5. Schmit, L. A., Kicher, T. P. and Morrow, W. M., "Structural Synthesis Capability for Integrally Stiffened Waffle Plates", AIAA Journal, Vol. 1, No. 12, pp. 2820-2836, 1963.
6. Kicher, T. P., "Structural Synthesis of Integrally Stiffened Cylinders", Journal of Spacecraft and Rockets, Vol.5, No. 1, pp. 62-68, 1968.
7. Schmit, L. A., Morrow, W. M., and Kicher, T. P., "Structural Synthesis Capability for Integrally Stiffened Cylindrical Shell Shells", AIAA Paper 68-327, Palm Springs, California, 1968.
8. Kicher, T. P. and Chao, T. L., "Minimum Weight Design of Stiffened Fiber Composite Cylinders", Journal of Aircraft, Vol. 8, No. 7, pp. 562-568, 1971.

9. R. M. Verette, "Stiffness, strength and stability optimization of laminated Composite", Report NOR-70-138, Northrop Aircraft Corp., Hawthorne, California, 1970.
10. Morz Z., "Optimal Design of Structures of Composite Materials", Int. J. Solids & Struct., Vol. 6, pp. 559, 1970.
11. Bryzgalin, G. J. "On some Optimal Design Criteria of Inhomogeneous anisotropic bodies", J. Appl. Maths & Mech., Vol. 36, pp. 716, 1972.
12. Love P.G. and Melchers R. E., "On the Theory of Optimal Constant Thickness Fiber Reinforced plates", Int. J. Mech. Sc. Vol.19, pp.311, 1972.
13. Lai Y.S. and Achenbach J. D., "Optimal Design of Layered Structures under Dynamic Loading", Int. J. Mech. Sc., Vol. 3, pp. 559, 1973.
14. Khot N.S. and others, "Optimization of Fiber Reinforced Composite Structures", J. Solids Struct. , Vol.19, pp. 1225, 1973.
15. Schmit Jr. L. A. and Farshi B., "Optimum Laminate Design for Strength and Stiffness", Int. J. Numer. Meth. Eng., Vol. 4, pp. 519, 1973.
16. Schmit Jr. L. A. and Farshi B., "Optimum Design of Laminated Fiber Composite Plates", Int. J. Numer. Meth. Eng., Vol. 7, pp. 623, 1977.
17. Hayashi T., "Optimization for Elastic Buckling Strength of Fiber Reinforced Composite Structures-Columns, Plates and Cylinders", Proc.Soc. Mat. Sc. Japan, pp. 399, 1974.
18. Chao C.C. and others, "Optimization of Buckling and Yield Strengths of Laminated Composites", J. AIAA, Vol. 13, pp. 1131, 1975.

19. Hayashi T., "Optimization Design of Cross- and Angle-Plied Laminated Composite Plates under Compression", Proc. Composite Materials Structures. Japan, pp. 18, 1974.
20. Bert C. W., "Optimal Design of Composite Materials Panels for Business Aircraft Meeting", Wichita, Kansas, Vol.1, 1977.
21. Housner, J. M. and Stein, M., "Numerical Analysis and Parametric Studies of the Buckling of Composite Orthotropic Compression and Shear Panels", NASA TN D-7996, 1975.
22. Hirano Y., "Optimum Design of Laminated Plates under Axial Compression", J. AIAA, Vol. 17, pp. 1017, 1979.
23. Bert C.W., "Optimal Design of a Composite Material Plate to Maximize its Fundamental Frequency", J. Sound & Vibration, Vol. 50, pp. 229, 1977.
24. Bert, C. W. "Design of Clamped Composite Material Plates to Maximize Fundamental Frequency", J. of Mech. Des. ASME, Vol. 100, pp. 274, 1978.
25. Adali, S. "Design of Shear-Deformable Antisymmetric Angle-Ply laminates to Maximize the Fundamental Frequency and Frequency Separation, Comp. Struct. Vol. 2, pp. 349, 1984.
26. Pedersen, P., "On Sensitivity Analysis and Optimal Design of Specially Orthotropic laminates", Proc. ASI CAD, Troia, Portugal, pp. 170, 1986.
27. Pedersen, P., "On Sensitivity Analysis and Optimal Design for laminates", In "Mechanical Behavior of Composites and Laminates" (eds. Green and Micunovic), Elsevier, pp. 274, 1987.

28. Joshi S.P., Iyengar N. G. R. "Studies on Optimization of laminated composite Plates ", Proc. 13 ICAS Cong., AIAA Sys. Conf, pp. 607, 1982.
29. Soni P.J., Iyengar N.G.R. "Optimal Design of Clamped Laminated Plates", J. Fibre Sci. & Tech., Vol.19, pp. 281, 1983.
30. Joshi S.P., Iyengar N.G.R. "Optimal Design of Laminated Composite Plates under Axial Compression", Trans. Can. Soc. Mech. Eng., Vol.9, pp. 45, 1986.
31. Khot, N. S., "Computer Program (OPTCOMP) for Optimization of Composite Structures for Minimum Weight Design", AFFDL TR-76-149, Wright-Patterson Air Force Base, Dayton, OH, 1977.
32. McKeown, J. J., "Optimal Composite Structures by Deflection-Variable Programming, Comput. Meths. Appl. Mech. Engrg., Vol.12, pp. 155, 1977.
33. Starnes, J.H. and Haftka, R.T., "Preliminary Design of Composite Wings AIAA, ASME Structures, Structural Dynamics and Material Conference, Bethesda, MD, 1978.
34. Schmit, L.A. and Mehrinfar, M., "Multilevel Optimum Design of Structures with Fiber-Composite Stiffened-Panel Components", J. AIAA, Vol. 16, pp.5, 1980.
35. Sobieszczanski-Sovieski, J., "An Integrated Computer Procedure for Sizing Composite Airframe Structures", NASA TP 1300, NASA Langley Research Center, Hampton, VA, 1979.
36. Park, J.W., "An Optimal Design of Simple Symmetric Laminates Under the First Ply Failure Criteria", AFWAL-TR-81-4175, Air Force Materials Laboratory, 1982.

37. Donaldson, S., "Simplified Weight Saving Techniques for Composite Panels", J. of Reinf. Plastics and Composites, 1983.
38. Wurzel, D.P., "On the Optimal Design of Bidirectional Composites", AFWAL-TR-83-4060, Air Force Materials Laboratory, 1983.
39. Massard, T.N., "Computer Sizing of Composite Laminates for Strength", J. Reinf. Plastics composites, Vol. 3, pp. 300, 1984.
40. Maksimovic, S., "Optimum Design of Composite Structures", Proc. 3rd Conf. Comp. Struct, Paisley, pp. 148, 1985.
41. Tsai, S.W., "Composites design", (eds. Tsai, S. W., Massard, T. N., Susuki, I.), 1985.
42. Watkins R.I., Morris A.J., "A Multicriteria Objective Function Optimization Scheme for Laminated Composites for use in Multilevel Structural Optimization Schemes", Comp. Meth. in Eng. Vol.60, pp. 233, 1987.
43. Iyengar N.G.R., "Optimal Design of Fiber Reinforced Composite Plates", Proc. Advances in Aerospace structures, Madras, pp. 71, 1988.
44. Pedersen, P., "On Optimal Orientation of Orthotropic Materials", to appear.
45. Leissa, A.W., "Buckling of Laminated Composite Plates and Shell Panels", AFWAL-TR-85-3069, 1985.
46. Muc, A., "Optimal Fibre Orientation for Simply-supported, Angle-Ply Plates under Biaxial Compression", Comp. Struct, Vol. 9, pp. 161, 1988.
47. Reissner, E. and Stavsky, Y., Trans. ASME J. Appl. Mech. (Vol. 28)(83), pp. 402, 1961.



48. Timoshenko, S. P. and Woinowsky-Krieger, S., "Theory of Plates and Shells", McGraw- Hill, New York, 1959.
49. Cook, R. D., "Concepts and Applications of Finite Element Analysis", John Wiley, New York, 1981.
50. Reissner E., "The effect of transverse shear deformation on the bending of elastic plates", ASME, J. Appl. Mech. Vol. 12, A69-A77, 1945.
51. Mindlin, R. D., "Influence of rotatory inertia and shear deformation on flexural motions of isotropic elastic plates", ASME, J. Appl. Mech., Vol.18, 31, 1951.
52. Zienkiewicz, O. C., Taylor, R.L. and Too, J.M., "Reduced integration techniques in general analysis of plates and shells", Int. J. Num. Meth. Engng., Vol. 3, 275, 1971.
53. Pawsey, S. E., Clough, R. W., "Improved numerical integration of thick shell finite elements", Int. J. Num. Meth. Engng., Vol. 3, 545, 1971.
54. Hughes, T. J. R., Taylor, R. L. and Kanoknukulchal, W., "A simple and efficient finite element for plate bending", Int. J. Num. Meth. Engng., Vol.11, 1529, 1977.
55. Pugh, E. D. L., Hinton, E. and Zienkiewicz, O. C., "A study of quadrilateral plate bending with reduced integration", Int. J. Num. Meth. Engng, Vol.12, 1059, 1978.
56. Lee, S. W., Pian, T.H., "Improvement of plate and shell finite elements by mixed formulations", AIAA J., Vol.16, 29, 1978.

57. Hughes, T. J. R., Tezduyar, T. E., "Finite Elements based upon Mindlin plate theory, with particular reference to the four-node bilinear isoparametric element", ASME, J. Appl. Mech. Vol.48, 587, 1981.
58. Lo, K. H., Christensen, R.M., Wu, E.M., "A high order theory of plate deformation part I: Homogeneous plates", ASME, J. Appl. Mech., Vol.44, 663, 1977.
59. Lo, K. H., Christensen, R.M., Wu, E.M., "A high order theory of plate deformation part II: Laminated plates", ASME, J. Appl. Mech., Vol. 44, 669, 1977.
60. Reissner, E., "On transverse bending of plates, including the effects of transverse shear deformation", Int. J. Solids Struct., Vol. 11, pp. 569, 1975.
61. Kant, T., Owen, D. R. J., Zienkiewicz, O. C., "A refined higher order Co plate bending element", Comput. Struct., Vol. 15, 177, 1982.
62. Reddy, J. N., "A simple higher order theory for laminated composite plates", ASME J. Appl. Mech., Vol. 51, 745, 1984.
63. Pandya, B. N., Kant, T., "A refined higher order generally orthotropic Co plate bending element", Comput. Struct., Vol. 28, 119, 1988.
64. Lakshminarayana, H.V., Ramani, T. S., "On improving the performance of a shear-flexible triangular laminated composite plate finite element", Proc. Int. Conf. Com. Mat. and Struct., Madras, 1988.
65. Prathap, G., Somashekar, B.R., "A field-consistent 8-noded laminated anisotropic plate element", Proc. Int. Conf. Com. Mat. and Struct., Madras, 1988.

66. Tessler, A., "An improved higher-order theory for orthotropic plates", Proc. Rev.Mech. Comp, Bal Harbour, Florida, 1988.
67. Miravete, A., "A Simple Finite Element Formulation for Three-Dimensional Laminated Composite Plates", Proc.5th Conf. Comp. Struct., Paisley, Scotland, 1989.
68. Zienkiewicz, O. C., "The finite element method", McGraw Hill, New York,1967.
69. Noor, A. K., Mathers, M. D., "Shear flexible finite element models of laminated composite plates", NASA TN D-8044, 1975.
70. Miravete, A, "The finite element Method applied to composites", Escribano, Zaragoza, Spain, 1987.
71. Tsai, S. W. and Hahn, H. T., "Introduction to Composite Materials", Technomic, Westport Com., pp. 457, 1980.
72. Tsai, S.W. and Wu, E. M., "A general Theory of Strength for Anisotropic Materials", J. Composite Mat, Vol. 5, pp. 58, 1971.
73. Khot N. S., Venkayya V. B., Berke L. "Optimum Design of Structures with Stress and Displacement Constraints", AIAA Journal, Vol. 14, pp. 131-132, 1976.
74. Roy, A. K. and Tsai, S. W., "3-D Effective Moduli of Laminated Orthotropic plates", to appear in Journal of Applied Mechanics.
75. Ashton, J.E., "Analysis of Anisotropic Plates II", J. Composite Mat., Vol.3, pp. 470, 1969.

76. Miravete A., "Análisis del Comportamiento Resistente de Laminados de Poliester Reforzado y su Aplicación a los Medios de Transporte", Ph.D. University of Zaragoza, Spain, 1984.
77. Miravete A., "Caracterisation et mise au Point d'un Element Fini de Grande Precision Applicable a des Lamines de Polyester Renforce avec Fibres de Verre", Composites. Vol. 4, pp. 20, 1986.

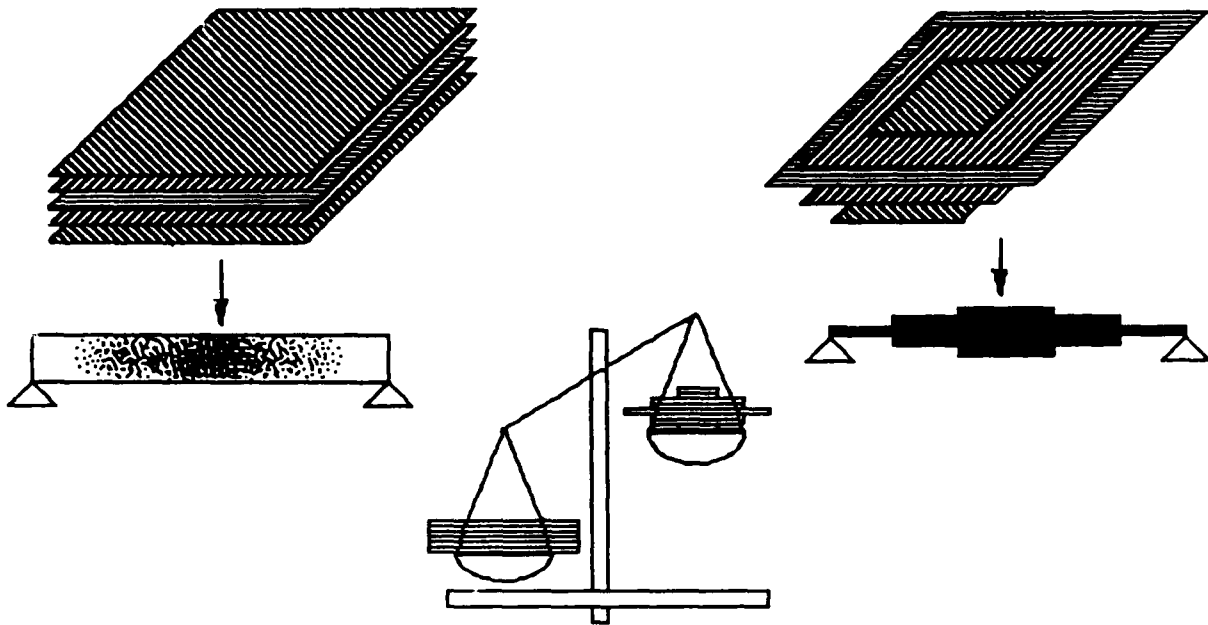


Figure 1. Schematic representation of a variable-thickness composite plate.

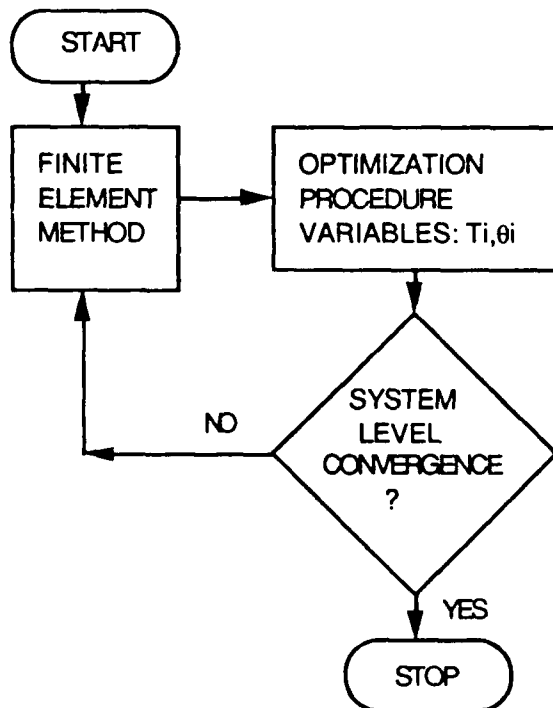


Figure 2. Representation of the optimization procedure.

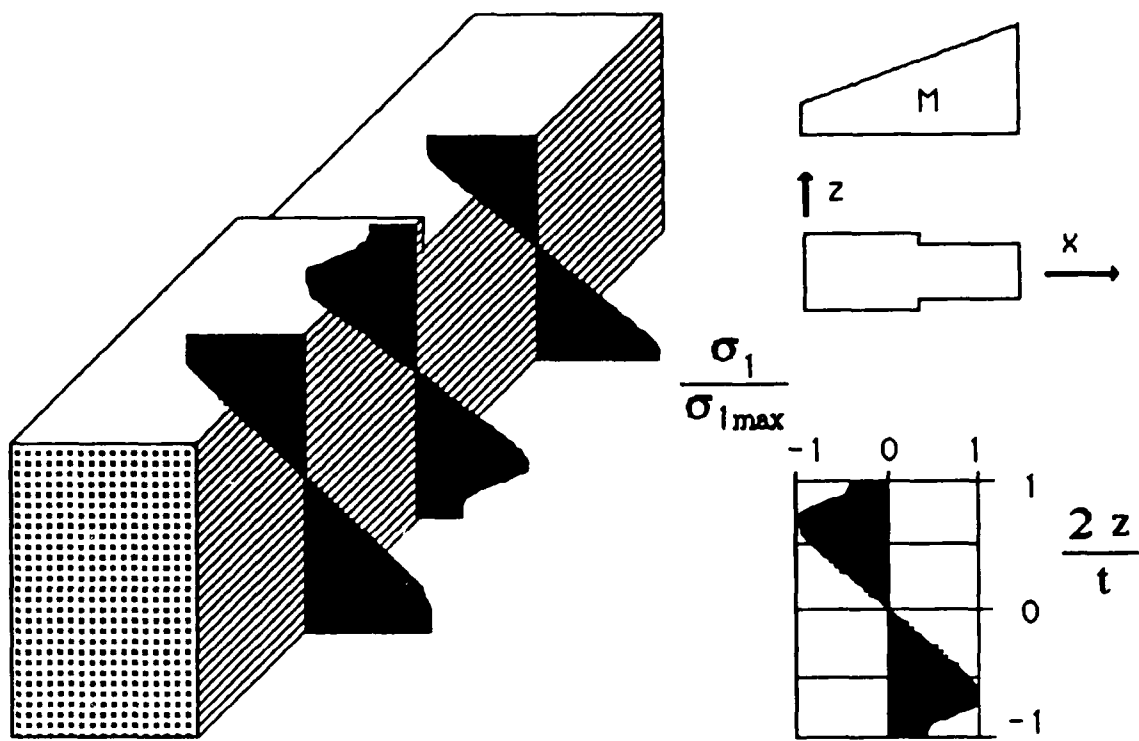


Figure 3. Distribution of  $\sigma_1$  for a two-sides tapered plate and  $\partial M / \partial x > 0$ .

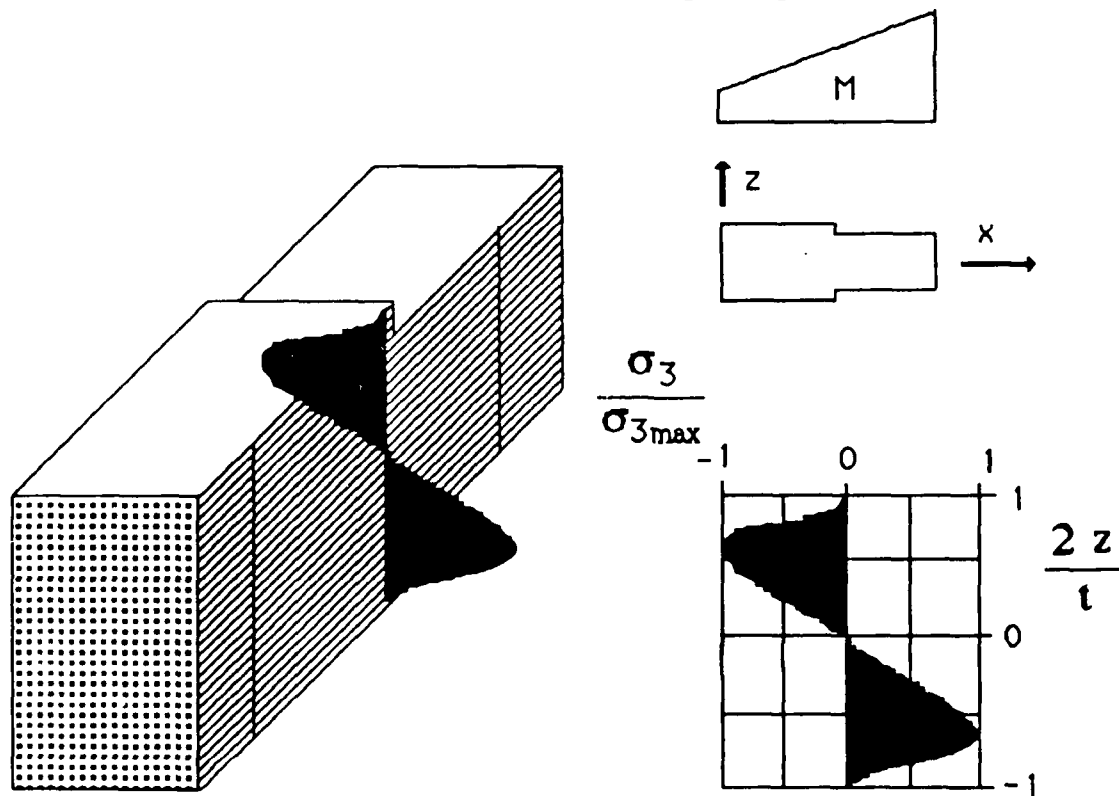


Figure 4. Distribution of  $\sigma_3$  for a two-sides tapered plate and  $\partial M / \partial x > 0$ .

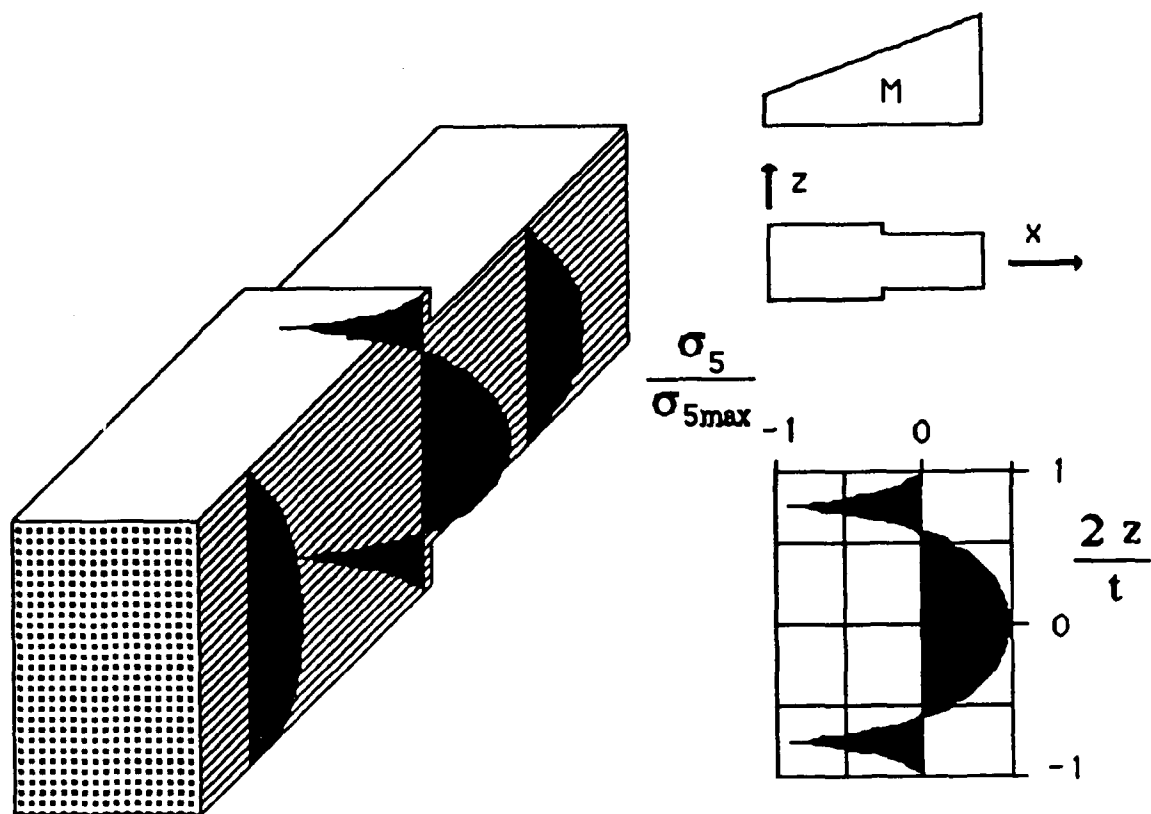


Figure 5. Distribution of  $\sigma_5$  for a two-sides tapered plate and  $\partial M / \partial x > 0$ .

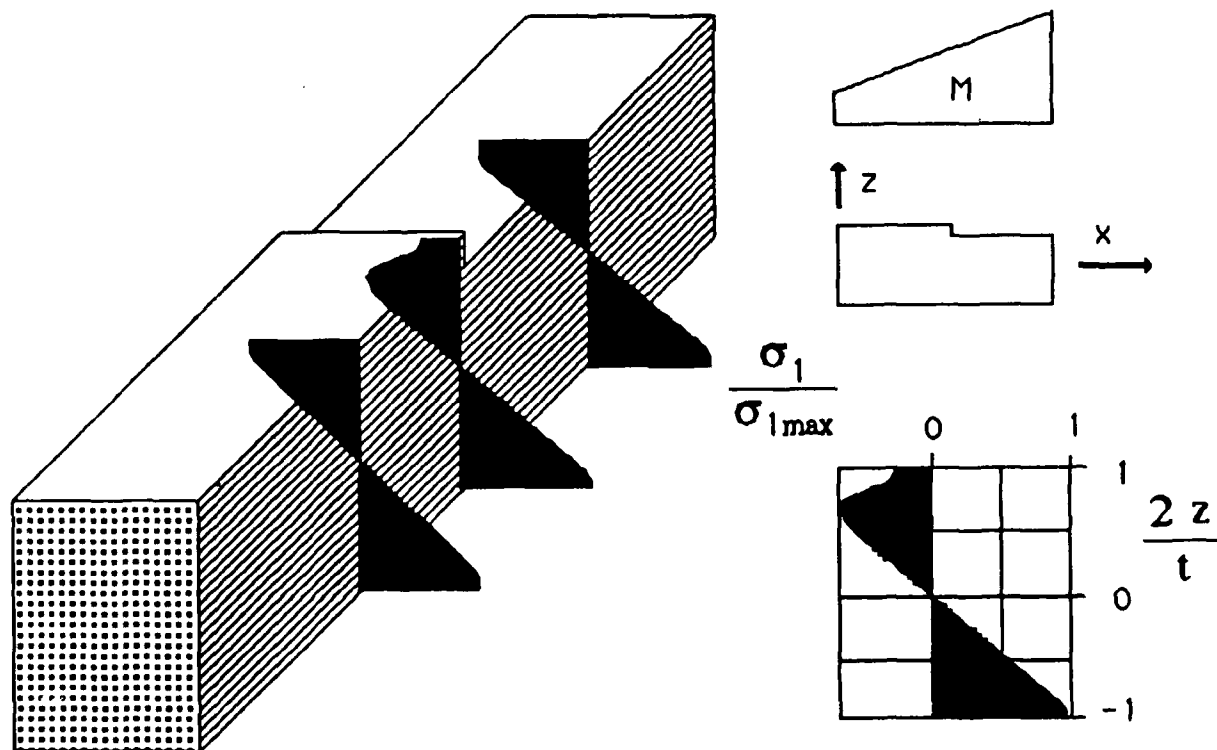


Figure 6. Distribution of  $\sigma_1$  for a one-side tapered plate and  $\partial M / \partial x > 0$ .

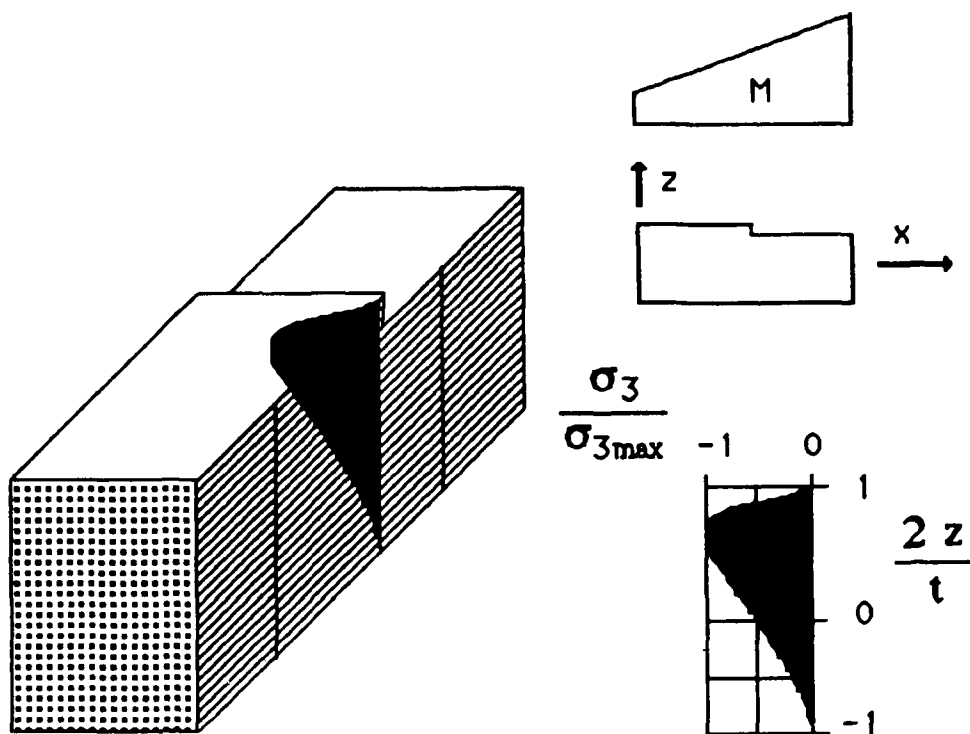


Figure 7. Distribution of  $\sigma_3$  for a one-side tapered plate and  $\partial M / \partial x > 0$ .

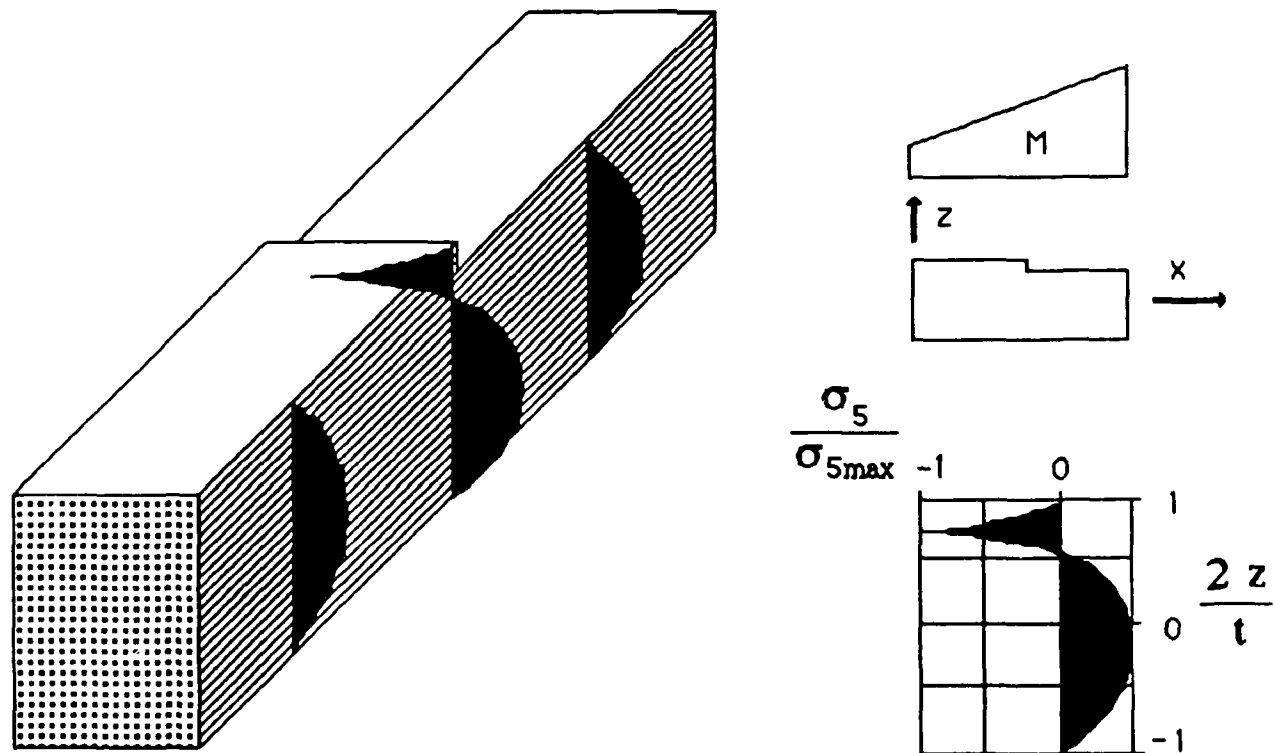


Figure 8. Distribution of  $\sigma_5$  for a one-side tapered plate and  $\partial M / \partial x > 0$ .



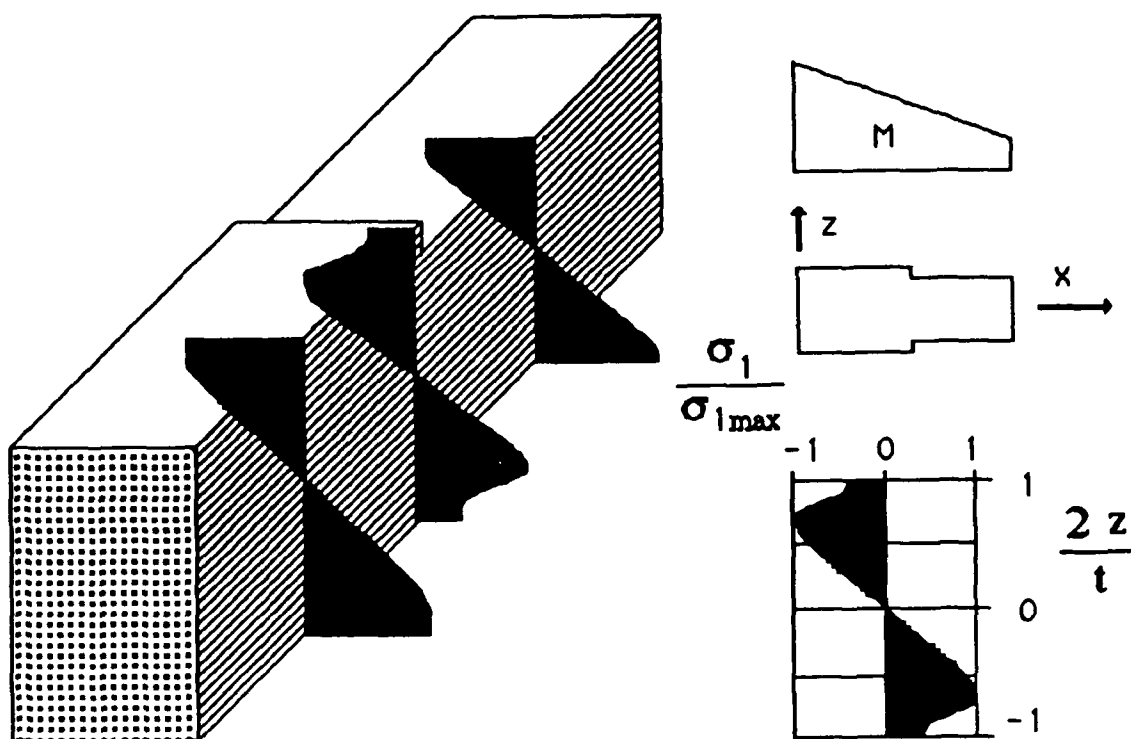


Figure 9. Distribution of  $\sigma_1$  for a two-sides tapered plate and  $\partial M / \partial x < 0$ .

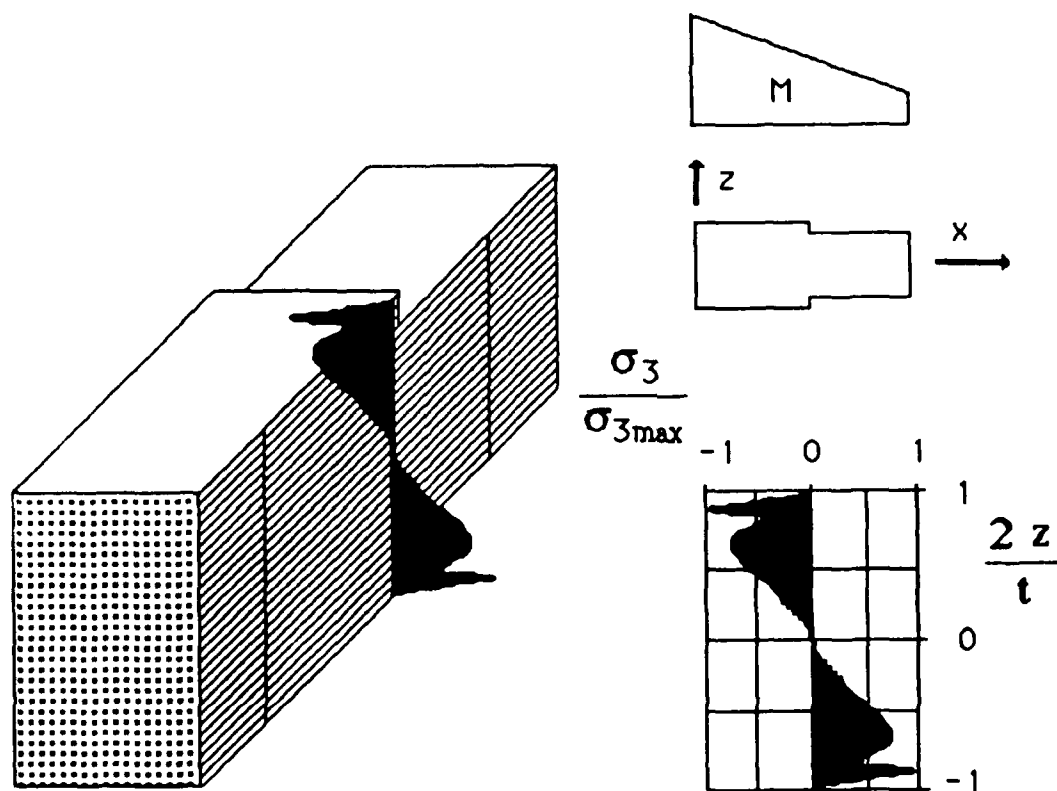


Figure 10. Distribution of  $\sigma_3$  for a two-sides tapered plate and  $\partial M / \partial x < 0$ .

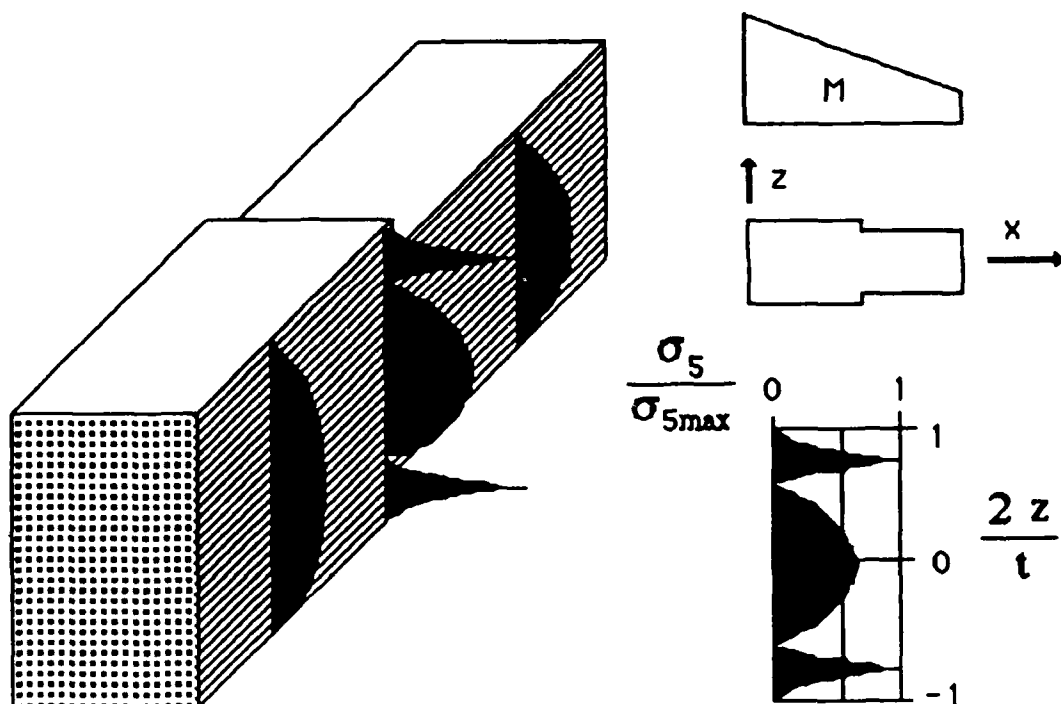


Figure 11. Distribution of  $\sigma_5$  for a two-sides tapered plate and  $\partial M / \partial x < 0$ .

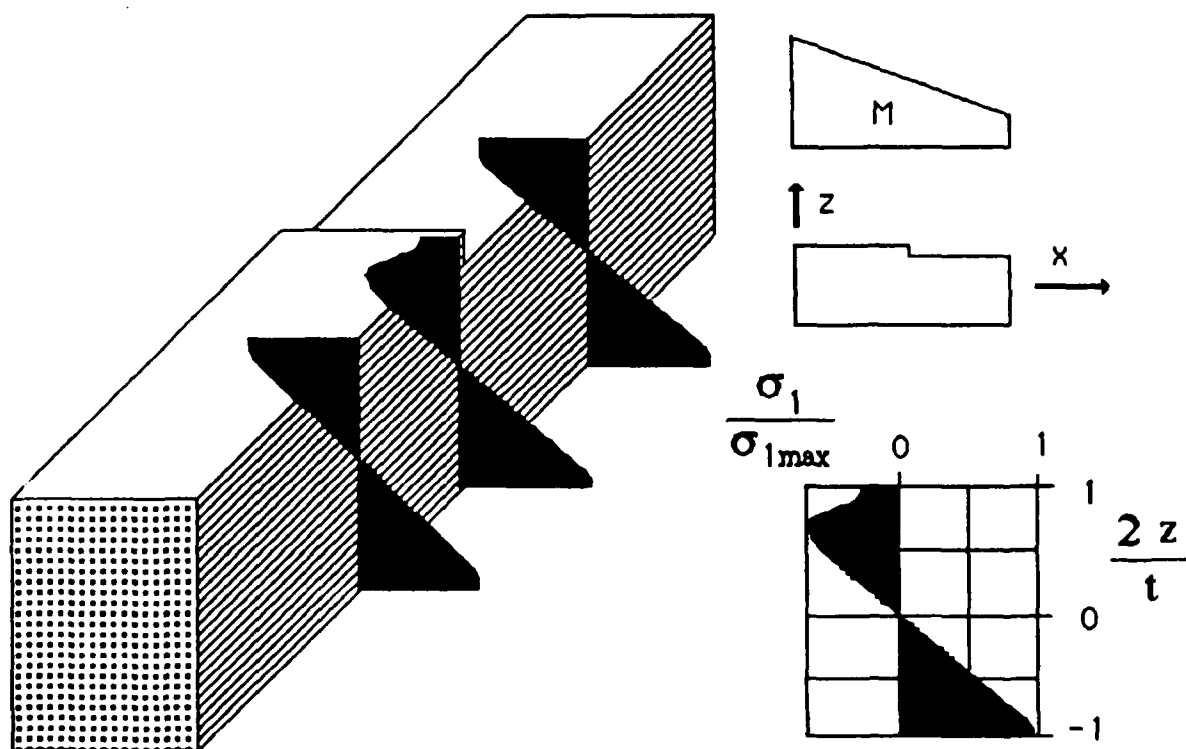


Figure 12. Distribution of  $\sigma_1$  for a one-side tapered plate and  $\partial M / \partial x < 0$ .

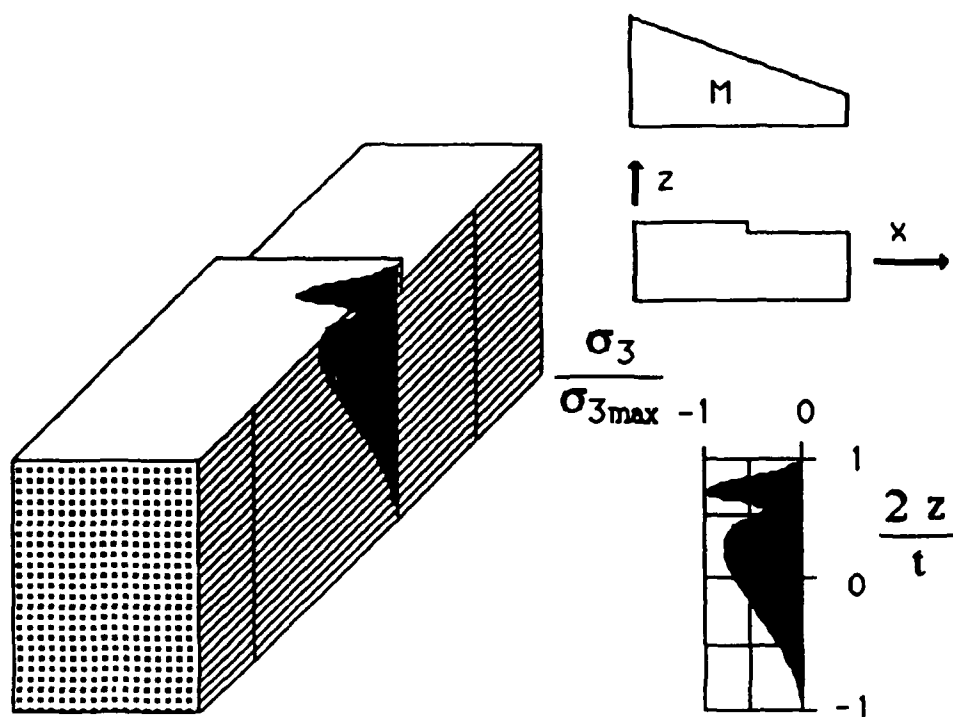


Figure 13. Distribution of  $\sigma_3$  for a one-side tapered plate and  $\partial M / \partial x < 0$ .

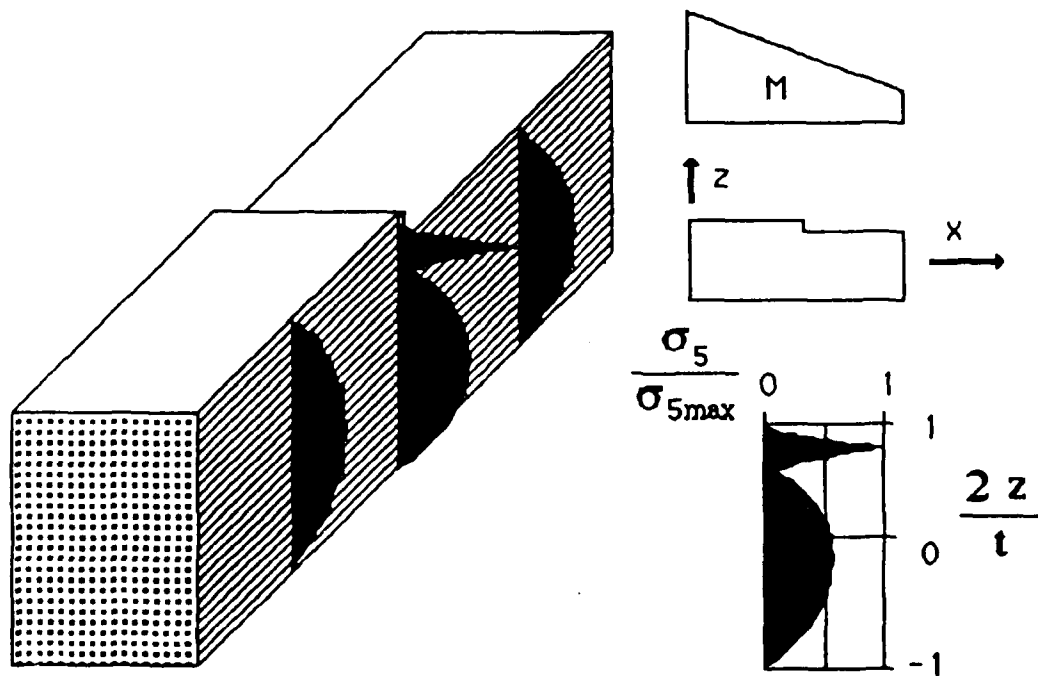


Figure 14. Distribution of  $\sigma_5$  for a one-side tapered plate and  $\partial M / \partial x < 0$ .

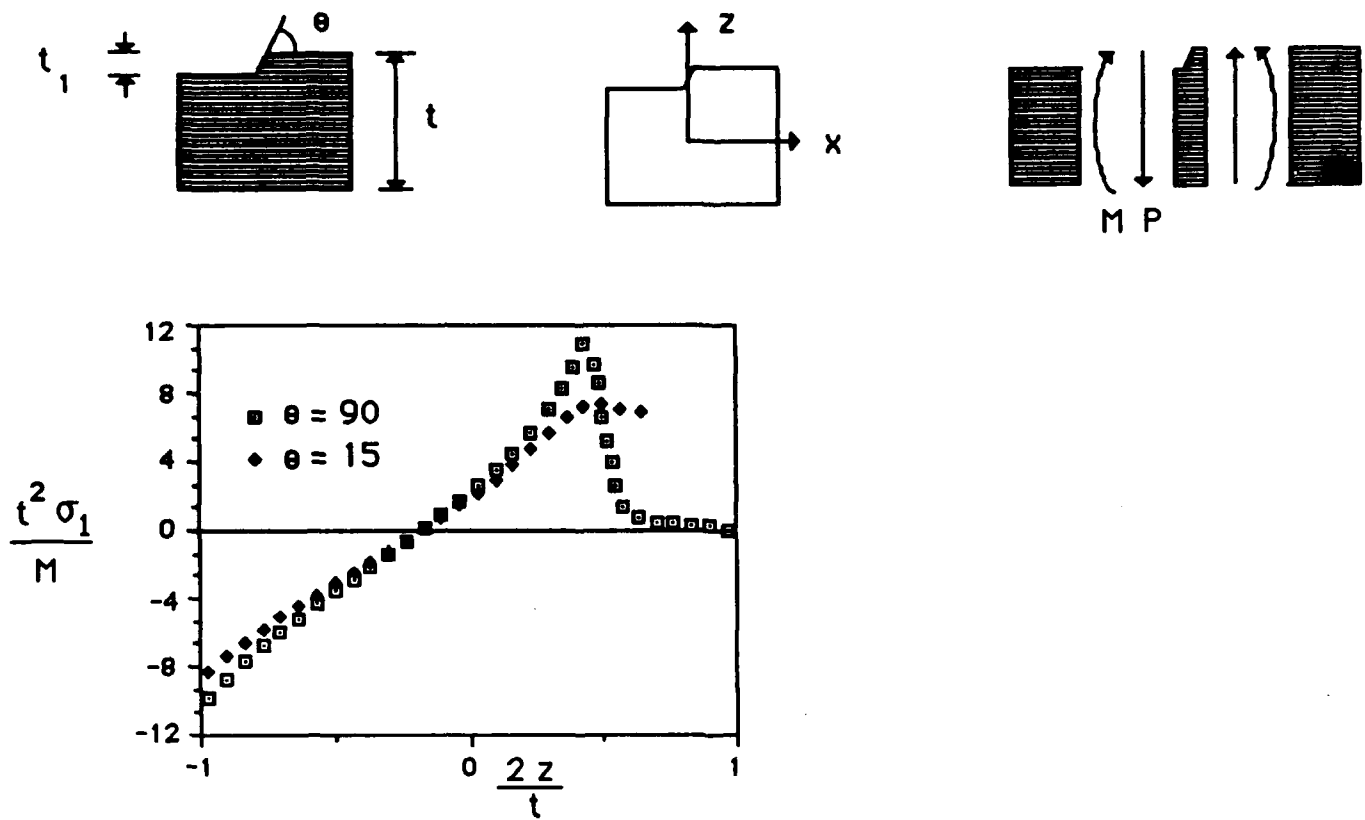


Figure 15. Distribution of  $\sigma_1$  for a one-side tapered plate,  $t_1/t=0.3$ ,  $M/Pt=5$  and  $\partial M/\partial x > 0$ .

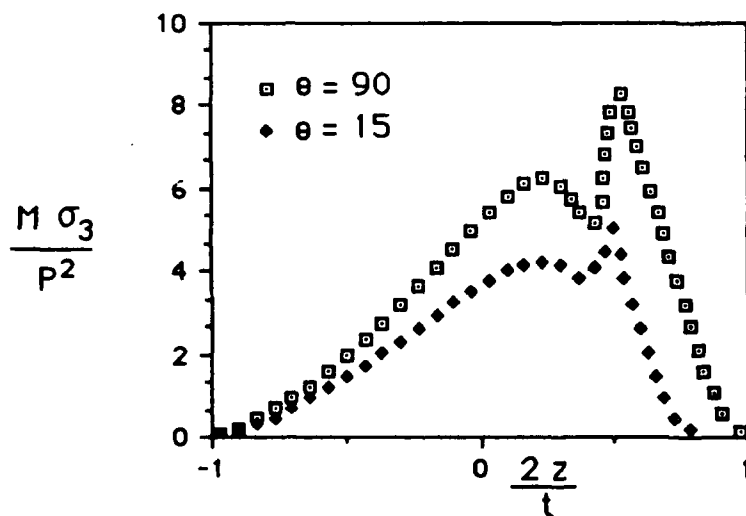


Figure 16. Distribution of  $\sigma_3$  for a one-side tapered plate,  $t_1/t=0.3$ ,  $M/Pt=5$  and  $\partial M/\partial x > 0$ .

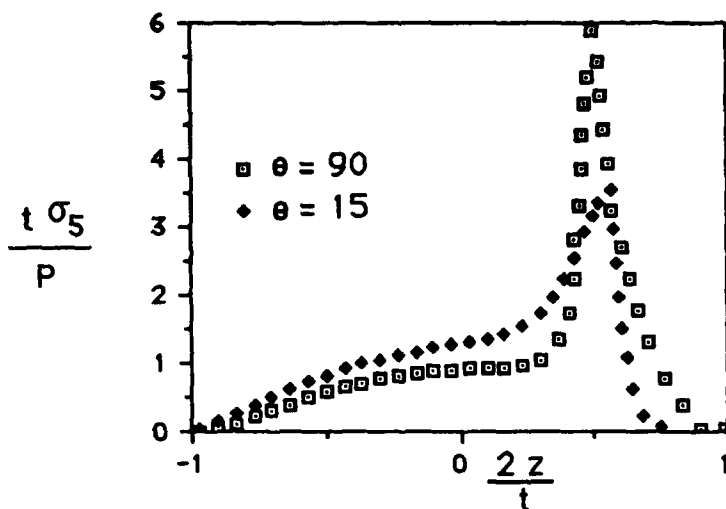
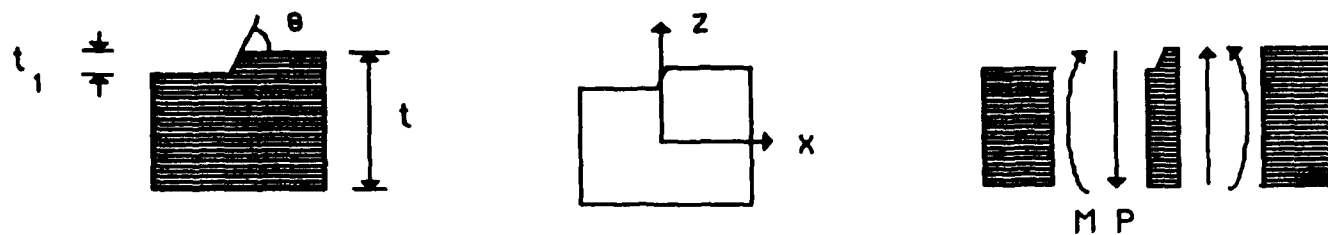


Figure 17. Distribution of  $\sigma_5$  for a one-side tapered plate,  $t_1/t=0.3$ ,  $M/Pt=5$  and  $\partial M/\partial x > 0$ .

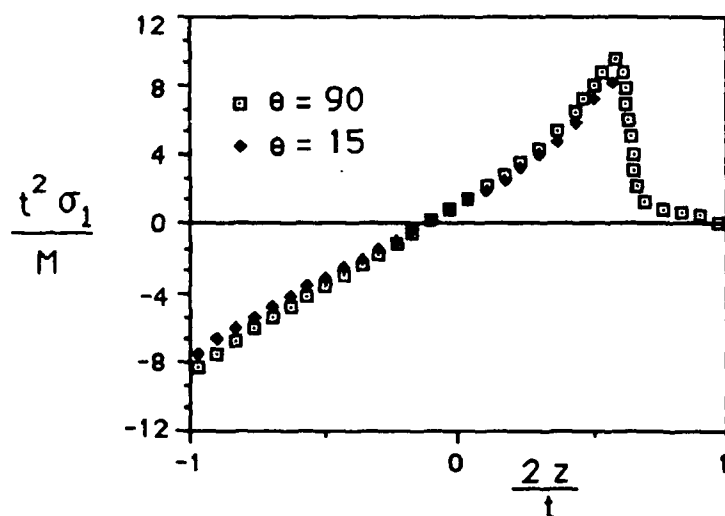


Figure 18. Distribution of  $\sigma_1$  for a one-side tapered plate,  $t_1/t=0.2$ ,  $M/Pt=5$  and  $\partial M/\partial x > 0$ .

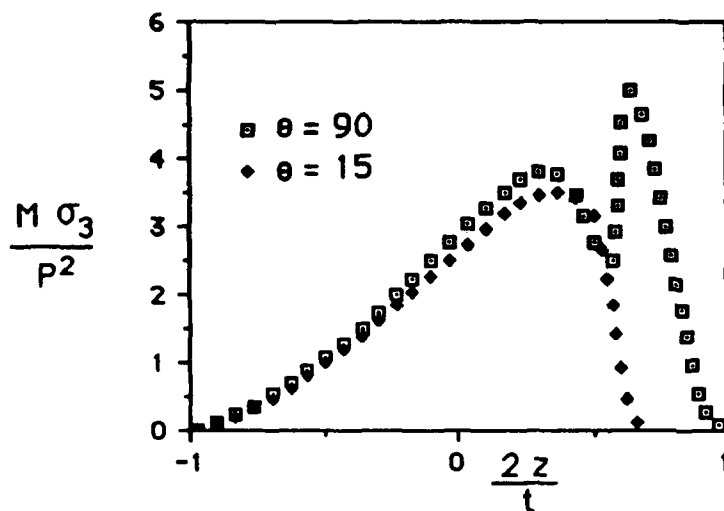
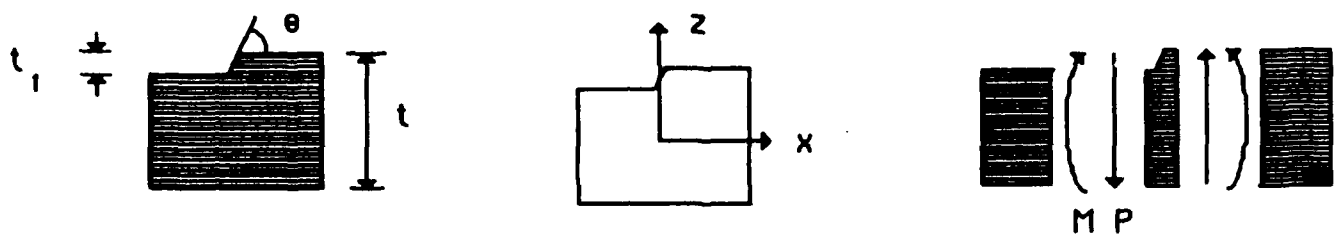


Figure 19. Distribution of  $\sigma_3$  for a one-side tapered plate,  $t_1/t=0.2$ ,  $M/Pt=5$  and  $\partial M/\partial x > 0$ .

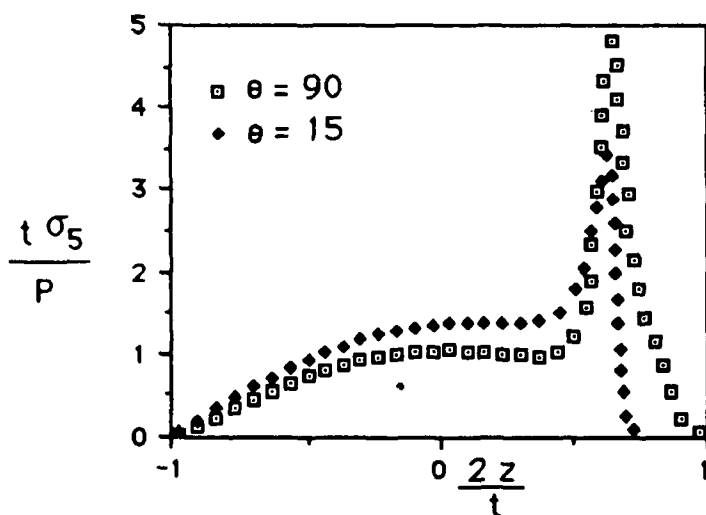


Figure 20. Distribution of  $\sigma_5$  for a one-side tapered plate,  $t_1/t=0.2$ ,  $M/Pt=5$  and  $\partial M/\partial x > 0$ .

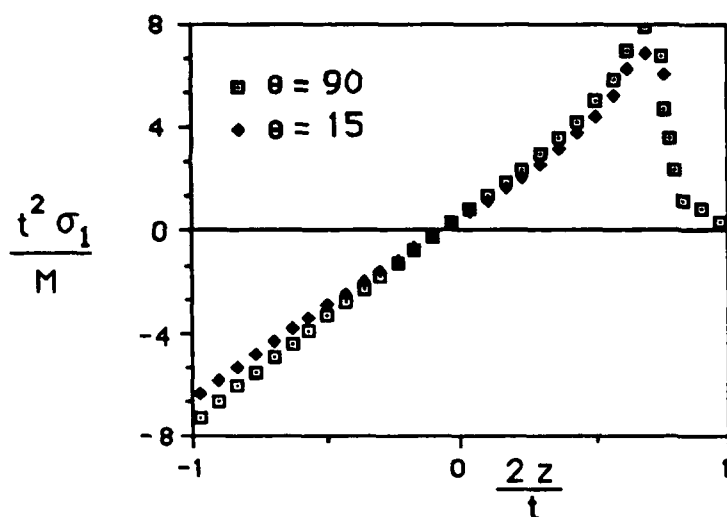
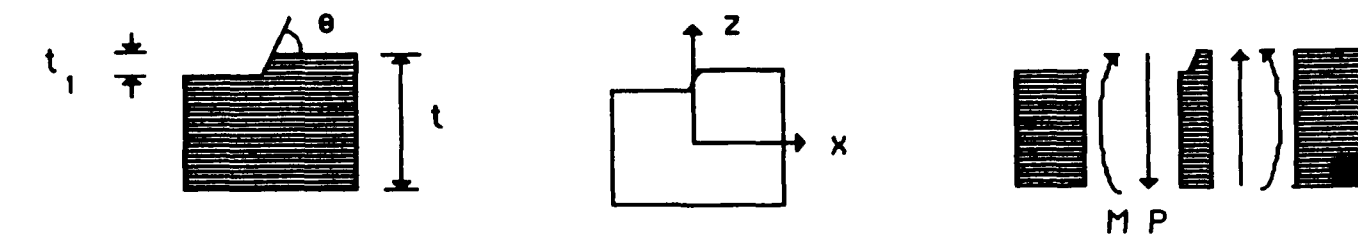


Figure 21. Distribution of  $\sigma_1$  for a one-side tapered plate,  $t_1/t=0.1$ ,  $M/Pt=5$  and  $\partial M/\partial x > 0$ .

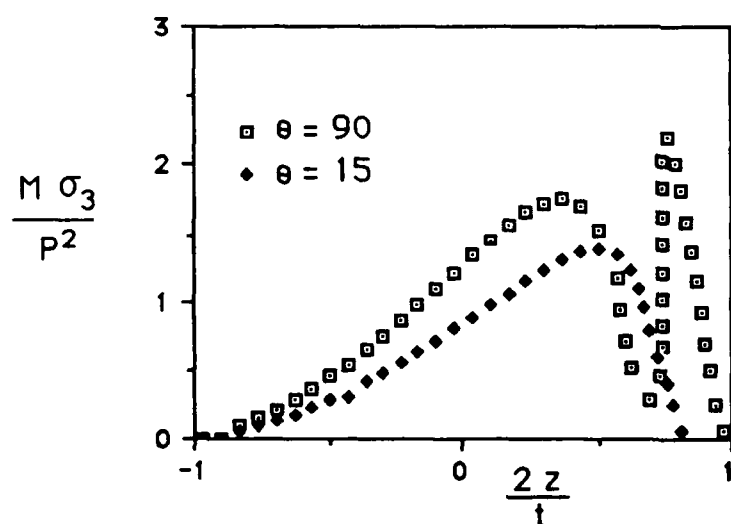


Figure 22. Distribution of  $\sigma_3$  for a one-side tapered plate,  $t_1/t=0.1$ ,  $M/Pt=5$  and  $\partial M/\partial x > 0$ .

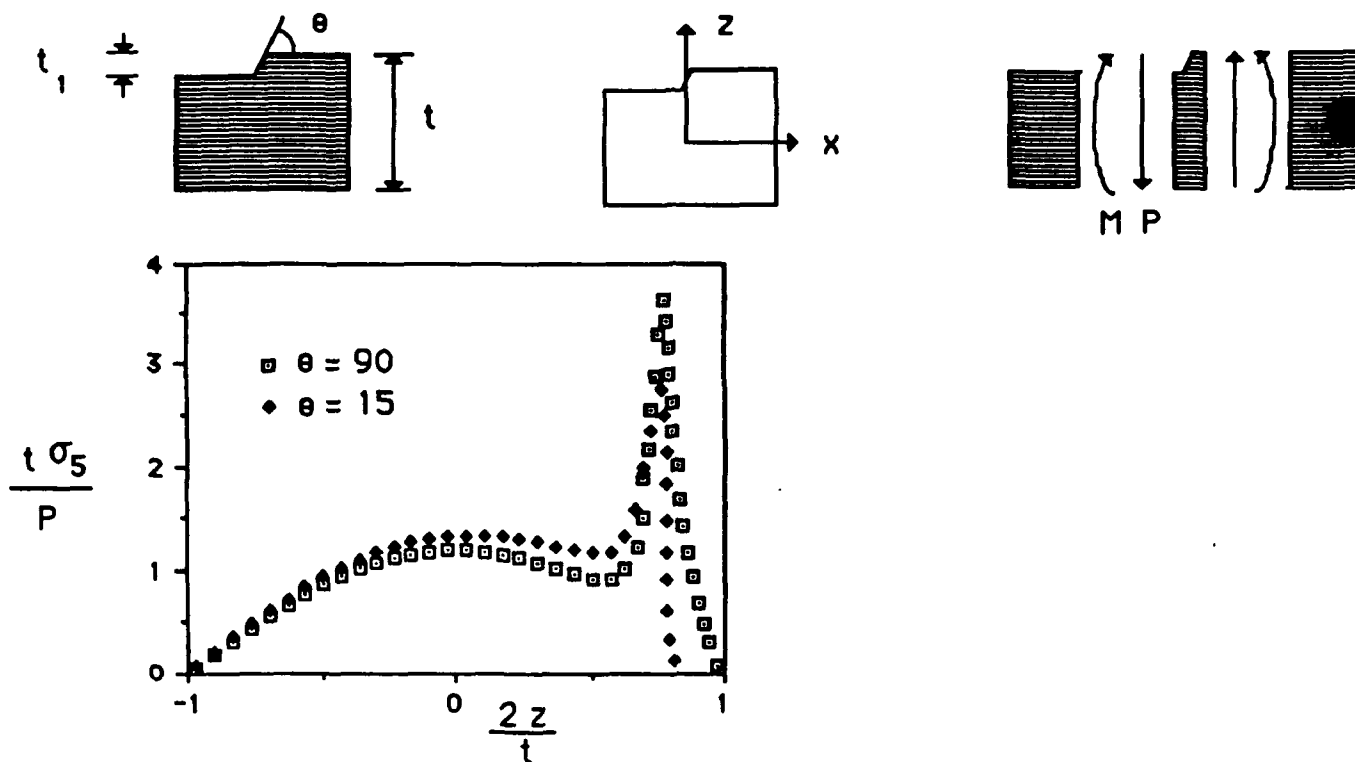


Figure 23. Distribution of  $\sigma_5$  for a one-side tapered plate,  $t_1/t=0.1$ ,  $M/Pt=5$  and  $\partial M/\partial x > 0$ .



Figure 24. Three-point bending test.



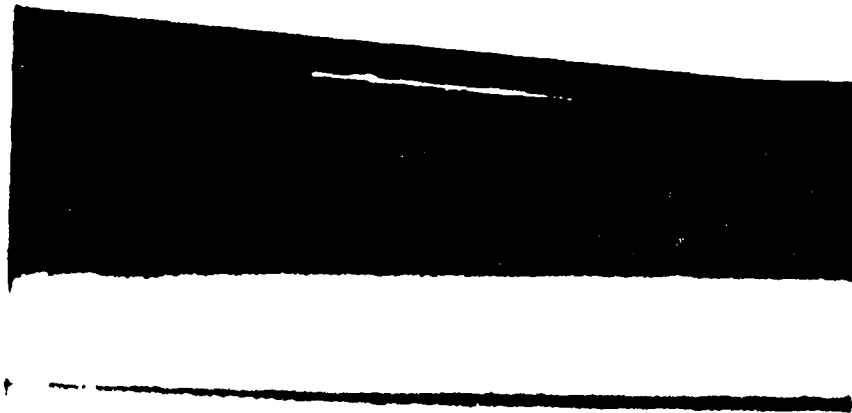


Figure 25. Delamination failure in the midplane.

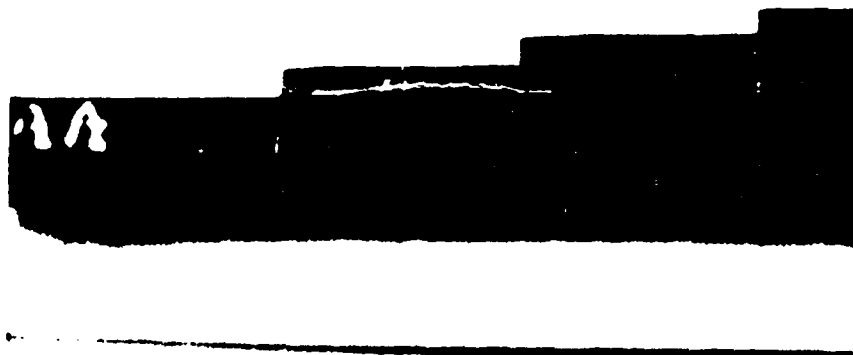


Figure 26. Delamination failure in the tapered surface.



Figure 27. SEM photograph of delamination fracture surface.



Figure 28. SEM photograph of detail of delamination fracture surface.

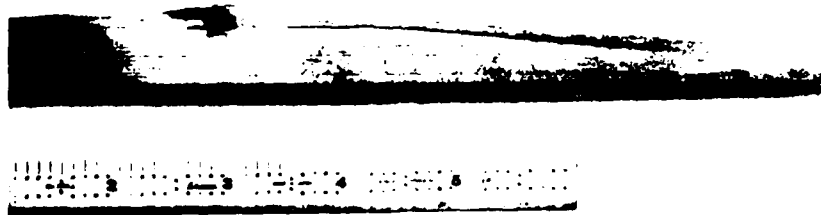


Figure 29. Photograph showing a mixed compression-interlaminar normal failure mode.

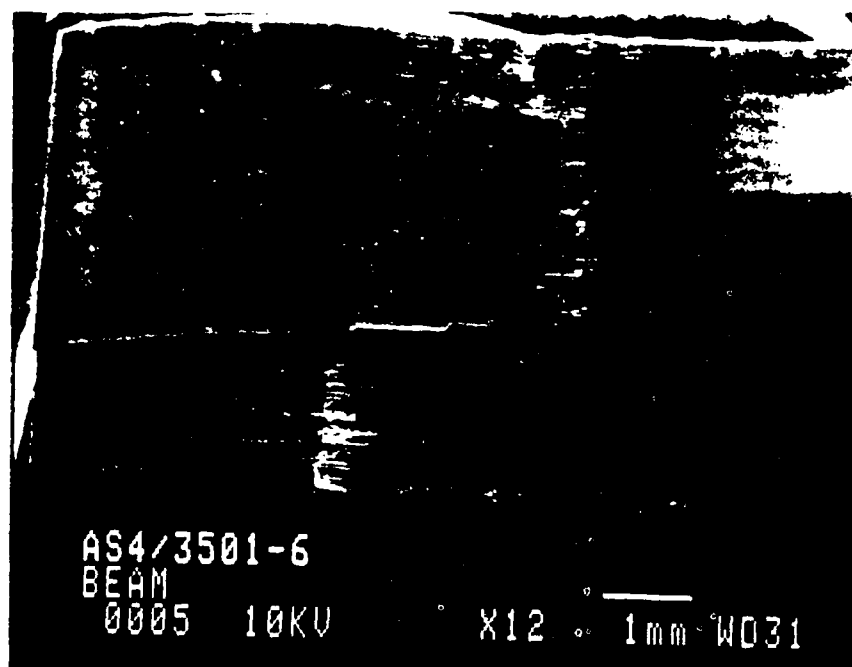


Figure 30. SEM photograph of mixed mode fracture surface

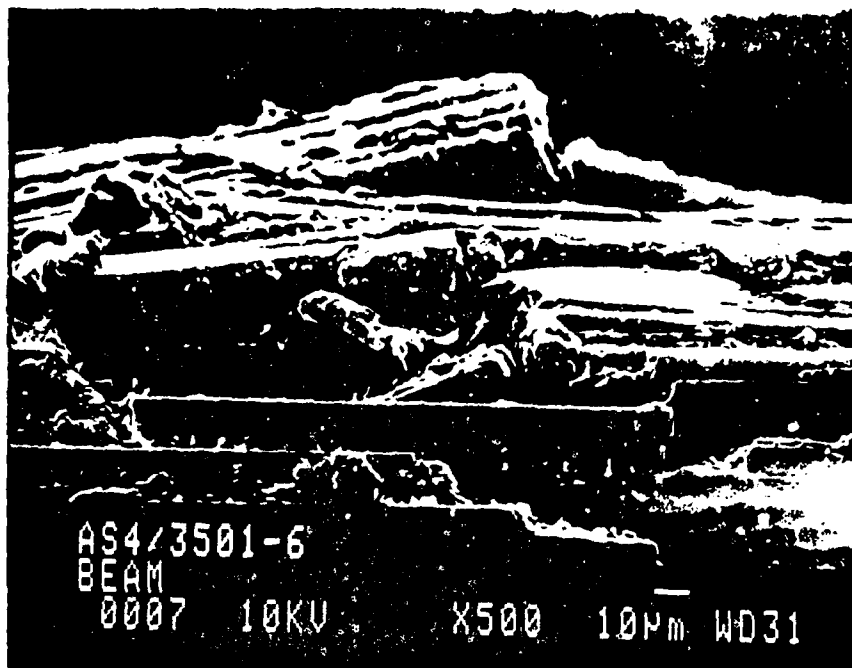


Figure 31. SEM image of top of mixed failure mode surface. Crushing due to a compressive interlaminar stress is detected.

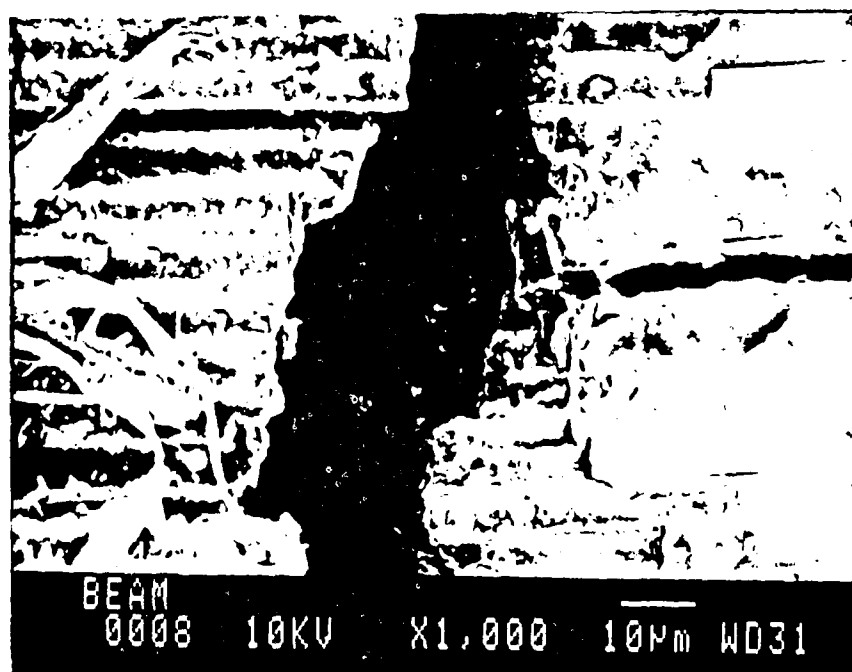


Figure 32. SEM photograph of the upper part of the mixed failure mode surface.



Figure 33. SEM photograph of the center part of the mixed failure mode surface.

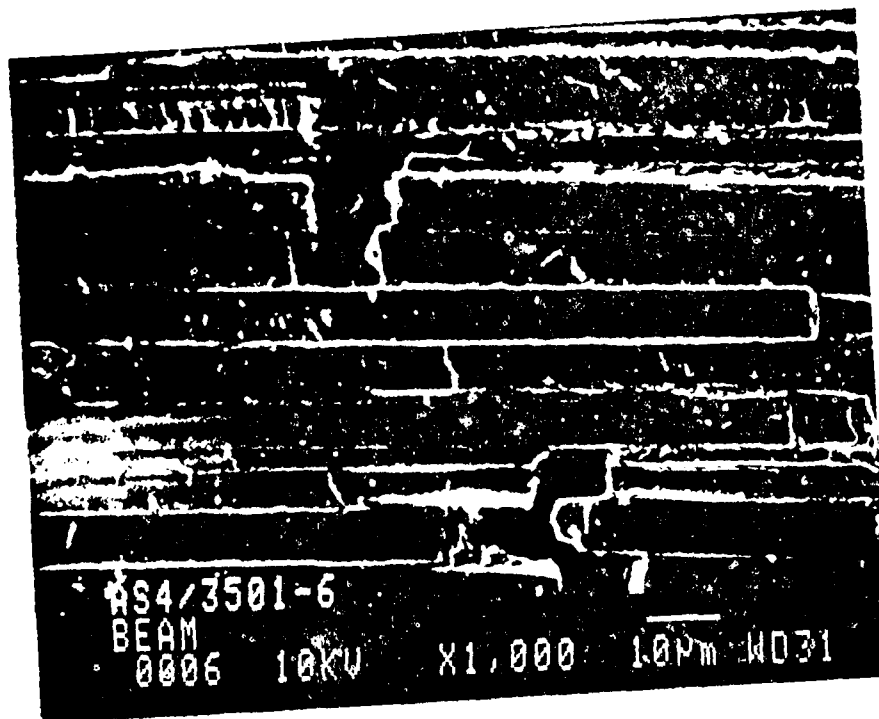


Figure 34. SEM image of the inner part of the mixed failure mode surface.

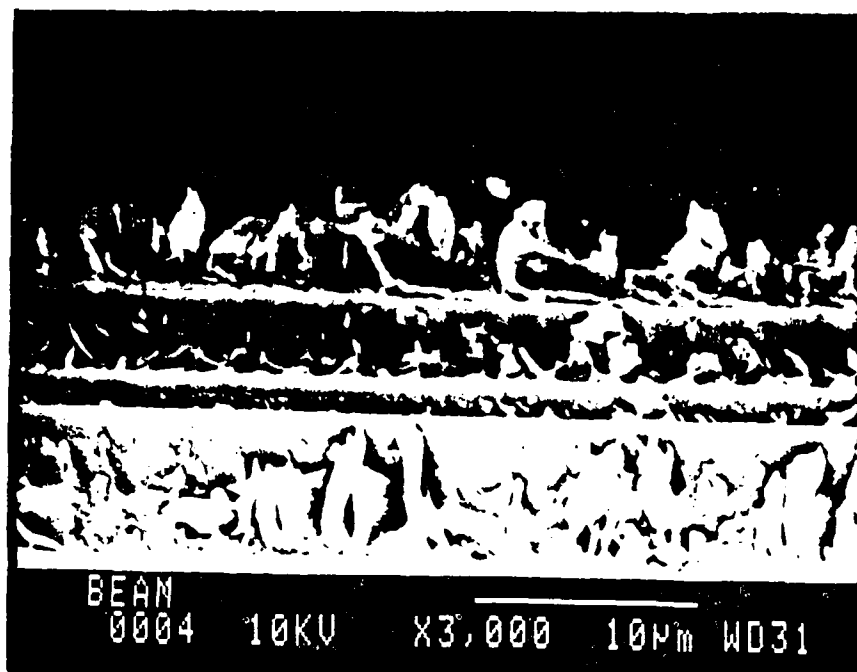


Figure 35. SEM image of the bottom of the mixed failure mode surface.

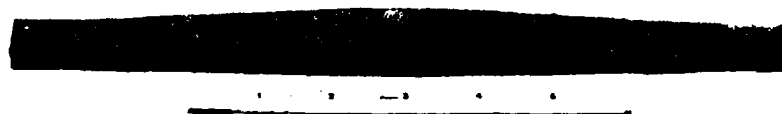


Figure 36. Photograph showing specimen OLCP\_7001.

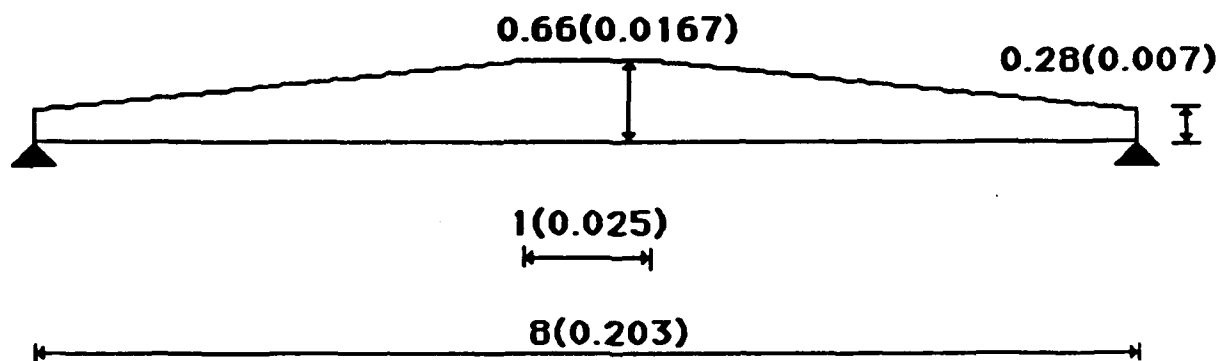


Figure 37. Measurements of specimen OLCP\_7001 in inches (meters).



Figure 38. Photograph showing detail of tapering of specimen OLCP\_7001.



Figure 39. Image of failure in specimen OLCP\_7001.

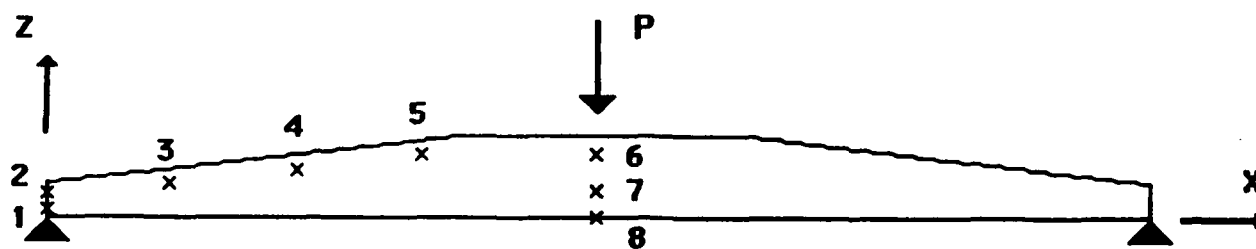


Figure 40. Representation of specimen OLCP\_7001 and position of gauges.





Figure 41. Photograph showing specimen OLC<sub>P</sub>\_7002.

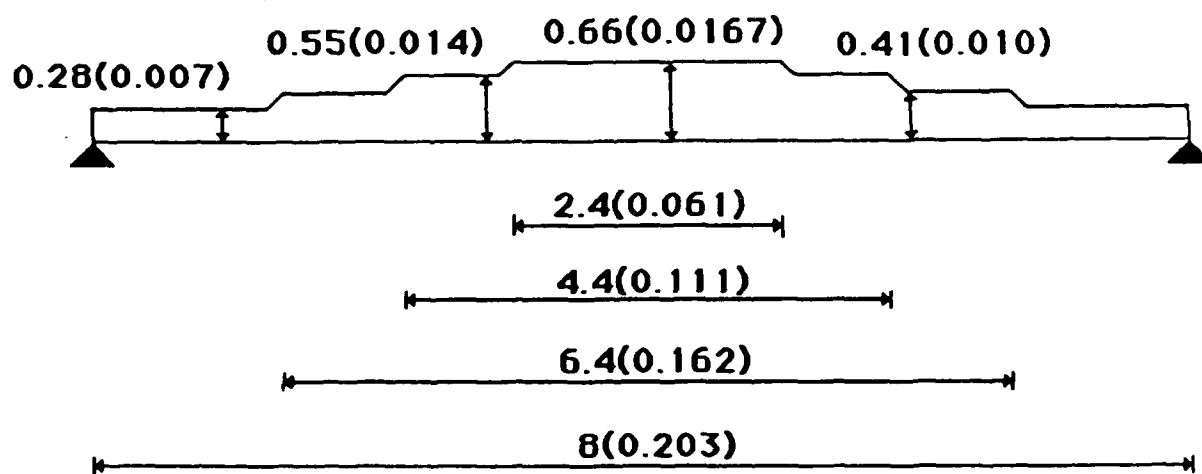


Figure 42. Measurements of specimen OLC<sub>P</sub>\_7002 in inches (meters).



Figure 43. Image of failure in specimen OLCP\_7002.

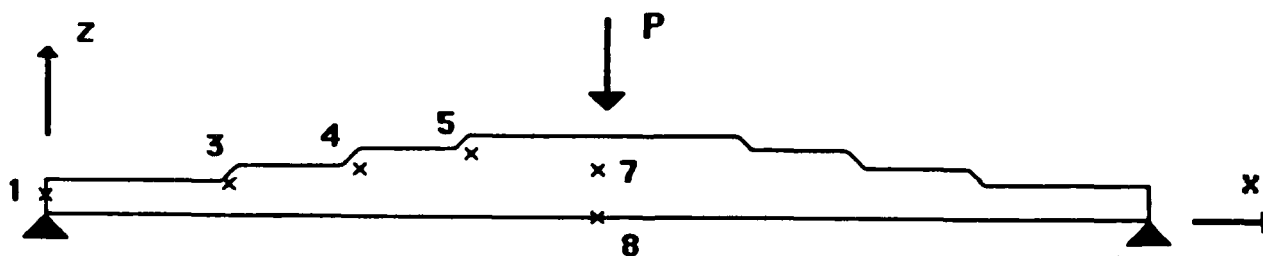


Figure 44. Representation of specimen OLCP\_7002 and position of gauges.

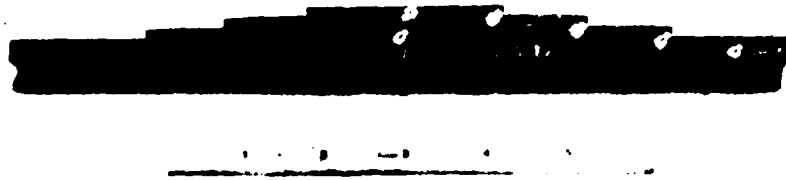


Figure 45. Photograph showing specimen OLCP\_7003.

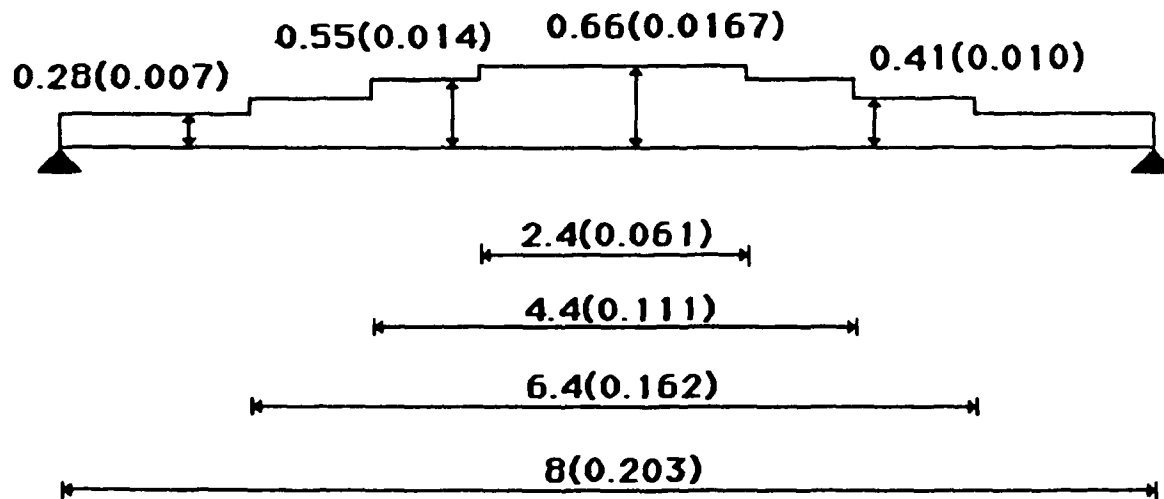


Figure 46. Measurements of specimen OLCP\_7003 in inches (meters).

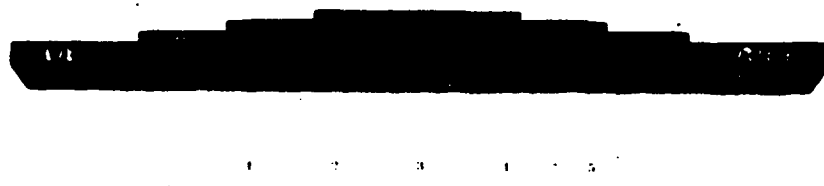


Figure 47. Image of failure in specimen OLCP\_7003.

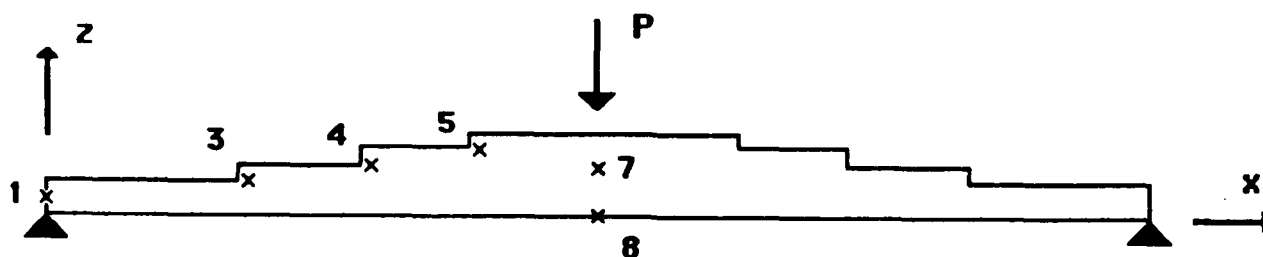


Figure 48. Representation of specimen OLCP\_7003 and position of gauges.

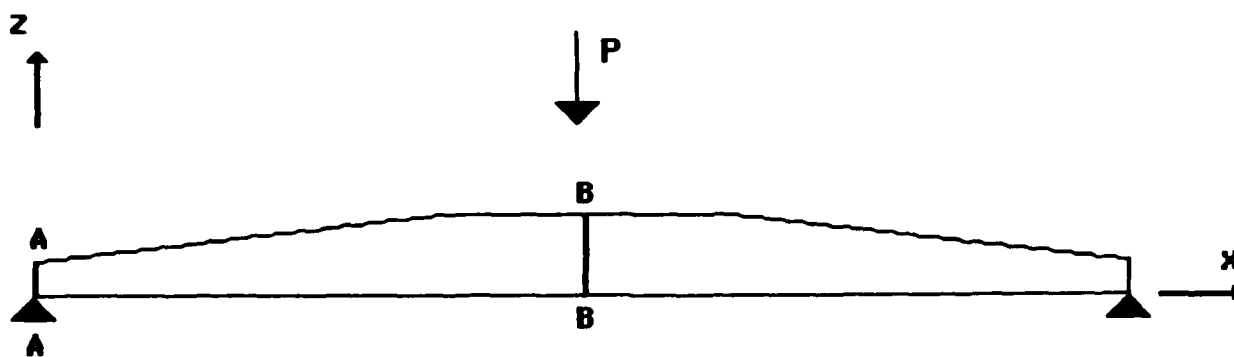


Figure 49. Representation of sections AA and BB.

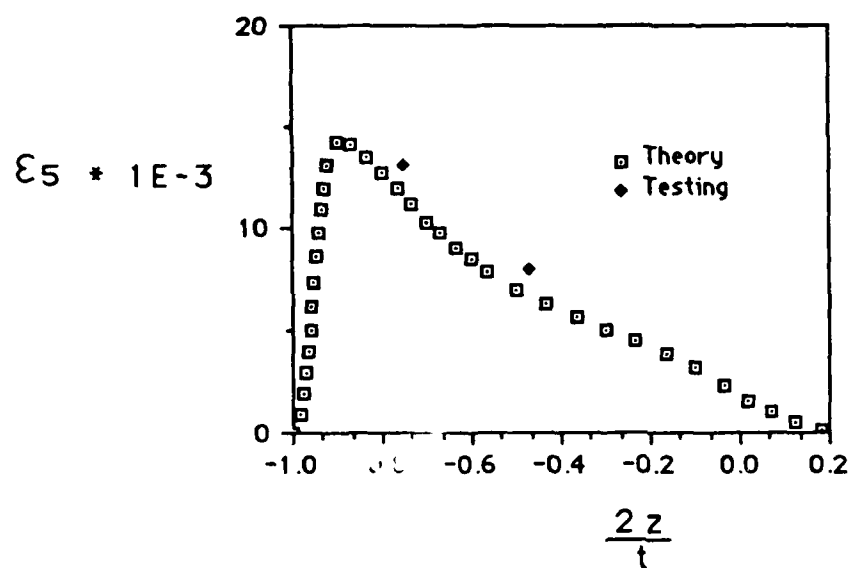


Figure 50. Distribution of  $\epsilon_5$  through the thickness in section AA

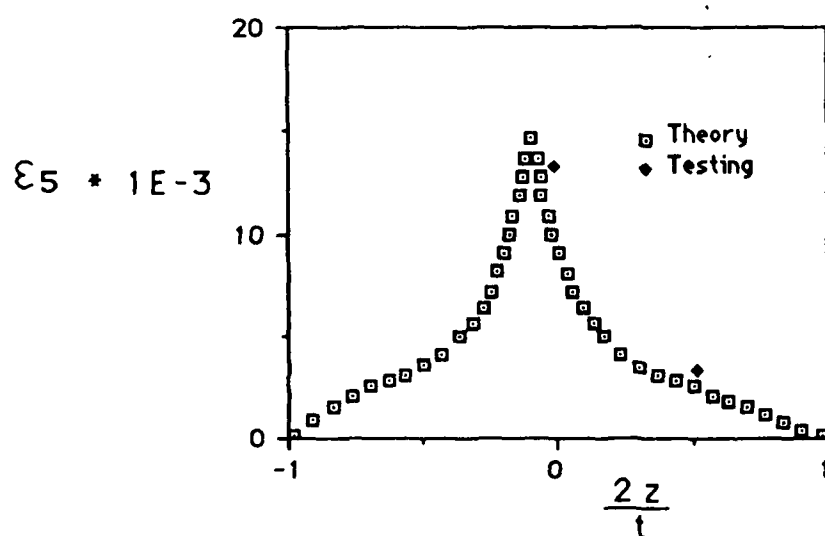


Figure 51. Distribution of  $\epsilon_5$  through the thickness in section BB.

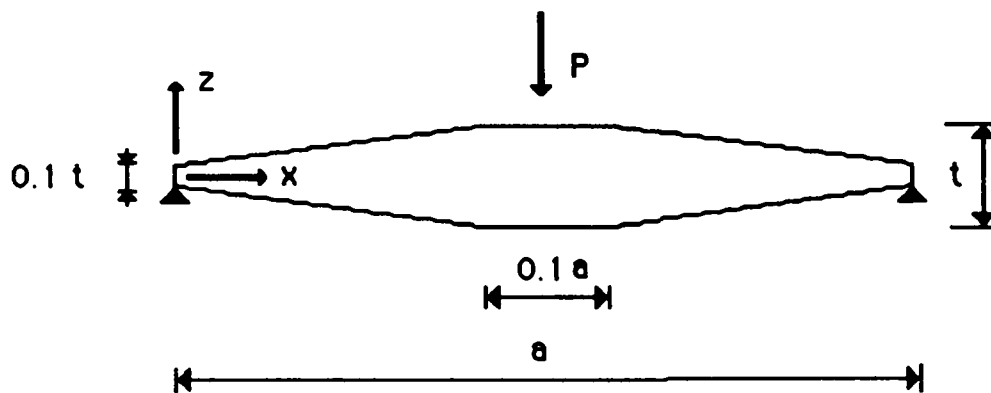


Figure 52. Description of structure used to compare both 2-D plane strain model and shear deformation plate model.

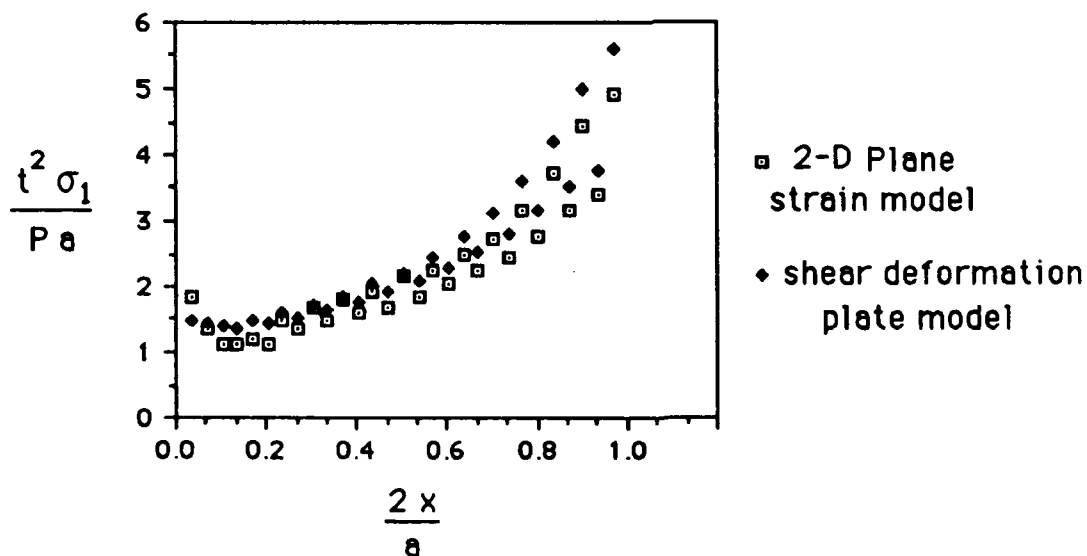


Figure 53. Distribution of  $\sigma_1$  through the thickness from a 2-D plane strain model and a shear deformation plate model.

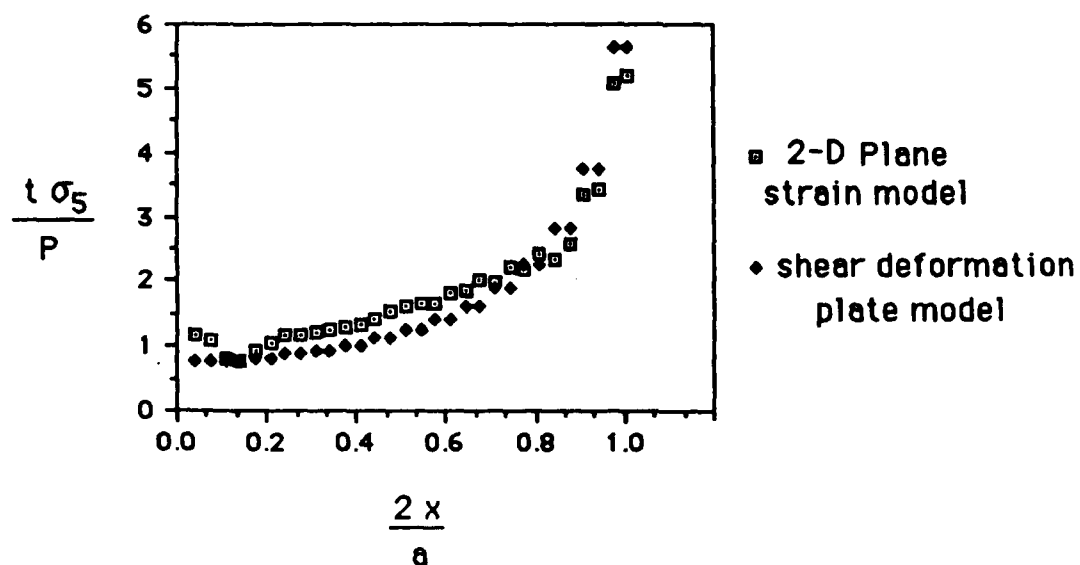


Figure 54. Distribution of  $\sigma_5$  through the thickness from a 2-D plane strain model and a shear deformation plate model.

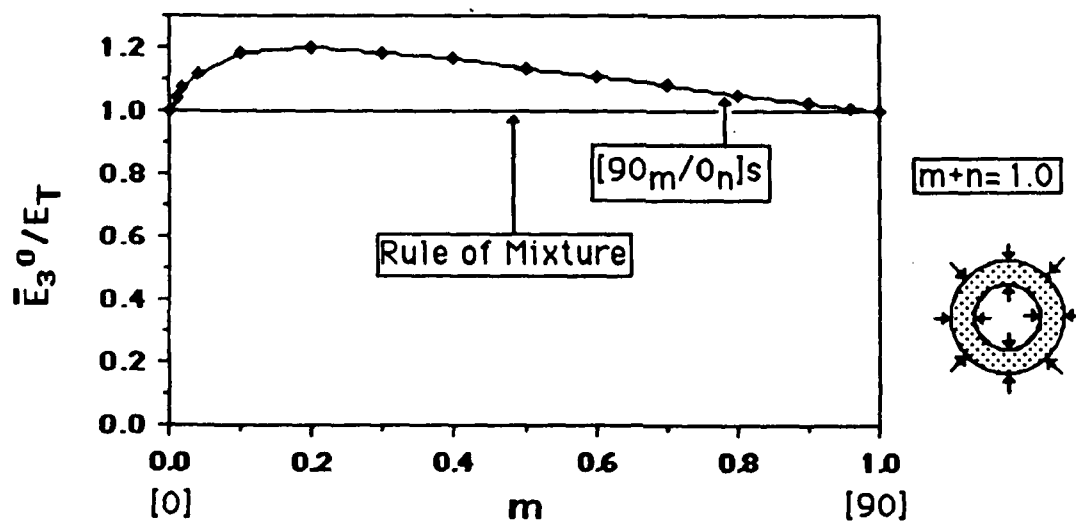


Figure 55. Variation of interlaminar normal modulus in function of  $m$  and  $n$  in a laminate T300/N5208  $[90_m/0_n]_s$ .

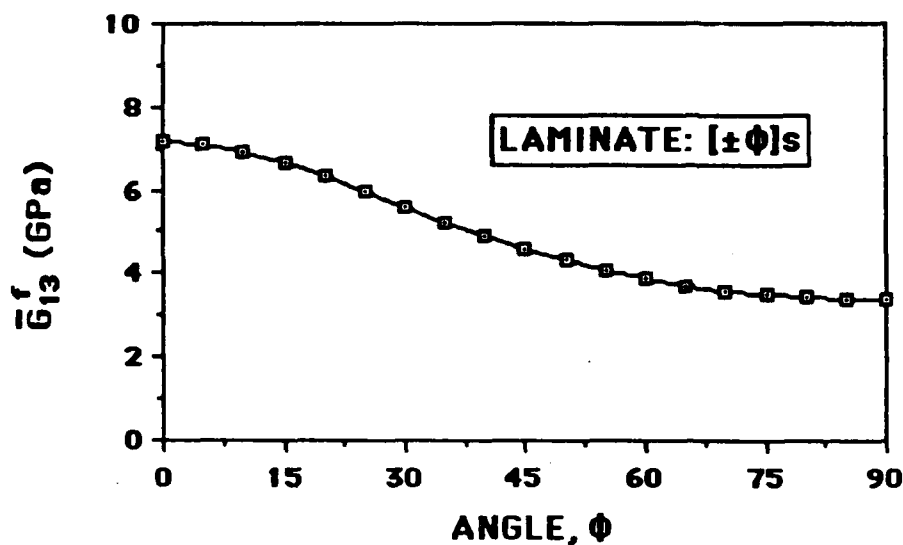


Figure 56. Variation of interlaminar shear modulus in function of  $\phi$  in a laminate T300/N5208  $[+\phi / -\phi ]_s$ .

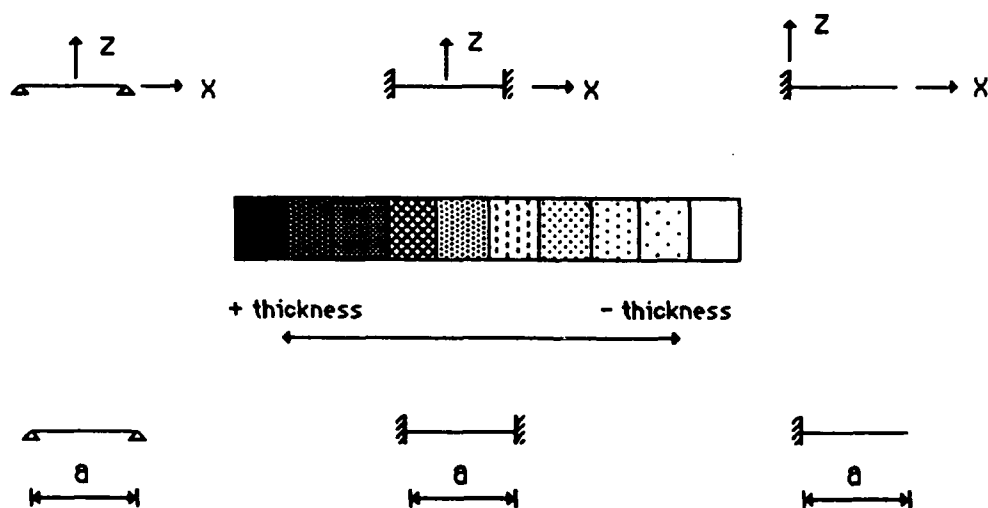


Figure 57. Definition of coordinates axis and key to colors for one-dimensional plates.



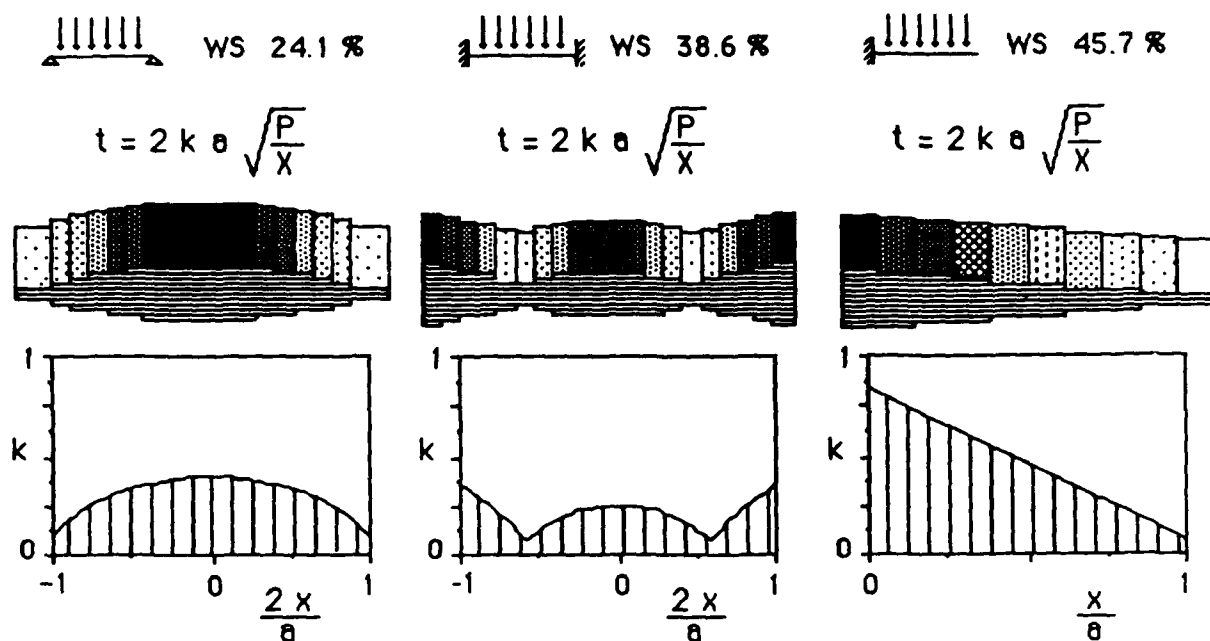


Figure 58. Representation of optimal thin one-dimensional plates subjected to a uniform distributed transverse load.

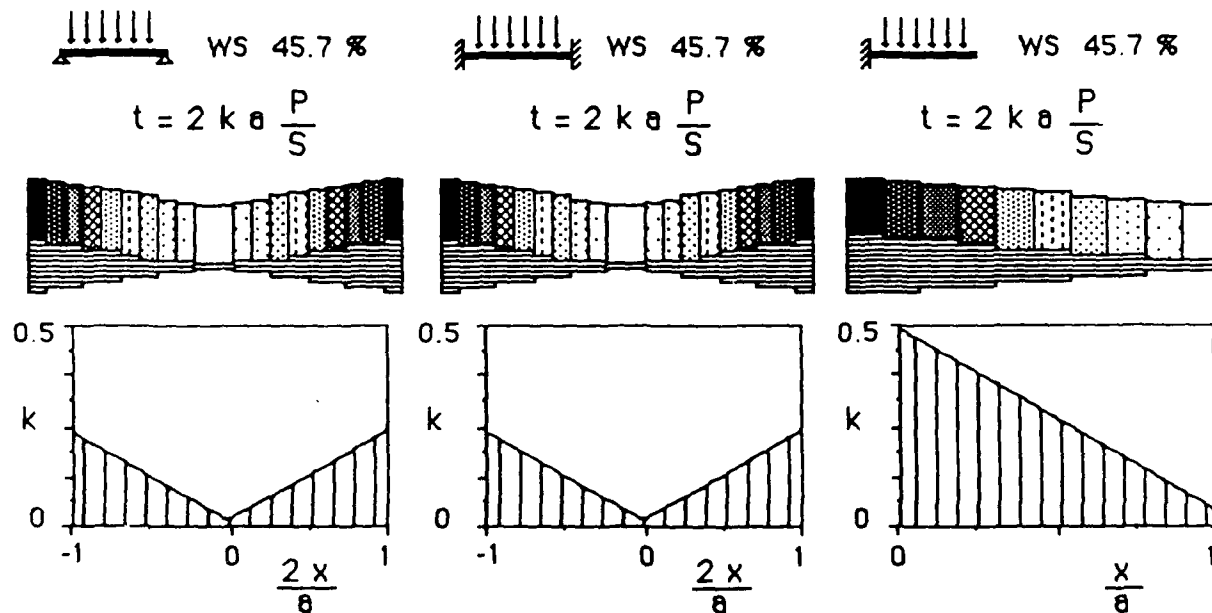


Figure 59. Representation of optimal thick one-dimensional plates subjected to a uniform distributed transverse load.

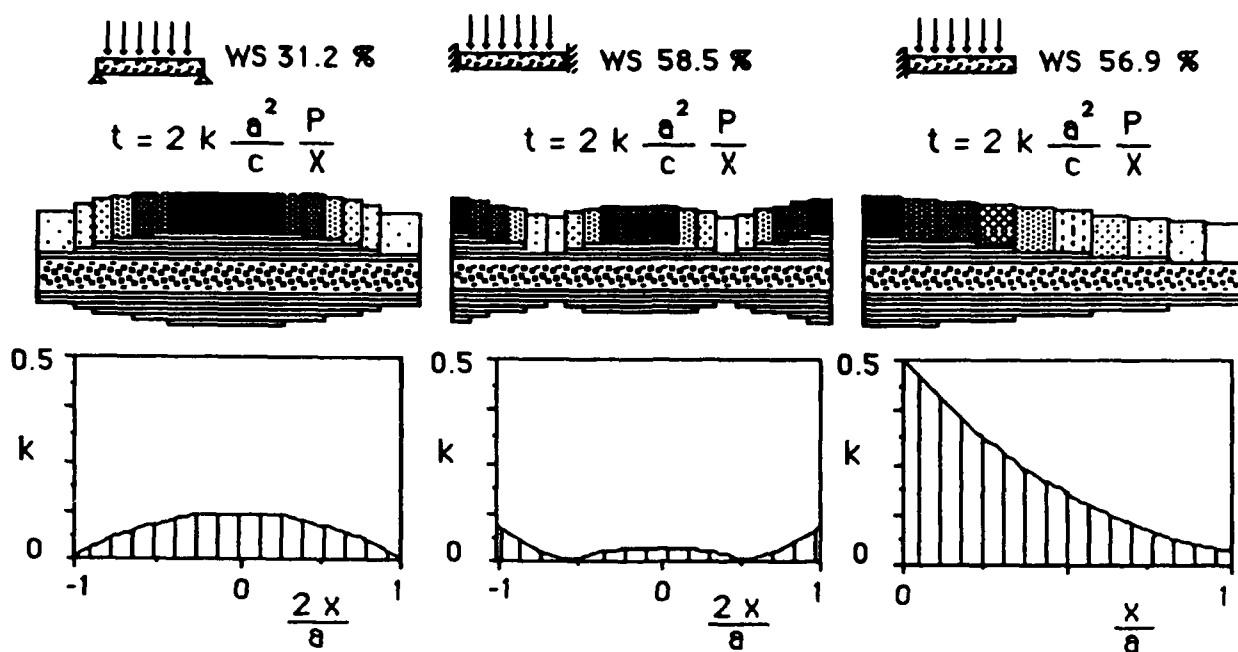


Figure 60. Representation of optimal one-dimensional sandwich panels subjected to a uniform distributed transverse load.

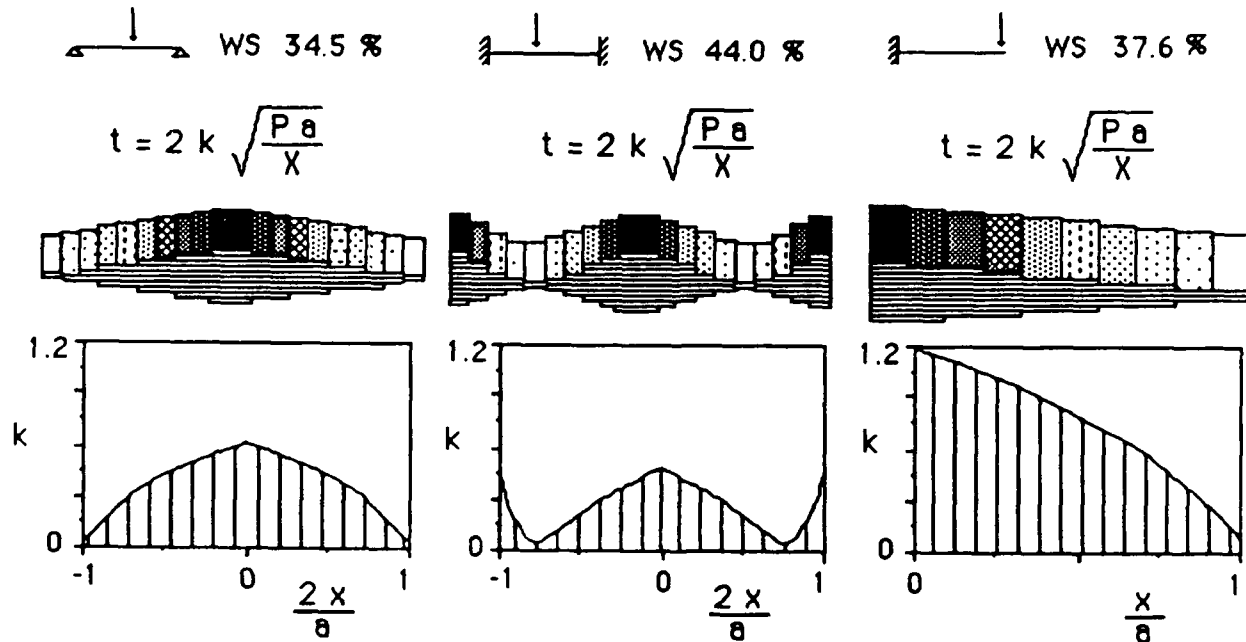


Figure 61. Representation of optimal thin one-dimensional plates subjected to a point transverse load.

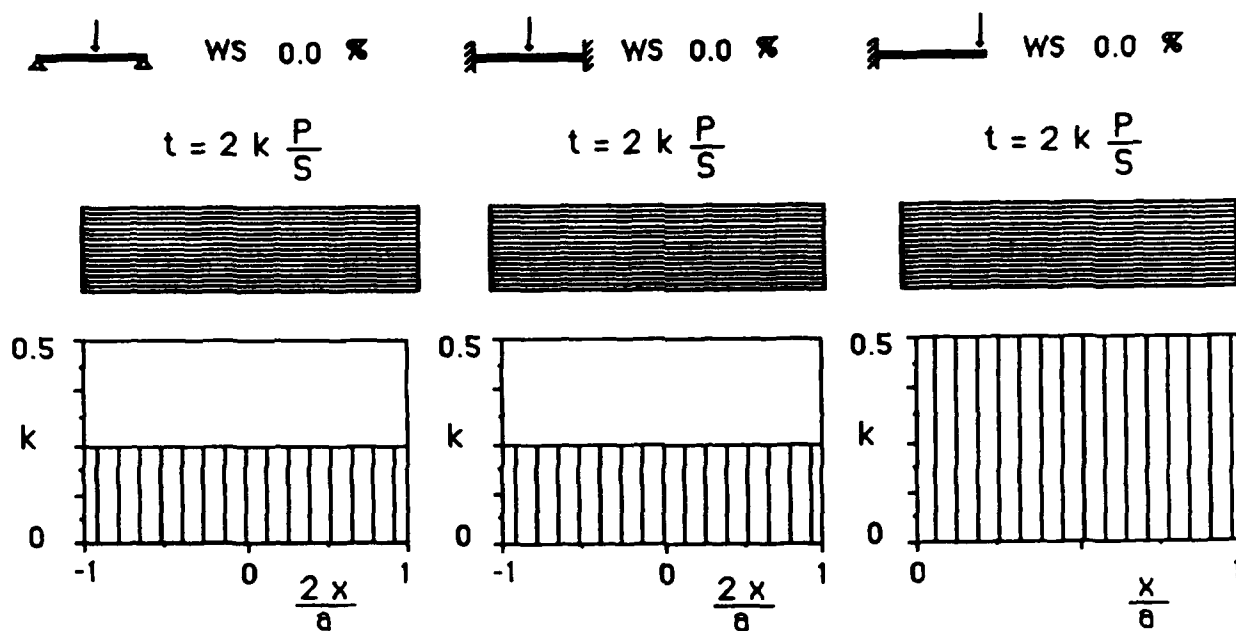


Figure 62. Representation of optimal thick one-dimensional plates subjected to a point transverse load.

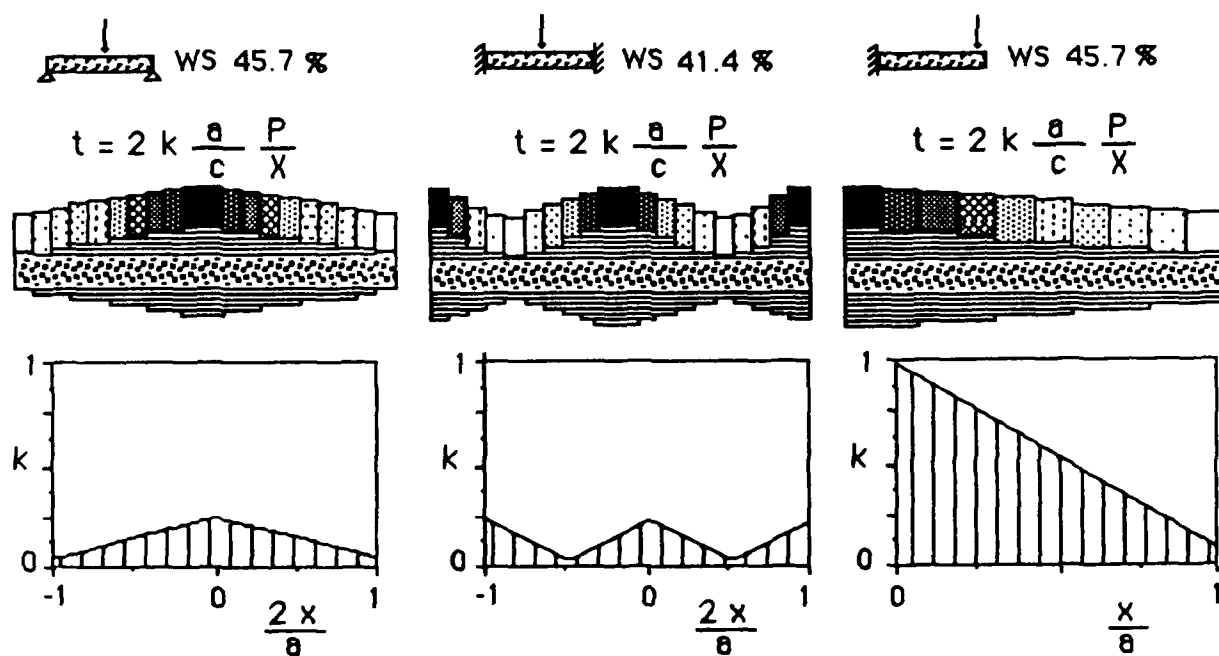


Figure 63. Representation of optimal one-dimensional sandwich panels subjected to a point transverse load.

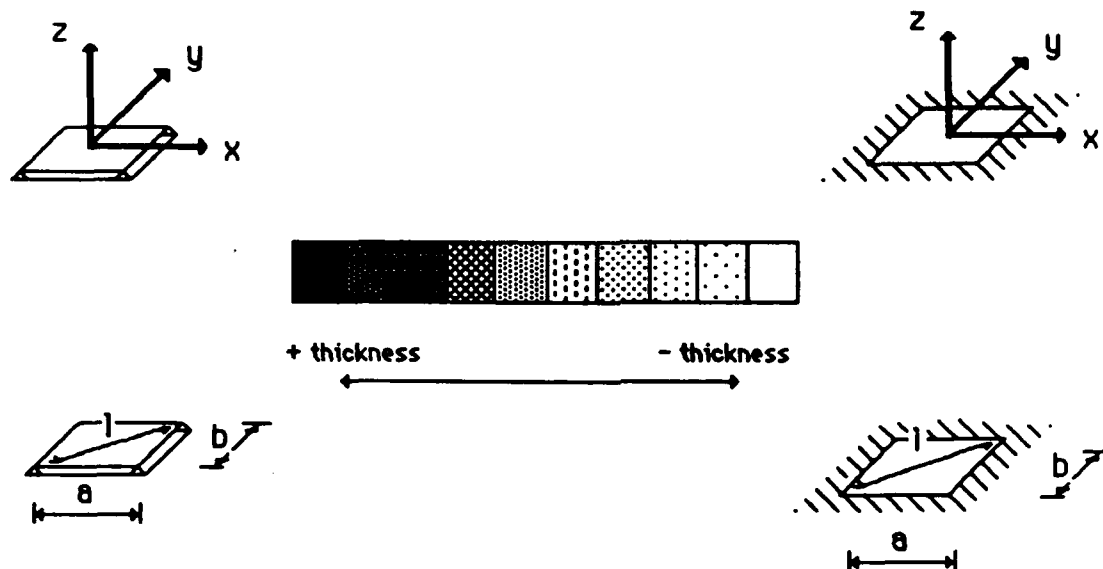


Figure 64. Definition of coordinate axis and key to colors for two-dimensional plates subjected to a transverse load.

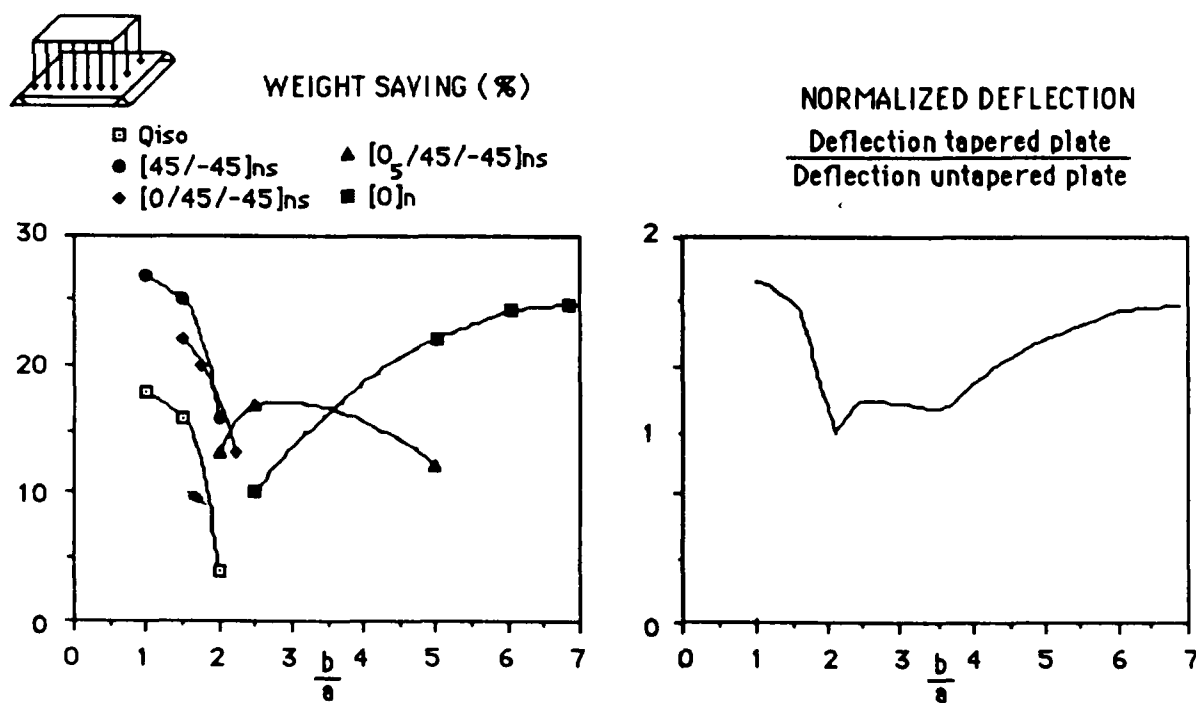
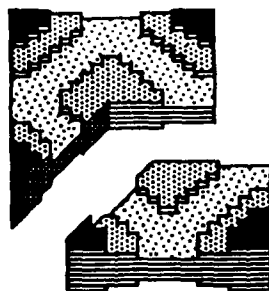
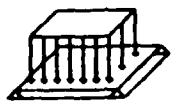


Figure 65. Weight saving and normalized deflection for a thin, simply supported plate subjected to a uniform distributed transverse load.



$$1 \leq \frac{b}{a} < 1.75$$

OPTIMUM SUBLAMINATE  
[ 45/-45]

$$t = 2 k a \sqrt{\frac{P}{X}}$$

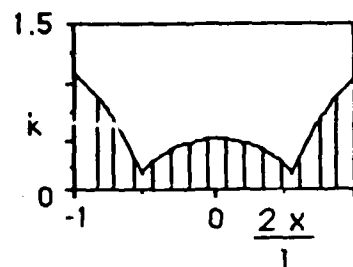
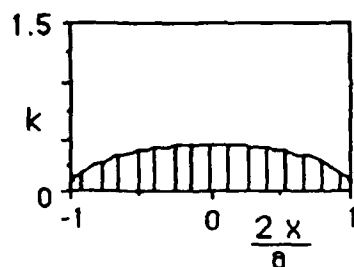
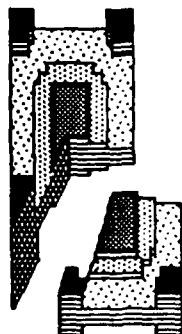
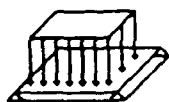


Figure 66. Representation of an optimal thin, simply supported plate subjected to a uniform distributed transverse load for aspect ratios between 1 and 1.75.



$$1.75 \leq \frac{b}{a} < 2.25$$

OPTIMUM SUBLAMINATE  
[0/45/-45]

$$t = 2 k a \sqrt{\frac{P}{X}}$$

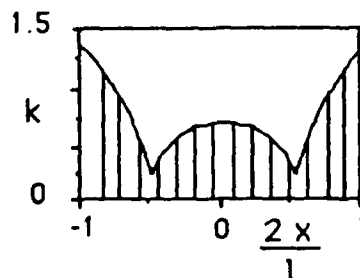
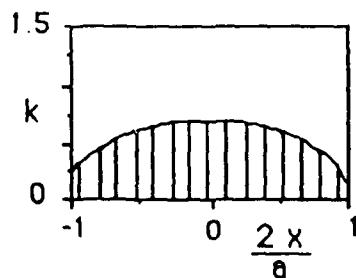
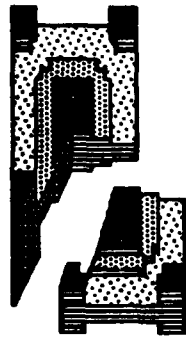
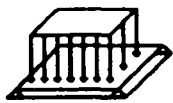


Figure 67. Representation of an optimal thin, simply supported plate subjected to a uniform distributed transverse load for aspect ratios between 1.75 and 2.25.



$$2.25 \leq \frac{b}{a} < 3.5$$

OPTIMUM SUBLAMINATE  
[0<sub>5</sub>/45/-45]

$$t = 2 k a \sqrt{\frac{P}{X}}$$

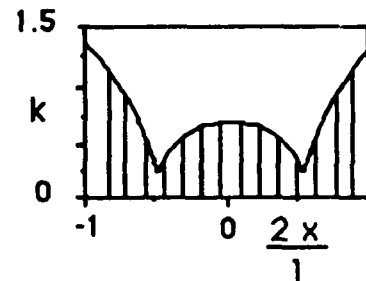
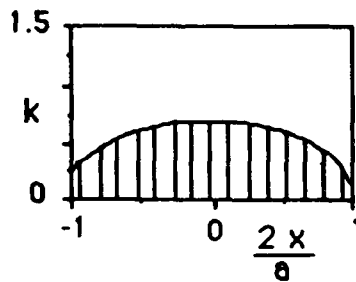
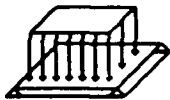


Figure 68. Representation of an optimal thin, simply supported plate subjected to a uniform distributed transverse load for aspect ratios between 2.25 and 3.5.



$$3.5 \leq \frac{b}{a}$$

OPTIMUM SUBLAMINATE  
[0]

$$t = 2 k a \sqrt{\frac{P}{X}}$$

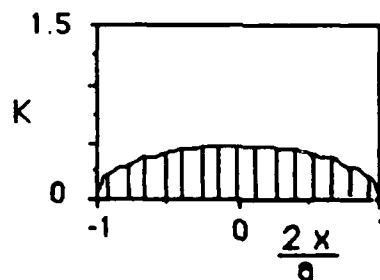


Figure 69. Representation of an optimal thin, simply supported plate subjected to a uniform distributed transverse load for aspect ratios higher than 3.5.

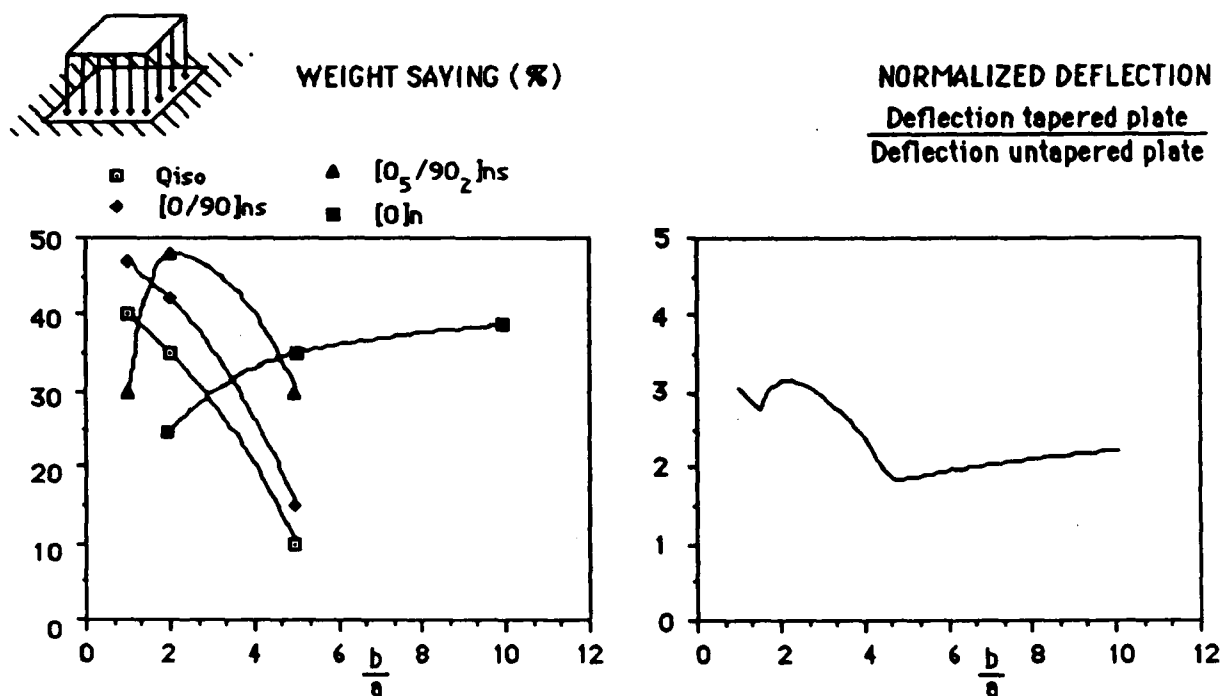


Figure 70. Weight saving and normalized deflection for a thin, clamped plate subjected to a uniform distributed transverse load.

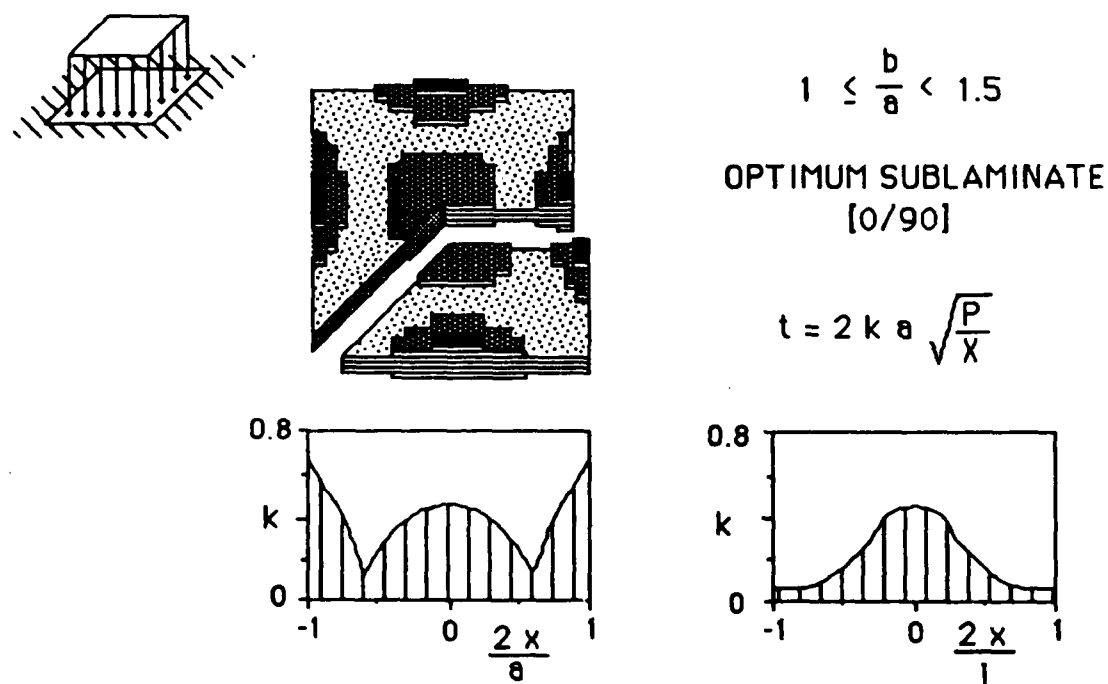
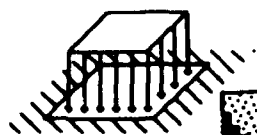


Figure 71. Representation of an optimal thin, clamped plate subjected to a uniform distributed transverse load for aspect ratios between 1 and 1.5.



$$1.5 \leq \frac{b}{a} < 4.4$$

OPTIMUM SUBLAMINATE  
[0<sub>5</sub>/90<sub>2</sub>]

$$t = 2 k a \sqrt{\frac{P}{X}}$$

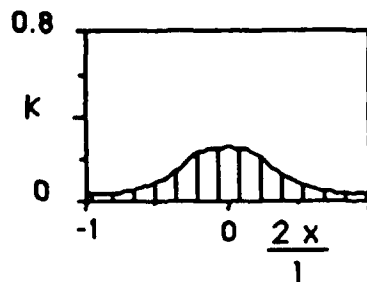
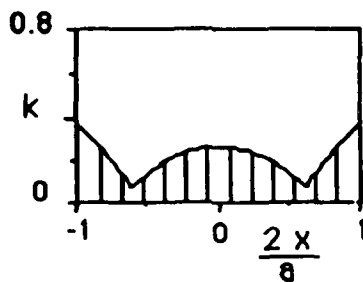
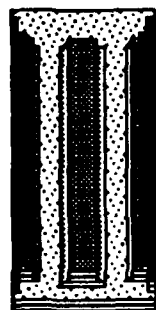
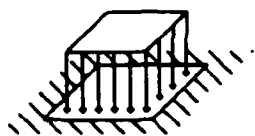


Figure 72. Representation of an optimal thin, clamped plate subjected to a uniform distributed transverse load for aspect ratios between 1.5 and 4.4.



$$4.4 \leq \frac{b}{a}$$

OPTIMUM SUBLAMINATE  
[0]

$$t = 2 k a \sqrt{\frac{P}{X}}$$

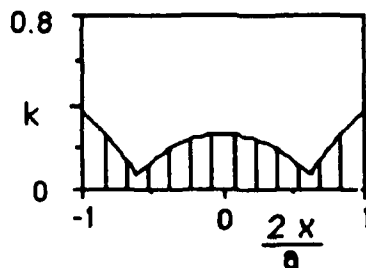
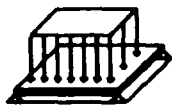


Figure 73. Representation of an optimal thin, clamped plate subjected to a uniform distributed transverse load for aspect ratios higher than 4.4.





WEIGHT SAVING (%)

- Qiso
- ◆ [45/-45]<sub>ns</sub>
- ▲ [0]<sub>n</sub>

NORMALIZED DEFLECTION

$\frac{\text{Deflection tapered plate}}{\text{Deflection untapered plate}}$

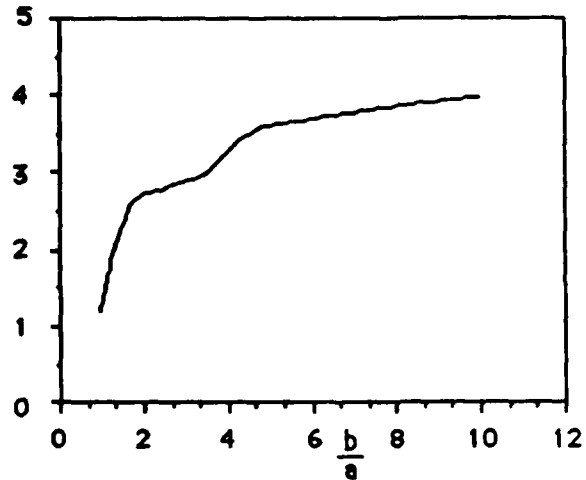
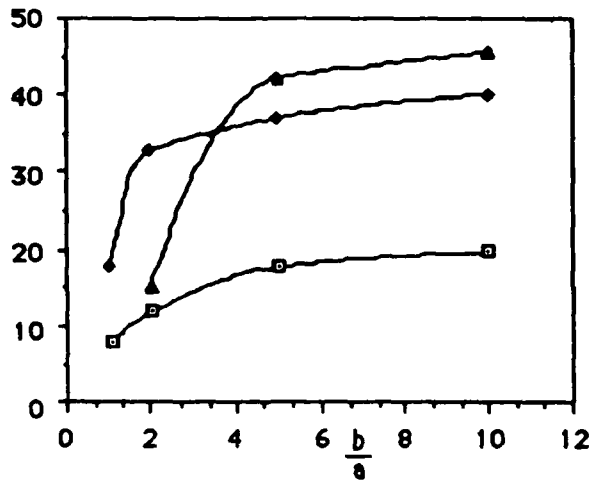
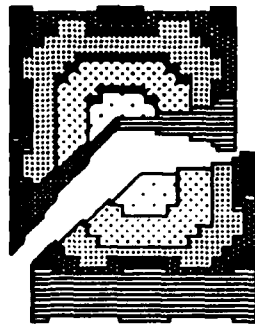
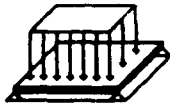


Figure 74. Weight saving and normalized deflection for a thick, simply supported plate subjected to a uniform distributed transverse load.



$$1 \leq \frac{b}{a} < 3.5$$

OPTIMUM SUBLAMINATE  
[45/-45]<sub>s</sub>

$$t = 2 k a \frac{P}{S}$$

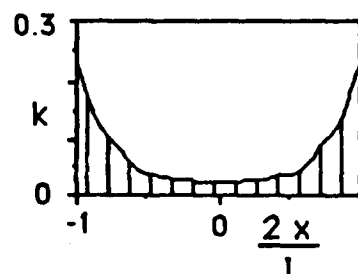
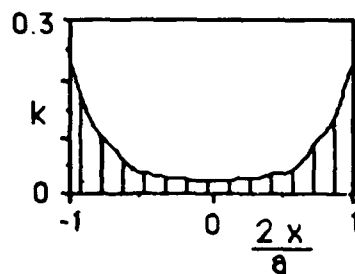
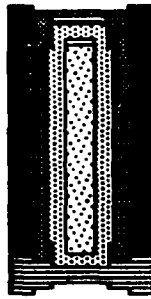
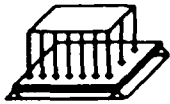


Figure 75. Representation of an optimal thick, simply supported plate subjected to a uniform distributed transverse load plates for aspect ratios between 1 and 3.5.



$$3.5 \leq \frac{b}{a}$$

OPTIMUM SUBLAMINATE  
[0]

$$t = 2 k a \frac{P}{S}$$

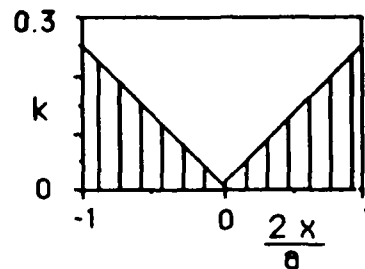
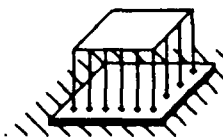


Figure 76. Representation of an optimal thick, simply supported plate subjected to a uniform distributed transverse load for aspect ratios higher than 3.5.



WEIGHT SAVING (%)

- Qiso
- ◆ [45/-45]<sub>ns</sub>
- ▲ [0]<sub>n</sub>

NORMALIZED DEFLECTION  
 $\frac{\text{Deflection tapered plate}}{\text{Deflection untapered plate}}$

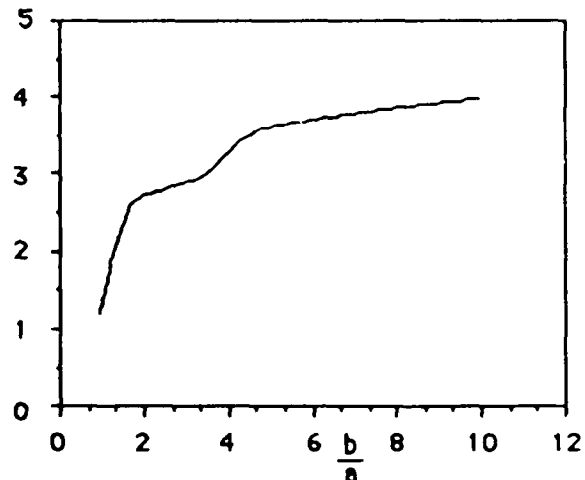
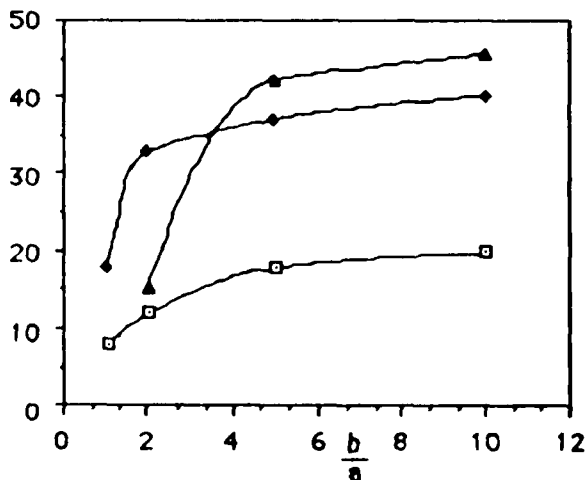
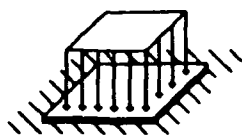


Figure 77. Weight saving and normalized deflection for a thick, clamped plate subjected to a uniform distributed transverse load.



$$1 \leq \frac{b}{a} < 3.5$$

OPTIMUM LAMINATE  
[45/-45]<sub>s</sub>

$$t = 2 k a \frac{P}{S}$$

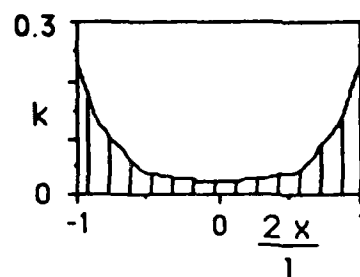
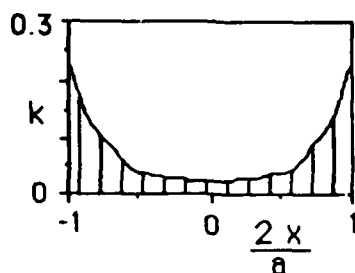
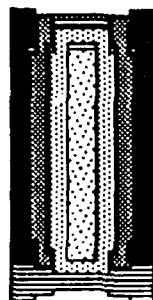
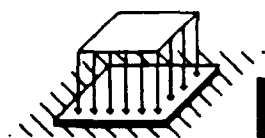


Figure 78. Representation of an optimal thick, clamped plate subjected to a uniform distributed transverse load for aspect ratios between 1 and 3.5.



$$3.5 \leq \frac{b}{a}$$

OPTIMUM SUBLAMINATE  
[0]

$$t = 2 k a \frac{P}{S}$$

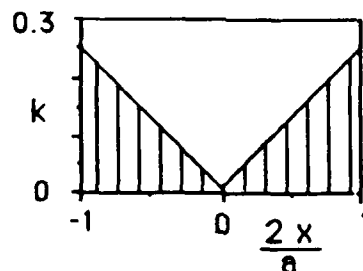
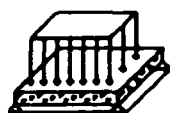
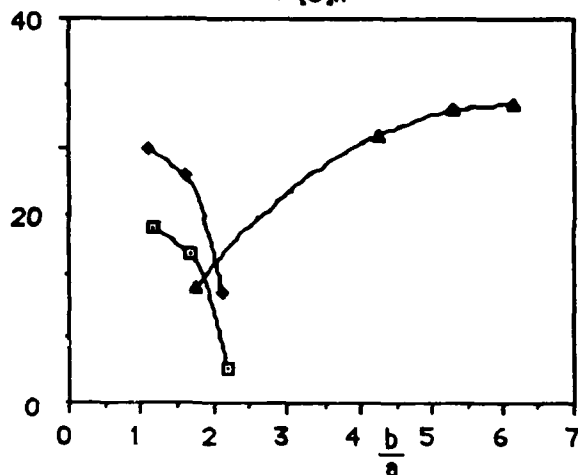


Figure 79. Representation of an optimal thick, clamped plate subjected to a uniform distributed transverse load for aspect ratios higher than 3.5.



WEIGHT SAVING (%)

- Qiso
- ◆ [45/-45]<sub>ns</sub>
- ▲ [0]<sub>n</sub>



NORMALIZED DEFLECTION

$\frac{\text{Deflection tapered plate}}{\text{Deflection untapered plate}}$

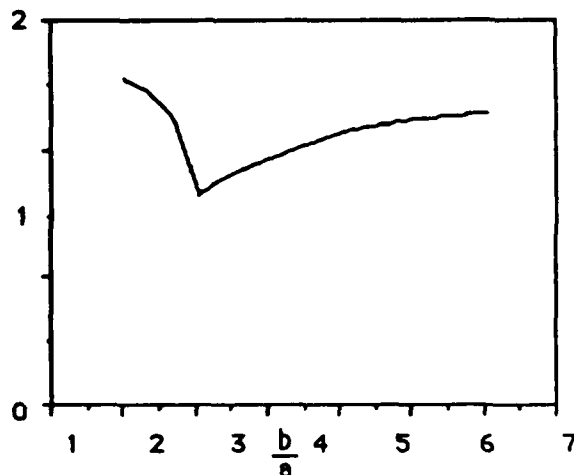
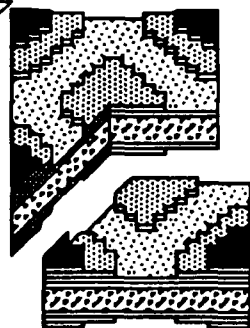
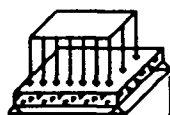


Figure 80. Weight saving and normalized deflection for a simply supported sandwich panel subjected to a uniform distributed transverse load.



$$1 \leq \frac{b}{a} < 1.5$$

OPTIMUM SUBLAMINATE  
[45/-45]

$$t = 2k \frac{a^2}{c} \frac{P}{X}$$

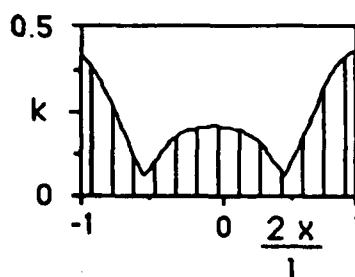
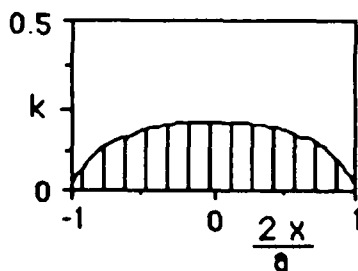
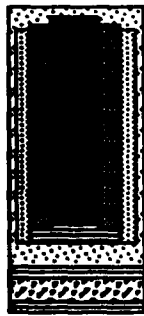
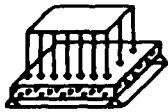


Figure 81. Representation of an optimal simply supported sandwich panel subjected to a uniform distributed transverse load for aspect ratios between 1 and 1.5.



$$1.5 \leq \frac{b}{a}$$

OPTIMUM SUBLAMINATE  
[0]

$$t = 2 k \frac{a^2}{c} \frac{P}{X}$$

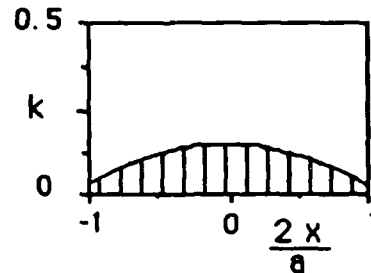
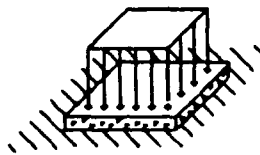


Figure 82. Representation of an optimal simply supported sandwich panel subjected to a uniform distributed transverse load. for aspect ratios higher than 1.5.



WEIGHT SAYING (%)

□ Qiso    ▲  $[0_5/90_2]_{ns}$   
♦  $[0/90]_{ns}$     ■  $[0]_n$

NORMALIZED DEFLECTION  
 $\frac{\text{Deflection tapered plate}}{\text{Deflection untapered plate}}$

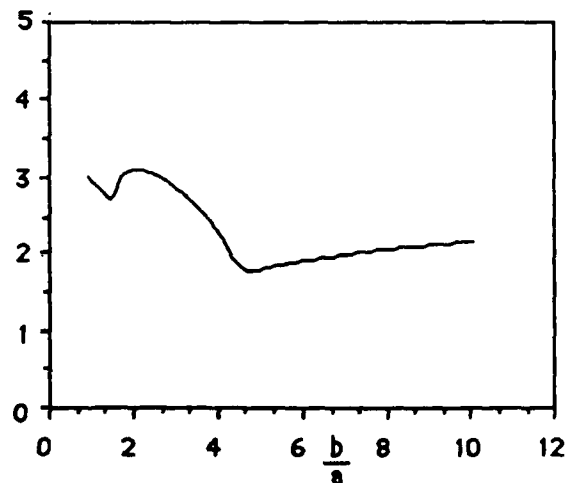
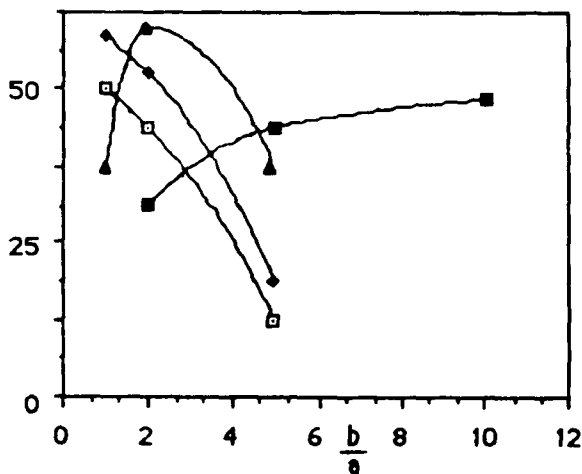


Figure 83. Weight saving and normalized deflection for a clamped sandwich panel subjected to a uniform distributed transverse load.

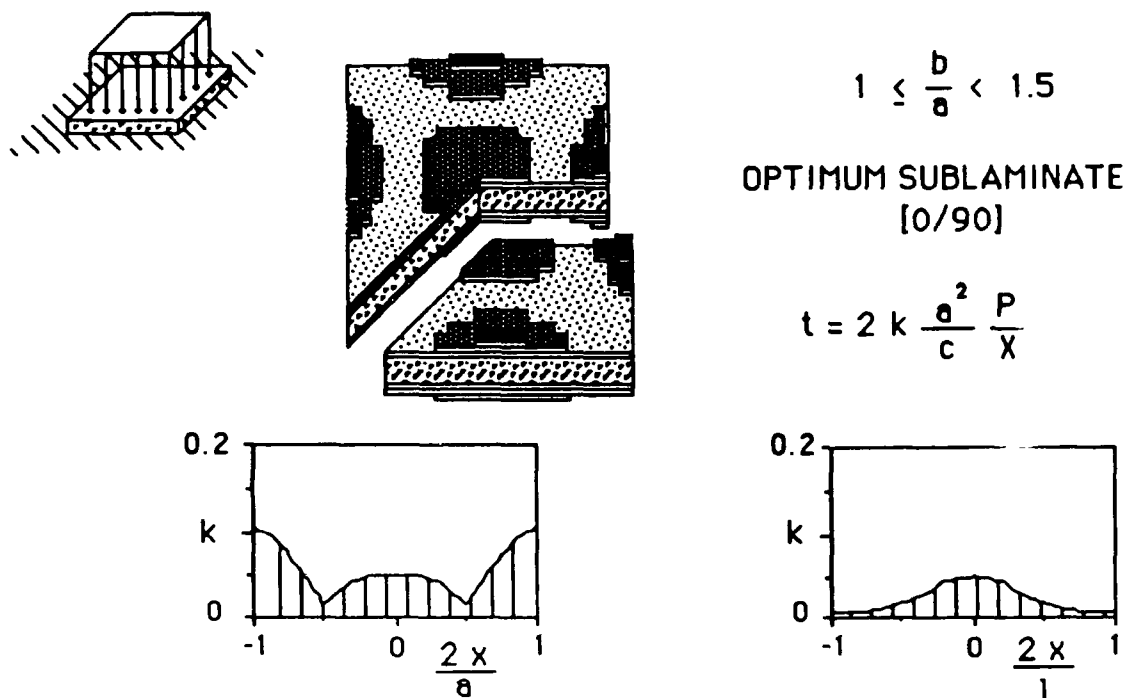


Figure 84. Representation of an optimal clamped sandwich panel subjected to a uniform distributed transverse load for aspect ratios between 1 and 1.5.

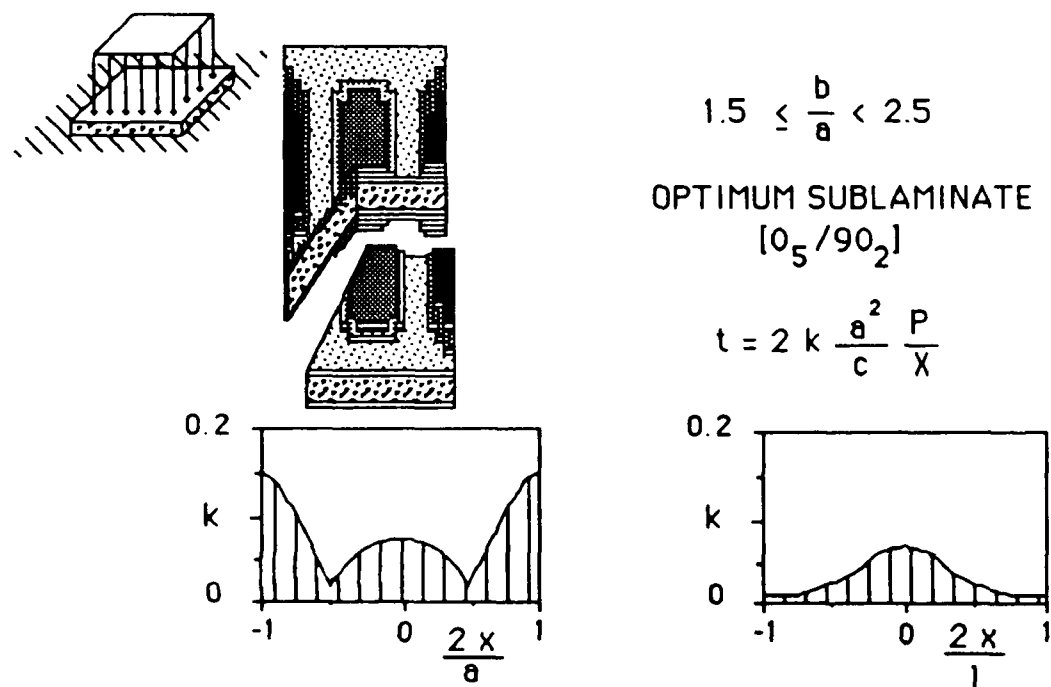
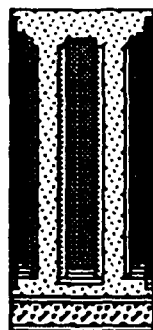
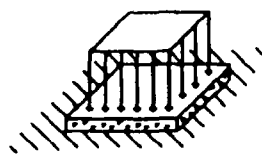


Figure 85. Representation of an optimal clamped sandwich panel subjected to a uniform distributed transverse load for aspect ratios between 1.5 and 2.5.



$$2.5 \leq \frac{b}{a}$$

OPTIMUM SUBLAMINATE  
[0]

$$t = 2 k \frac{a^2}{c} \frac{P}{X}$$

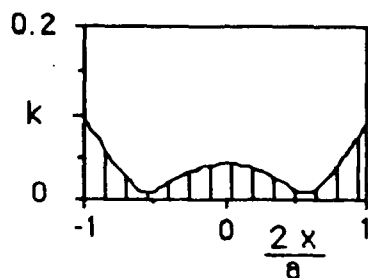


Figure 86. Representation of an optimal clamped sandwich panel subjected to a uniform distributed transverse load for aspect ratios higher than 2.5.

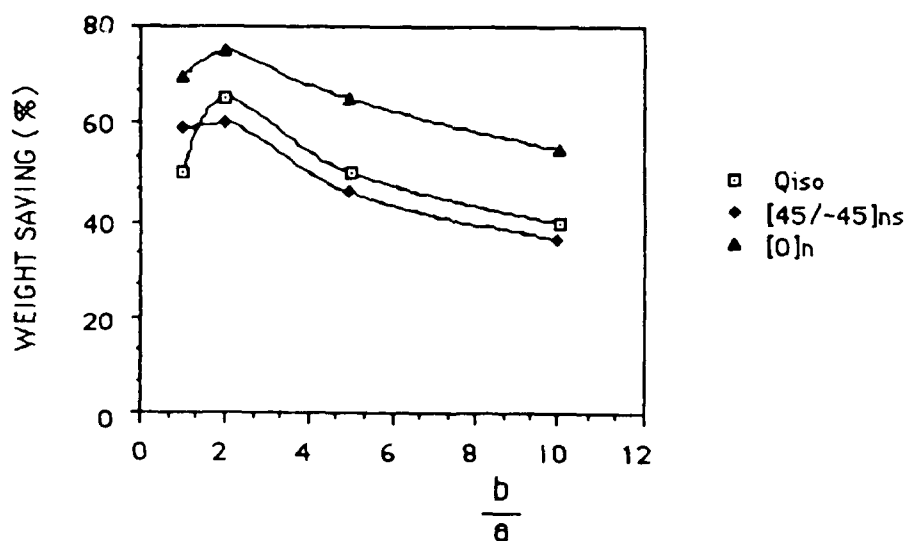
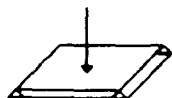
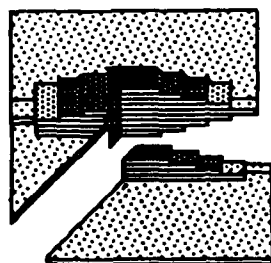
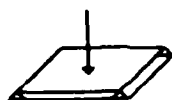


Figure 87. Weight saving for a thin, simply supported plate subjected to a point transverse load.



$$1 \leq \frac{b}{a} < 2$$

OPTIMUM SUBLAMINATE

[0]

$$a = 0.2 \text{ m}$$

$$P = 2.0 \text{ E4 N}$$

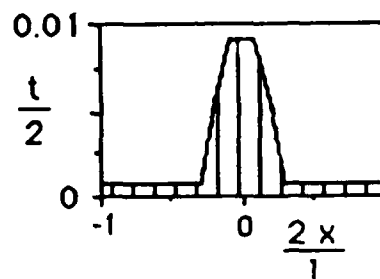
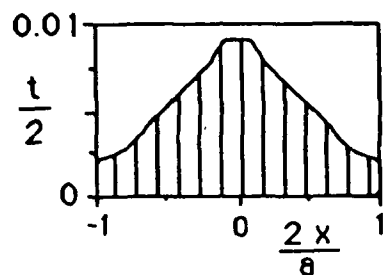
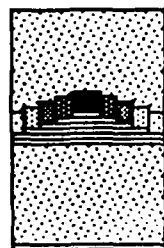
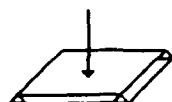


Figure 88. Representation of an optimal thin, simply supported plate subjected to a point transverse load for aspect ratios between 1 and 2.



$$2 \leq \frac{b}{a} < 5$$

OPTIMUM SUBLAMINATE

[0]

$$a = 0.2 \text{ m}$$

$$P = 2.0 \text{ E4 N}$$

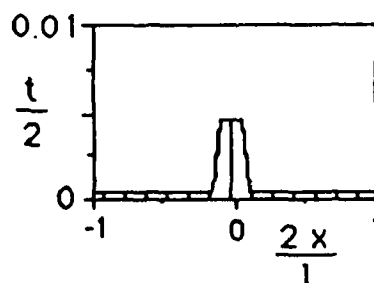
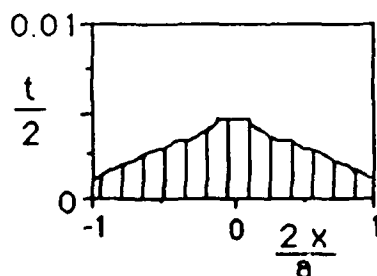
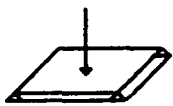


Figure 89. Representation of an optimal thin, simply supported plate subjected to a point transverse load for aspect ratios between 2 and 5.





$$5 \leq \frac{b}{a}$$

OPTIMUM SUBLAMINATE  
[0]

$$a = 0.2 \text{ m}$$

$$P = 2.0 \text{ E}4 \text{ N}$$

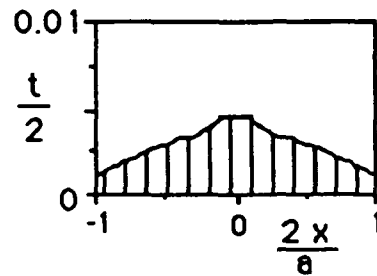


Figure 90. Representation of an optimal thin, simply supported plate subjected to a point transverse load for aspect ratios higher than 5.

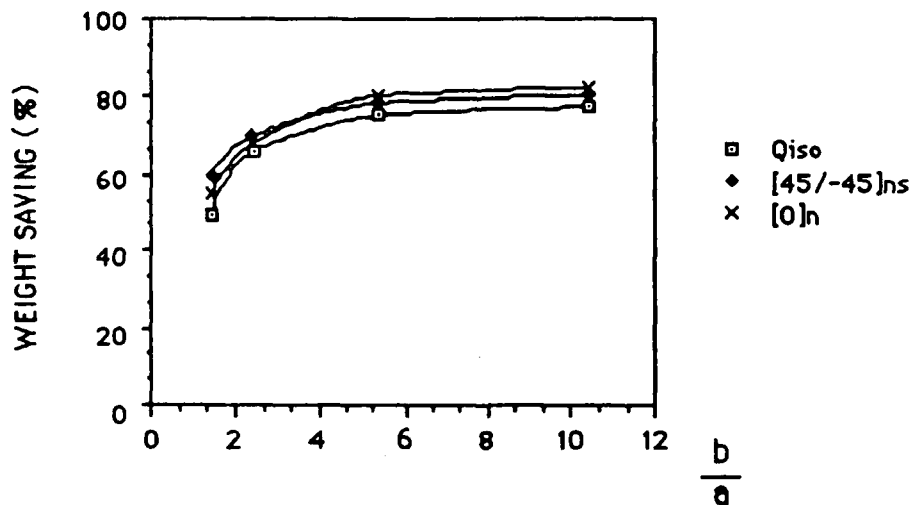
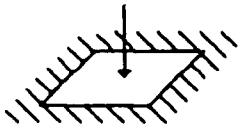
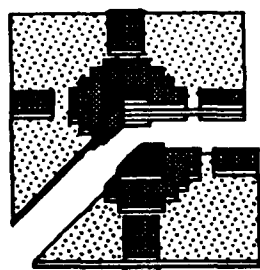
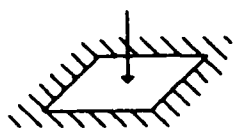


Figure 91. Weight saving for a thin, clamped plate subjected to a point transverse load.



$$1 \leq \frac{b}{a} < 1.5$$

OPTIMUM SUBLAMINATE  
[45/-45]

$$a = 0.2 \text{ m}$$

$$P = 2.0 \text{ E4 N}$$

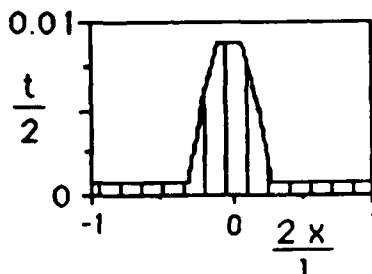
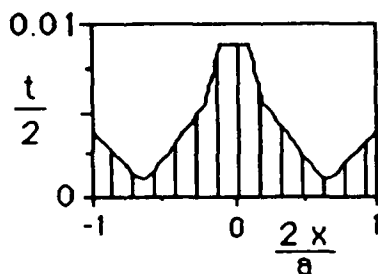
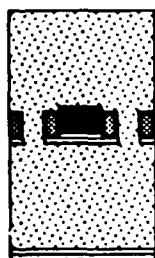
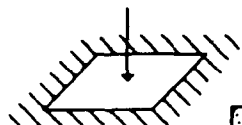


Figure 92. Representation of an optimal thin, clamped plate subjected to a point transverse load for aspect ratios between 1 and 1.5.



$$1.5 \leq \frac{b}{a} < 5$$

OPTIMUM SUBLAMINATE  
[0]

$$a = 0.2 \text{ m}$$

$$P = 2.0 \text{ E4 N}$$

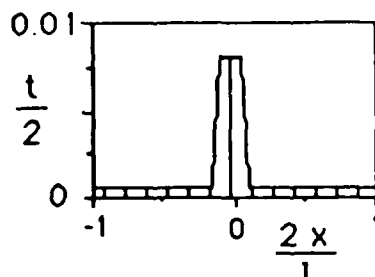
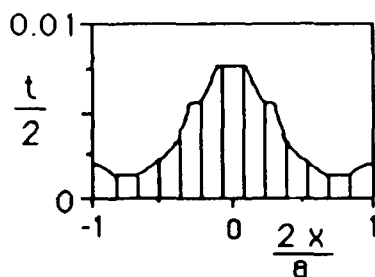
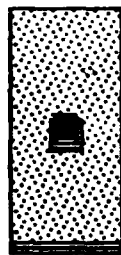
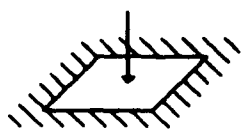


Figure 93. Representation of an optimal thin, clamped plate subjected to a point transverse load for aspect ratios between 1.5 and 5.



$5 \leq \frac{b}{a}$   
 OPTIMUM SUBLAMINATE  
 [0]

$a = 0.2 \text{ m}$   
 $P = 2.0 \text{ E4 N}$

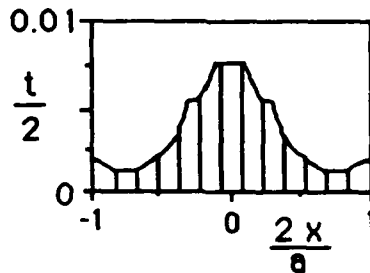


Figure 94. Representation of an optimal thin, clamped plate subjected to a point transverse load for aspect ratios higher than 5.

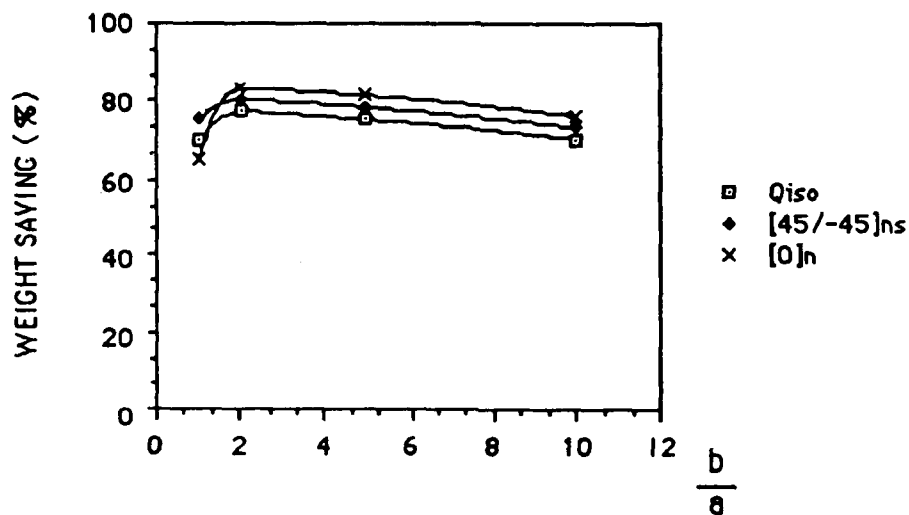
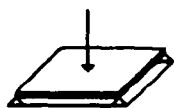
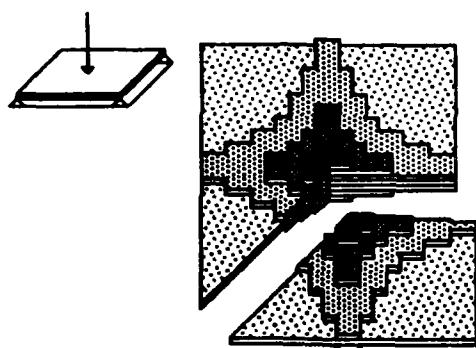


Figure 95. Weight saving for a thick, simply supported plate subjected to a point transverse load.



$$1 \leq \frac{b}{a} < 2.25$$

OPTIMUM SUBLAMINATE  
[45/-45]

$$a = 0.01 \text{ m}$$

$$P = 4.0 \text{ E3 N}$$

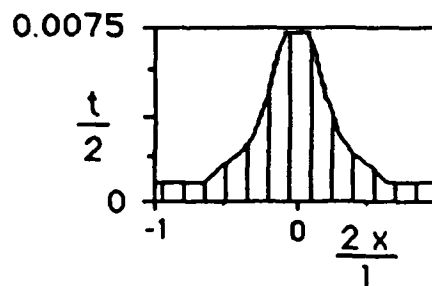
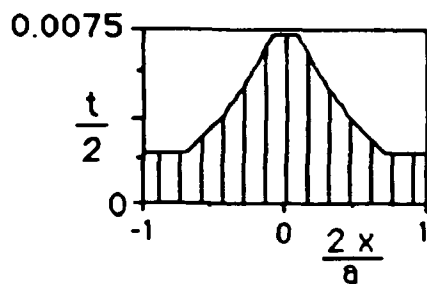
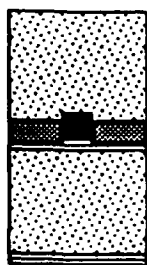
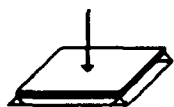


Figure 96. Representation of an optimal thick, simply supported plate subjected to a point transverse load for aspect ratios between 1 and 2.25.



$$2.25 \leq \frac{b}{a}$$

OPTIMUM SUBLAMINATE  
[0]

$$a = 0.01 \text{ m}$$

$$P = 4.0 \text{ E3 N}$$

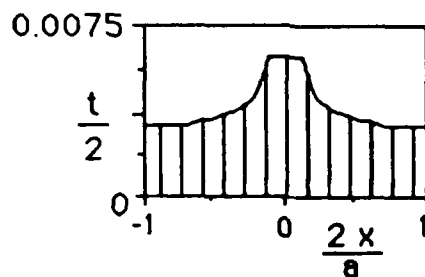


Figure 97. Representation of an optimal thick, simply supported plate subjected to a point transverse load for aspect ratios higher than 2.25.

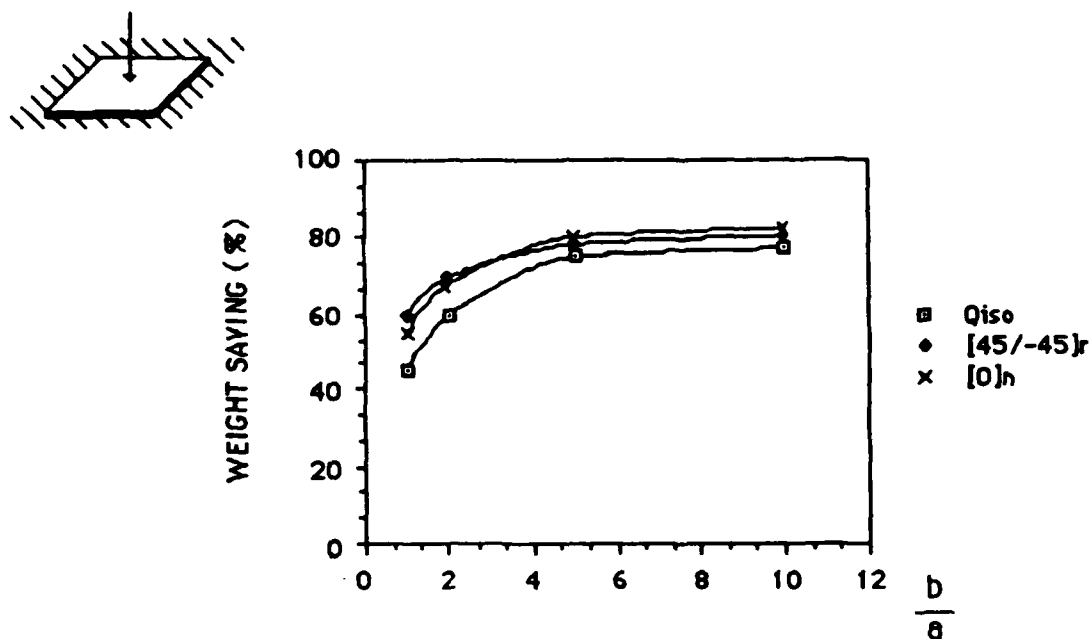


Figure 98. Weight saving for a thick, clamped plate subjected to a point transverse load.

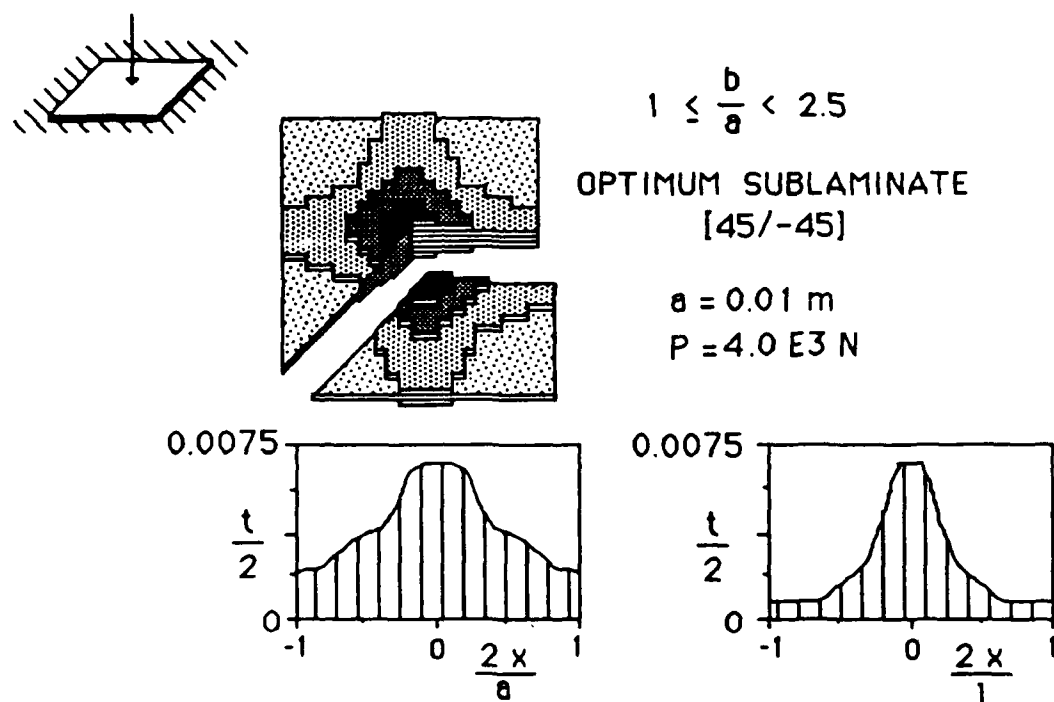
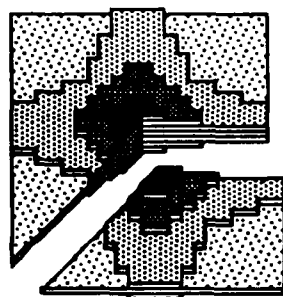
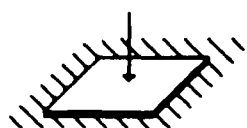


Figure 99. Representation of an optimal thick, clamped plate subjected to a point transverse load for aspect ratios between 1 and 2.5.



$$1 \leq \frac{b}{a} < 2.5$$

OPTIMUM SUBLAMINATE  
[45/-45]

$$a = 0.01 \text{ m}$$

$$P = 4.0 \text{ E3 N}$$

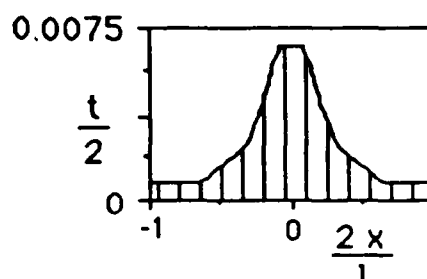
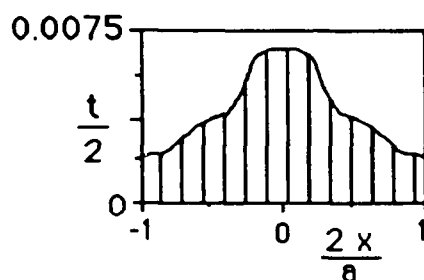
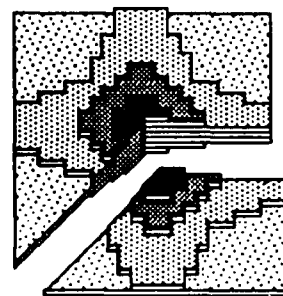
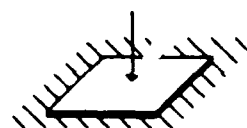


Figure 100. Representation of an optimal thick, clamped plate subjected to a point transverse load for aspect ratios between 2.5 and 5.



$$1 \leq \frac{b}{a} < 2.5$$

OPTIMUM SUBLAMINATE  
[45/-45]

$$a = 0.01 \text{ m}$$

$$P = 4.0 \text{ E3 N}$$

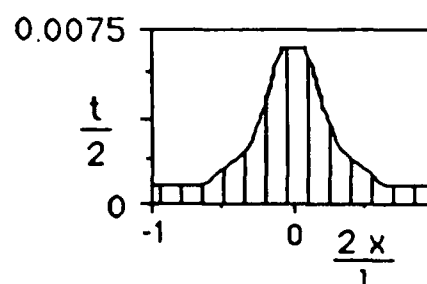
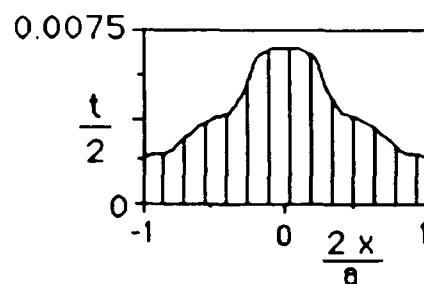


Figure 101. Representation of an optimal thick, clamped plate subjected to a point transverse load for aspect ratios higher than 5.

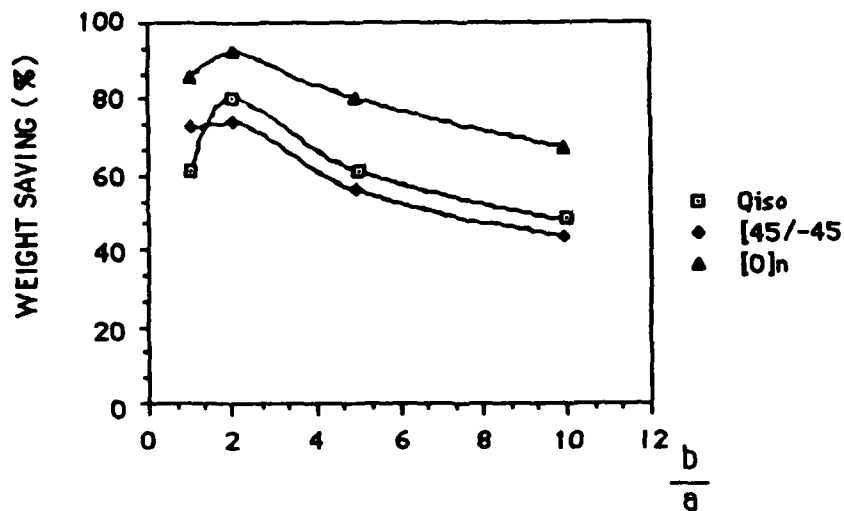
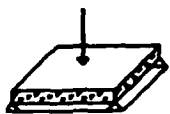
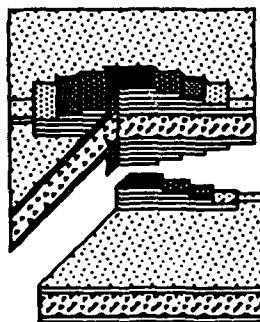
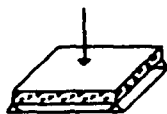


Figure 102. Weight saving for a simply supported sandwich panel subjected to a point transverse load.



$$1 \leq \frac{b}{a} < 2$$

OPTIMUM SUBLAMINATE  
[45/-45]

$$a = 1 \text{ m}$$

$$c = 0.1 \text{ m}$$

$$P = 2.0 \text{ E4 N}$$

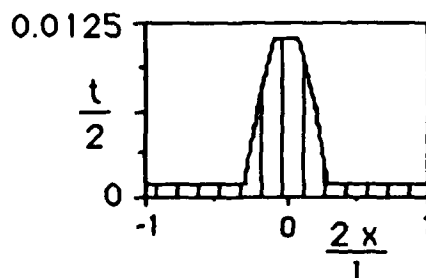
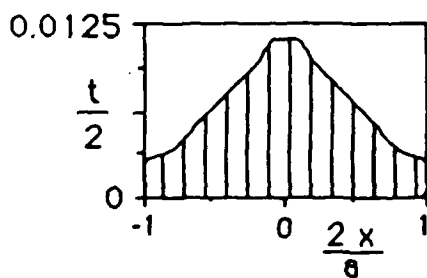
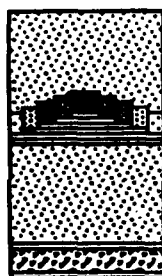
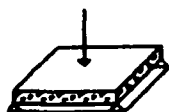


Figure 103. Representation of an optimal simply supported sandwich panel subjected to a point transverse load for aspect ratios between 1 and 2.



$2 \leq \frac{b}{a} < 5$   
 OPTIMUM SUBLAMINATE  
 [0]

$a = 1 \text{ m}$   
 $c = 0.1 \text{ m}$   
 $P = 2.0 \text{ E}4 \text{ N}$

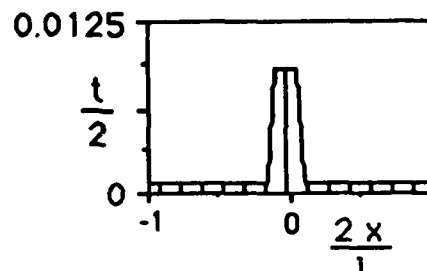
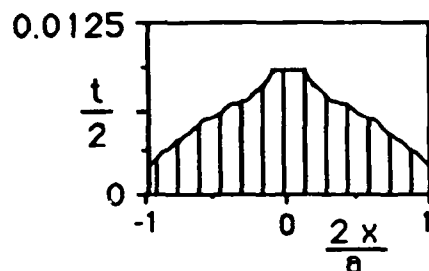
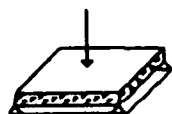


Figure 104. Representation of an optimal simply supported sandwich panel subjected to a point transverse load for aspect ratios between 2 and 5.



$5 \leq \frac{b}{a}$   
 OPTIMUM SUBLAMINATE  
 [0]

$a = 1 \text{ m}$   
 $c = 0.1 \text{ m}$   
 $P = 2.0 \text{ E}4 \text{ N}$

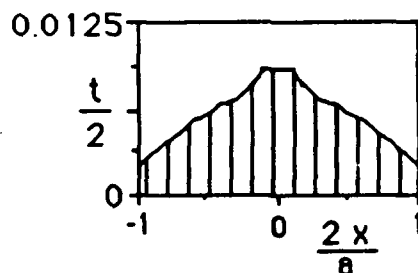


Figure 105. Representation of an optimal simply supported sandwich panel subjected to a point transverse load for aspect ratios higher than 5.



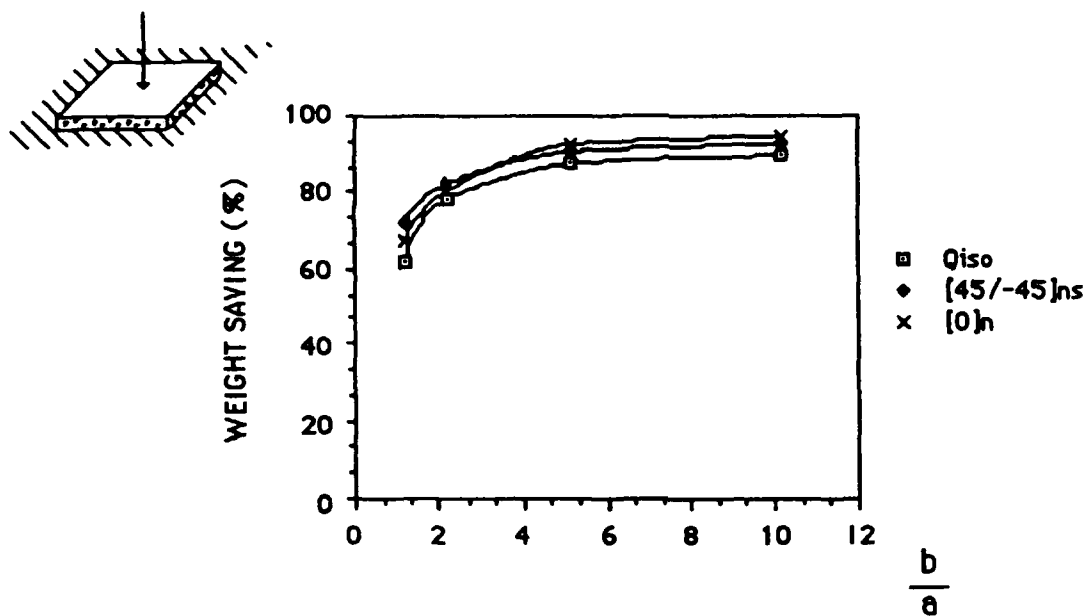


Figure 106. Weight saving for a clamped sandwich panel subjected to a point transverse load.

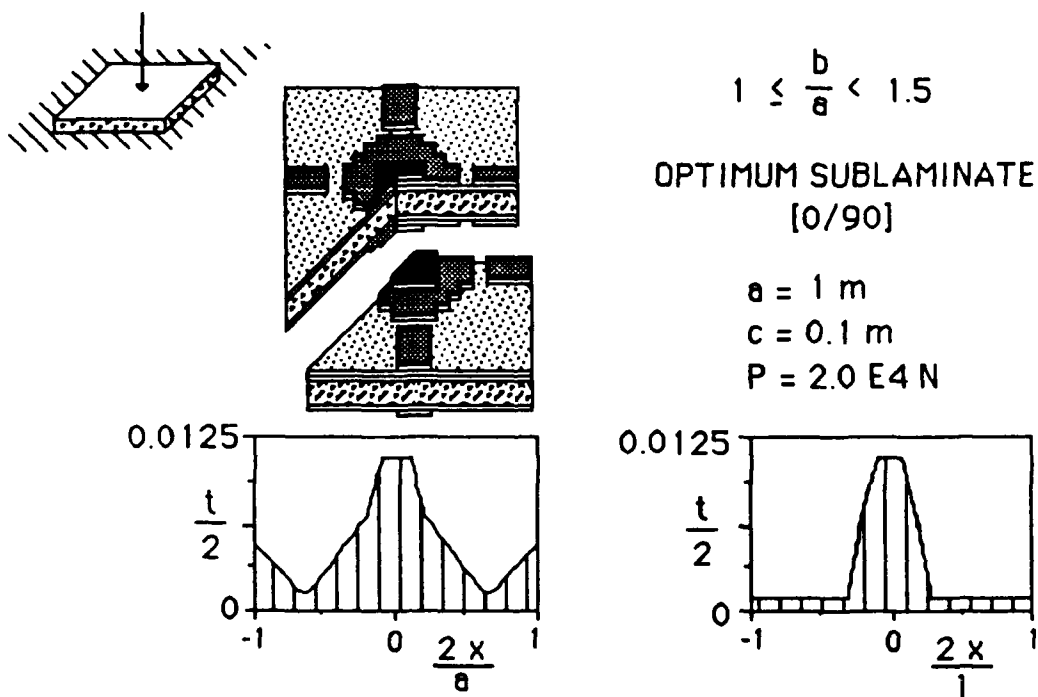


Figure 107. Representation of an optimal clamped sandwich panel subjected to a point transverse load for aspect ratios between 1 and 1.5.

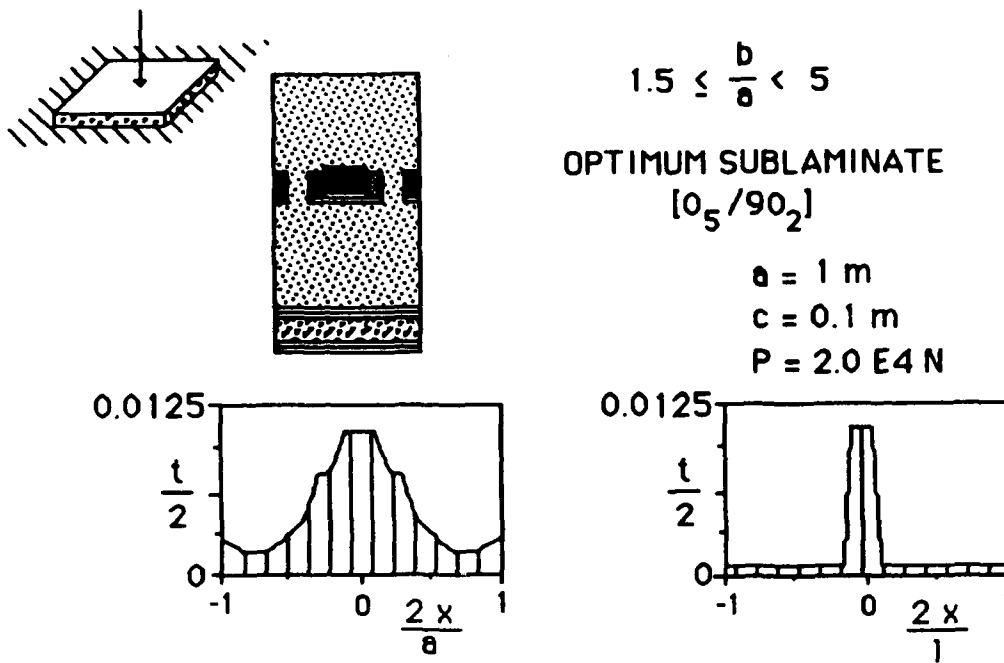


Figure 108. Representation of an optimal clamped sandwich panel subjected to a point transverse load for aspect ratios between 1.5 and 5.

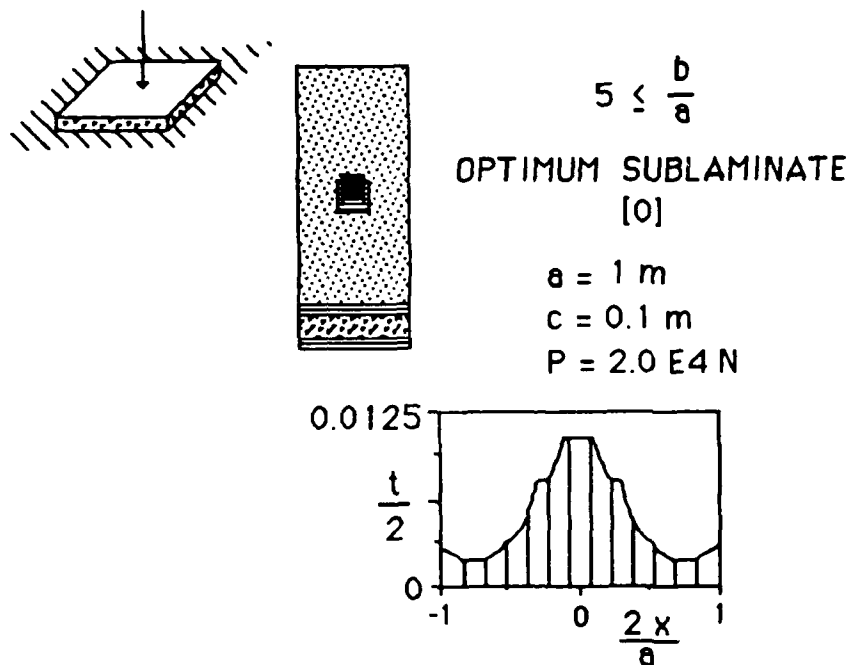


Figure 109. Representation of an optimal clamped sandwich panel subjected to a point transverse load for aspect ratios higher than 5.

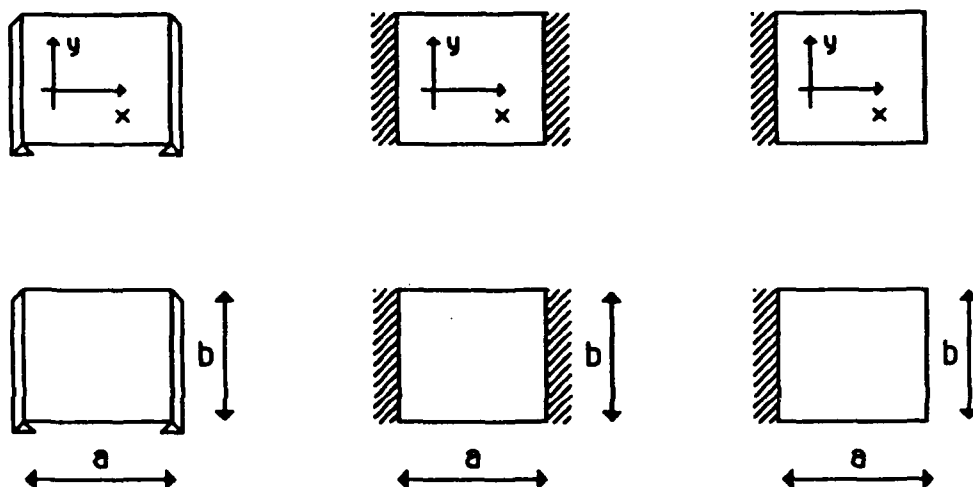
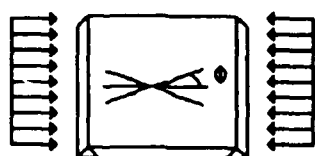


Figure 110. Definition of coordinate axis for one-dimensional plates subjected to a uniform uniaxial compression load.



$$\frac{N_{xcr} b^2}{Q_{yy} t^3}$$

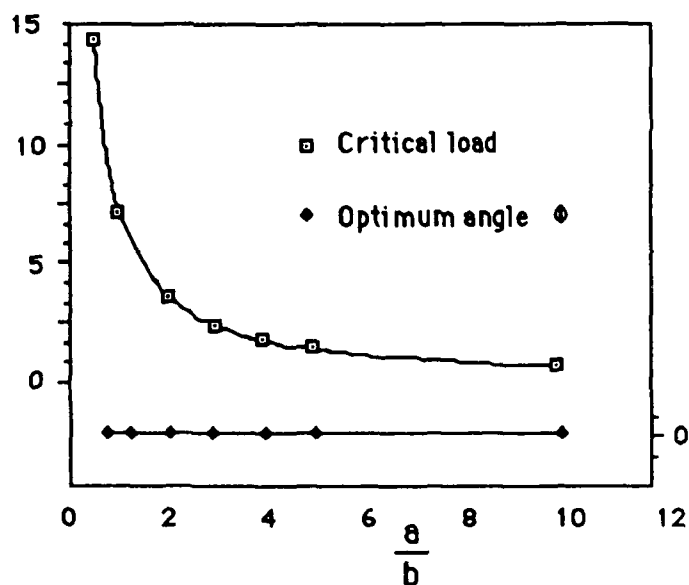


Figure 111. Critical load and optimum angle for an one-dimensional simply supported plate.

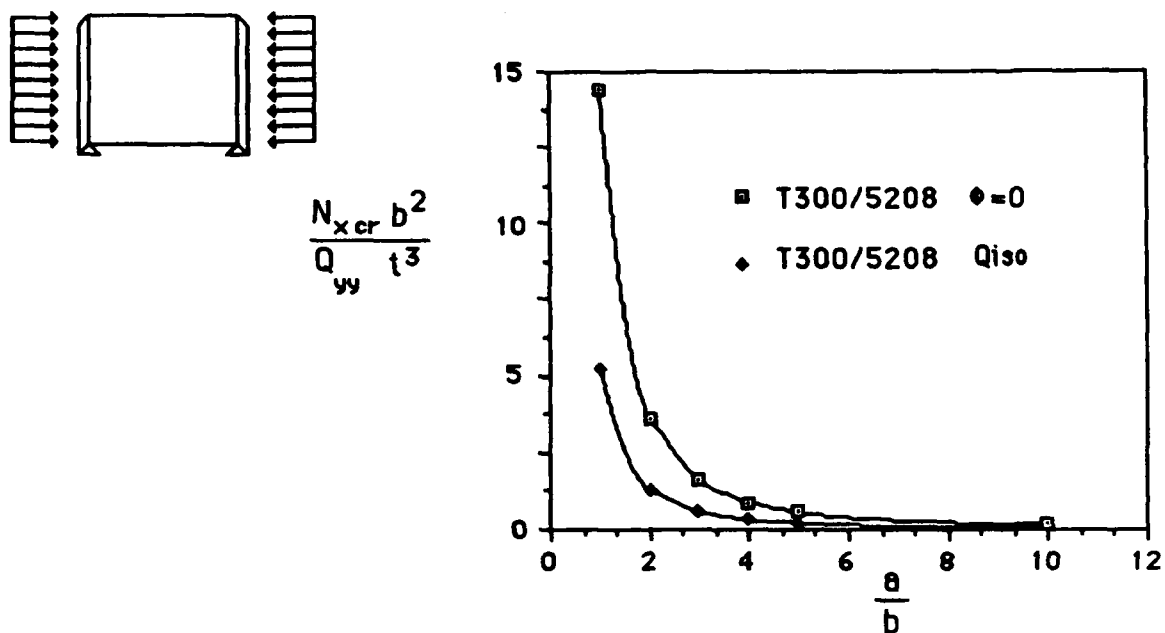


Figure 112. Comparison between critical loads of optimum configuration and quasi-isotropic laminate (one-dimensional simply supported plates).

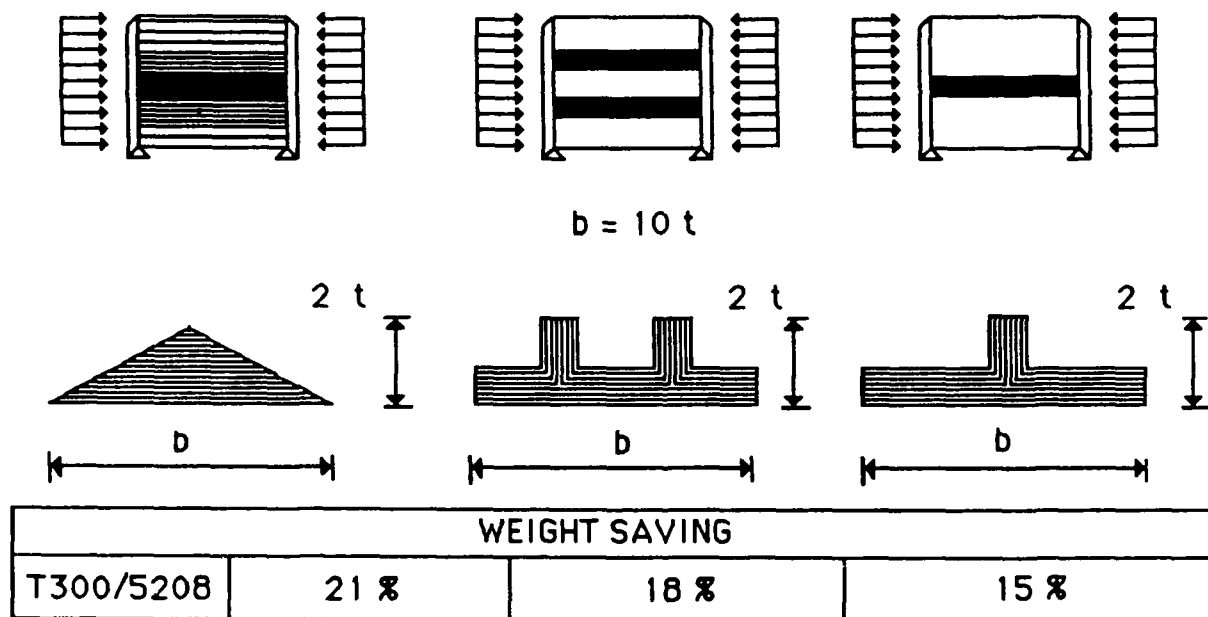


Figure 113. Weight saving for different cross sections whose height is twice the laminate thickness (one-dimensional simply supported plates).

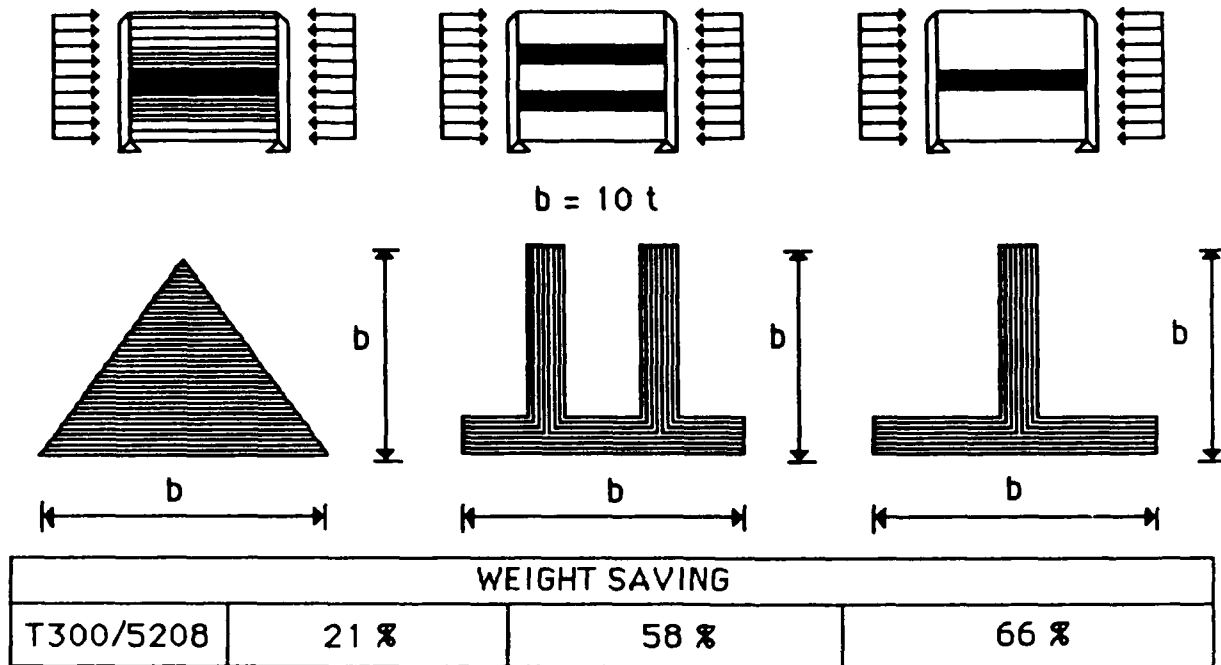


Figure 114. Weight saving for different cross sections whose height is ten times the laminate thickness (one-dimensional simply supported plates).

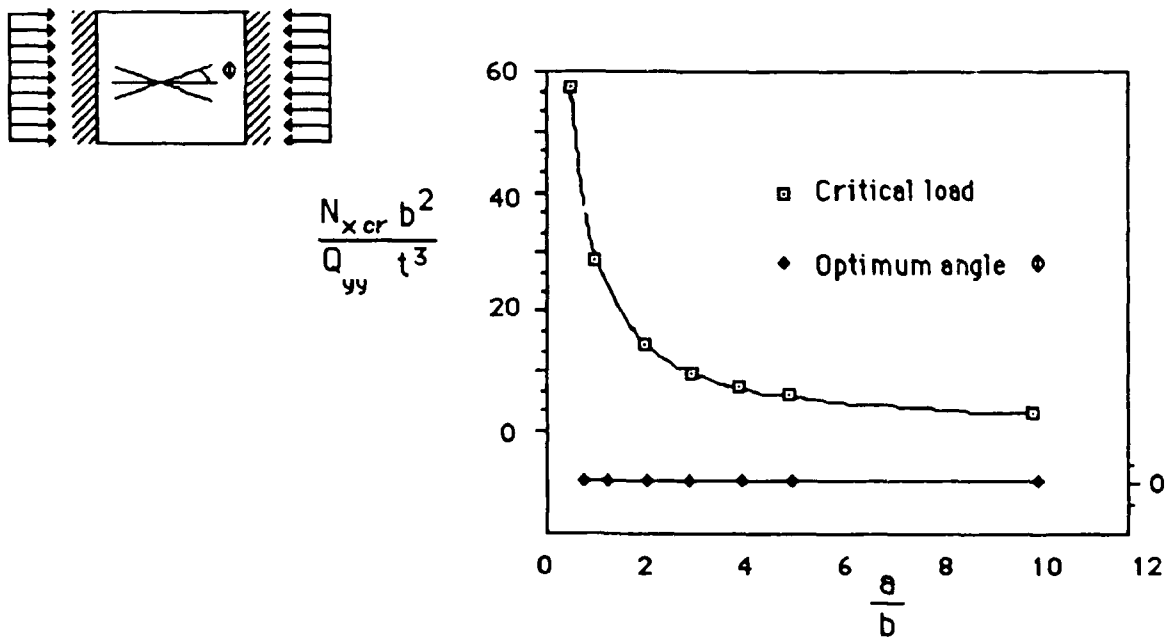


Figure 115. Critical load and optimum angle for an one-dimensional clamped plate.

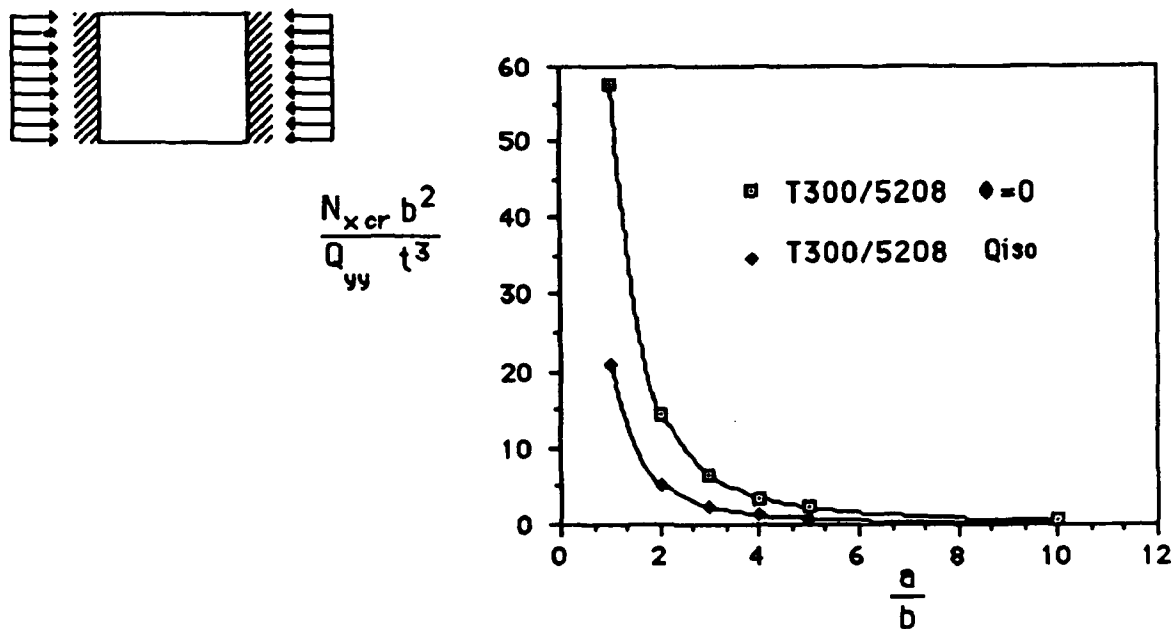


Figure 116. Comparison between critical loads of optimum configuration and quasi-isotropic laminate (one-dimensional clamped plates).

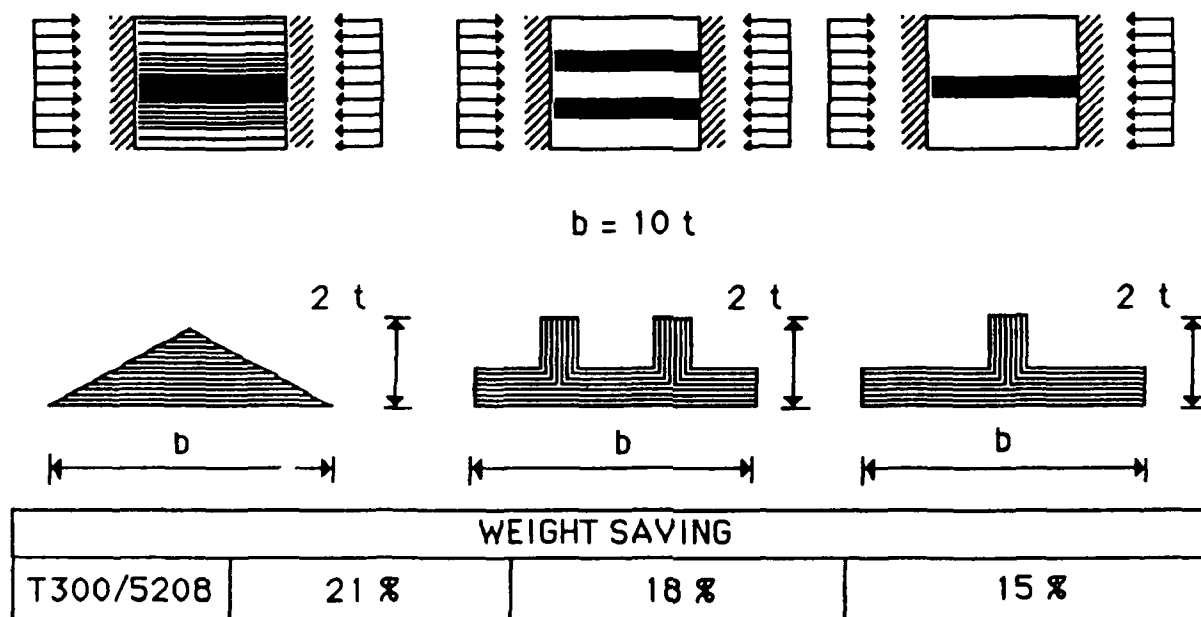


Figure 117. Weight saving for different cross sections whose height is twice the laminate thickness (one-dimensional clamped plates).

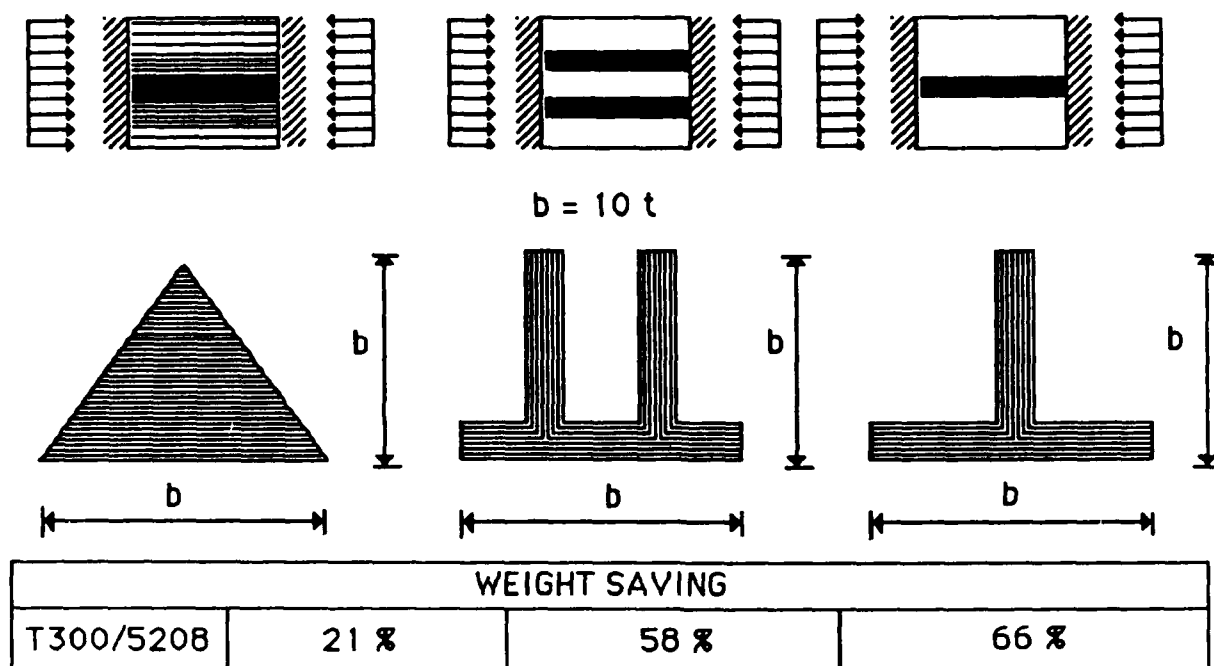


Figure 118. Weight saving for different cross sections whose height is ten times the laminate thickness (one-dimensional simply supported plates).

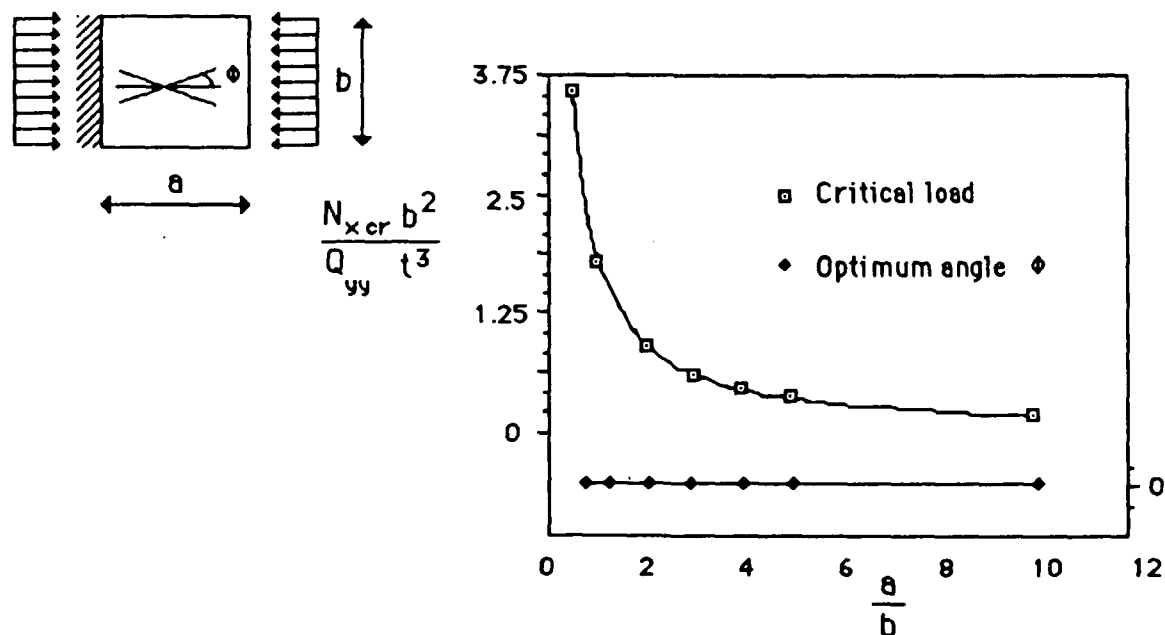


Figure 119. Critical load and optimum angle for an one-dimensional cantilever plate.

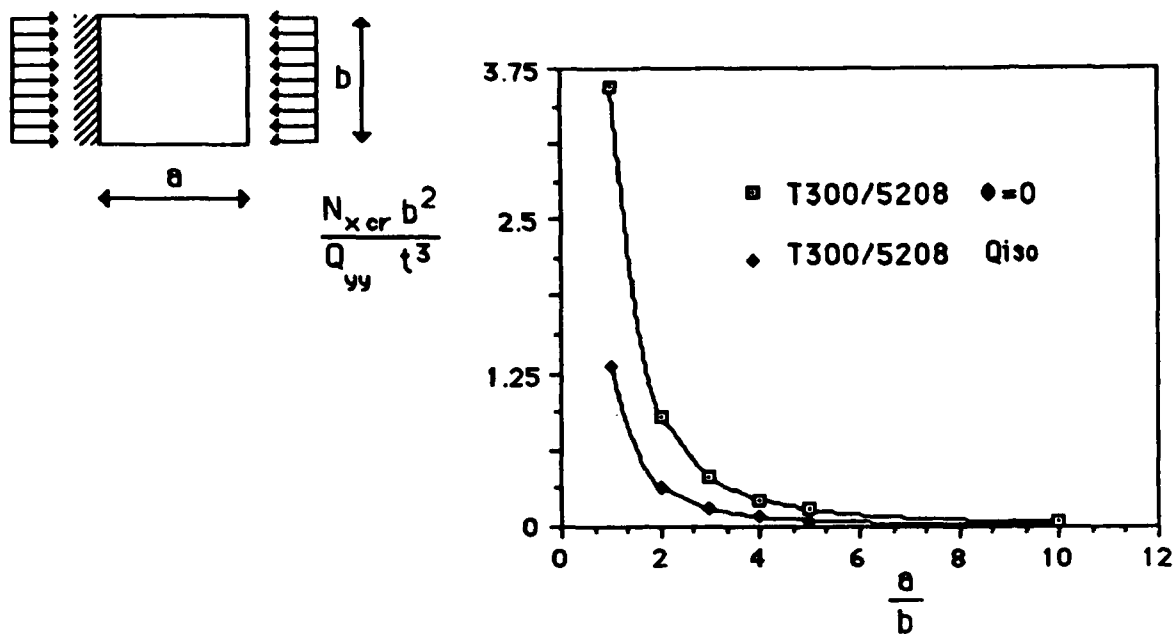


Figure 120. Comparison between critical loads of optimum configuration and quasi-isotropic laminate (cantilever simply supported plates).

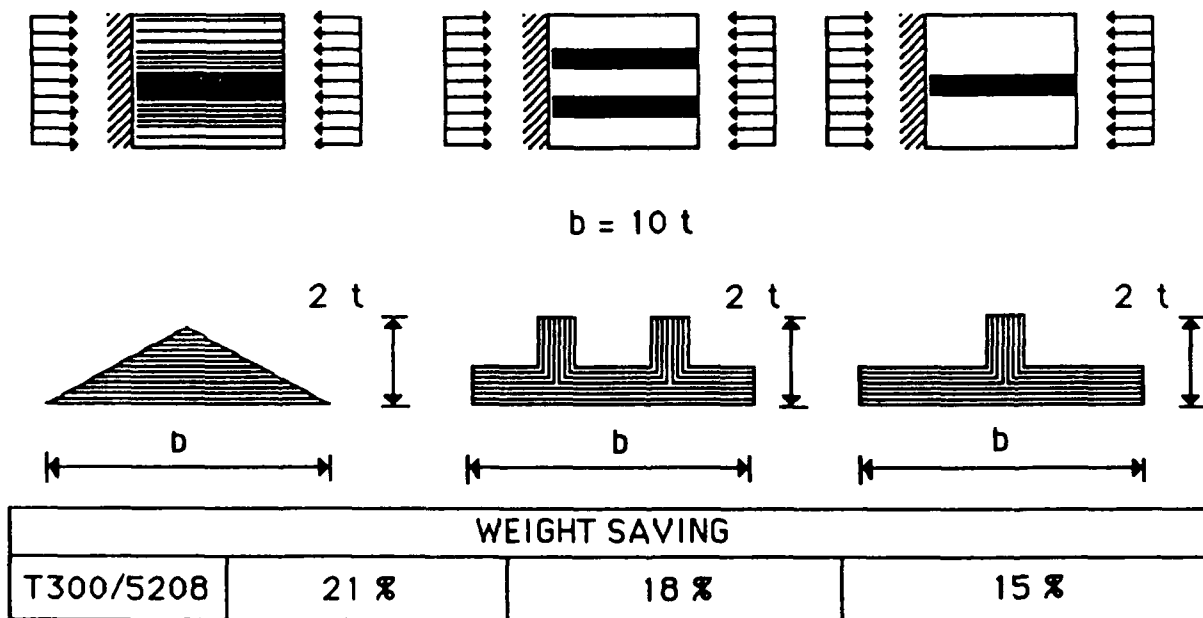


Figure 121. Weight saving for different cross sections whose height is twice the laminate thickness (one-dimensional cantilever plates).



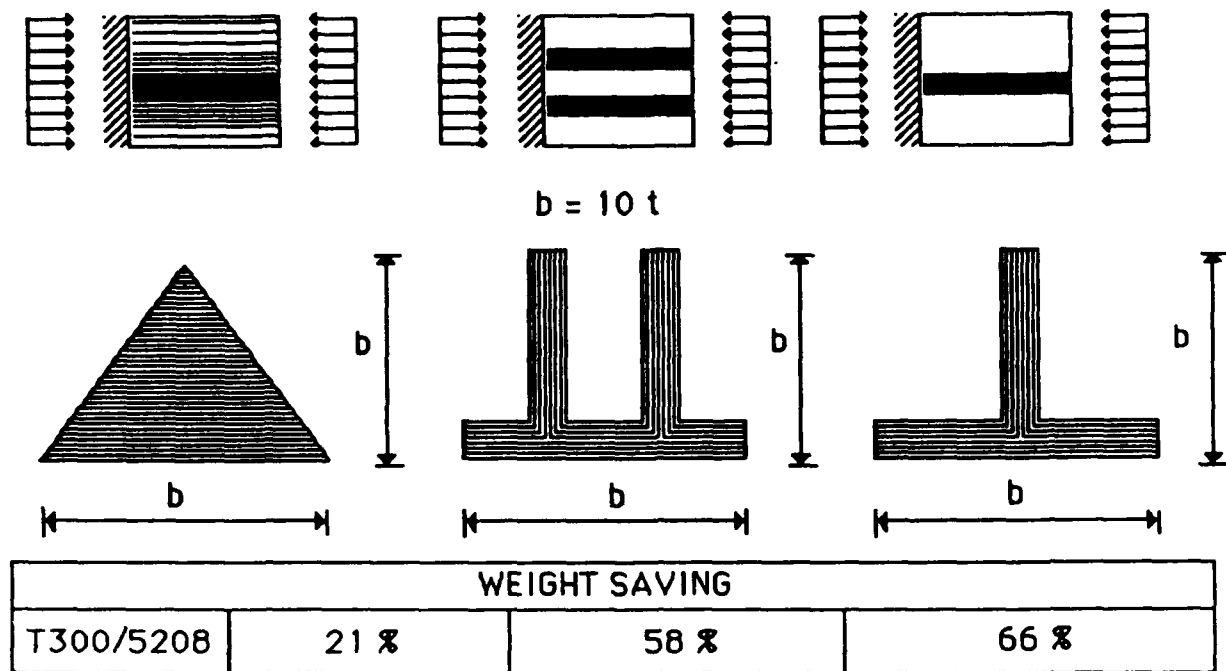


Figure 122. Weight saving for different cross sections whose height is ten times the laminate thickness (one-dimensional simply supported plates).

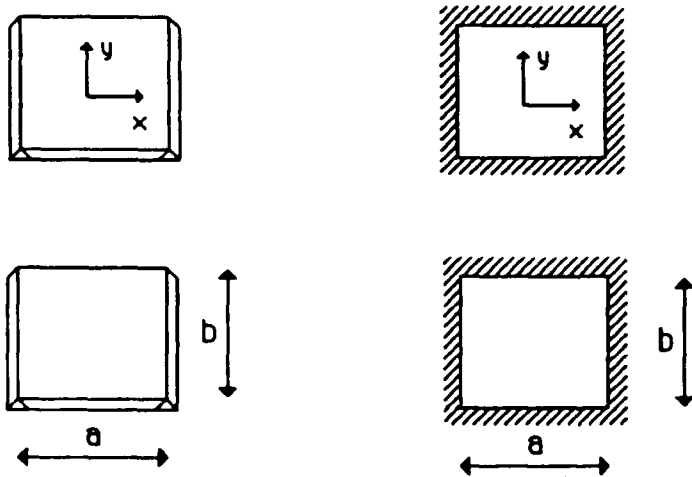


Figure 123. Definition of coordinate axis for two-dimensional plates subjected to uniform uniaxial compression, biaxial compression, shear or combined load.

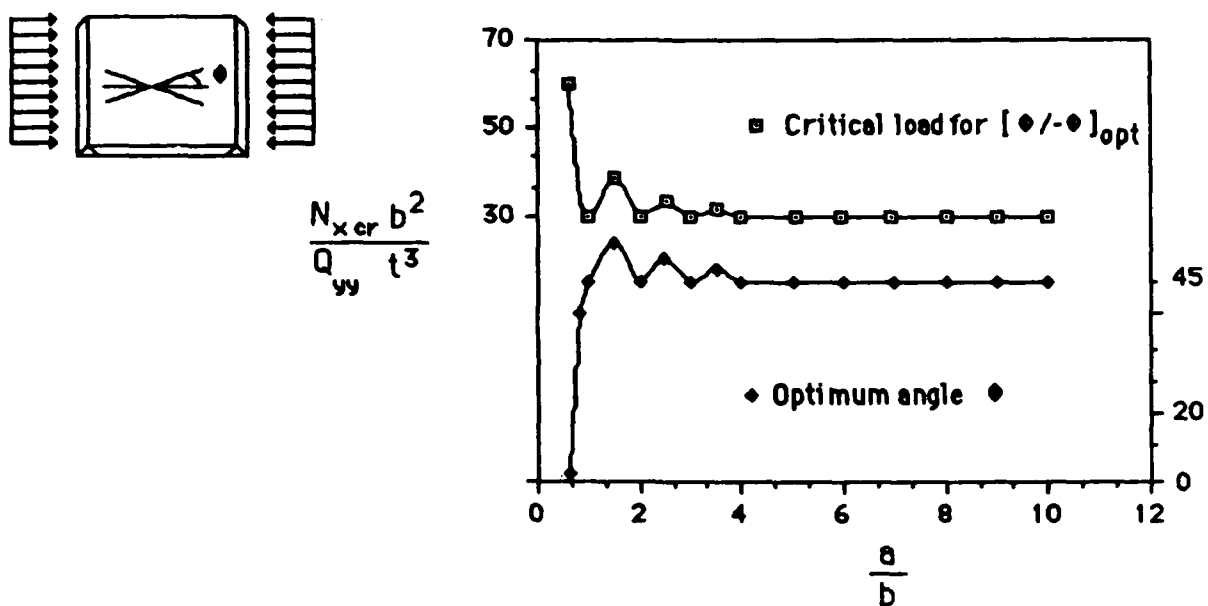


Figure 124. Critical load and optimum angle for a simply supported plate subjected to a uniform uniaxial compression load.

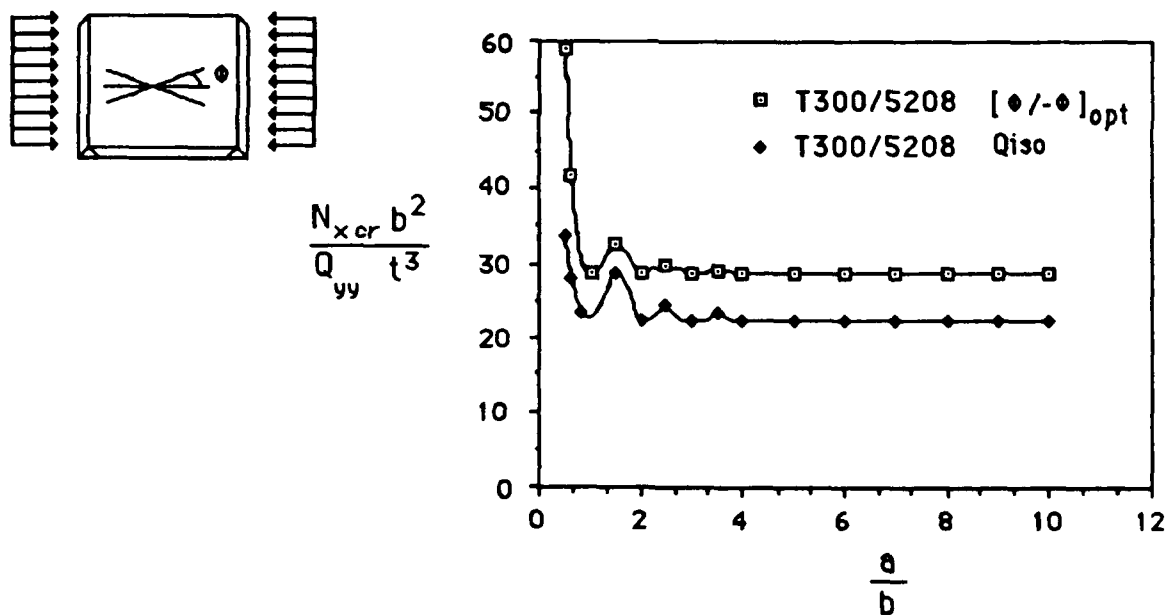
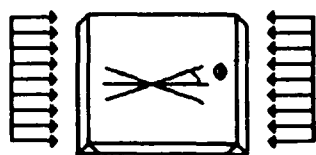


Figure 125. Comparison between critical loads of optimum configuration and quasi-isotropic laminate (simply supported plates subjected to a uniform uniaxial compression load).



$$\frac{N_{xcr} b^2}{Q_{yy} t^3}$$

$$\frac{a}{b} = 1$$

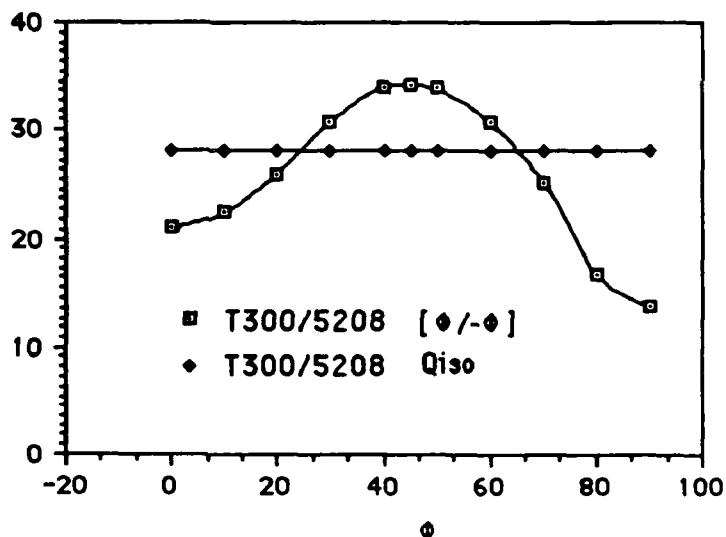
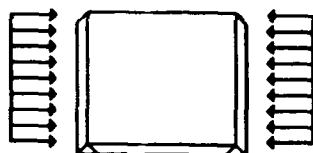


Figure 126. Comparison of critical loads for cross-ply and quasi-isotropic laminate for a square plate (simply supported plates subjected to a uniform uniaxial compression load).



RELATIVE WEIGHT  
RESPECT TO  
[ $\phi/-\phi$ ] opt

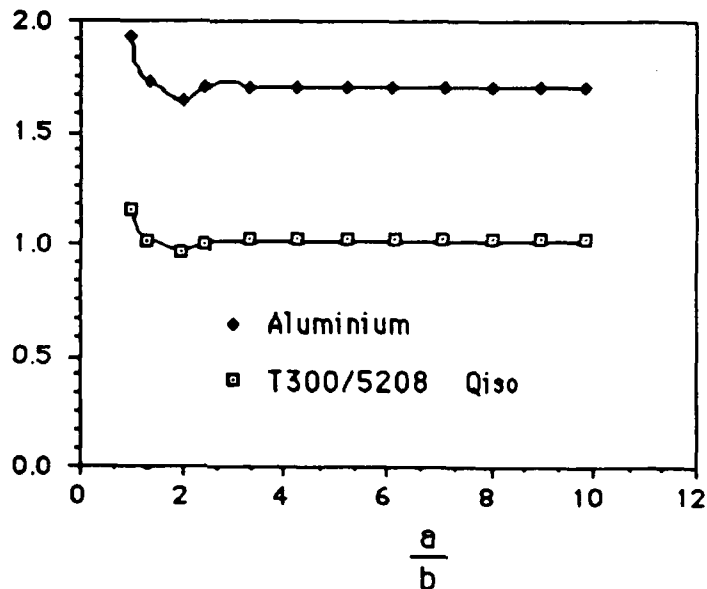


Figure 127. Comparison between weights of aluminium and the optimum configuration of T300/N5208 (simply supported plates subjected to a uniform uniaxial compression load).

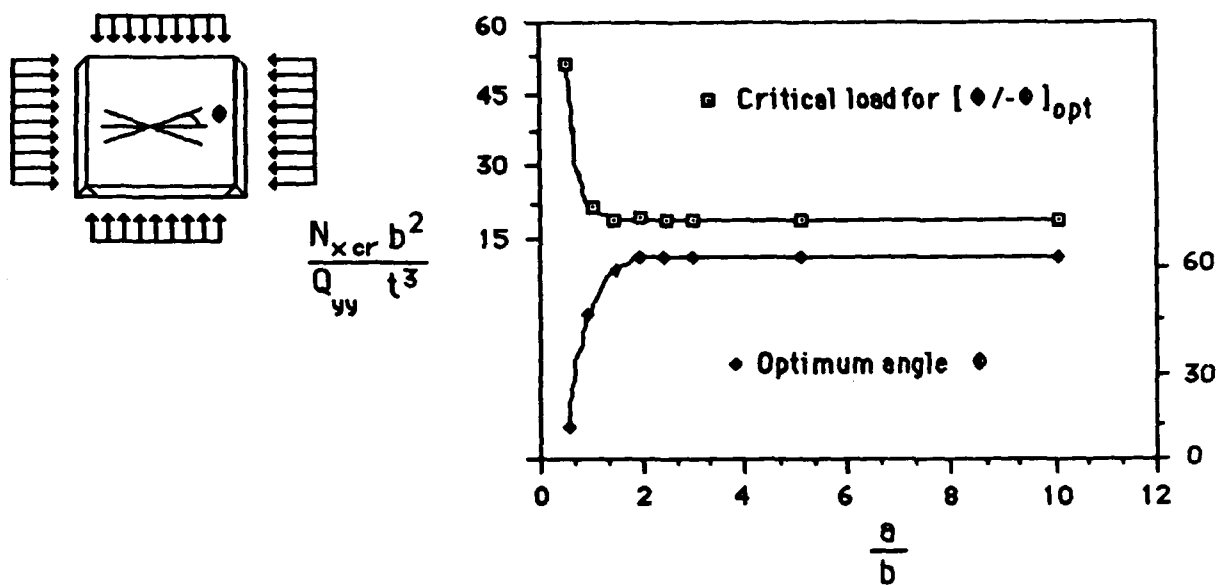


Figure 128. Critical load and optimum angle for a simply supported plate subjected to a uniform biaxial compression load ( $N_y = N_x/2$ ).

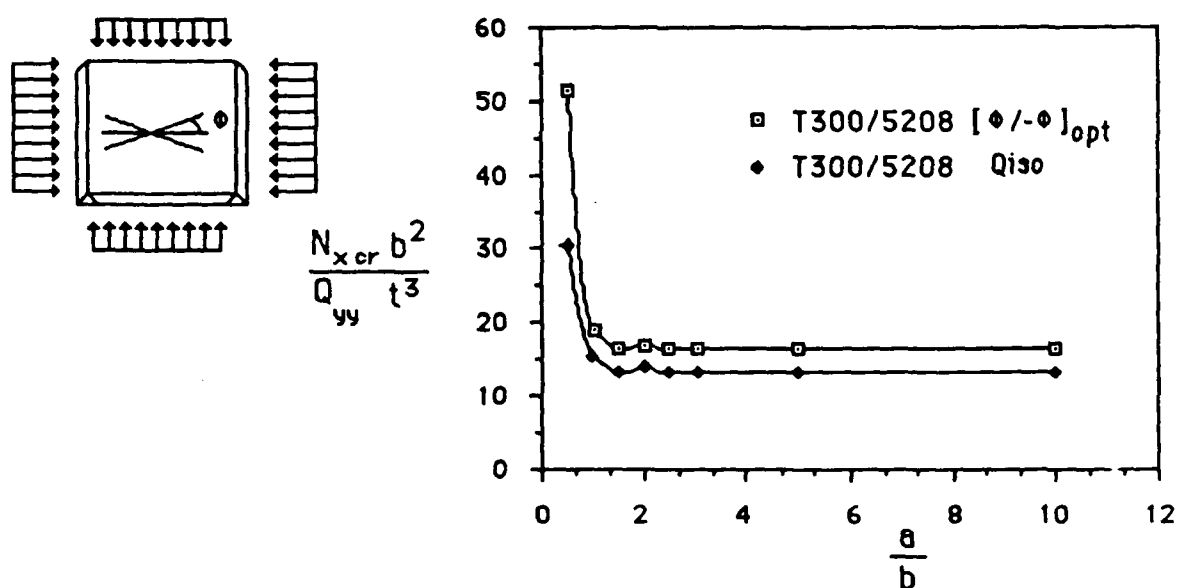


Figure 129. Comparison between critical loads of optimum configuration and quasi-isotropic laminate (simply supported plates subjected to a uniform biaxial compression load ( $N_y = N_x/2$ )).

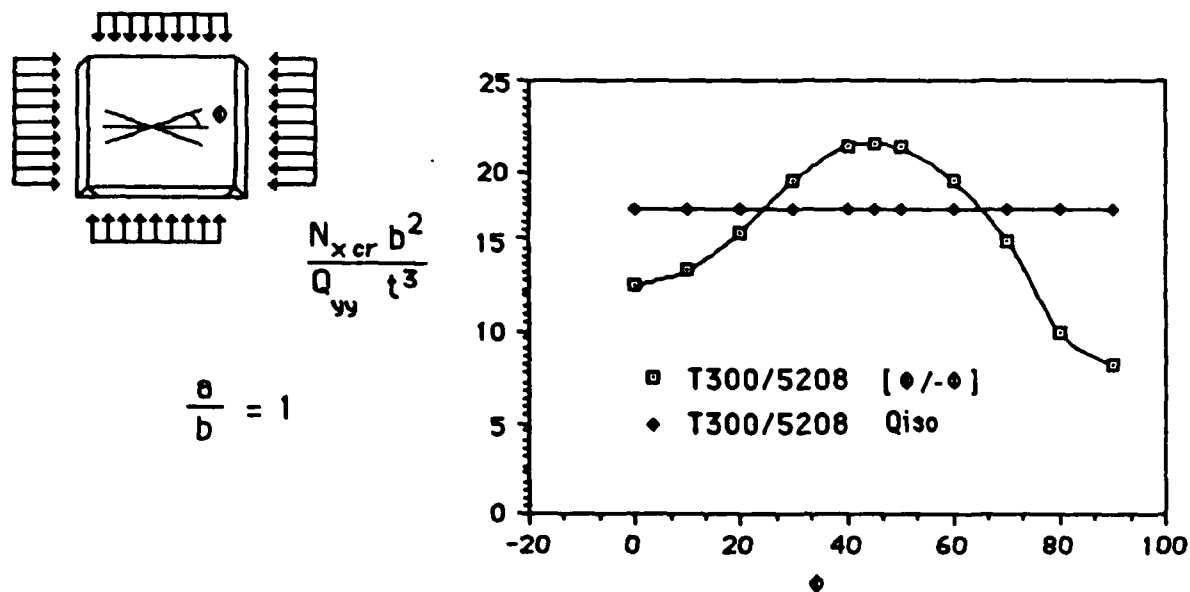


Figure 130. Comparison of critical loads for cross-ply and quasi-isotropic laminate for a square plate (simply supported plates subjected to a uniform biaxial compression load ( $N_y=N_x/2$ )).

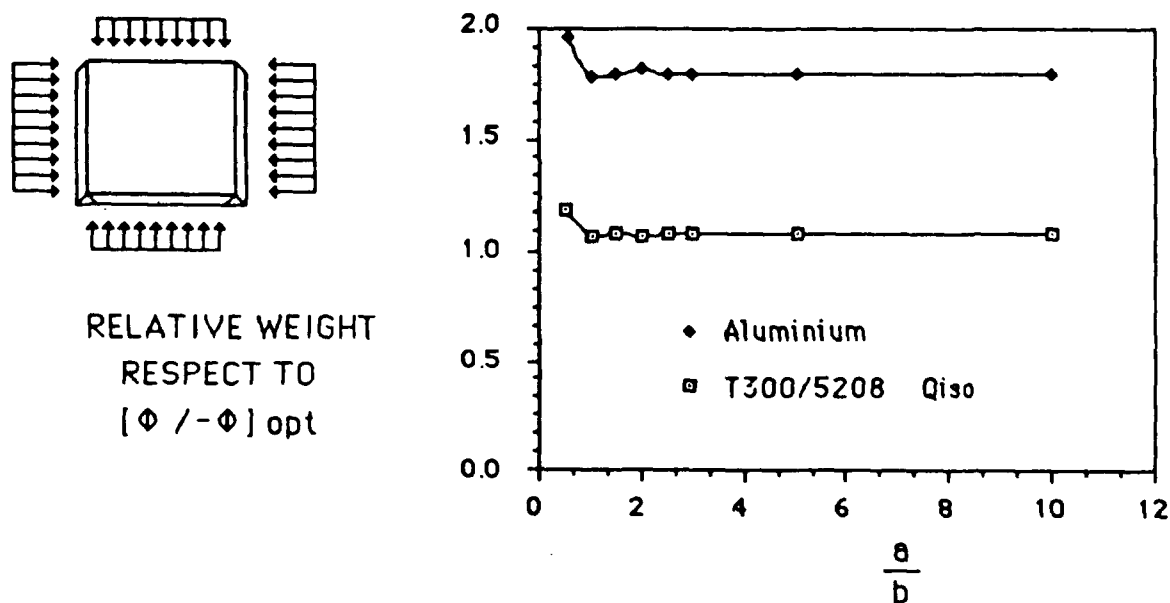


Figure 131. Comparison between weights of aluminium and the optimum configuration of T300/N5208 (simply supported plates subjected to a uniform biaxial compression load ( $N_y=N_x/2$ )).

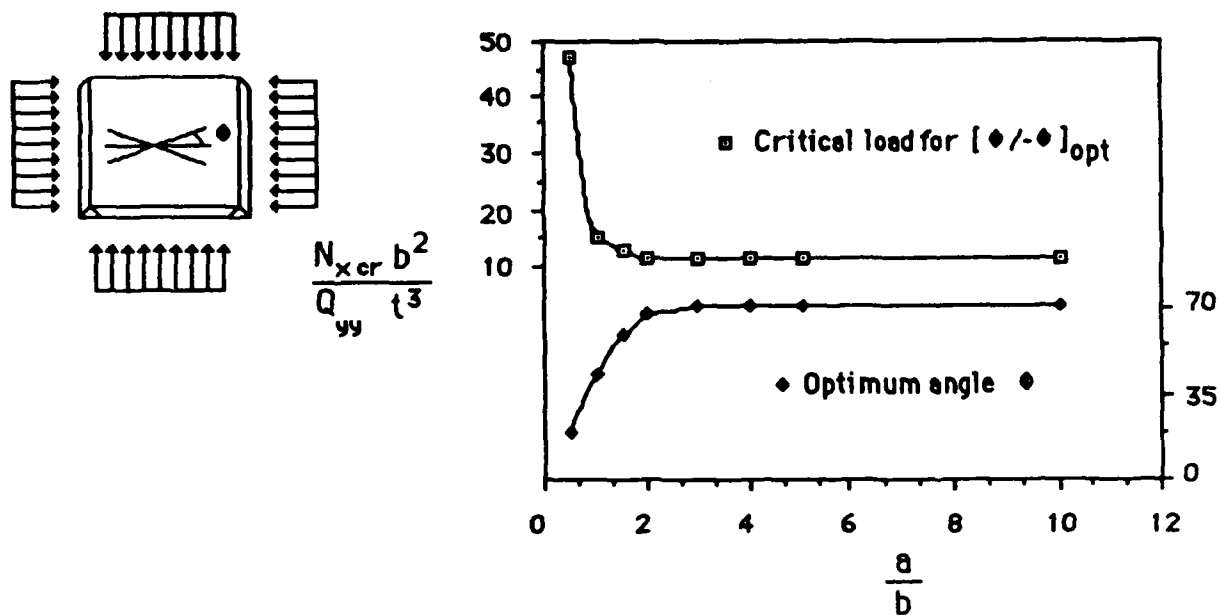


Figure 132. Critical load and optimum angle for a simply supported plate subjected to a uniform biaxial compression load ( $N_y=N_x$ ).

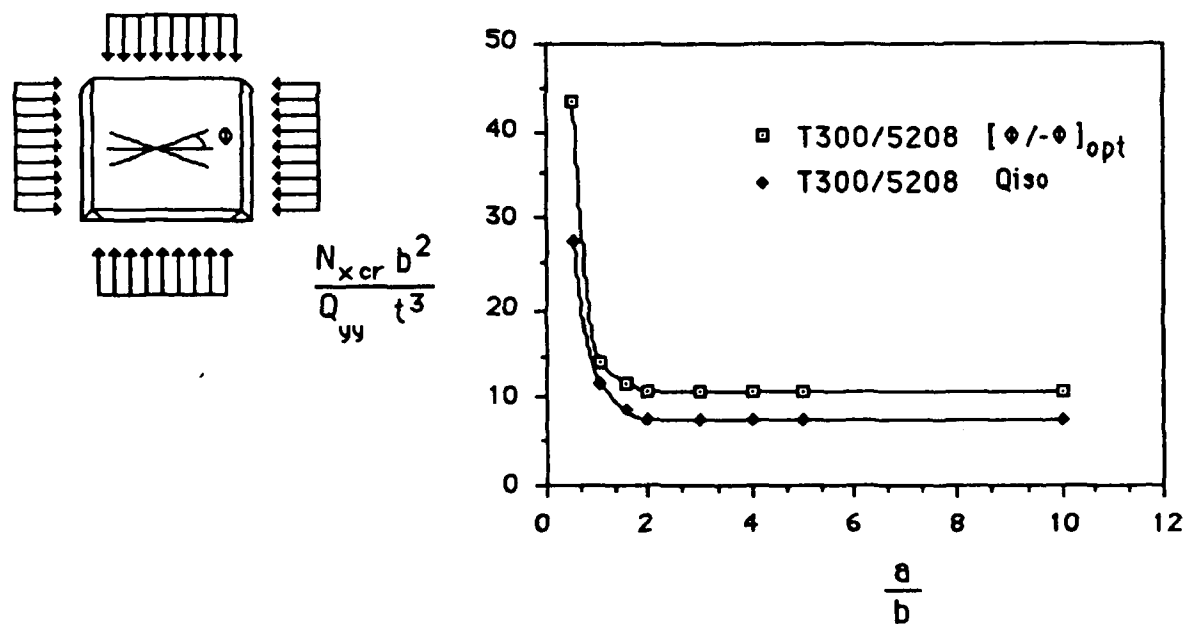


Figure 133. Comparison between critical loads of optimum configuration and quasi-isotropic laminate. (simply supported plates subjected to a uniform biaxial compression load ( $N_y=N_x$ )).

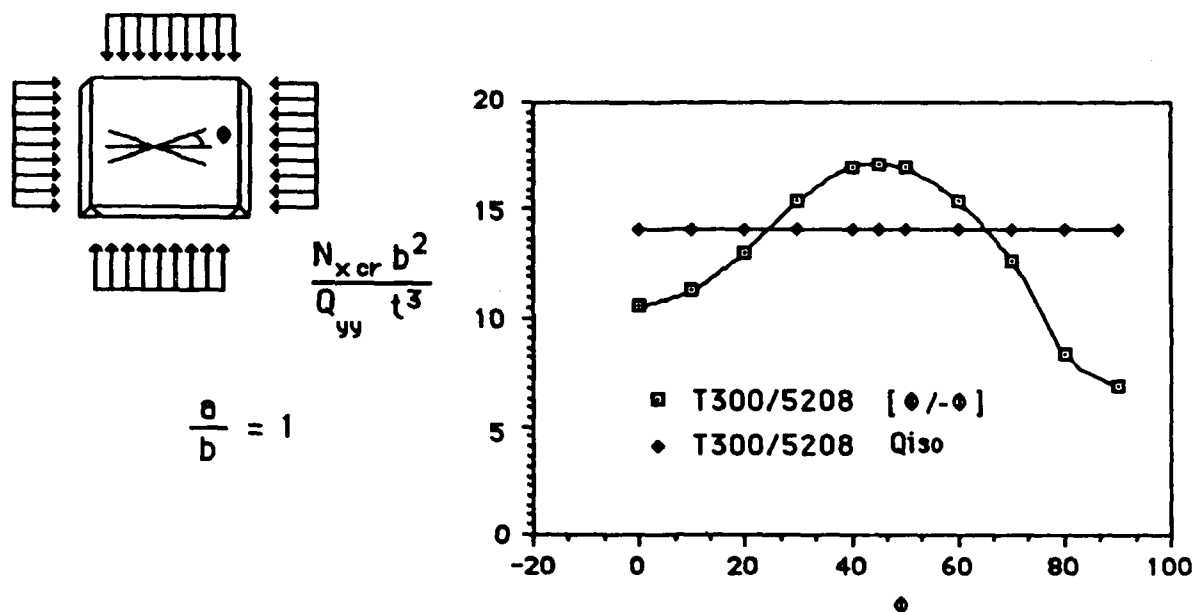


Figure 134. Comparison of critical loads for cross-ply and quasi-isotropic laminate for a square plate (simply supported plates subjected to a uniform biaxial compression load ( $N_y = N_x$ )).

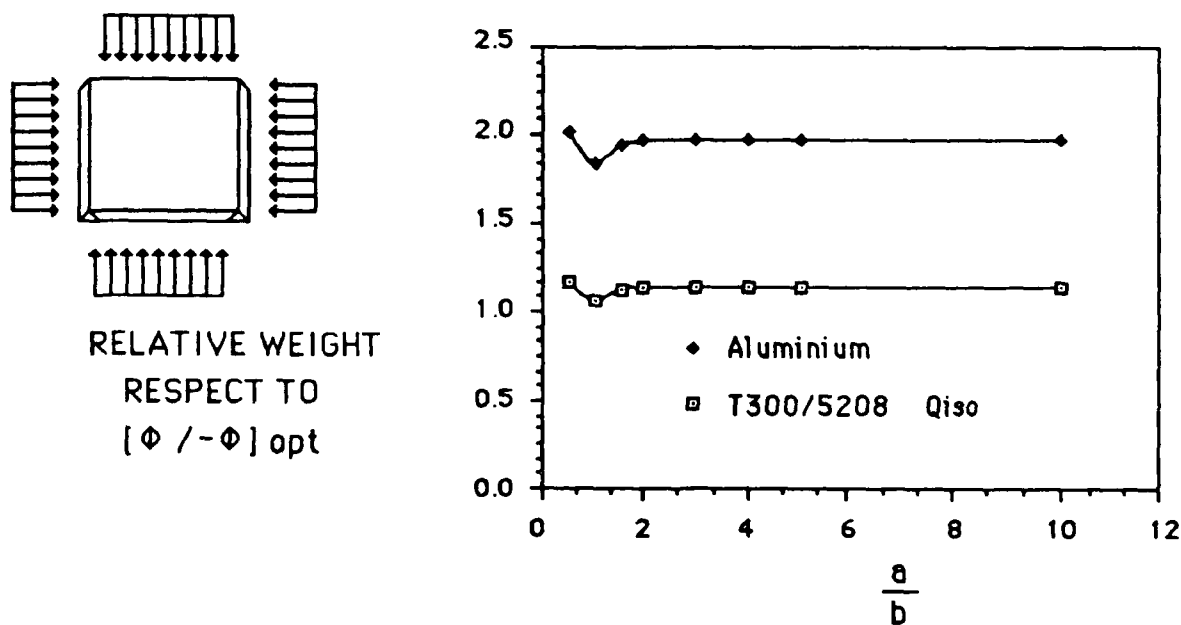


Figure 135. Comparison between weights of aluminium and the optimum configuration of T300/N5208 (simply supported plates subjected to a uniform biaxial compression load ( $N_y = N_x$ )).

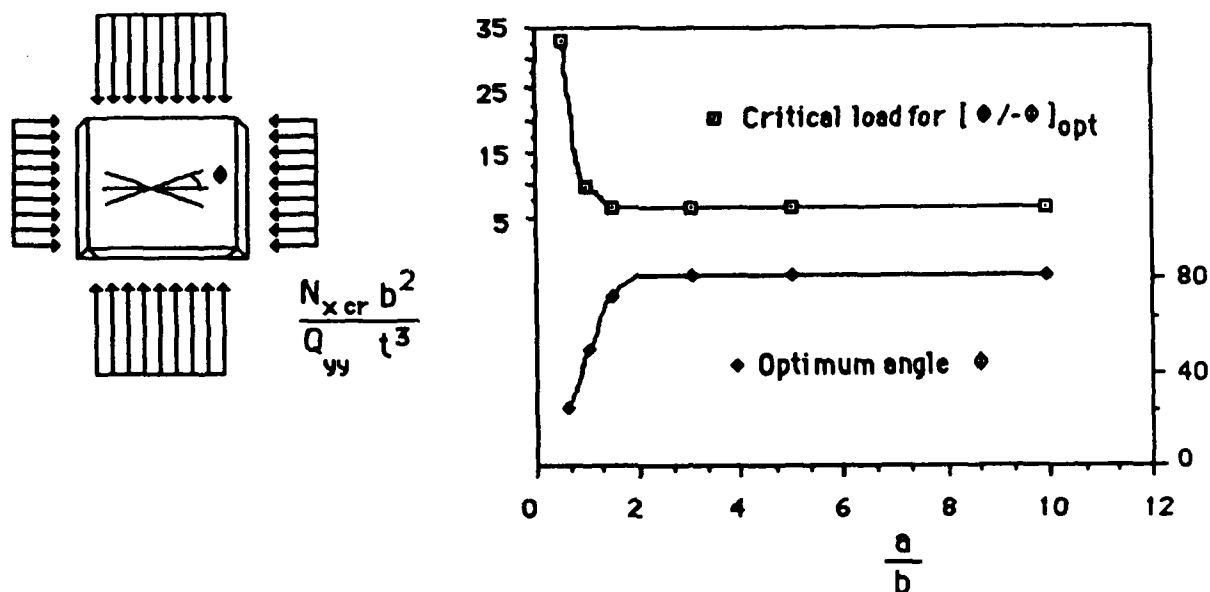


Figure 136. Critical load and optimum angle for a simply supported plate subjected to a uniform biaxial compression load ( $N_y=2*N_x$ ).

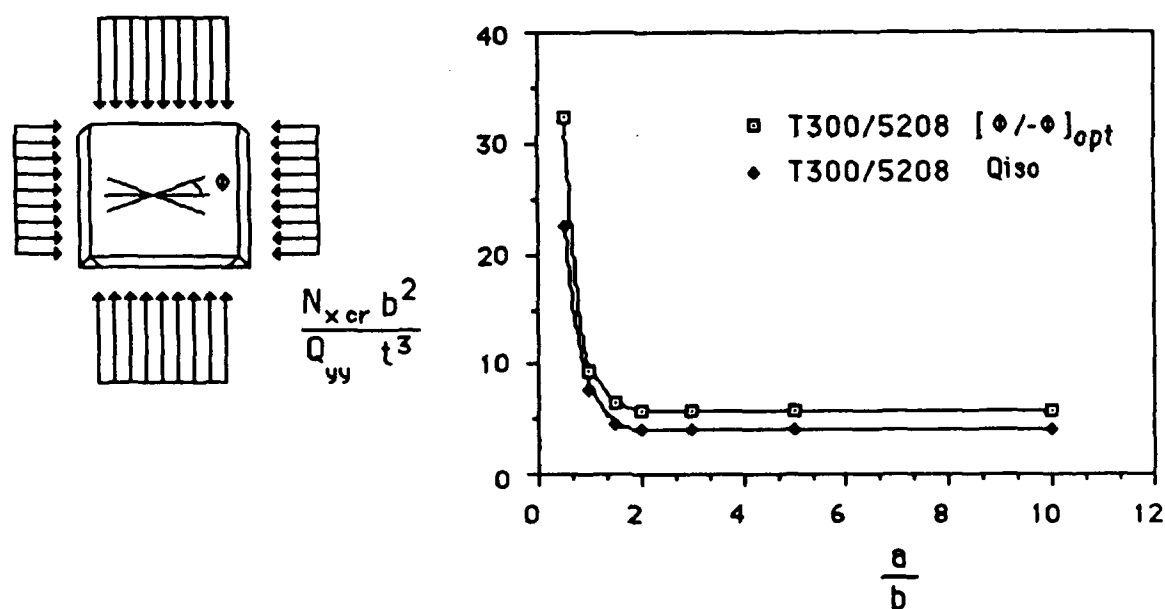


Figure 137. Comparison between critical loads of optimum configuration and quasi-isotropic laminate (simply supported plates subjected to a uniform biaxial compression load ( $N_y=2*N_x$ )).



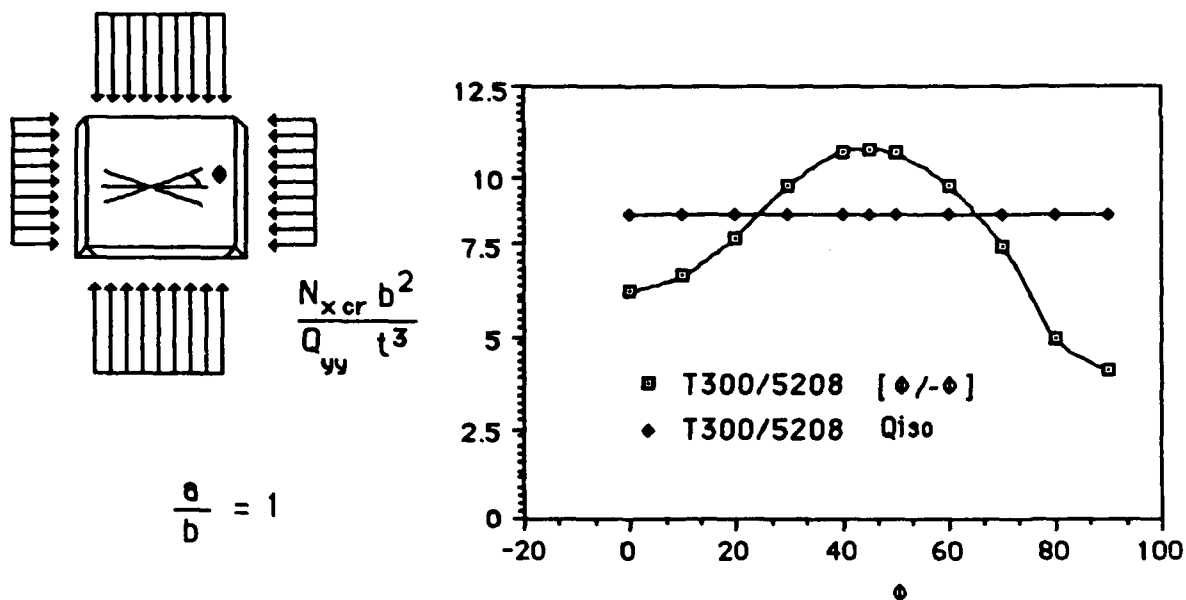


Figure 138. Comparison of critical loads for cross-ply and quasi-isotropic laminate for a square plate (simply supported plates subjected to a uniform biaxial compression load ( $N_y=2*N_x$ )).

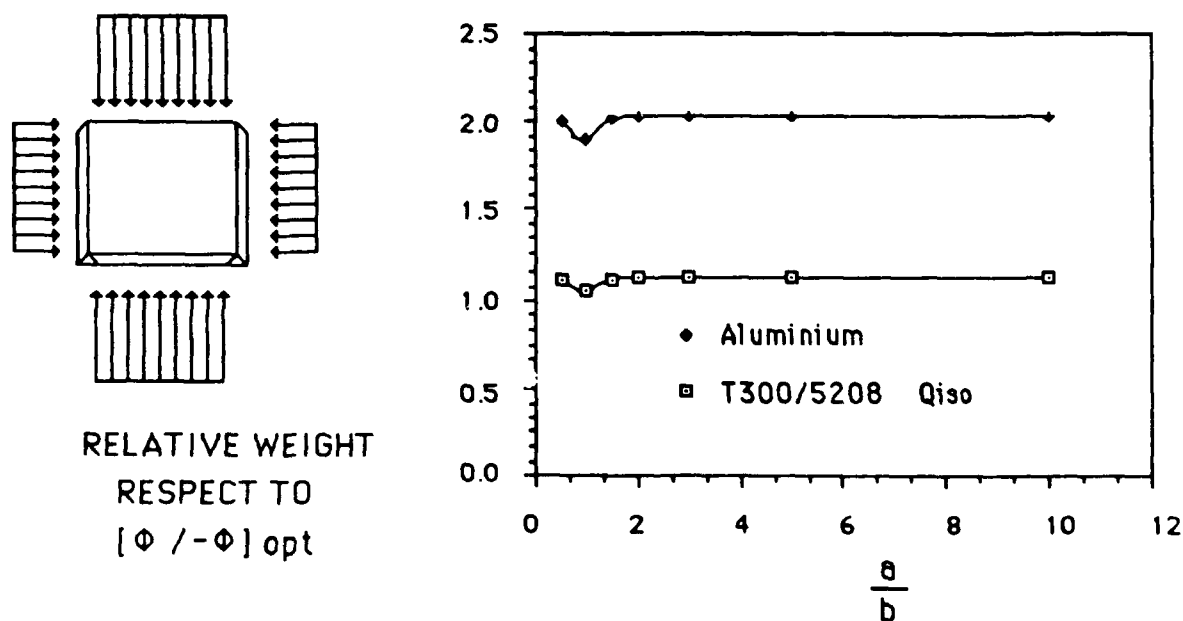


Figure 139. Comparison between weights of aluminium and the optimum configuration of T300/N5208 (simply supported plates subjected to a uniform biaxial compression load ( $N_y=2*N_x$ )).

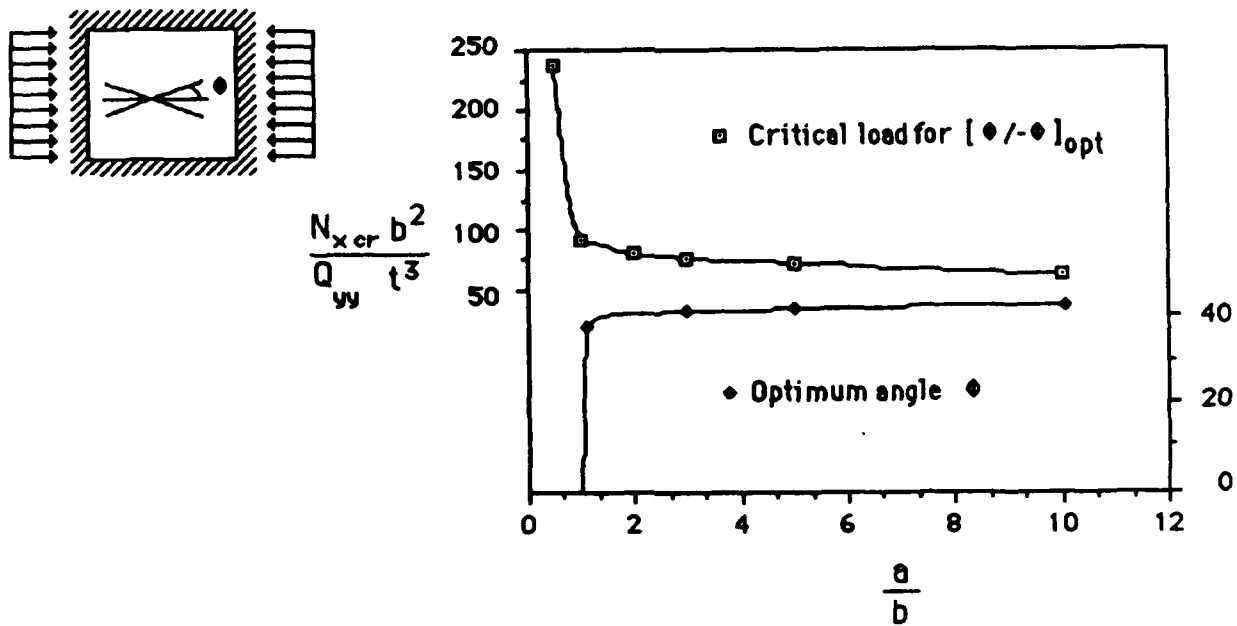


Figure 140. Critical load and optimum angle for a clamped plate subjected to a uniform uniaxial compression load.

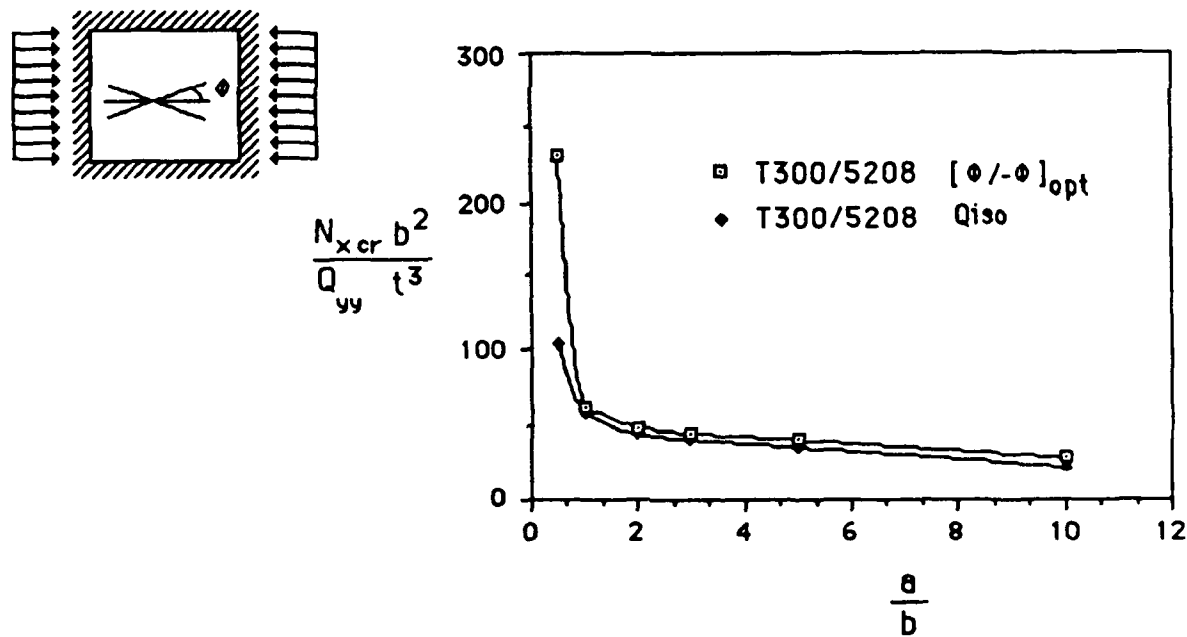
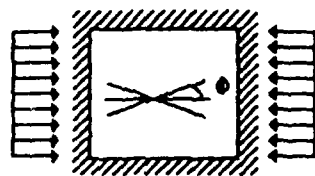


Figure 141. Comparison between critical loads of optimum configuration and quasi-isotropic laminate (clamped plates subjected to a uniform uniaxial compression load).



$$\frac{N_{xcr} b^2}{Q_{yy} t^3}$$

$$\frac{a}{b} = 1$$

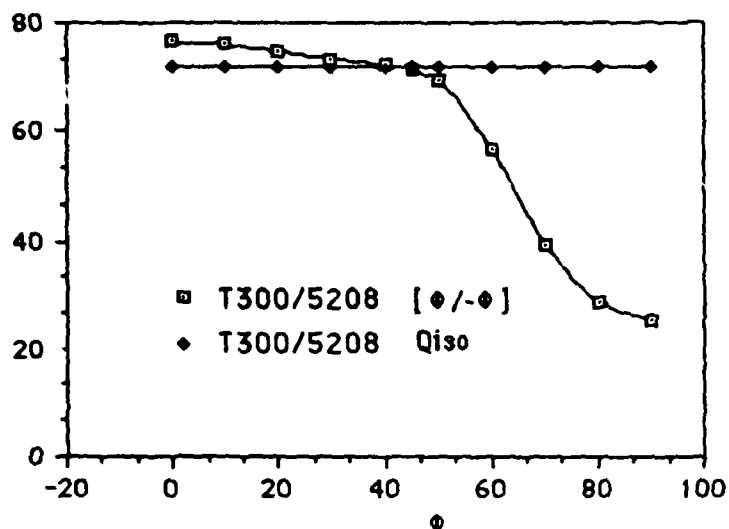
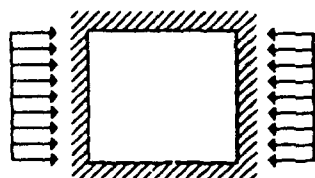


Figure 142. Comparison of critical loads for cross-ply and quasi-isotropic laminate for a square plate (clamped plates subjected to a uniform uniaxial compression load).



RELATIVE WEIGHT  
RESPECT TO  
[ $\phi$  / -  $\phi$ ] opt

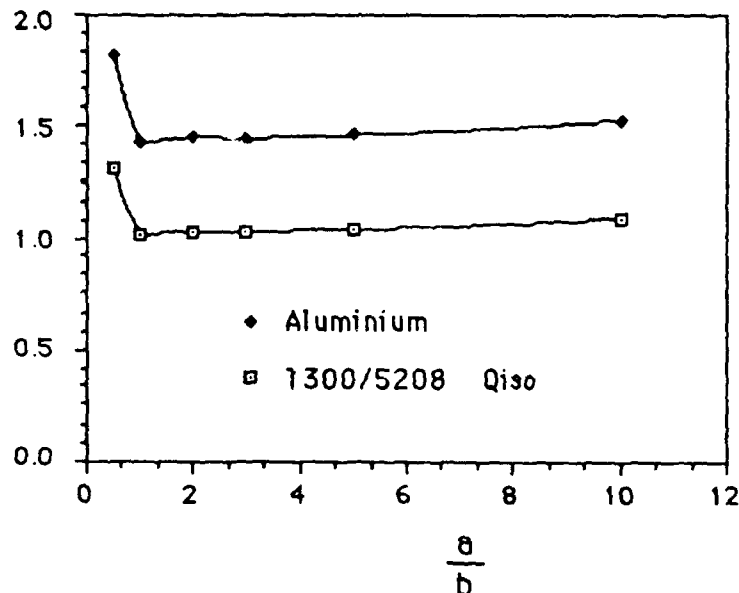


Figure 143. Comparison between weights of aluminium and the optimum configuration of T300/N5208 (clamped plates subjected to a uniform uniaxial compression load).

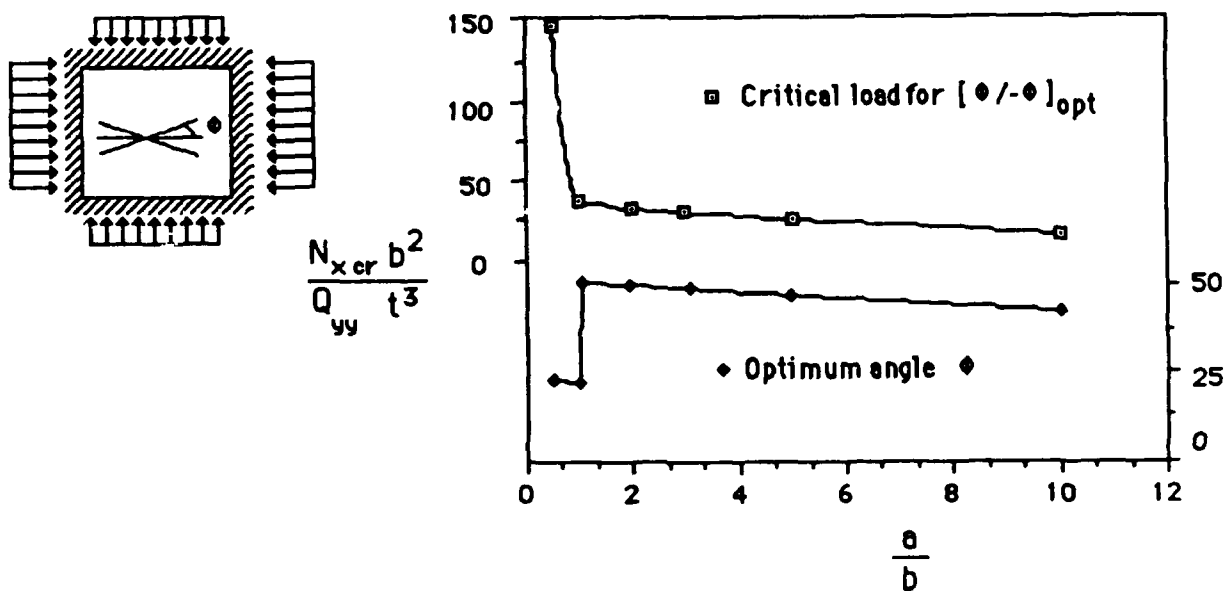


Figure 144. Critical load and optimum angle for a clamped plate subjected to a uniform biaxial compression load ( $N_y = N_x/2$ ).

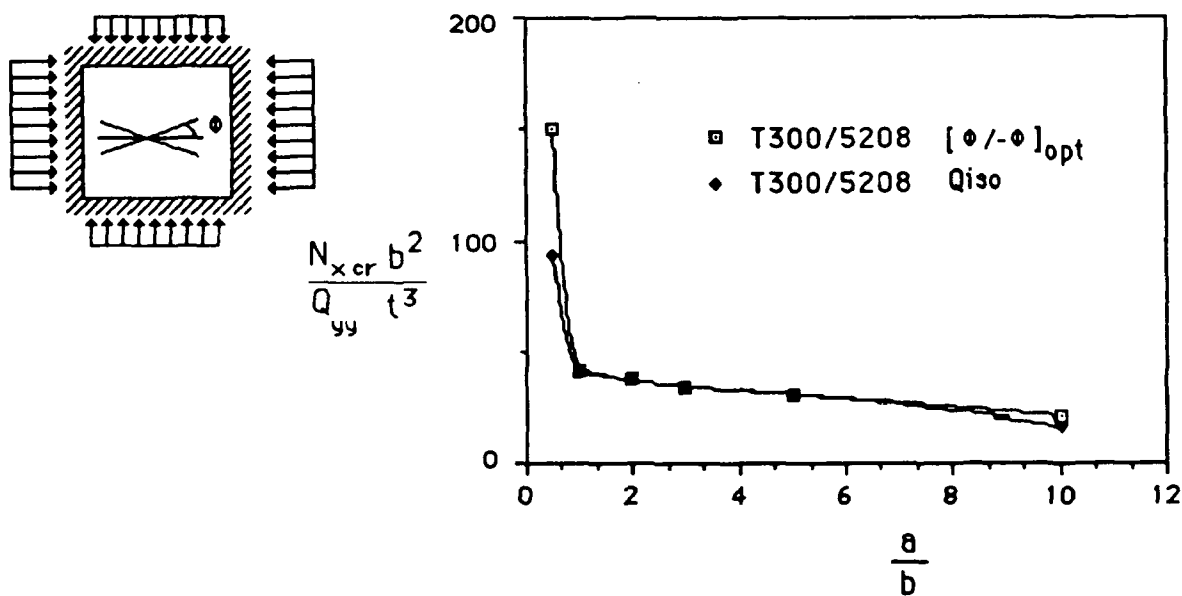


Figure 145. Comparison between critical loads of optimum configuration and quasi-isotropic laminate (clamped plates subjected to a uniform biaxial compression load ( $N_y = N_x/2$ )).

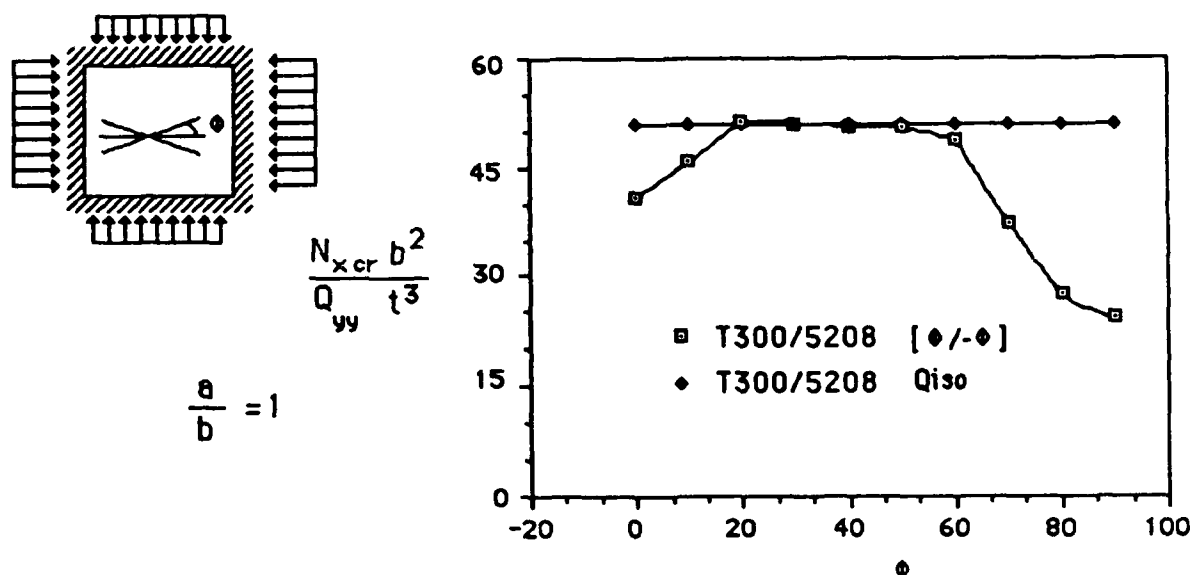


Figure 146. Comparison of critical loads for cross-ply and quasi-isotropic laminate for a square plate (clamped plates subjected to a uniform biaxial compression load ( $N_y = N_x/2$ )).

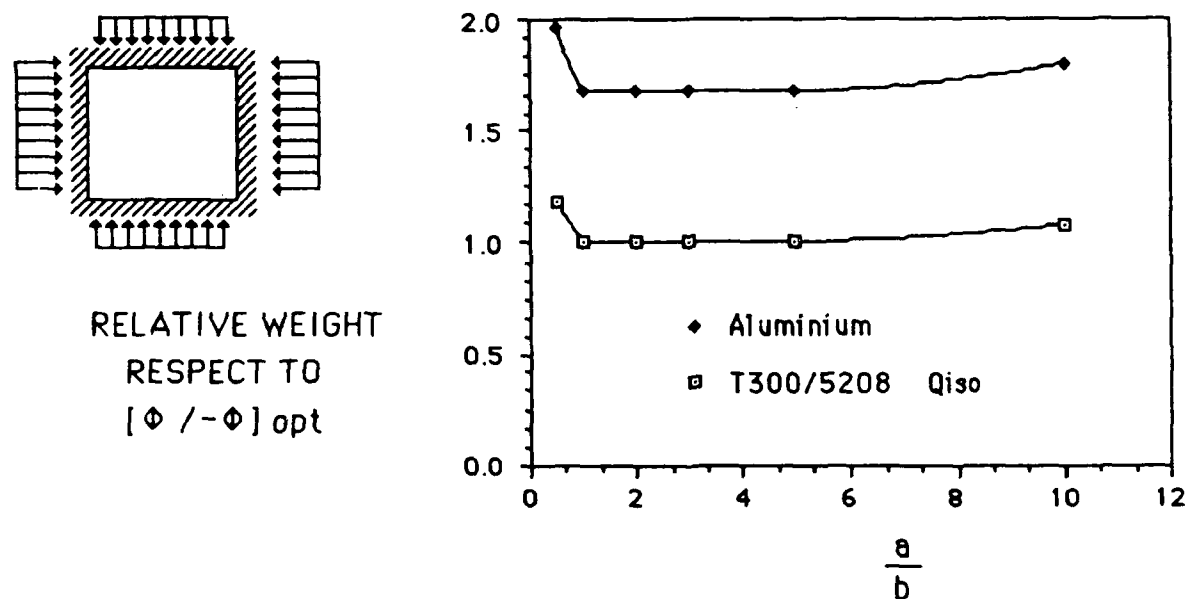


Figure 147. Comparison between weights of aluminium and the optimum configuration of T300/N5208 (clamped plates subjected to a uniform biaxial compression load ( $N_y = N_x/2$ )).

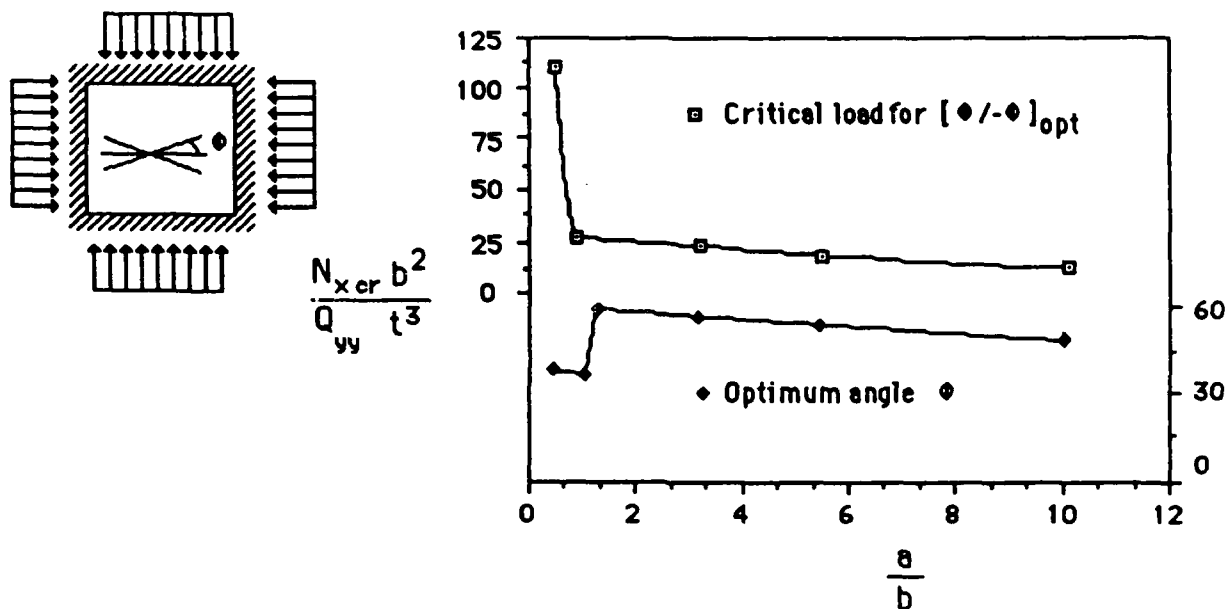


Figure 148. Critical load and optimum angle for a clamped plate subjected to a uniform biaxial compression load ( $N_y=N_x$ ).

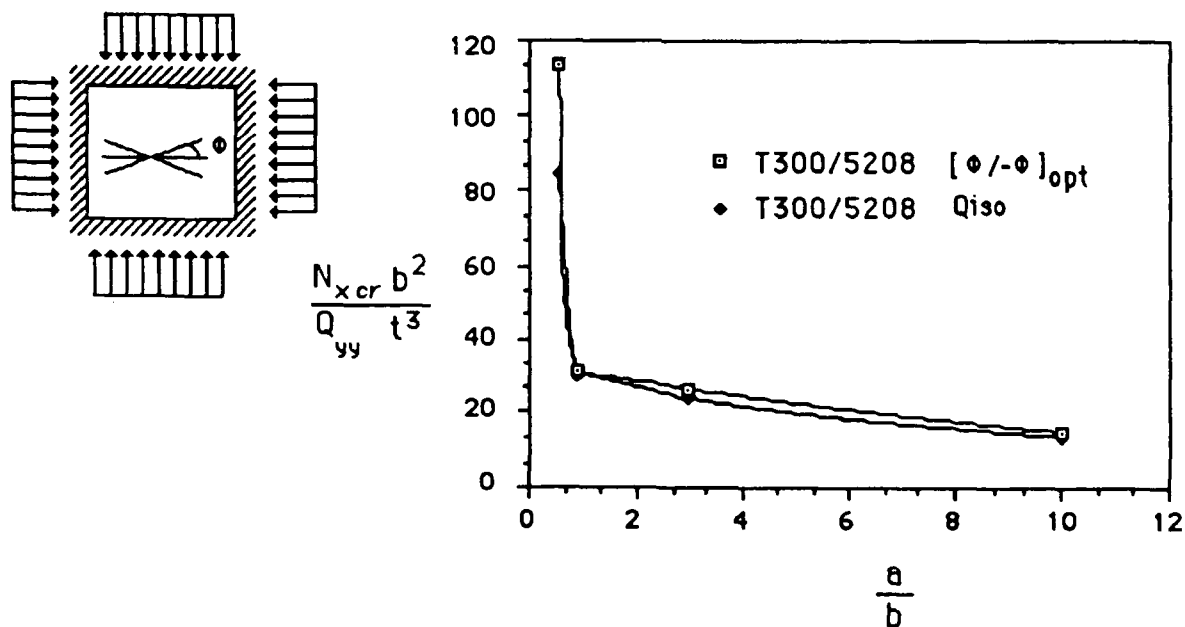


Figure 149. Comparison between critical loads of optimum configuration and quasi-isotropic laminate (clamped plates subjected to a uniform biaxial compression load ( $N_y=N_x$ )).

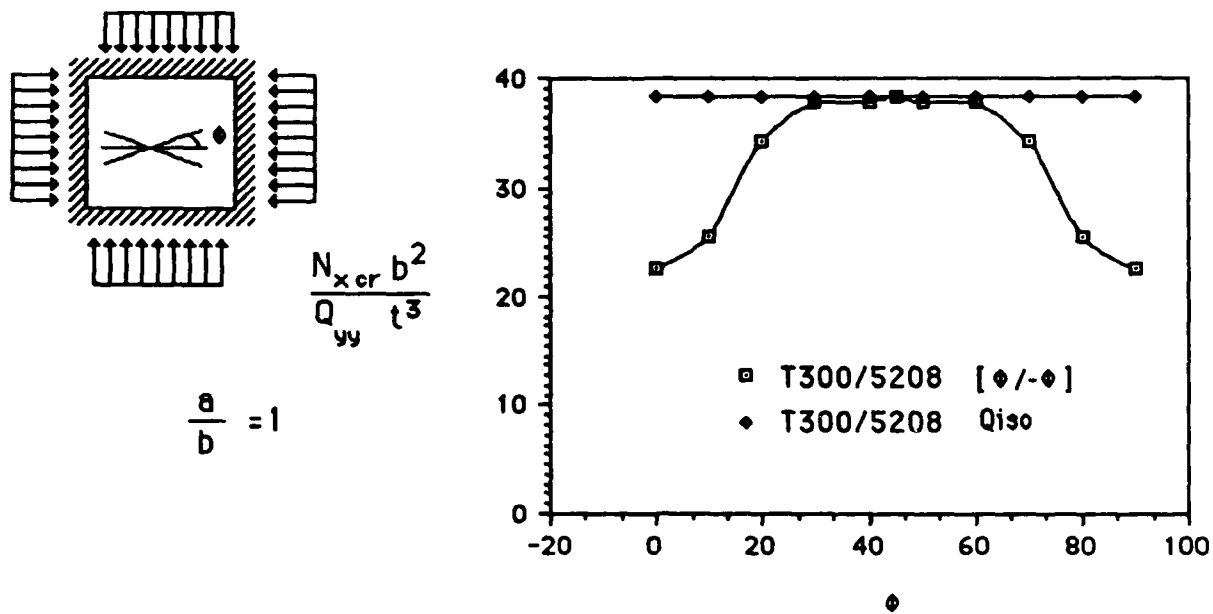


Figure 150. Comparison of critical loads for cross-ply and quasi-isotropic laminate for a square plate (clamped plates subjected to a uniform biaxial compression load ( $N_y=N_x$ )).

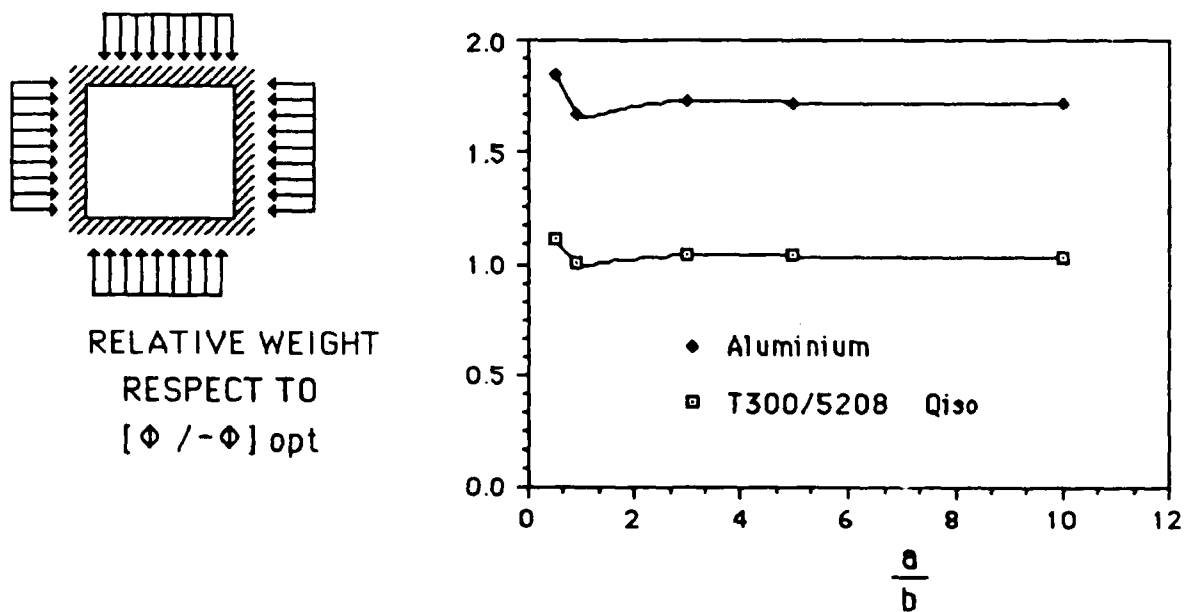


Figure 151. Comparison between weights of aluminium and the optimum configuration of T300/N5208 (clamped plates subjected to a uniform biaxial compression load ( $N_y=N_x$ )).

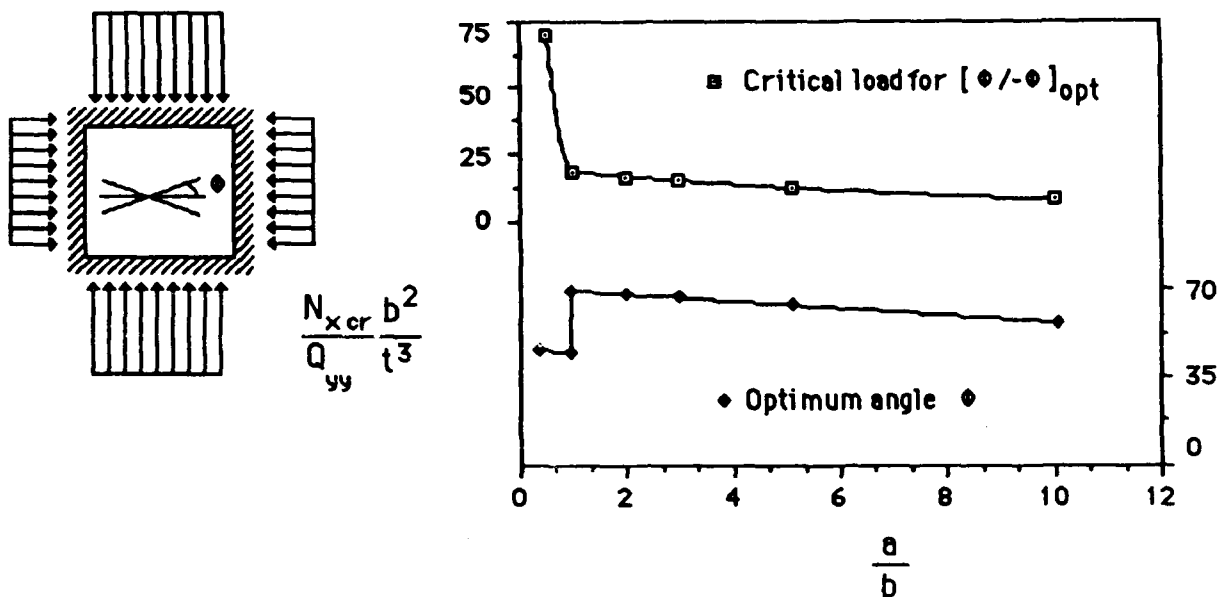


Figure 152. Critical load and optimum angle for a clamped plate subjected to a uniform biaxial compression load ( $N_y=2*N_x$ ).

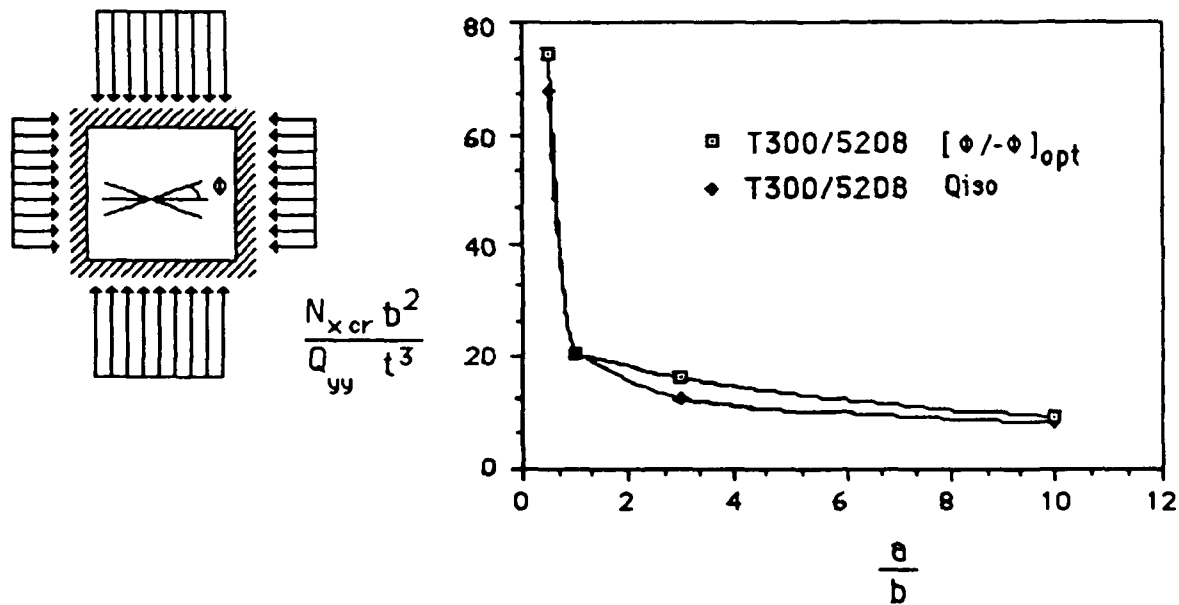


Figure 153. Comparison between critical loads of optimum configuration and quasi-isotropic laminate (clamped plates subjected to a uniform biaxial compression load ( $N_y=2*N_x$ )).



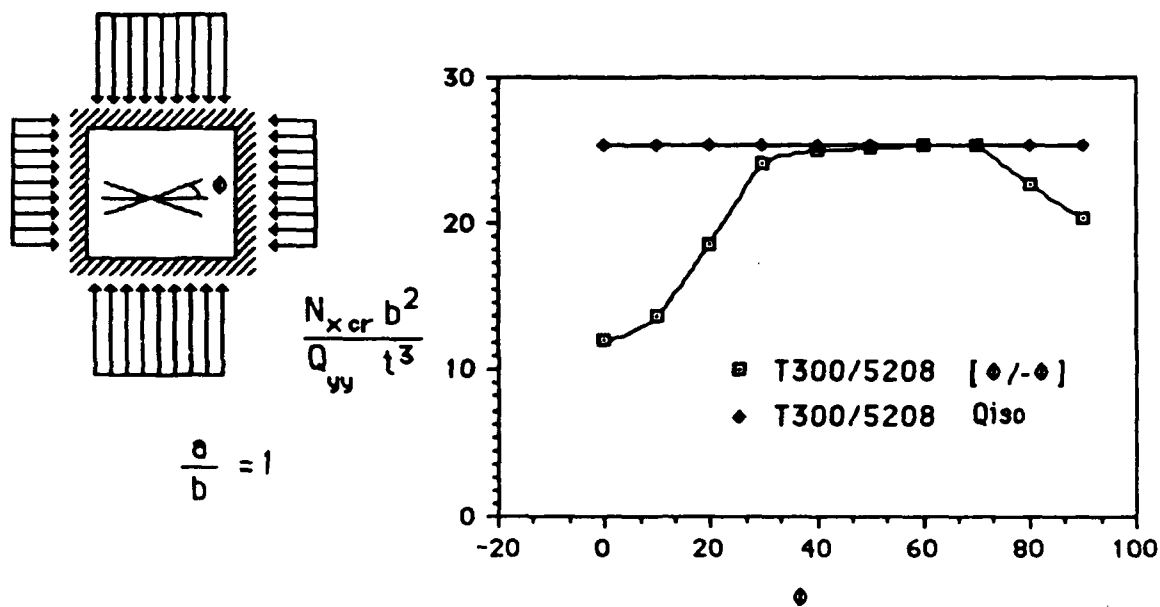


Figure 154. Comparison of critical loads for cross-ply and quasi-isotropic laminate for a square plate (clamped plates subjected to a uniform biaxial compression load ( $N_y=2*N_x$ )).

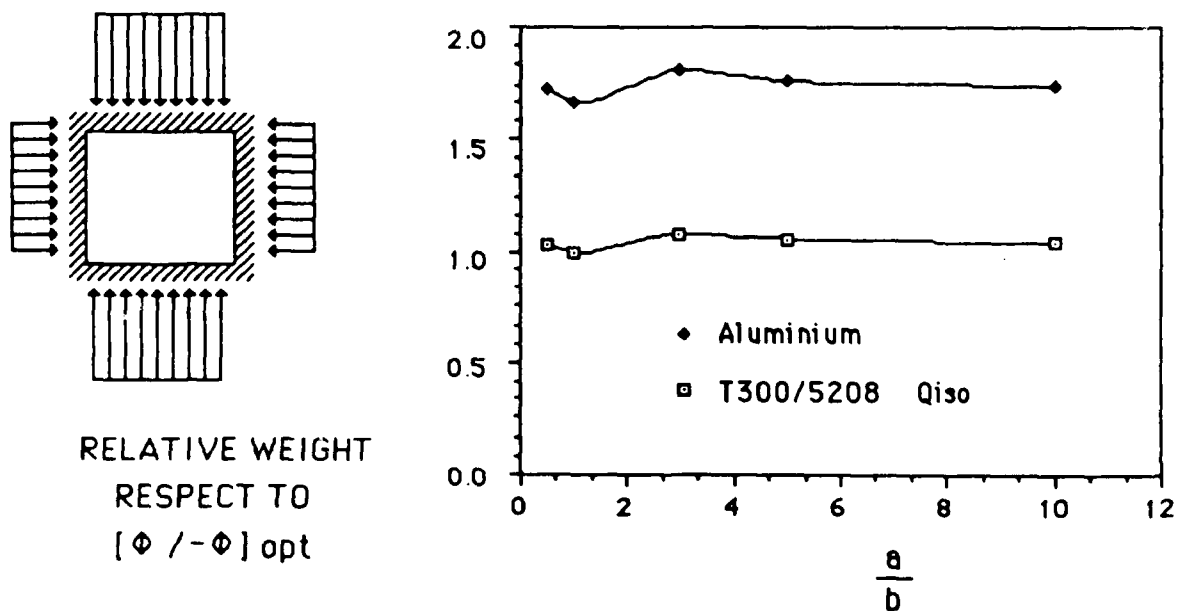


Figure 155. Comparison between weights of aluminium and the optimum configuration of T300/N5208 (clamped plates subjected to a uniform biaxial compression load ( $N_y=2*N_x$ )).

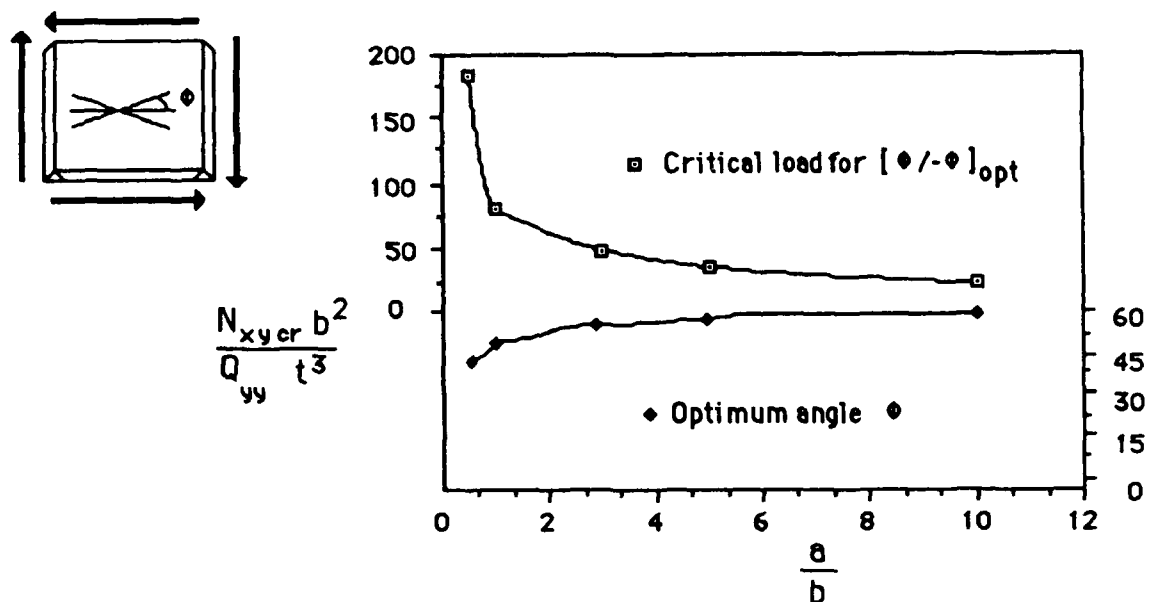


Figure 156. Critical load and optimum angle for a simply supported plate subjected to a uniform shear load.

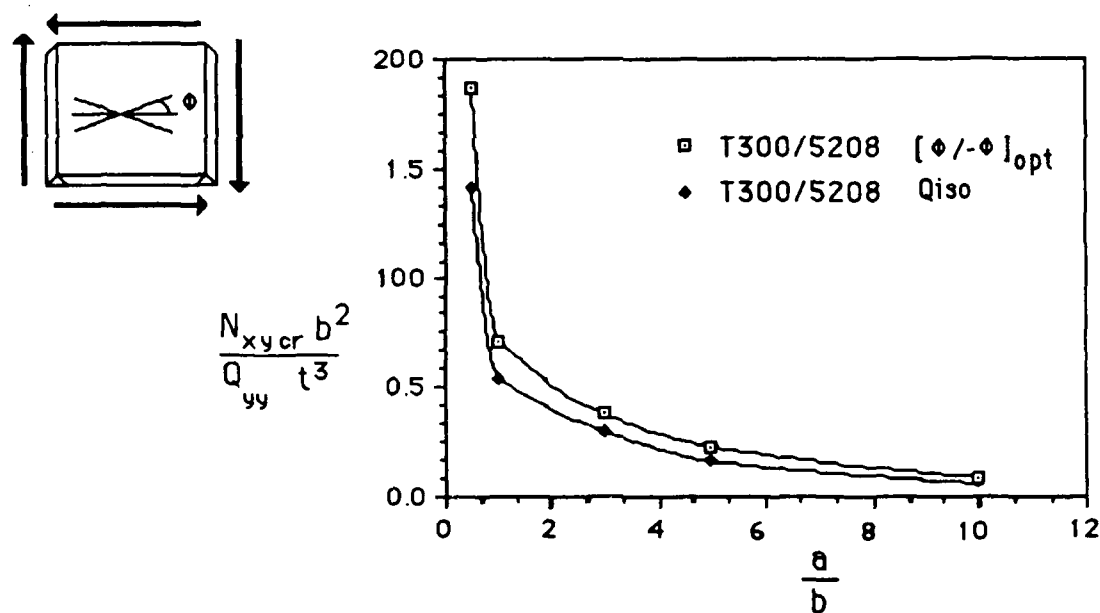
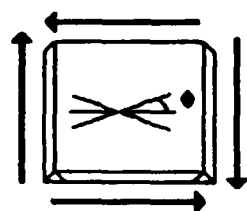


Figure 157. Comparison between critical loads of optimum configuration and quasi-isotropic laminate (simply supported plates subjected to a uniform shear load).



$$\frac{N_{xy cr} b^2}{Q_{yy} t^3}$$

$$\frac{a}{b} = 1$$

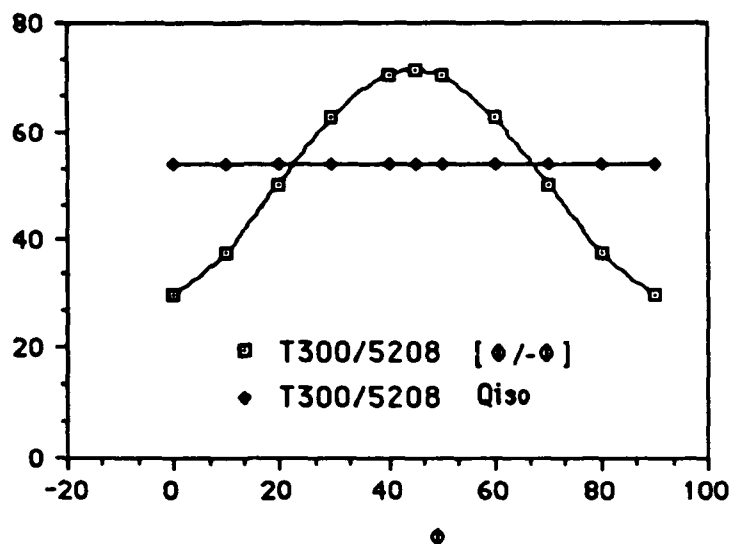
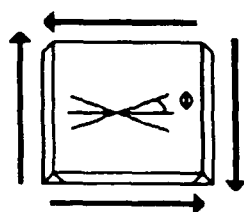


Figure 158. Comparison of critical loads for cross-ply and quasi-isotropic laminate for a square plate (simply supported plates subjected to a uniform shear load).



RELATIVE WEIGHT  
RESPECT TO  
[0 / -90] opt

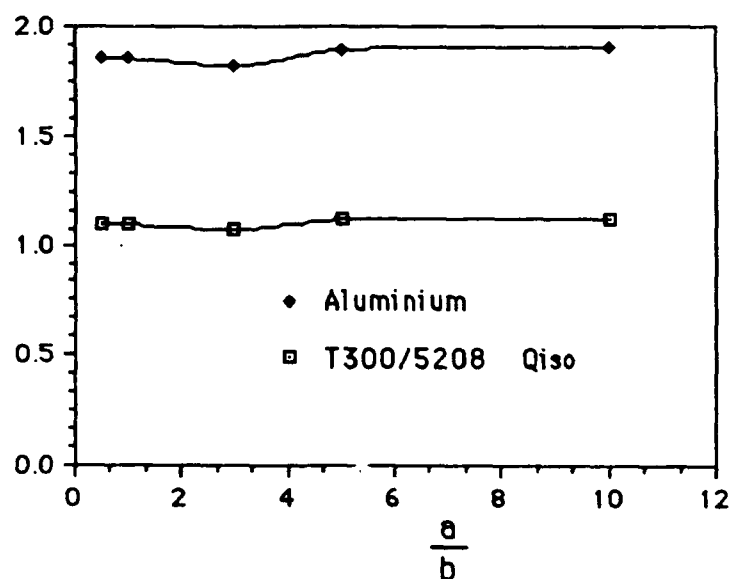
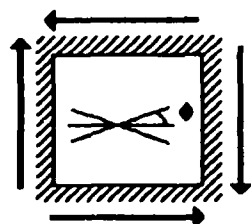


Figure 159. Comparison between weights of aluminium and the optimum configuration of T300/N5208 (simply supported plates subjected to a uniform shear load).



$$\frac{N_{xy cr} b^2}{Q_{yy} t^3}$$

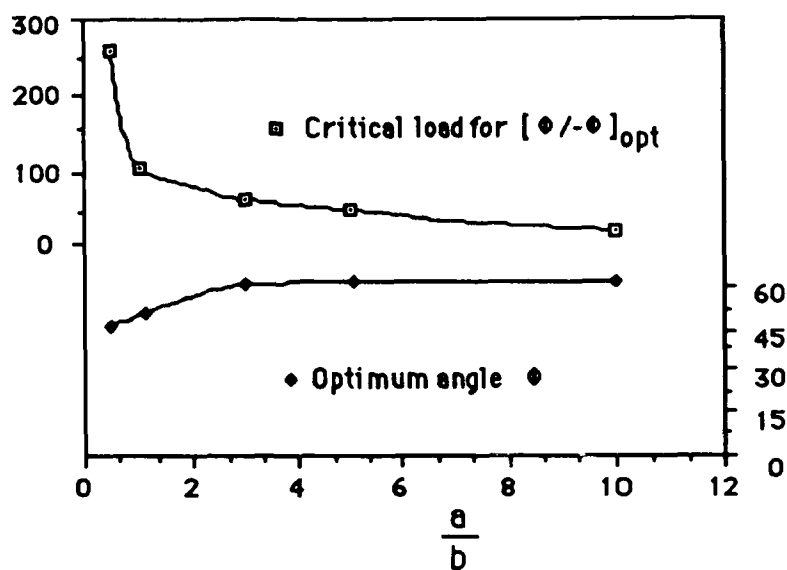
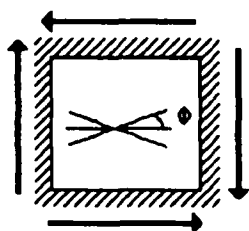


Figure 160. Critical load and optimum angle for a clamped plate subjected to a uniform shear load.



$$\frac{N_{xy cr} b^2}{Q_{yy} t^3}$$

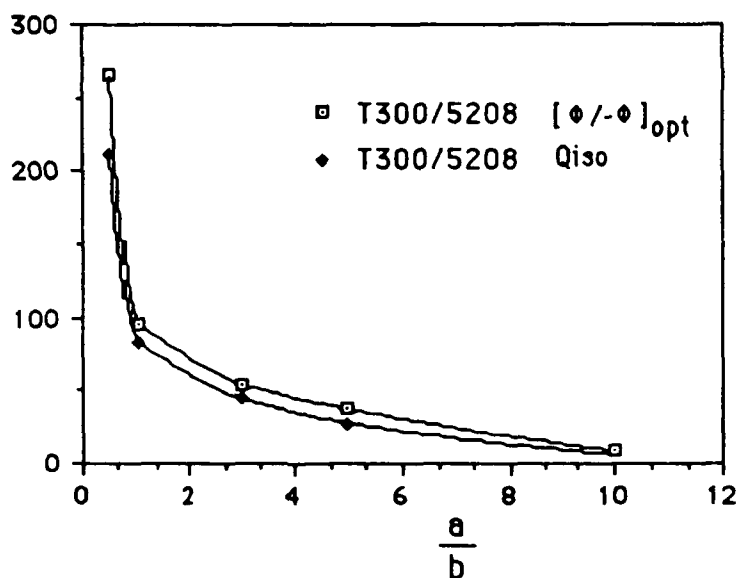


Figure 161. Comparison between critical loads of optimum configuration and quasi-isotropic laminate (clamped plates subjected to a uniform shear load).

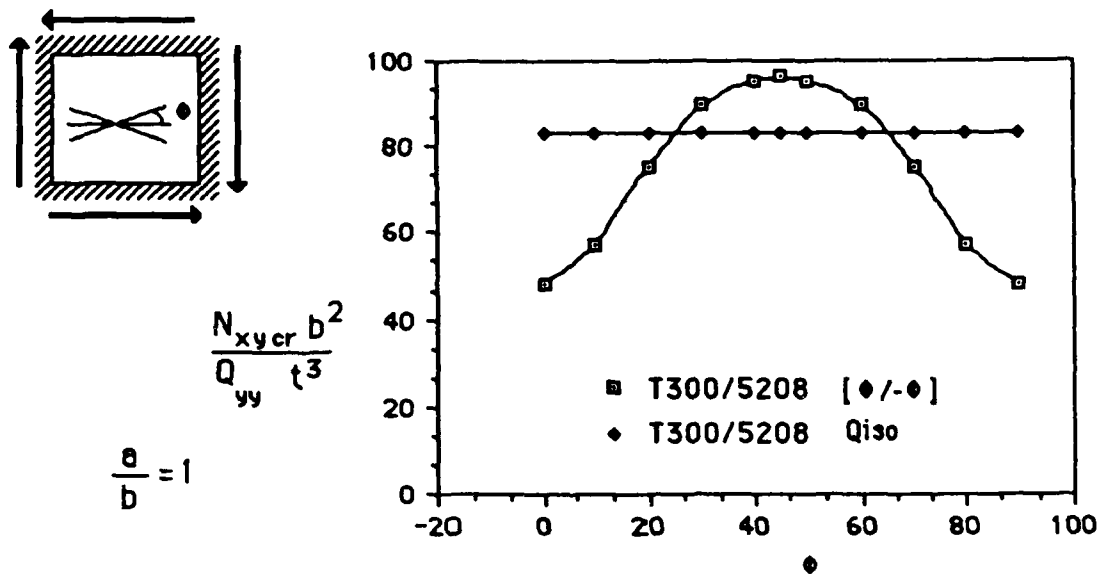


Figure 162. Comparison of critical loads for cross-ply and quasi-isotropic laminate for a square plate (clamped plates subjected to a uniform shear load).

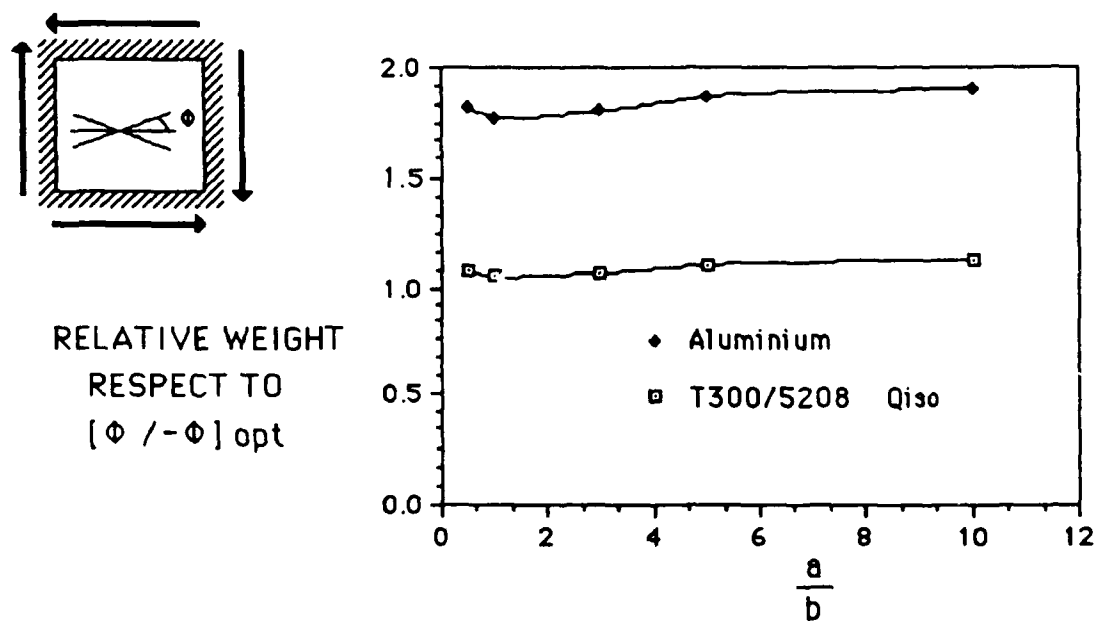


Figure 163. Comparison between weights of aluminium and the optimum configuration of T300/N5208 (clamped plates subjected to a uniform shear load).

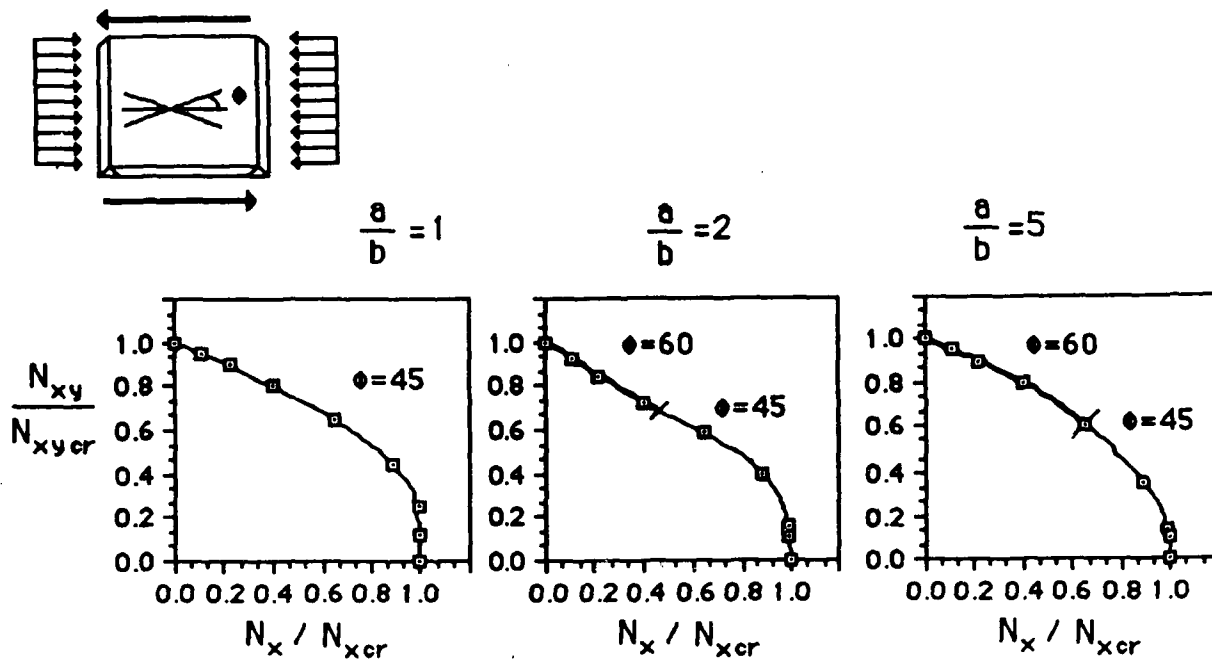


Figure 164. Buckling parameters for simply supported plates subjected to combined uniform uniaxial compression and shear.

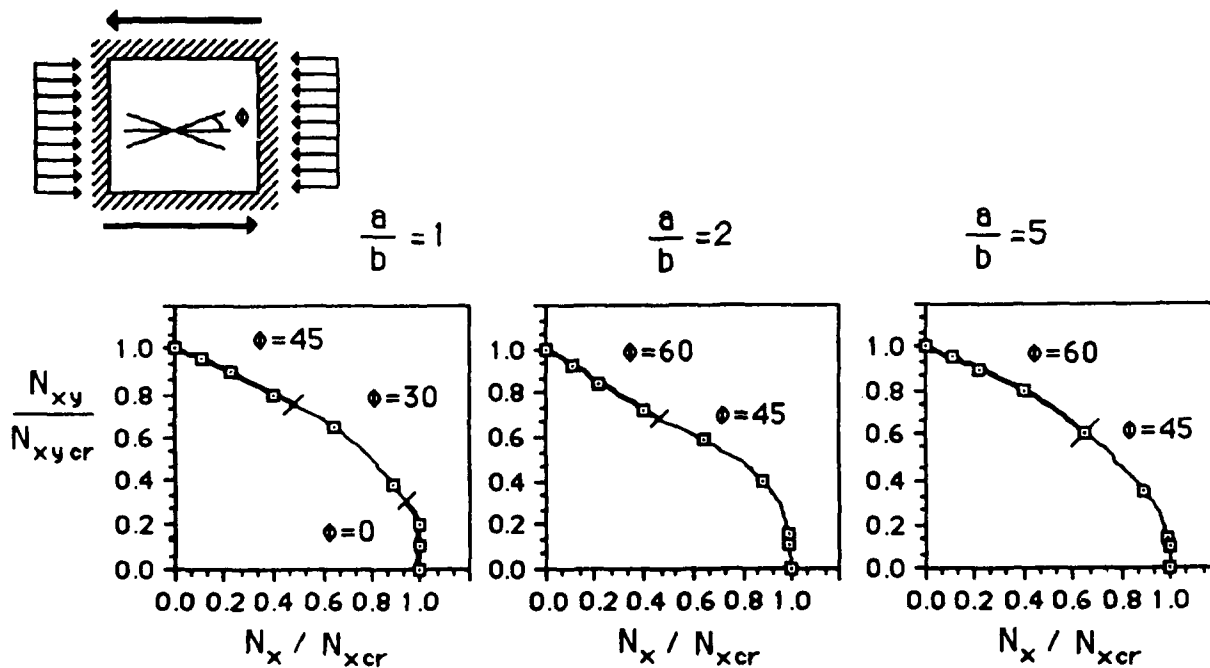


Figure 165. Buckling parameters for clamped plates subjected to combined uniform uniaxial compression and shear.